

**Forschungsbericht 2012-08**

**Development of a Forecast Model  
for Global Air Traffic Emissions**

Martin Schaefer

Deutsches Zentrum für Luft- und Raumfahrt  
Institut für Antriebstechnik  
Köln

235 Seiten  
137 Bilder  
70 Tabellen  
133 Literaturstellen



**DLR**

**Deutsches Zentrum  
für Luft- und Raumfahrt e.V.**

in der Helmholtz-Gemeinschaft



---

Development of a Forecast Model  
for Global Air Traffic Emissions

Dissertation  
zur Erlangung des Grades  
Doktor-Ingenieur

der Fakultät für Maschinenbau  
der Ruhr-Universität Bochum

von  
Martin Schaefer  
aus Nürnberg

Bochum 2012

---

---

Dissertation eingereicht am:	07. März 2012
Tag der mündlichen Prüfung:	29. Juni 2012
Erster Referent:	Prof. Dr.-Ing. Reinhard Mönig (Ruhr-Universität Bochum)
Zweiter Referent:	Prof. Dr. rer. nat. Johannes Reichmuth (RWTH Aachen)

---



---

## CONTENTS

	<b>LIST OF FIGURES</b> .....	<b>V</b>
	<b>LIST OF TABLES</b> .....	<b>XI</b>
	<b>LIST OF ABBREVIATIONS</b> .....	<b>XIV</b>
	<b>PREFACE</b> .....	<b>XIX</b>
<b>1</b>	<b>EXECUTIVE SUMMARY</b> .....	<b>1</b>
1.1	Objectives of this Study .....	1
1.2	Abstract of Methodology .....	1
1.3	Summary of Results .....	4
1.3.1	Overview on Application Studies.....	4
1.3.2	Emissions from Air Traffic 2000-2010 .....	5
1.3.3	Forecast of Emissions from Air Traffic 2011-2030 .....	6
<b>2</b>	<b>ECOLOGICAL AND TECHNOLOGICAL BACKGROUND</b> .....	<b>9</b>
2.1	Development of Air Traffic .....	9
2.2	Climate Impact of Aviation Emissions.....	11
2.3	Technology Measures to Limit Aviation Emissions.....	15
2.3.1	Improving Aircraft Fuel Efficiency.....	15
2.3.2	Reducing Engine NO <sub>x</sub> Emissions.....	18
2.3.3	Optimizing Air Traffic Management and Aircraft Operations.....	21
2.3.4	Alternative Fuels .....	22
2.4	Approach and Focus of this Study .....	23
<b>3</b>	<b>METHODOLOGY FOR AVIATION EMISSIONS CALCULATION</b> .....	<b>25</b>
3.1	Model Overview .....	25
3.2	VarMission – Flight Mission and Emissions Module.....	26
3.2.1	Overview .....	26
3.2.2	The BADA Aircraft Performance Model .....	27
3.2.3	Flight Mission Simulation in VarMission.....	30
3.2.4	Emission Calculation in VarMission .....	34
3.2.4.1	Overview on Calculation Methods.....	34
3.2.4.2	Emissions of CO <sub>2</sub> and H <sub>2</sub> O.....	34
3.2.4.3	Emissions of NO <sub>x</sub> , CO and HC.....	35
3.2.4.4	Emissions of Soot / Black Carbon .....	38

3.2.5	VarMission Validation.....	39
3.2.5.1	Mission Fuel Burn Validation .....	39
3.2.5.2	Validation of Emissions Calculations .....	42
3.2.6	“Emission Profiles” – Look-up Tables of Aircraft Emissions .....	44
3.3	Air Traffic Emissions Module .....	46
3.3.1	Overview .....	46
3.3.2	OAG Schedules and Flight Movements .....	47
3.3.3	Load Factors and Payload .....	48
3.3.4	ATM Efficiency .....	51
3.3.5	Fuel Burn and Emissions of Global Air Traffic.....	53
3.3.5.1	Procedure for Calculating Fuel Burn and Emissions .....	53
3.3.5.2	Simplifications and Uncertainties.....	57
3.3.6	Contents of the Flight Movements and Emissions Database.....	59
3.3.7	Link to the FATE Global Inventory Software .....	60
3.4	Air Traffic Emissions Forecast Module .....	62
3.4.1	Overview .....	62
3.4.2	Simplifying Assumptions for the Forecast .....	63
3.4.3	Traffic Growth Model .....	66
3.4.4	Fleet Rollover Model .....	68
3.4.4.1	Approach and Assumptions.....	68
3.4.4.2	Aircraft Retirements .....	71
3.4.4.3	Aircraft Deliveries and Assignment to Flight Movements .....	75
3.4.4.4	Aircraft Production Periods.....	81
3.4.5	Models of Future Aircraft-Engine Combinations.....	82
3.4.5.1	Approach and Overview .....	82
3.4.5.2	Widebody Aircraft of the Near Future .....	83
3.4.5.3	Narrowbody Aircraft of the Near Future .....	87
3.4.5.4	A Generic Narrowbody Aircraft Family of the 2020s.....	90
3.4.5.5	Aircraft Representation for Fuel Burn and Emissions Calculation .....	94
3.4.6	Other Assumptions.....	95
3.4.6.1	Fuel Efficiency Improvement by Serial Modification .....	95
3.4.6.2	Reduction of NO <sub>x</sub> Emissions by Improved Engine Combustors .....	96
3.4.6.3	Load Factor Development .....	99
3.4.6.4	Improvement of ATM Efficiency.....	100

---

<b>4</b>	<b>AIR TRAFFIC EMISSIONS 2000-2030 .....</b>	<b>101</b>
4.1	Overview on Application Studies .....	101
4.2	Air Traffic Emissions 2000-2010 .....	102
4.2.1	Results Summary .....	102
4.2.2	Transport Performance .....	103
4.2.3	Fuel Consumption .....	104
4.2.4	NO <sub>x</sub> Emissions .....	106
4.2.5	CO and HC Emissions .....	108
4.2.6	Emissions of Soot / Black Carbon .....	110
4.3	Forecast of Air Traffic Emissions 2011-2030 .....	112
4.3.1	Results Summary .....	112
4.3.2	Transport Performance .....	113
4.3.3	Fleet Composition .....	115
4.3.4	Fuel Consumption .....	119
4.3.5	NO <sub>x</sub> Emissions .....	122
4.4	Selected Sensitivities and Case Studies .....	125
4.4.1	Influence of Traffic Growth .....	125
4.4.2	Influence of Assumptions about Future Engine Combustors .....	128
4.4.3	Delayed Introduction of New Aircraft .....	131
4.4.4	New Single-Aisle Aircraft instead of Re-Engineed A320 and 737 .....	135
<b>5</b>	<b>PERSPECTIVES .....</b>	<b>138</b>
5.1	Outlook on Future Air Traffic .....	138
5.2	Past and Future Model Application .....	142
5.3	Prospective Model Improvements .....	143
	<b>REFERENCES .....</b>	<b>145</b>
	<b>APPENDICES .....</b>	<b>155</b>
	Appendix A Aircraft Speeds and Accelerations .....	156
	Appendix B Engine Thrust Levels .....	158
	Appendix C Format of VarMission and FATE Emission Profiles .....	160
	Appendix D Typical Cruise Flight Levels .....	162
	Appendix E Specific Soot Particle Number vs. Altitude .....	164
	Appendix F OAG Aircraft and VarMission Models .....	165
	Appendix G En-Route Extension .....	171

---

Appendix H	ATM Efficiency in Air Traffic Emissions Module .....	174
Appendix I	Database Structure of Air Traffic Emissions Module .....	177
Appendix J	Growth Rates for Passenger and Cargo Air Traffic .....	180
Appendix K	Standardization of Aircraft Capacities.....	185
Appendix L	Development of Retirement Curves.....	189
Appendix M	Fleet Forecast Details.....	192
Appendix N	Aircraft Delivery Periods, Capacities and Lifetime Assumptions .....	194
Appendix O	Visualization of Aircraft Delivery Periods .....	204
Appendix P	Aircraft Replacement Schemes .....	208
Appendix Q	Aircraft and Engine Models of the Near Future .....	213
Appendix R	Design Approach for a Future Narrowbody Aircraft Family .....	217
Appendix S	Assumptions for Cargo Aircraft.....	219
Appendix T	Assumed Stringency of NO <sub>x</sub> Emission Standards .....	221
Appendix U	Tabulated Results for Baseline Scenario.....	222
Appendix V	Visualization of Air Traffic Emissions.....	231

---

## LIST OF FIGURES

Figure 1: Schematic of model architecture .....	1
Figure 2: Schematic of VarMission Module .....	2
Figure 3: Schematic of Air Traffic Emissions Module .....	3
Figure 4: Schematic of Air Traffic Emissions Forecast Module .....	3
Figure 5: Development of transport performance, fuel burn and NO <sub>x</sub> emissions .....	4
Figure 6: Comparison of fuel burn and NO <sub>x</sub> emissions calculations for global aviation.....	6
Figure 7: Forecasted fleet shares for large passenger aircraft.....	7
Figure 8: Forecasted fuel consumption and NO <sub>x</sub> emissions until 2030 .....	8
Figure 9: Development of air traffic and sold aviation fuel.....	9
Figure 10: Combustion process and typical share of emissions in cruise .....	11
Figure 11: Global distribution of fuel burn from civil aviation .....	12
Figure 12: Aviation radiative forcing components in 2005.....	14
Figure 13: Development of aircraft fuel efficiency .....	15
Figure 14: The link of TSFC to thermal and propulsive efficiency .....	16
Figure 15: NO <sub>x</sub> emission standards and NO <sub>x</sub> levels for selected engine families.....	18
Figure 16: Schematic of RQL and LDI combustor concepts .....	19
Figure 17: Fuel staging in TAPS combustor .....	20
Figure 18: Schematic of tool chain applied in this study.....	23
Figure 19: Schematic of the VarMission module .....	26
Figure 20: VarMission main input mask (screenshot) .....	29
Figure 21: Typical flight profile, flaps/slats schedule, departure and approach procedures for an Airbus A319 example mission.....	33
Figure 22: Overview on methods for emission calculation used in this study .....	34
Figure 23: EI NO <sub>x</sub> vs. fuel flow at sea level static conditions for a CFM56-5A3 engine.....	36
Figure 24: Comparison of mission fuel burn (B747-400, VarMission vs. Airline Software) ...	39
Figure 25: Comparison of mission fuel burn (B747-300, VarMission vs. FDR data) .....	40
Figure 26: Comparison of NO <sub>x</sub> between VarMission and VarCycle (DLR method).....	42

Figure 27: Comparison of NO <sub>x</sub> between VarMission and VarCycle (Boeing method) .....	43
Figure 28: Schematic of Air Traffic Emissions Module with link to the FATE software.....	46
Figure 29: Contents of OAG flight schedule data files .....	47
Figure 30: Contents of data sources for load factor assignment .....	49
Figure 31: Principle of load factor assignment.....	50
Figure 32: Flight inefficiency due to Air Traffic Management (ATM).....	51
Figure 33: Selected contents of the ASCEND Fleets Database .....	54
Figure 34: En-route extension vs. great-circle distance from EUROCONTROL statistics.....	56
Figure 35: Contents and structure of the Movements and Emissions Database .....	59
Figure 36: Visualization of scheduled aviation's CO <sub>2</sub> and NO <sub>x</sub> emissions .....	61
Figure 37: Schematic of the Forecast Module with optional link to the FATE software .....	62
Figure 38: Deviation of OAG seat capacities from baseline seating configurations .....	64
Figure 39: Schematic of traffic growth rate assignment.....	67
Figure 40: Examples of historical and forecasted aircraft numbers vs. time (method 1) .....	72
Figure 41: Typical retirement curves from this study and ICAO CAEP.....	72
Figure 42: Example of reference retirement curve and parameter variation.....	73
Figure 43: Examples of historical and forecasted aircraft numbers vs. time (method 2) .....	74
Figure 44: Schematic of relations between aircraft types .....	77
Figure 45: Example of an aircraft replacement scheme for widebody passenger aircraft .....	78
Figure 46: Aircraft delivery periods in the baseline scenario of the forecast.....	81
Figure 47: Lift-to-drag characteristics assumed for a model of the Boeing 787-8 .....	84
Figure 48: Characteristic NO <sub>x</sub> levels assumed for engines of the near future and NO <sub>x</sub> emissions as function of thrust assumed for the GENx-1B model.....	85
Figure 49: Fuel efficiency and specific NO <sub>x</sub> emissions of future widebody aircraft.....	86
Figure 50: Lift-to-drag characteristics assumed for the A320 NEO in cruise flight .....	88
Figure 51: Fuel efficiency and specific NO <sub>x</sub> emissions of future narrowbody aircraft .....	89
Figure 52: Parabolic drag polars assumed for future narrowbody aircraft in cruise flight .....	91
Figure 53: NO <sub>x</sub> emission characteristics assumed for future UHBR engines .....	93
Figure 54: Fuel efficiency and specific NO <sub>x</sub> emissions of future narrowbody aircraft .....	93

---

Figure 55: NO <sub>x</sub> standards and technology goals (left); NO <sub>x</sub> stringency in forecast .....	97
Figure 56: Load factors according to ICAO and forecast assumptions .....	99
Figure 57: ATM efficiency goals from the CANSO report.....	100
Figure 58: Comparison of model results based on OAG with ICAO statistics.....	103
Figure 59: Comparison of fuel consumption in IEA statistics and emission inventories.....	105
Figure 60: Comparison of NO <sub>x</sub> emissions in emission inventories .....	106
Figure 61: Comparison of the average NO <sub>x</sub> emission index in emission inventories .....	106
Figure 62: Comparison of CO emissions in emission inventories .....	108
Figure 63: Comparison of the average CO emission index in emission inventories .....	108
Figure 64: Comparison of HC emissions in emission inventories .....	109
Figure 65: Comparison of the average HC emission index in emission inventories.....	110
Figure 66: Comparison of soot emissions in emission inventories.....	110
Figure 67: Comparison of the average soot emission index in emission inventories .....	111
Figure 68: Comparison of model results with Airbus and Boeing forecasts .....	113
Figure 69: Comparison of model results with ICAO Outlook for Air Transport .....	114
Figure 70: Development of fleet shares for passenger aircraft.....	115
Figure 71: Development of aircraft number and ASK by seat category .....	116
Figure 72: Comparison of simulated fleet development with Airbus GMF.....	117
Figure 73: Delivery numbers by seat category in reference forecasts and model.....	118
Figure 74: Influence of increased load factors, fleet rollover process and ATM efficiency improvement on fuel consumption.....	119
Figure 75: Comparison of fuel burn with reference studies .....	120
Figure 76: Comparison of fuel efficiency with reference studies .....	120
Figure 77: Distribution of fuel burn and tonne-kilometres amongst seat categories.....	121
Figure 78: Comparison of NO <sub>x</sub> forecast with reference studies.....	122
Figure 79: Comparison of specific NO <sub>x</sub> emissions with reference studies.....	123
Figure 80: Comparison of forecasted EI NO <sub>x</sub> with reference studies .....	124
Figure 81: Distribution of NO <sub>x</sub> emissions and tonne-kilometres amongst seat categories ..	124
Figure 82: Transport performance in alternative traffic growth scenarios.....	125

---

Figure 83: Flight movements, total distance, fuel consumption and NO <sub>x</sub> emissions as function of traffic growth.....	126
Figure 84: Number of aircraft in service in 2030 and delivered during 2011-2030 .....	127
Figure 85: Fuel efficiency and specific NO <sub>x</sub> emissions as function of traffic growth .....	127
Figure 86: Variation of NO <sub>x</sub> Emissions with Technology Assumptions .....	129
Figure 87: Fleet shares of large passenger aircraft in baseline scenario and in scenario with delivery delays .....	132
Figure 88: Effects of delivery delays on fuel burn and emissions of air traffic .....	133
Figure 89: Effects of delivery delays on fuel efficiency .....	133
Figure 90: Effects of delivery delays on fuel efficiency and specific NO <sub>x</sub> emissions - exemplary analysis for the fleet segment with 121-210 seats .....	134
Figure 91: Fleet shares of large single-aisle passenger aircraft in baseline scenario and in scenario with new single-aisle aircraft types.....	135
Figure 92: Comparison of fuel efficiency and spec. NO <sub>x</sub> emissions in different scenarios ..	136
Figure 93: Distribution of fuel consumption between aircraft size categories .....	137
Figure 94: Comparison of global fuel burn and NO <sub>x</sub> emissions in different scenarios .....	137
Figure 95: Development of transport performance, fuel burn and NO <sub>x</sub> emissions.....	138
Figure 96: IATA environmental targets and potential effects of alternative fuels.....	139
Figure 97: Analysis of IATA's long term target for CO <sub>2</sub> emissions.....	140
Figure 98: Example of an information file .....	160
Figure 99: Example of a profile file .....	161
Figure 100: Maximum flight level of Airbus A321 by mission distance in flight movements of the Aero2k inventory for December 2002 .....	162
Figure 101: Average soot particle number per gram of soot vs. flight altitude.....	164
Figure 102: Contributions to route extension .....	171
Figure 103: Direct route extension in Europe and the US per distance category .....	172
Figure 104: Direct route extension as function of great-circle distance (approximation) .....	172
Figure 105: En-route extension vs. great-circle distance.....	176
Figure 106: Movements and Emissions Database based on OAG flight schedules.....	177
Figure 107: ICAO TFS data as used by the Air Traffic Emissions Module .....	178



---

Figure 108: ICAO Air Carrier data as used by the Air Traffic Emissions Module .....	178
Figure 109: Data from airline publications as used by the Air Traffic Emissions Module ....	178
Figure 110: Excerpt of the VarMission database as used by the Air Traffic Emissions Module for the assignment of aircraft models to flight movements .....	179
Figure 111: Excerpt of ASCEND fleets data as used by the Air Traffic Emissions Module for the assignment of engine types to flight movements .....	179
Figure 112: Deviation of OAG seat capacities from baseline seating configurations .....	186
Figure 113: Analysis of typical aircraft lifetimes by aircraft category .....	190
Figure 114: Reference retirement curves for different groups of aircraft.....	191
Figure 115: Estimated aircraft numbers vs. time (without detailed fleet statistics).....	193
Figure 116: Aircraft delivery periods in the baseline scenario of the forecast .....	204
Figure 117: Aircraft delivery periods in an alternative fleet scenario assuming development and delivery delays of future aircraft types .....	205
Figure 118: Aircraft delivery periods in an alternative fleet scenario assuming all-new single-aisle aircraft instead of re-engined A320 and 737 families.....	206
Figure 119: Aircraft delivery periods in a hypothetical fleet scenario assuming no new aircraft types after the year 2010 .....	207
Figure 120: Replacement scheme for widebody jet aircraft in baseline forecast .....	208
Figure 121: Replacement scheme for narrowbody jet aircraft in baseline forecast.....	209
Figure 122: Replacement scheme for regional jet aircraft in baseline forecast.....	210
Figure 123: Replacement scheme for aircraft with turboprop engines in baseline forecast	211
Figure 124: Replacement scheme for all-cargo aircraft / freighter in baseline forecast .....	212
Figure 125: Fuel flow and NO <sub>x</sub> emission index vs. thrust for GEnx-1B engine.....	214
Figure 126: Fuel flow and NO <sub>x</sub> emission index vs. thrust for Trent 1000 engine.....	215
Figure 127: Fuel flow and NO <sub>x</sub> emission index vs. thrust for Trent XWB engine.....	215
Figure 128: Fuel flow and NO <sub>x</sub> emission index vs. thrust for PW 1217G engine.....	215
Figure 129: Fuel flow and NO <sub>x</sub> emission index vs. thrust for A321 NEO engine .....	216
Figure 130: Payload-range performance of new aircraft types.....	216
Figure 131: Fuel flow and NO <sub>x</sub> emission index vs. thrust for UHBR engine .....	217

Figure 132: Payload-range performance of a future narrowbody aircraft family compared to the Airbus A320 family..... 218

Figure 133: Visualization of global scheduled aviation’s fuel consumption in September 2000 and September 2010..... 231

Figure 134: Visualization of global scheduled aviation’s NO<sub>x</sub> emissions in September 2000 and September 2010..... 232

Figure 135: Visualization of global scheduled aviation’s CO emissions in September 2000 and September 2010..... 233

Figure 136: Visualization of global scheduled aviation’s HC emissions in September 2000 and September 2010..... 234

Figure 137: Visualization of global scheduled aviation’s soot emissions in September 2000 and September 2010..... 235

---

## LIST OF TABLES

Table 1: Transport performance and emissions of scheduled aviation .....	5
Table 2: Forecast of flight movements, transport performance and emissions until 2030 .....	7
Table 3: Potential measures for improving aircraft fuel efficiency .....	17
Table 4: Operations performance parameters in BADA .....	28
Table 5: Available flight phases in VarMission .....	31
Table 6: Default flight mission as sequence of flight phases.....	32
Table 7: Emission indices for CO <sub>2</sub> , H <sub>2</sub> O and SO <sub>x</sub> from various studies .....	35
Table 8: Summary of fuel burn comparison with FDR data.....	40
Table 9: Comparison of emission calculations between VarMission and VarCycle on a Boeing 747-400 example flight mission.....	43
Table 10: Estimation of errors from model assumptions .....	57
Table 11: Future passenger aircraft assumed in a baseline fleet scenario .....	65
Table 12: Excerpt of regional growth rates for passenger air traffic .....	66
Table 13: Aircraft deliveries by seat category.....	80
Table 14: Characteristic weights of future widebody aircraft .....	83
Table 15: Engine parameters of simulated engines for widebody aircraft .....	84
Table 16: Characteristic weights of future regional jet and A320 NEO models.....	87
Table 17: Engine parameters of simulated engines for narrowbody aircraft .....	88
Table 18: Design specification for a future narrowbody aircraft family .....	90
Table 19: Characteristic weights of future narrowbody aircraft.....	91
Table 20: Engine parameters of future narrowbody aircraft (highest thrust version) .....	92
Table 21: Assumptions for passenger aircraft without available simulation model .....	94
Table 22: Assumptions for future combustor updates in aircraft engines.....	96
Table 23: NO <sub>x</sub> stringency assumptions in the baseline scenario of the forecast.....	98
Table 24: Transport performance, fuel burn and emissions for scheduled aviation .....	102
Table 25: Influence of calculation method on global NO <sub>x</sub> emissions and average EI NO <sub>x</sub> ..	107
Table 26: Forecasted transport performance, fuel burn and emissions for aviation.....	112

Table 27: Baseline and alternative assumptions for future low-NO <sub>x</sub> combustors .....	128
Table 28: Assumptions about delivery delays of future aircraft types in sensitivity study....	131
Table 29: Assignment of VarMission / BADA models to OAG aircraft types, part 1 .....	165
Table 30: Assignment of VarMission / BADA models to OAG aircraft types, part 2 .....	166
Table 31: Assignment of VarMission / BADA models to OAG aircraft types, part 3 .....	167
Table 32: Assignment of VarMission / BADA models to OAG aircraft types, part 4 .....	168
Table 33: Assignment of VarMission cargo aircraft models to OAG aircraft types .....	169
Table 34: Assignment of VarMission passenger aircraft models to future aircraft types .....	170
Table 35: Development of en-route extension in Europe.....	171
Table 36: Average annual growth rates for passenger air traffic, part 1 .....	180
Table 37: Average annual growth rates for passenger air traffic, part 2 .....	181
Table 38: Average annual growth rates for passenger air traffic, part 3 .....	182
Table 39: Average annual growth rates for cargo air traffic, part 1 .....	182
Table 40: Average annual growth rates for cargo air traffic, part 2 .....	183
Table 41: Average annual growth rates for cargo air traffic, part 3 .....	184
Table 42: Cargo volumes of different unit load devices .....	186
Table 43: Description of identifier for aircraft retirement curves .....	194
Table 44: Aircraft production periods and capacities, seat categories 6-7 .....	195
Table 45: Aircraft production periods and capacities, seat category 5 .....	196
Table 46: Aircraft production periods and capacities, seat category 4 .....	197
Table 47: Aircraft production periods and capacities, seat category 3 .....	198
Table 48: Aircraft production periods and capacities, seat category 2 .....	199
Table 49: Aircraft production periods and capacities, seat category 1 .....	200
Table 50: Aircraft production periods and capacities, seat category 0 .....	201
Table 51: Aircraft production periods and capacities, seat category 101-103 .....	202
Table 52: Aircraft production periods and capacities, seat category 200 .....	203
Table 53: Aerodynamic assumptions for aircraft models in cruise flight .....	213
Table 54: Characteristic weights of major cargo aircraft types .....	219
Table 55: Characteristic weights of major cargo aircraft types (continued) .....	219

---

Table 56: Characteristic weights of major cargo aircraft types (continued).....	219
Table 57: Characteristic weights of major cargo aircraft types (continued).....	220
Table 58: Assumptions for future cargo aircraft without available performance models .....	220
Table 59: Stringency of NO <sub>x</sub> emission standards in baseline scenario .....	221
Table 60: Stringency of NO <sub>x</sub> emission standards in scenario with development delays .....	221
Table 61: Transport performance and emissions for historical scheduled air traffic .....	222
Table 62: Transport performance and emissions for forecasted scheduled air traffic.....	222
Table 63: Number of active aircraft by aircraft type, seat categories 6-7 .....	223
Table 64: Number of active aircraft by aircraft type, seat category 5 .....	224
Table 65: Number of active aircraft by aircraft type, seat category 4 .....	225
Table 66: Number of active aircraft by aircraft type, seat category 3 .....	226
Table 67: Number of active aircraft by aircraft type, seat category 2 .....	227
Table 68: Number of active aircraft by aircraft type, seat category 1 .....	228
Table 69: Number of active aircraft by aircraft type, seat categories 101-103 .....	229
Table 70: Number of active aircraft by aircraft type, seat category 200 .....	230

## LIST OF ABBREVIATIONS

AAGR	Average Annual Growth Rate
ACARE	Advisory Council for Aeronautics Research in Europe
ADS-B	Automatic Dependent Surveillance Broadcast
AEDT	Aviation Environment Design Tool
ASTM	American Society for Testing and Materials
ASCII	American Standard Code for Information Interchange
ASK	Available Seat Kilometres
ATA	Air Transport Association
ATM	Air Traffic Management
BADA	Base of Aircraft Data
BM2	Boeing Fuel Flow Correlation Method 2 for Calculation of NO <sub>x</sub> Emissions
BPR	Bypass Ratio
BTL	Biomass to Liquid
CAEP	Committee on Aviation Environmental Protection
CANSO	Civil Air Navigation Services Organisation
CAS	Calibrated Airspeed
CASFE	Commercial Aircraft System Fuel Efficiency
CO	Carbon Monoxide
CO <sub>2</sub>	Carbon Dioxide
CO <sub>2e</sub>	Equivalent Carbon Dioxide
DLR	Deutsches Zentrum für Luft- und Raumfahrt (German Aerospace Center)
EI	Emission Index
EIS	Entry into Service
FAA	Federal Aviation Administration
FATE	Four-dimensional Calculation of Aircraft Trajectories and Emissions
FDR	(Computer) Flight Data Recorder
FESG	Forecasting and Economic Analysis Support Group

---

FL	Flight Level
FOCA	Swiss Federal Office of Civil Aviation
FOI	Swedish Defence Research Agency
FTKO	Freight Tonne Kilometres Offered (Available)
FTKT	Freight Tonne Kilometres Transported
F-T	Fischer-Tropsch
GCD	Great Circle Distance
GDP	Gross Domestic Product
GHG	Greenhouse Gas
GMF	Global Market Forecast
HC	Hydrocarbons
HEFA	Hydroprocessed Esters and Fatty Acids
H <sub>2</sub> O	Water (or water vapour)
IATA	International Air Transport Association
ICAO	International Civil Aviation Organization
IEA	International Energy Agency
IFR	Instrument Flight Rules
ISA	International Standard Atmosphere
LDI	Lean Burn Direct Injection
LF	Load Factor
LOSU	Level of Scientific Understanding
LTO	Landing and Take-off Cycle
MFC	Maximum Fuel Capacity
MLW	Maximum Landing Weight
MTOW	Maximum Take-off Weight
MTW	Maximum Taxi Weight
NASA	National Aeronautics and Space Administration
NO <sub>x</sub>	Nitric Oxides
OAG	Official Airline Guide

OEW	Operational Empty Weight
OPR	Overall Pressure Ratio
PL	Payload
PM	Particulate Matter
RF	Radiative Forcing
RPK	Revenue Passenger Kilometres
RQL	Rich-Burn / Quick-Mix / Lean-Burn
SAGE	System for Assessing Aviation's Global Emissions
SESAR	Single European Sky ATM Research
SFC	Specific Fuel Consumption
SO <sub>x</sub>	Sulphur Oxides
SQL	Structured Query Language
TAPS	Twin Annular Premixing Swirler
TAS	True airspeed
TFS	Traffic by Flight Stage
TKM	Tonne Kilometres
TMA	Terminal Control Area
TKO	Tonne Kilometres Offered
TKT	Tonne Kilometres Transported
TRL	Technology Readiness Level
TSFC	Thrust Specific Fuel Consumption
UHBR	Ultra High Bypass Ratio
UTC	Universal Time Coordinates
VarCycle	Software for thermodynamic engine simulation used at DLR
VarMission	Software for flight mission analysis used at DLR
VBA	Visual Basic for Applications
VFR	Visual Flight Rules



---

**Symbols used in Formulae**

C	Concentration [g/m <sup>3</sup> ]
C <sub>D</sub>	Drag coefficient [-]
C <sub>L</sub>	Lift coefficient [-]
D	Aerodynamic drag force [N]
D <sub>p</sub>	NO <sub>x</sub> emissions (“deposit”) of an aircraft engine in the ICAO LTO cycle [g]
EI	Emission index [g/kg fuel]
F	Force [N]
F <sub>00</sub>	Maximum rated thrust of an aircraft engine at sea-level static conditions [kN]
f	Fuel flow of an aircraft [kg/s]
g	Gravitational acceleration [m/s <sup>2</sup> ]
h	Altitude [m]
H	Humidity correction factor [-]
L	Aerodynamic lift force [N]
m	Aircraft mass [kg]
M	Mach number [-]
n	Number [-]
p	Pressure [Pa]
S	Wing surface area [m <sup>2</sup> ]
t	Time [s]
T	Thrust [N] or Temperature [K]
v	Velocity [m/s or kt]
w	Fuel flow [kg/s]
φ	Bank angle [rad] or equivalence ratio [-]
η	Thrust specific fuel consumption [g/s/kN]
μ	Bypass ratio of an engine [-]
π	Overall pressure ratio [-]
ρ	Density [kg/m <sup>3</sup> ]
ω	Specific humidity [-]

**Units**

ft	Feet
g	Gram
h	Hour
kg	Kilogram
km	Kilometre
kN	Kilonewton
kt	Knot
K	Kelvin
lb	Pound
lbf	Pound-Force
m	Metre
Mt	Megatons
N	Newton
NM	Nautical miles
Pa	Pascal
Pkm	Passenger-Kilometres
s	Second
t	Metric ton
tkm	Tonne-Kilometres
W	Watt

## PREFACE

Aviation contributes to economic growth, but also has negative impacts on the environment. Considering traffic growth in the order of 5% per year, sustainability of the air transport sector is difficult to achieve. This study deals with gaseous and particulate emissions from global air traffic. It describes a newly developed simulation tool that quantifies historical emissions and forecasts emissions in the future. In order to demonstrate the functionality of this tool, fuel burn and emissions are calculated for the years 2000 until 2010. In addition, a forecast of emissions from air traffic until the year 2030 is conducted.

A summary of major results from this study is found in chapter 1. An overview on aviation's impact on atmospheric physics and climate is presented in chapter 2 of the report. This chapter also describes technical measures to limit aviation's impact on the environment. The newly developed simulation model that can be used to quantify emissions of current and future aviation is presented in chapter 3. This model can be regarded as an automated chain of software consisting of the following programs:

- The engine performance software VarCycle.
- The flight mission simulation tool VarMission.
- The Air Traffic Emissions Module based on worldwide flight schedules.
- The Air Traffic Emissions Forecast Module considering traffic growth and future fleet composition.
- The FATE software that creates four-dimensional inventories of global air traffic emissions.

While VarCycle and FATE are well-established and validated software developed at DLR, the remaining modules have been specifically created by the author. These modules are based on publicly available data, can be run on any personal computer with Microsoft Windows and can be adopted easily for a number of different assessments.

Results from an application of the model are discussed in chapter 4. Emissions from scheduled air traffic have been calculated for the years 2000 until 2010 and are supplemented by a forecast until the year 2030. The assessment for the years 2000-2010 covers transport performance and fuel burn as well as emissions of nitric oxides (NO<sub>x</sub>), carbon monoxide (CO), hydrocarbons (HC) and soot. In the forecast until 2030, future transport performance, fleet composition, fuel burn and emissions of NO<sub>x</sub> are predicted. An evaluation of selected sensitivities regarding e.g. the variability of future emissions with traffic growth and fleet composition are also discussed in chapter 4.

---

---

# 1 EXECUTIVE SUMMARY

## 1.1 OBJECTIVES OF THIS STUDY

This report describes the methodology of a newly developed simulation model that can be used to quantify gaseous and particulate emissions from air traffic. The automated tool provides a means to calculate historical emissions from air traffic and to forecast emissions in the short-term and medium-term future. It consists of a chain of software modules that are flexible enough to perform a range of different assessments. Developed at the DLR Institute of Propulsion Technology, the software will be used to quantify the environmental effects of future aircraft and engine technology both for flight missions and for global air traffic. While some modules in the tool chain have been specifically developed for this study, others are based on existing software, namely the VarCycle engine performance tool used at the DLR Institute of Propulsion Technology and the FATE software for global emission inventories developed by the DLR Institute of Air Transport and Airport Research.

First results from an application of the simulation model are presented in this study and cover emissions from scheduled air traffic for the years 2000 to 2010 as well as forecasted emissions until the year 2030. These results have been validated against reference data from various sources including statistics from the International Civil Aviation Organization (ICAO), the International Energy Agency (IEA) and simulation results from research projects. Besides total emission quantities, three-dimensional emission inventories can be calculated by the model that can be processed further to assess aviation's impact on climate.

## 1.2 ABSTRACT OF METHODOLOGY

The simulation model developed for this study is a chain of software tools covering engine performance and emissions, aircraft flight simulation, air traffic movements and forecast scenarios. A schematic of the automated tool chain is shown in Figure 1. The model calculates fuel burn and emissions of air traffic in a bottom-up approach, i.e. starting from a database of flight movements and calculating emissions for each flight. As will be described below, this approach is followed both for historical air traffic and for the emissions forecast.

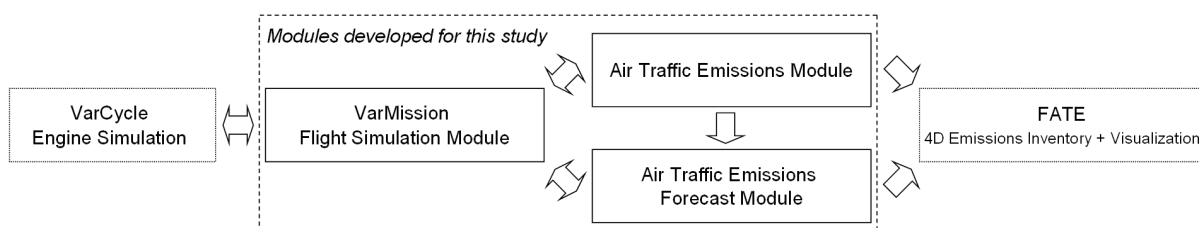


Figure 1: Schematic of model architecture

The first tool in the chain is the software VarCycle, which simulates an engine’s performance and emissions at different operating conditions. Developed at the DLR Institute of Propulsion Technology, the well-established and validated software can be linked to a newly developed flight simulation module named VarMission.

The VarMission module is an aircraft performance tool capable of calculating fuel burn and emissions on given flight missions (see Figure 2). A flight mission can be described as any sequence of flight segments. Using the EUROCONTROL BADA database of aircraft models [46] in combination with emission correlation methods developed by Boeing [14] and DLR [31], VarMission covers a broad range of aircraft-engine combinations. Besides BADA, aircraft models from other sources and in different formats can be used with this module. VarMission is coupled to the VarCycle engine simulation. This way, detailed performance and emissions models of aircraft engines can be evaluated on flight mission level.

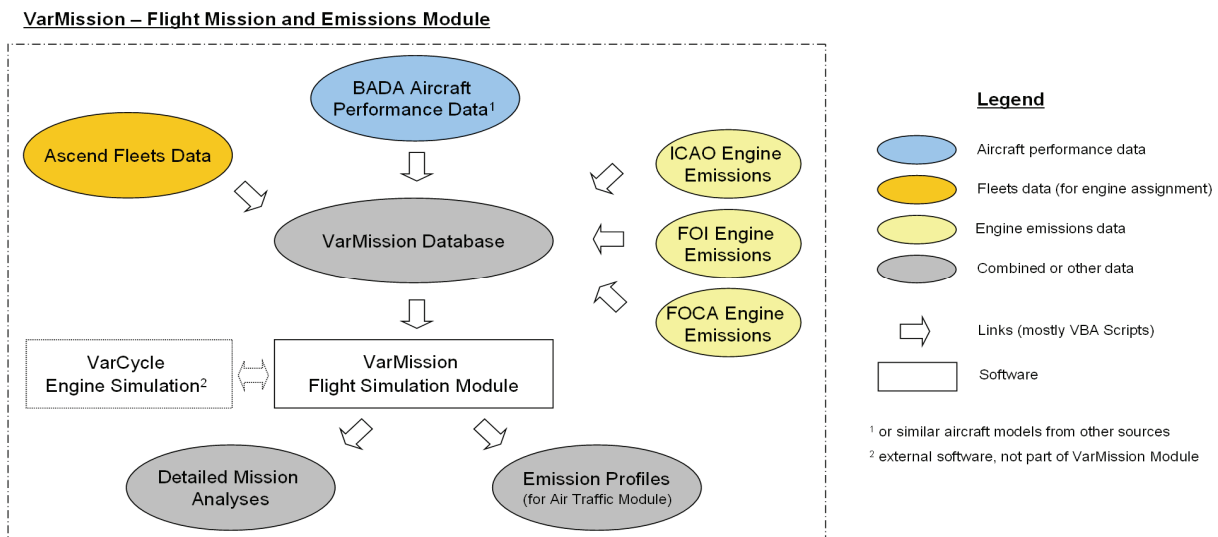


Figure 2: Schematic of VarMission Module

The Air Traffic Emissions Module developed for this study is based on worldwide flight schedules compiled by the Official Airline Guide (OAG) [100]. The module consists of several database scripts linking and combining information from various sources. Initially, OAG flight schedules are converted into a database of flight movements. The movements data is supplemented by information on engine types from the ASCEND fleets database [11] and by load factors from ICAO statistics [77]. Provided with this information, the module uses on look-up tables produced by VarMission to calculate fuel burn and emissions for each flight. Assumptions are made regarding inefficiencies from Air Traffic Management which influence fuel burn and emissions of air traffic. In order to account for these inefficiencies, the module simulates flight distance extensions compared to the great-circle, holding patterns and increased taxi times on the ground based on information from the Civil Air Navigation Services Organization (CANSO) [27]. A schematic of the module is shown in Figure 3.

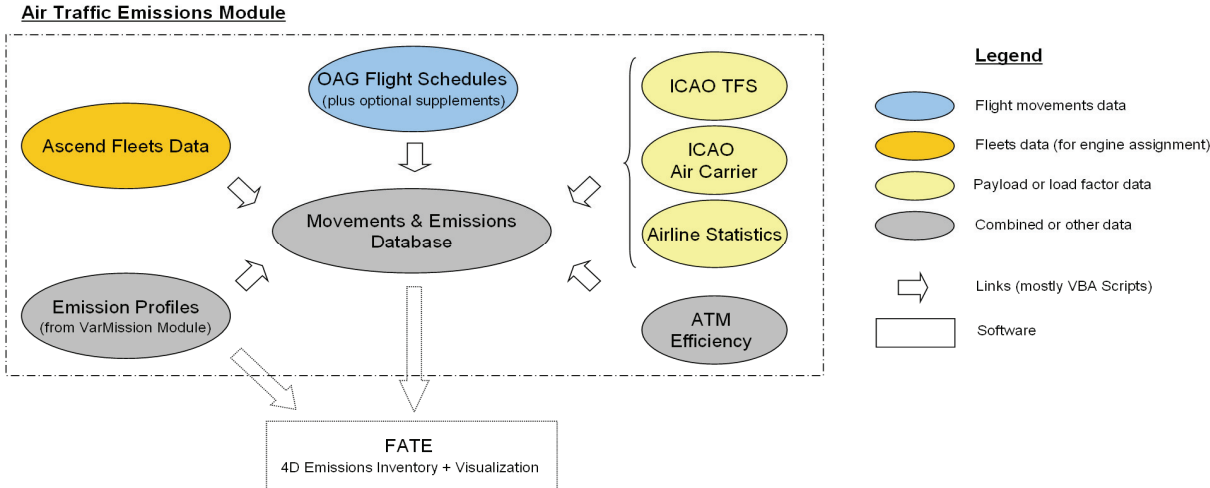


Figure 3: Schematic of Air Traffic Emissions Module

The Air Traffic Emissions Forecast Module, which has been newly developed for this study, predicts fuel burn and emissions of air traffic in the short-term and medium-term future. Using a common database structure with the Air Traffic Emissions Module, the model applies regional traffic growth rates from the Airbus Global Market Forecast (GMF) [4] to flight movements for a base year. It predicts the future fleet composition based on fleet statistics, typical aircraft lifetimes, assumptions about new aircraft types and aircraft market shares. In a year-by-year forecast, traffic growth and fleet rollover are simulated and applied to the base year flight movements. Similar to the approach for historical aviation, VarMission is used to determine fuel burn and emissions of each flight. For this purpose, simplified models of future aircraft types have been developed for VarMission, which are used in combination with engine models simulated by VarCycle. Assumptions about future load factors, ATM efficiency and regulatory standards for engine NO<sub>x</sub> emissions are also used for emissions prediction. Figure 4 presents a schematic of the Air Traffic Emissions Forecast Module.

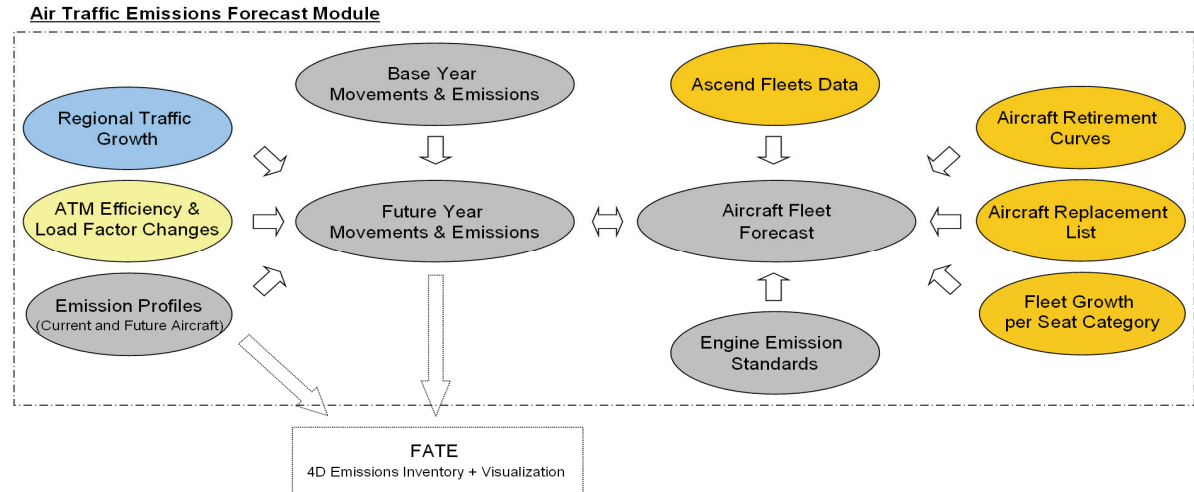


Figure 4: Schematic of Air Traffic Emissions Forecast Module

Both the Air Traffic Emissions and Emissions Forecast Modules provide an optional link to the FATE software developed at the DLR Institute of Air Transport and Airport Research. This software is capable of calculating four-dimensional emission inventories, i.e. emission quantities in a three-dimensional grid around the Earth, supplemented by an additional time coordinate. Gridded emissions are typically used to evaluate aviation’s influence on climate. The flight movements data required by FATE can be created directly by the Air Traffic Emissions Module and the Emissions Forecast Module.

### 1.3 SUMMARY OF RESULTS

#### 1.3.1 OVERVIEW ON APPLICATION STUDIES

To demonstrate the capabilities of the newly developed tool chain, it was applied to calculate aviation’s fuel consumption and emissions from 2000 until 2030. Flight schedules from the Official Airline Guide (OAG) [100] covering the years 2000 and 2003-2010 were used for the simulation of air traffic. The forecast until 2030 is based on traffic growth rates from the Airbus Global Market Forecast [4]. Simulation models of future aircraft and engine types are used for fuel burn and emissions prediction.

Figure 5 shows the development of passenger-kilometres and tonne-kilometres for scheduled aviation. The diagram also includes fuel consumption and emissions of nitric oxides (NO<sub>x</sub>) obtained from the simulation. Forecast results shown in the figure refer to a baseline scenario using technology assumptions that are regarded as “most likely”. Selected variations from this scenario were also evaluated and are presented in chapter 4.4. By use of the newly developed tool chain, additional scenarios for future aviation can be evaluated at comparably low effort. Such analyses are planned for the near future.

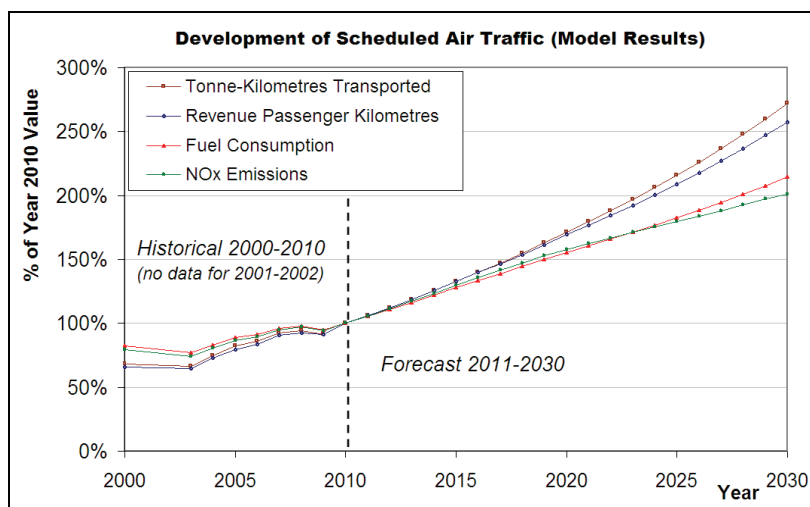


Figure 5: Development of transport performance, fuel burn and NO<sub>x</sub> emissions 2000-2030



### 1.3.2 EMISSIONS FROM AIR TRAFFIC 2000-2010

The Air Traffic Emissions Module was applied to calculate fuel burn and emissions for historical air traffic. Besides emissions of nitric oxides (NO<sub>x</sub>), the module considers emissions of carbon monoxide (CO), hydrocarbons (HC) and soot. Results are summarized in Table 1.

Year	RPK [10 <sup>12</sup> Pkm]	TKT [10 <sup>9</sup> tkm]	Fuel [10 <sup>9</sup> kg]	NO <sub>x</sub> [10 <sup>9</sup> kg]	CO [10 <sup>6</sup> kg]	HC [10 <sup>6</sup> kg]	Soot [10 <sup>6</sup> kg]
2000*	3.24	412	155	1.95	630	1073	6.78
2003**	3.20	399	145	1.83	554	804	5.62
2004**	3.60	451	156	1.99	582	795	5.83
2005**	3.92	495	168	2.14	600	804	6.01
2006	4.15	519	172	2.21	603	771	6.02
2007	4.48	557	181	2.34	615	740	6.08
2008	4.58	567	185	2.40	621	713	6.17
2009	4.53	549	178	2.33	583	622	5.75
2010	4.95	603	188	2.47	604	622	6.09

\* September 2000 schedules available only. Results have been scaled for the estimation of yearly values.  
 \*\* January and July schedules available for 2003-2005. Results have been scaled to estimate yearly values.

*Table 1: Transport performance and emissions of scheduled aviation*

The transport performance of scheduled aviation measured in revenue passenger-kilometres (RPK) has increased by 53% between 2000 and 2010. Tonne-kilometres transported (TKT), which include both passenger and freight transport, have increased by 46%. According to the model, fuel consumption has grown by 21% from 155 Mt to 188 Mt while NO<sub>x</sub> emissions have increased by 27%. HC emissions show a decreasing trend while emissions of CO and soot remain approximately constant. Soot emissions were estimated by use of a DLR-developed correlation method [33]. Only limited reference data is available to validate this method, particularly on air traffic system level. As yet, the accuracy of any calculations of soot emissions from global aviation must be regarded as low.

From 2000 to 2010, the relative growth in fuel consumption is lower than the increase in transport performance, which is caused by a more fuel efficient aircraft fleet and – to a smaller degree – by improved load factors and air traffic management. Using fuel burn per tonne-kilometres as a measure of fuel efficiency, efficiency has improved from 376 g/tkm to 313 g/tkm. This corresponds to a 17% improvement between 2000 and 2010. In the same timeframe, specific emissions of NO<sub>x</sub> have decreased by 13% from 4.74 g/tkm to 4.11 g/tkm.

Fuel consumption and emissions calculated in this study compare well to results from reference studies using similar methodologies (see Figure 6). This includes publications by NASA ([13], [14], [126]), DLR ([26], [118]), AERO-MS [95] and ANCAT [63], but also more recent calculations from AERO2k [53], the SAGE inventories ([55], [87]) and AEDT [133]. Differences between results from the aforementioned studies can be explained by different

coverage of global air traffic and by the applied emission models. The comparably large delta between fuel burn calculations from inventories of global aviation to statistics from the International Energy Agency (IEA) can be explained by real-world inefficiencies not considered in the simulations (e.g. wind and weather conditions, aircraft and engine deterioration) and by incomplete coverage of global flight movements particularly in the military sector.

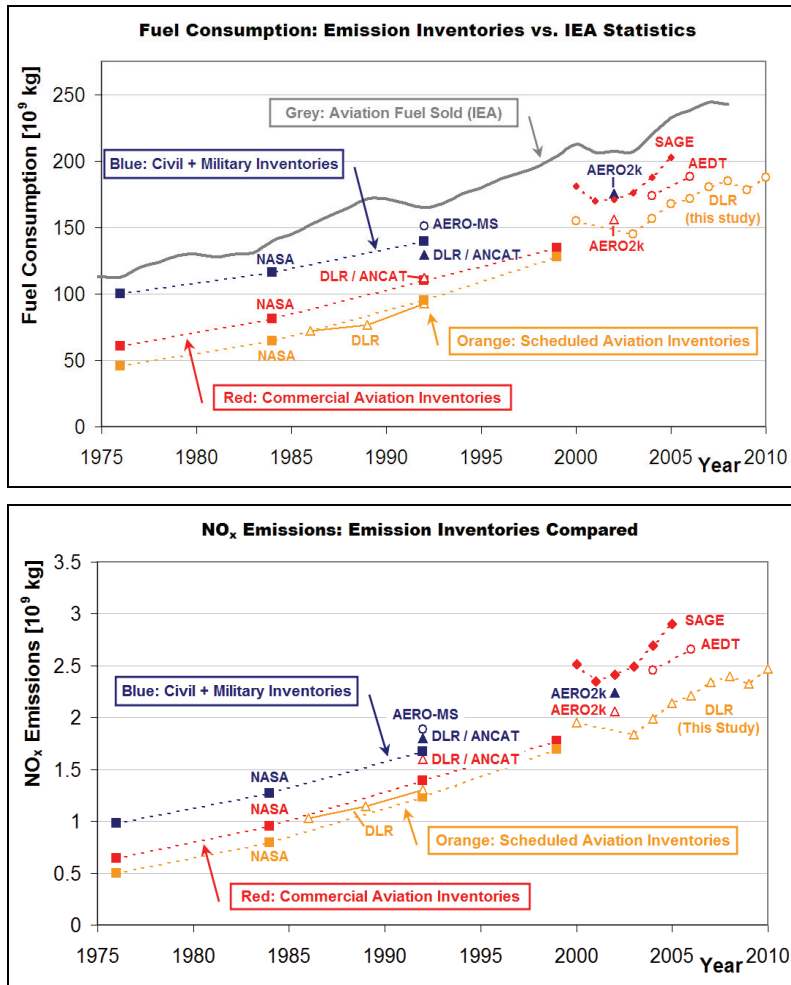


Figure 6: Comparison of fuel burn and NO<sub>x</sub> emissions calculations for global aviation

### 1.3.3 FORECAST OF EMISSIONS FROM AIR TRAFFIC 2011-2030

Using 2010 as a base year, the Air Traffic Emissions Forecast Module was applied to predict emissions from civil aviation until the year 2030. For this purpose, the model assumes regional traffic growth rates from the Airbus Global Market Forecast (GMF) [4]. A fleet rollover model accounts for the retirement of old aircraft and the introduction of new aircraft types. The Air Traffic Emissions Forecast Module covers transport performance, fuel burn and NO<sub>x</sub> emissions of scheduled aviation whereas emissions of CO, HC and soot are currently not forecasted. Table 2 summarizes the main results.

Year	Flights [10 <sup>6</sup> ]	Distance [10 <sup>9</sup> km]	RPK [10 <sup>12</sup> Pkm]	TKT [10 <sup>9</sup> tkm]	Fuel [10 <sup>9</sup> kg]	NO <sub>x</sub> [10 <sup>9</sup> kg]
2010	30.5	37.5	4.95	603	188	2.47
2015	38.1	47.7	6.59	801	241	3.20
2020	46.2	58.8	8.38	1032	293	3.89
2025	54.2	70.1	10.33	1301	344	4.43
2030	64.1	84.0	12.74	1640	405	4.96

Table 2: Forecast of flight movements, transport performance and emissions until 2030

Transport performance in terms of passenger-kilometres is expected to increase by 157% between 2010 and 2030, while transported tonne-kilometres will increase by 172%. Major changes in the worldwide fleet of aircraft include the introduction of new aircraft types, most notably the Boeing 787, 737 MAX, Airbus A350 XWB and A320 NEO aircraft. A successor (or major update) of the Boeing 777 aircraft family is also assumed in the baseline scenario, while older aircraft types are gradually phased out. Figure 7 shows the forecasted fleet of large passenger aircraft.

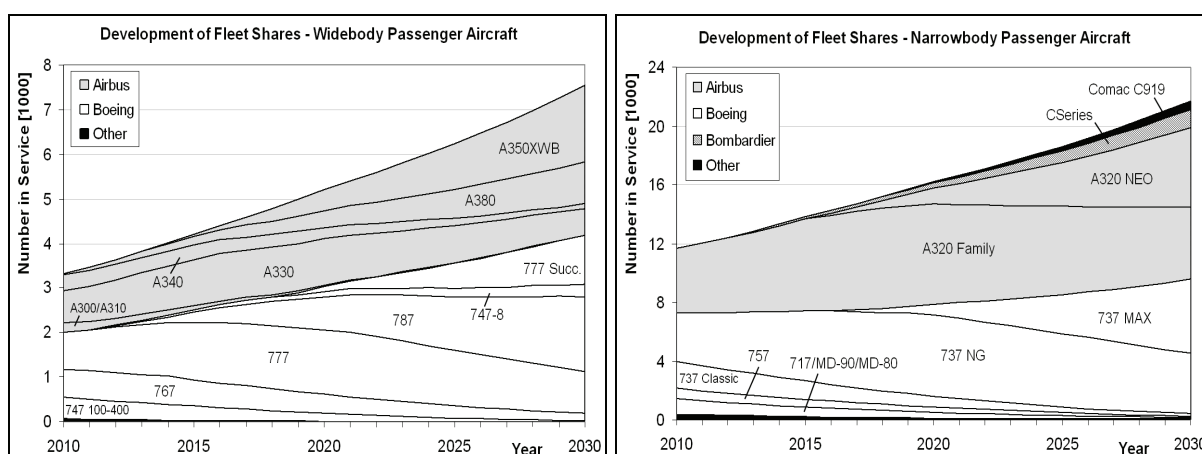


Figure 7: Forecasted fleet shares for large passenger aircraft

Simulation models of the most influential new aircraft and engine types have been created for this study and were applied for fuel burn and emissions prediction. According to these models, fuel consumption of scheduled aviation will grow from 188 Mt in 2010 to 405 Mt in 2030, which corresponds to a 115% increase. Fuel efficiency is forecasted to improve from 313 g/tkm to 247 g/tkm, a 21% improvement. NO<sub>x</sub> emissions will increase from 2.47 Mt to 4.96 Mt, which implies an improvement of specific NO<sub>x</sub> emissions by 27% from 4.1 g/tkm in 2010 to 3.0 g/tkm in 2030. The comparably high improvement of NO<sub>x</sub> emissions per tonne-kilometre is caused by a large-scale introduction of lean burn combustors for aircraft engines assumed for the timeframe 2015-2025. Given the uncertainty of many forecast assumptions (e.g. future traffic growth, development of the fleet and improvement of engine combustors), alternative scenarios have been evaluated and are discussed in the main part of this study.

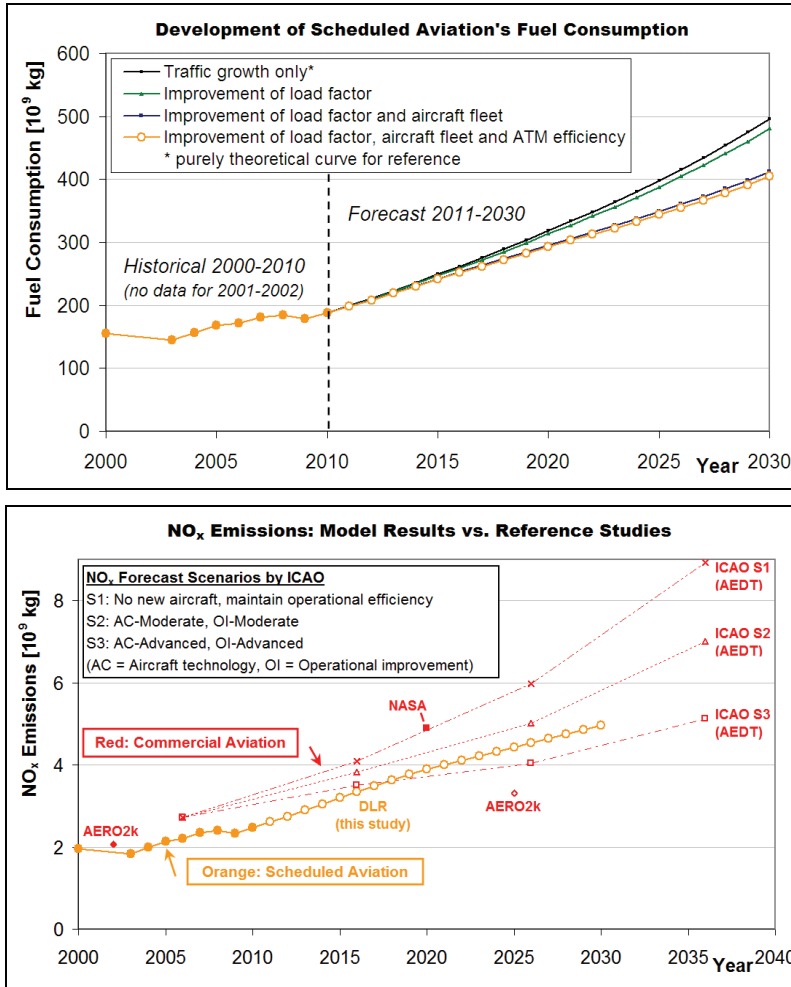


Figure 8: Forecasted fuel consumption and NO<sub>x</sub> emissions until 2030

The upper diagram in Figure 8 highlights the individual contributions to the improvement of fuel efficiency that are considered in the simulation. Between 2010 and 2030, fuel efficiency is predicted to improve by 1.18% per year on average. The aircraft fleet rollover has the largest contribution and is responsible for an annual efficiency improvement of 0.76% on average. Increasing load factors (0.16% p.a.) and ATM improvements (0.1% p.a.) also contribute to improved fuel efficiency. Another 0.15% annual improvement results from the above-average growth of the cargo sector and a trend towards longer distances per flight. The lower diagram in the above figure compares the NO<sub>x</sub> forecast from this study to reference studies from NASA [125], Aero2k [53] and ICAO CAEP [82]. Different base year emissions between the aforementioned studies are partly due to different coverage of global air traffic. The calculation method applied for the prediction of NO<sub>x</sub> emissions during cruise flight also affects the emissions in the base year. The NO<sub>x</sub> forecast from this study is in between the NASA and Aero2k predictions for 2020 and 2025 respectively. From 2020 onwards, the slope of the forecasted NO<sub>x</sub> increase is roughly comparable to the ICAO S2 scenario whereas in earlier years a higher slope similar to the ICAO S1 scenario is predicted.

## 2 ECOLOGICAL AND TECHNOLOGICAL BACKGROUND

### 2.1 DEVELOPMENT OF AIR TRAFFIC

Aviation creates economic and social benefits at the cost of adverse environmental impacts. Civil aviation facilitates tourism and trade in our globalized world. Aircraft and airline industries are major direct and indirect employers. In the past decades, growth rates of air traffic have shown a close link to the growth of the world gross domestic product (GDP). Negative effects of aviation include noise and gaseous emissions from aircraft, the use of limited resources like fossil fuels as well as land use for airport infrastructure. Besides noise and local air quality around airports, which have a negative influence on human health, the potential contribution of aviation to climate change has recently come into the public focus.

Since 1980, the transport performance of civil aviation measured in passenger-kilometres has increased by roughly 5% per year on average. This corresponds to a doubling of traffic volumes every 15 years. Annual growth rates in the cargo sector are even larger and in the order of 6%. Latest forecasts by Airbus and Boeing predict continuous traffic growth of similar magnitude in the foreseeable future<sup>1</sup>. It is the rapid growth of air traffic that gives rise to concerns, particularly regarding aviation's atmospheric impact. The consumption of fossil fuel is a major factor in this respect: Fuel burn is directly related to emissions of carbon dioxide (CO<sub>2</sub>) that are contributing to global warming. Figure 9 compares the development of passenger air traffic to the demand for aviation fuels compiled by the International Energy Agency (IEA) [84].

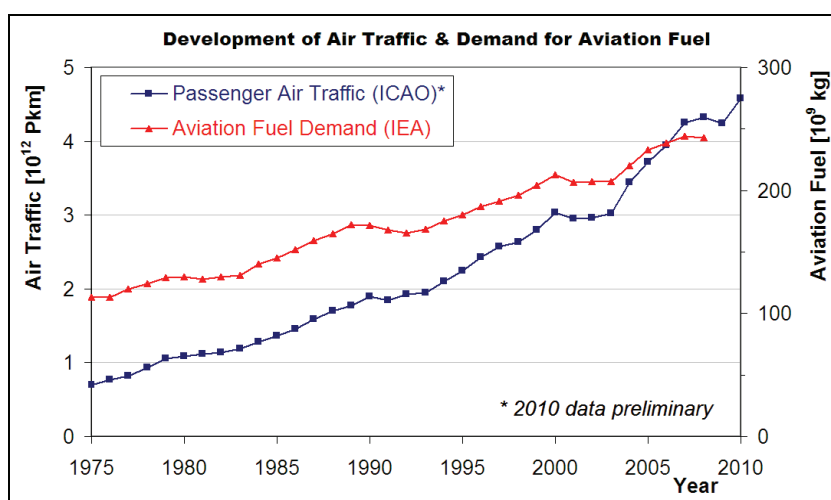


Figure 9: Development of air traffic and sold aviation fuel [74], [84]

<sup>1</sup> 4.8% average annual growth of passenger air traffic from 2011 to 2030 according to Airbus [4];

5.1% (passenger) / 5.6% (cargo) annual growth of air traffic from 2011 to 2030 according to Boeing [19]

As can be seen in Figure 9, the fuel use of aviation is increasing, yet at lower rates than the transport performance measured in passenger-kilometres<sup>2</sup>. This implies an improvement of fuel efficiency with time, which is attributable (to a large extent) to progress in aircraft and engine technology. So far, efficiency improvements cannot keep pace with the rapid growth of air transport. This development, which exemplifies the challenges of high-growth industries, cannot be considered sustainable from an ecological point of view.

Considering growth rates in the order of 5% per year, it is difficult to uncouple traffic growth and environmental effects. Aircraft fuel efficiency, for example, has improved by 50-70% since the 1960s, depending on metrics and reference point [104]. As technology has matured, further efficiency improvements are increasingly hard to achieve. Ambitious targets have been set by the aircraft industry, governments and airline associations in order to limit aviation's environmental effects in the future: Besides goals for aircraft noise and emissions of nitric oxides (NO<sub>x</sub>), the Advisory Council for Aeronautics Research in Europe (ACARE) aims at a 50% reduction of aircraft fuel burn between 2000 and 2020 [10]. This target, which must be regarded as challenging, requires substantial innovation in aircraft and engine technology along with a contribution from air traffic management. The more recent Flightpath 2050 [52] published by the European Commission aims at a 75% reduction of aircraft CO<sub>2</sub> emissions per passenger kilometre by 2050 compared to year 2000 levels. On the global level, the International Civil Aviation Organization (ICAO) agreed on a fuel efficiency improvement of 2% per year as a target through 2050 [75]. Similarly, the International Air Transport Association (IATA) targets a 1.5% annual improvement of fuel efficiency until 2020 and "carbon-neutral growth" from 2020 onwards [68]. Until 2050, IATA aims at reducing aviation's greenhouse gas emissions to 50% of the emissions from 2005 [68]. It is almost impossible to reach such ambitious targets by evolutionary improvements of aircraft and engine technology. Besides innovation in aircraft design, aircraft operations and air traffic management, the potential of biofuels regarding a reduction of life-cycle CO<sub>2</sub> emissions as well as carbon offset mechanisms (i.e. emissions trading with other sectors) are to be taken into account if the objectives are to be met [68].

Besides emissions of CO<sub>2</sub>, other gaseous and particulate emissions that result from the combustion of fuel in aircraft engines influence atmospheric physics and local air quality. This includes emissions of nitric oxides (NO<sub>x</sub>), carbon monoxide (CO), unburned hydrocarbons (HC) and soot particles. Given the focus of this study on global aviation emissions, the atmospheric impact of such emissions will be described shortly in the following chapter. Measures to reduce aviation emissions will be covered in chapter 2.3.

---

<sup>2</sup> IEA data in Figure 9 refer to fuels for civil and military aviation; civil aviation is the largest consumer [84].

## 2.2 CLIMATE IMPACT OF AVIATION EMISSIONS

Gaseous and particulate emissions from aviation result from the combustion of fuel in aircraft engines. Kerosene-based fuels like JET A-1 are used by jets and turboprops, which account for the majority of all large transport aircraft. The main combustion products of such hydrocarbon fuels are carbon dioxide (CO<sub>2</sub>) and water vapour (H<sub>2</sub>O). Emissions of CO<sub>2</sub> and H<sub>2</sub>O are proportional to fuel burn: The combustion of 1 kg of JET A-1 with air results in emissions of 3.156 kg of CO<sub>2</sub> and 1.237 kg of H<sub>2</sub>O [108]<sup>3</sup>.

As the combustion of fuel in aircraft engines is not an ideal process, products of non-ideal combustion are also found in the exhaust. This includes nitric oxide (NO) and nitrogen dioxide (NO<sub>2</sub>), together called nitric oxides (NO<sub>x</sub>). Carbon monoxide (CO) and unburned hydrocarbons (H<sub>x</sub>C<sub>y</sub> – mostly referred to as HC) are also emitted. The emission rates of these products from non-ideal combustion depend on engine and combustor technology, ambient conditions and the operating point of the engine: Emissions of nitric oxides (NO<sub>x</sub>) are influenced by pressure and temperature in the combustor and are mostly produced at high engine power settings [67]. Emissions of CO and HC, on the contrary, are mainly emitted at low power settings, when fuel/air mixing processes are rather inefficient [67]. Unlike NO<sub>x</sub>, emissions of CO and HC are of minor importance with respect to aviation's climate impact.

Furthermore, emissions from aircraft engines include sulphur oxides (SO<sub>x</sub>) due to the sulphur content in the fuel. Particulate emissions include soot, often referred to as black carbon. Soot from aircraft engines consists of 10<sup>14</sup> to 10<sup>15</sup> carbonaceous particles per kg of burnt fuel which have a diameter of 10-30nm and which may quickly form larger aggregates [120]. Besides, volatile aerosols are also emitted by aircraft engines or formed within milliseconds in the exhaust plume [120]. Figure 10 gives an overview on the combustion process and visualizes the approximate shares of different emissions in cruise flight.

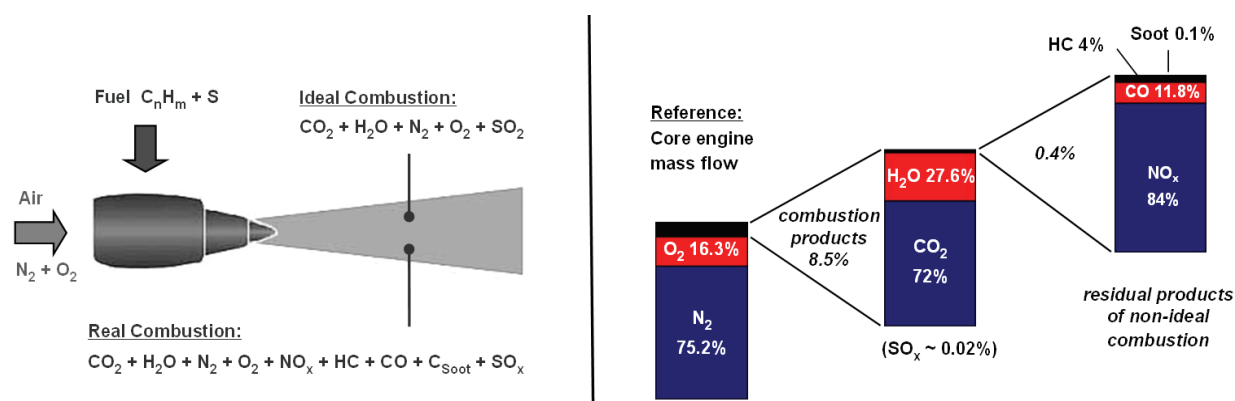


Figure 10: Combustion process (left) and typical share of emissions in cruise (right) [67]

<sup>3</sup> See chapter 3.2.4 for more details about emissions quantification.



Together with anthropogenic emissions from other sources, air traffic emissions influence the energy balance of the earth-atmosphere system. The regional distribution of aviation's fuel burn (and hence CO<sub>2</sub> and H<sub>2</sub>O emissions) is shown in Figure 11. Air traffic is predominantly performed in the northern hemisphere between 30° and 60° northern latitude. Unlike emissions from ground-based sources, aviation emissions occur to a large extent around the tropopause level, where ambient conditions, background concentrations and residence times e.g. of NO<sub>x</sub> are different from ground conditions.

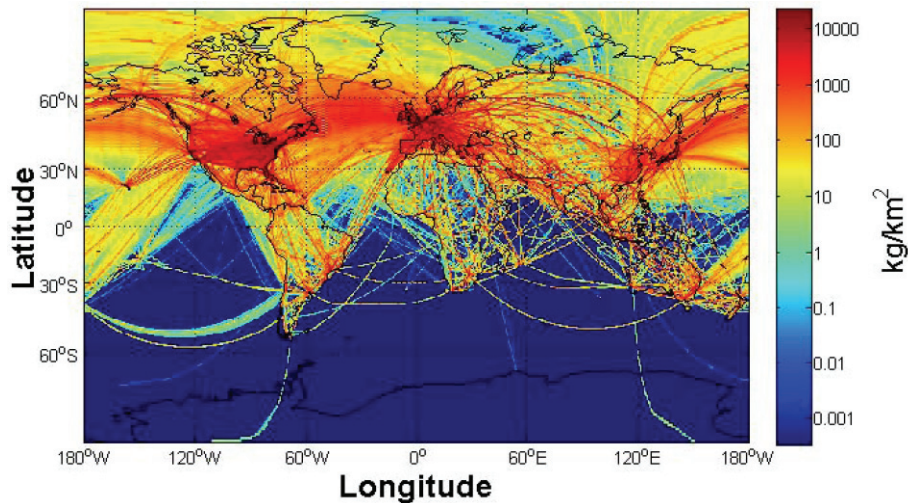


Figure 11: Global distribution of fuel burn from civil aviation [133]

The atmospheric effects of aviation emissions that influence climate can be grouped into three categories [67]:

- Direct emissions of greenhouse gases (CO<sub>2</sub> and H<sub>2</sub>O).
- Emissions that contribute to the formation of greenhouse gases (NO<sub>x</sub>).
- Emissions that influence the formation of contrails and clouds (e.g. soot particles).

CO<sub>2</sub> is a greenhouse gas with an atmospheric residence time in the order of 100 years [67]. Consequently, CO<sub>2</sub> emissions from various sources get widely distributed by atmospheric exchange processes. Aviation is responsible for around 2.5% of the yearly CO<sub>2</sub> emissions from fossil fuel consumption, which corresponds to 12% of the CO<sub>2</sub> emitted by the transportation sector [89]. Water vapour is also a greenhouse gas. Besides its radiative effect of small magnitude, aviation-induced H<sub>2</sub>O is influencing contrail formation [121].

NO<sub>x</sub> emissions from aircraft engines influence atmospheric ozone (O<sub>3</sub>) and methane (CH<sub>4</sub>) concentrations via chemical reactions and transport processes [67]. Aviation emissions alter the concentration of NO<sub>x</sub> at cruise altitude and have a significant influence on atmospheric chemistry. The production rate of tropospheric O<sub>3</sub> was found to be enhanced by NO<sub>x</sub> [67]. This leads to a warming effect, as O<sub>3</sub> around the tropopause level acts as a greenhouse gas.



Besides increasing tropospheric O<sub>3</sub>, which has a lifetime of months, NO<sub>x</sub> causes a decrease of CH<sub>4</sub>. CH<sub>4</sub> is a greenhouse gas with a lifetime of approximately 10 years. The CH<sub>4</sub> reduction has a cooling effect and reduces aviation's contribution to global warming [120].

Soot and sulphate particles emitted by aircraft engines alter the aerosol concentration in the upper troposphere. The radiative effect of these aerosols is rather small, but they may influence the formation of condensation trails (contrails) and cirrus clouds [121]. Contrails form at low ambient temperature, when the warm and moist engine exhaust mixes with cold air and saturation with respect to water is reached in the plume. They result from condensation and freezing of water vapour on aerosol particles [121]. Contrails are typically linearly shaped and short-lived, but may sometimes persist for hours or longer, depending on ambient conditions. In addition to their influence on contrails, particles emitted by aircraft may later act as condensation nuclei for cirrus clouds [121]. Scientists assume an influence of aircraft emissions on cloud properties including frequency of formation [121].

Greenhouse gases like CO<sub>2</sub>, O<sub>3</sub>, CH<sub>4</sub> and H<sub>2</sub>O influence the Earth's mean surface temperature by absorbing and reemitting outgoing radiation. Clouds affect both energy and water budgets of the Earth. A cloud cover absorbs and reflects solar radiation back to the ground and infrared radiation back to space. Integrated over day and night, both contrails and cirrus clouds have a warming effect [89]. In order to quantify and compare various anthropogenic impacts on climate, radiative forcing may be used as a metric. Radiative forcing (RF) is a measure of the perturbation of the Earth's energy budget since preindustrialized times. RF results for example from changes in atmospheric gas or particle concentrations and is measured in units of watts per square metre at the top of the atmosphere [89]. Positive RF causes a warming of the planet while negative values indicate a cooling effect. An approximately linear relationship can be assumed between a change in RF and the corresponding change of the equilibrium mean surface temperature [67].

By means of climate models, the RF of global aviation can be estimated [67], [112], [89]. Figure 12 presents the radiative forcing components from aviation and classifies the level of scientific understanding (LOSU) for the individual effects. The total RF from aviation until 2005 is currently estimated as 0.055 W/m<sup>2</sup> [89]. Main contributors are CO<sub>2</sub>, the impact of NO<sub>x</sub> on O<sub>3</sub> and CH<sub>4</sub> as well as linear contrails. Not included in the total are the potential effects of aviation emissions on cirrus cloudiness, as the level of scientific understanding in this respect must still be regarded as very low. Until 2005, aviation is responsible for about 3.5% of the total anthropogenic RF. When including current estimates for aviation-induced cirrus clouds, this share would even rise to 4.9% [89]. Until 2050, RF from aviation is expected to increase by a factor of 3-4, depending on traffic growth and technological progress. This also implies an increasing share of aviation amongst the total anthropogenic RF, which may reach 4-4.7% (without cirrus cloud effects) by 2050 [89].

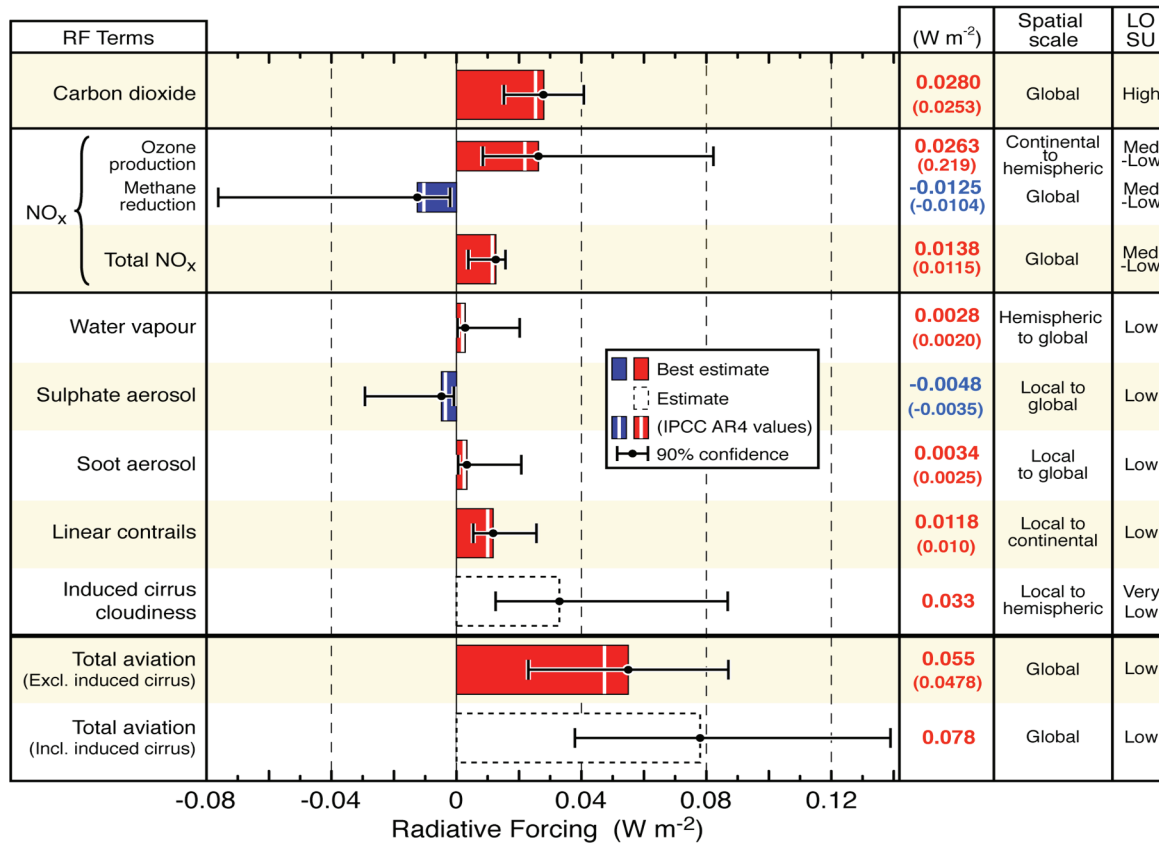


Figure 12: Aviation radiative forcing components in 2005 [89]

Global warming must be regarded as a risk for human society and the Earth’s ecosystem. The economic impact of rising surface temperatures, rising sea levels or glacial retreat is difficult to assess and even more difficult to quantify. The extensive Stern Review on the Economics of Climate Change (2006) produced for the British government estimates a loss of 5-20% of the global GDP if current emission trends continue [123]. The report also suggests that spending 1% of the world’s GDP annually on emissions reduction would avoid the most serious damage.

Given current limitations with respect to the scientific understanding of climate change and its economic effects, the quantitative results of the Stern Review must be treated with caution. Nevertheless, a considerable economic impact of global warming seems plausible. As a consequence, it is desirable to limit the anthropogenic influence on climate by reducing anthropogenic emissions. Technological measures can be taken in order to reduce emissions from aviation. These measures will be described shortly in the following section.

## 2.3 TECHNOLOGY MEASURES TO LIMIT AVIATION EMISSIONS

### 2.3.1 IMPROVING AIRCRAFT FUEL EFFICIENCY

Aircraft fuel efficiency has improved by roughly 50-70% since the beginning of the jet age, depending on chosen metrics and reference aircraft [104]. Figure 13 shows the development of aircraft fuel burn per available seat kilometre (ASK) from the 1960s until today. More than half of the improvement can be attributed to progress in the field of propulsion systems [67]. As aircraft and engine technology have matured, further progress is increasingly hard to achieve. The following key drivers for improved aircraft fuel efficiency can be identified:

- Improvements in aerodynamics (i.e. increasing the lift-to-drag ratio).
- Improvements in engine efficiency (i.e. reducing thrust-specific fuel consumption).
- Progress in lightweight construction (i.e. reducing aircraft mass).

Compared to state-of-the-art aircraft, evolutionary improvements in aerodynamics like advanced wingtip devices and wing design methods have only a limited potential to improve the lift-to-drag ratio of future aircraft. Methods for laminar flow control are currently in development and may result in more drastic reductions of friction and form drag components. From 2020 onwards, laminar flow control could be applied in new aircraft designs and is expected to deliver fuel efficiency benefits in the order of 5-15% [71]. For the more distant future, non-conventional configurations like blended wing bodies are on the roadmaps of aircraft manufacturers. Such concepts integrate fuselage and wings resulting in better aerodynamic properties than for conventional aircraft configurations. However, these concepts have disadvantages, e.g. with respect to pressurization and passenger comfort, which make it difficult to predict whether and when such aircraft will be used in civil aviation.

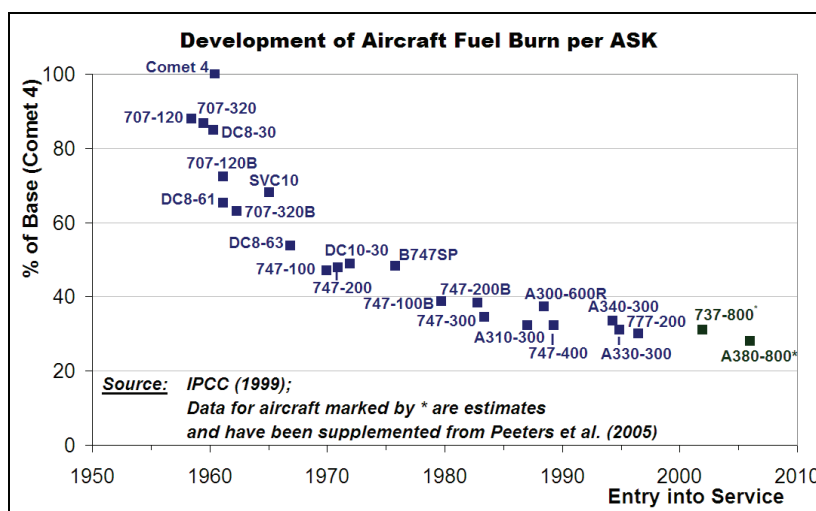


Figure 13: Development of aircraft fuel efficiency [67], [104]

On the engine side, thrust-specific fuel consumption (TSFC) is mainly dependent on an engine's thermal and propulsive efficiencies. Most modern turbofan engines have higher overall pressure ratios (OPR) and combustor exit temperatures than their predecessors, which translates into improved thermal efficiency. In addition, the increased bypass-ratios (BPR) of recent turbofans enable a larger propulsive efficiency than reached by earlier designs. The trends towards higher OPRs, temperatures and BPRs are expected to continue in the future. Besides advanced turbofans with ultra-high BPRs, geared-turbofan and open rotor concepts are currently in the focus of the engine industry. A geared turbofan enables higher BPRs by decoupling the rotational speeds of fan and low pressure turbine. Pratt & Whitney claim a fuel burn advantage in the order of 15% for its PW1000G geared turbofan engine compared to its predecessors [98]. The PW1000G will be used on the Bombardier CSeries and the Airbus A320 NEO aircraft that are planned to be introduced in 2013 and 2016 respectively. Open rotor or propfan engines may enable even lower TSFCs at the cost of reduced flight speed and increased noise emissions: a 20% fuel burn advantage compared to current turbofans can be expected [71]. Considering the challenges particularly with respect to noise and aircraft-engine integration, it is questionable if open rotor engines will be used for the next generation of short and medium range aircraft in the 2020s.

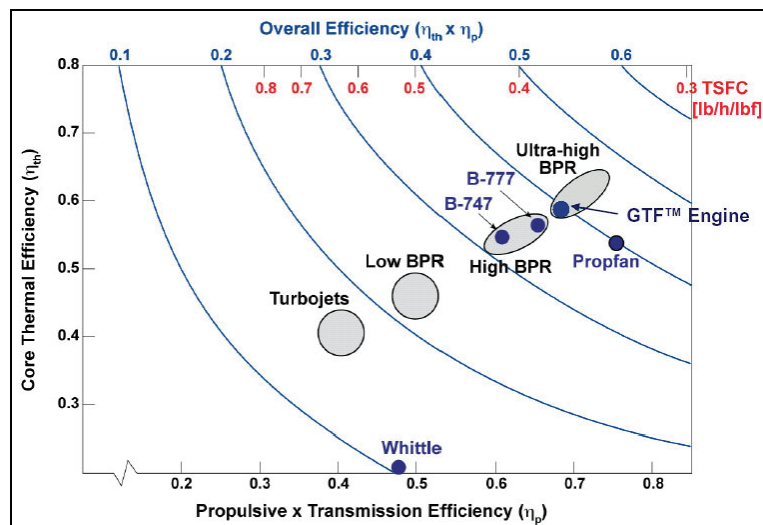


Figure 14: The link of TSFC to thermal and propulsive efficiency [39]

Besides lift-to-drag ratio and engine TSFC, the mass of an aircraft has a considerable influence on its fuel efficiency. Light-weight composite materials are increasingly used for modern aircraft, supplemented by advanced aluminium alloys and titanium. Major parts of the Boeing 787 and Airbus A350 XWB aircraft that are due to enter service in 2011 and 2013 are made from composites. The 787 consists of 50% composites, 20% aluminium, 15% titanium and 15% other materials (by mass) [128]. While weight has a direct influence on fuel burn, light and heat-resistant materials as well as advanced manufacturing processes enable further improvements in engine technology and aerodynamics.

Time Horizon	Technology	TRL*	Fuel Reduction Benefit	Combined Benefit**
New Aircraft before 2020	New engine systems architecture	5	15-20%	25-35%
	Hybrid laminar flow	6	10-15%	
	Natural laminar flow	6	5-10%	
New Aircraft 2020-2030	Variable cycle engine (2 <sup>nd</sup> GEN)	4	10-20%	25-50%
	Hybrid-wing-body	4	10-25%	
	Truss-braced wing	2	10-15%	
	Fuel cell system	5	1-5%	
<p>* Technology Readiness Level ranging from 1 (basic principles observed and reported) to 9 (system flight proven).  ** The technologies are not independent; the combined effect may be smaller than the sum of individual effects.</p>				

*Table 3: Potential measures for improving aircraft fuel efficiency [71]*

The Boeing 787 and Airbus A350 XWB long-range aircraft that will be introduced in the near future are claimed to be 15-25% more fuel-efficient than their predecessors [9]. Given numerous interrelations and trade-offs between aerodynamics, engine TSFC and aircraft weight, it is difficult to predict the combined effect of new technologies for the more distant future. Engines with ultra-high BPR, for example, have large dimensions, resulting in drawbacks with respect to drag and weight. Active laminar flow control systems also add weight to the aircraft and require additional power. Better fuel efficiency, on the other hand, leads to smaller fuel amounts that are to be carried, which may finally reduce aircraft weight. The aircraft gross weight (including fuel and payload) influences lift and thrust requirements. Such trade-offs and “snow-ball effects” are to be considered during aircraft design and make it difficult to forecast future fuel efficiency. Table 3 summarizes results from a recent IATA study, which predicts a potential efficiency improvement in the order of 25-35% for a hypothetical short-range aircraft introduced before 2020. Until 2030, an efficiency improvement of 25-50% compared to current aircraft is forecasted in the report [71].

### 2.3.2 REDUCING ENGINE NO<sub>x</sub> EMISSIONS

While emissions of CO<sub>2</sub> are proportional to fuel burn, emissions of nitric oxides (NO<sub>x</sub>) depend on engine and combustor technology, the actual power setting of the engine and ambient conditions. NO<sub>x</sub> emissions are mainly produced at high power settings, e.g. during the take-off, climb and cruise flight segments. The emission index (EI) for NO<sub>x</sub>, i.e. the mass of NO<sub>x</sub> emitted per kg fuel, is influenced by both the combustion temperature and pressure as well as by the residence time of the fuel/air mixture in the peak temperature regions of the combustor. The higher these influencing factors, the higher the resulting EI NO<sub>x</sub> [67]. The peak temperatures in the combustor depend on combustor air inlet temperature and pressure and on the local fuel to air mass ratio [67]. As high combustor temperatures and pressures are favourable to minimize fuel consumption, advanced combustor technology is required in order to keep NO<sub>x</sub> emissions under control.

In Annex 16 to the Convention on International Civil Aviation [73] the ICAO defines emission standards for large jet engines which include limits for NO<sub>x</sub>. These standards are set by the ICAO Committee on Aviation Environmental Protection (CAEP) and were originally created to reduce adverse effects of aircraft emissions on air quality around airports. The regulations refer to a generic landing and take-off (LTO) cycle, for which limits regarding the emissions (D<sub>p</sub>) of an engine per kilo-Newton take-off thrust (F<sub>00</sub>) are defined. The limits for NO<sub>x</sub> have been strengthened several times and depend on an engine's overall pressure ratio (π<sub>00</sub>) at take-off conditions. Figure 15 shows the latest emission standards and also the mid-term and long-term technology goals defined by a group of independent experts for the years 2016 and 2026 [109]. Today, the CAEP/6 standard is to be met by newly certified aircraft engines while the CAEP/2 requirement still defines the limit for in-production engines. A production cut-off for engines not compliant to CAEP/6 was agreed for the year 2013. In 2014, the more stringent CAEP/8 regulation for newly certified engines will come into effect [81].

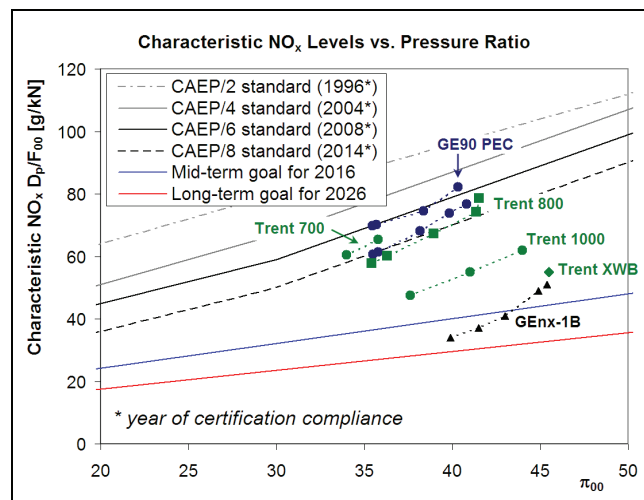


Figure 15: NO<sub>x</sub> emission standards and NO<sub>x</sub> levels for selected engine families [78], [110]

Advanced combustor technology enables a reduction of LTO and cruise  $\text{NO}_x$  emissions, while minimizing trade-offs e.g. with respect to flame stability, fuel burn or CO/HC emissions. Most modern aero engines use the Rich-Burn / Quick-Mix / Lean-Burn (RQL) concept for reasons of stability and performance (see left hand side of Figure 16). The RQL concept can also be used to limit  $\text{NO}_x$  production. As peak flame temperatures and peak  $\text{NO}_x$  formation rates are reached at the stoichiometric fuel to air ratio, the RQL concept aims at minimizing the residence time at stoichiometric conditions by means of fast fuel/air mixing [109]. The Rolls-Royce Trent 1000 engines for the Boeing 787 use an advanced RQL combustor with improved characteristics regarding  $\text{NO}_x$  emissions compared e.g. to Trent 700 engines used on the Airbus A330. Evolutionary improvement of the RQL concept can be expected in the future, enabled by progress in computational fluid dynamics and modelling capabilities. It is regarded as likely that RQL combustors will meet the mid-term goal for  $\text{NO}_x$  emissions that is shown in Figure 15 [109].

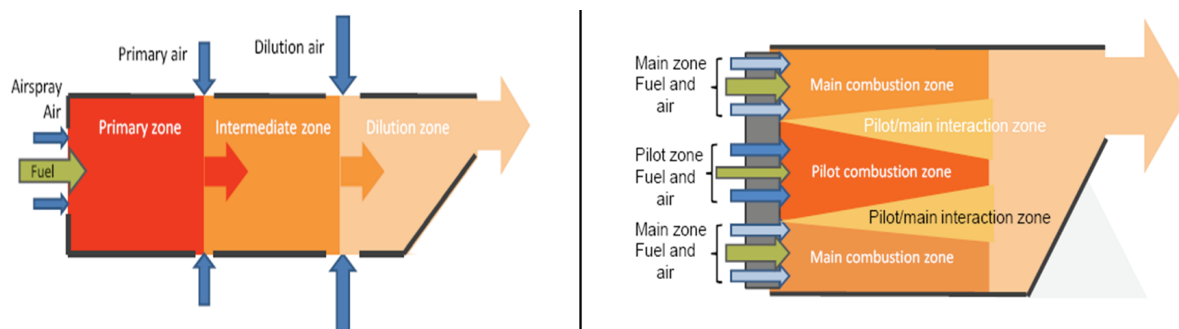


Figure 16: Schematic of RQL (left) and LDI (right) combustor concepts [110]

A more drastic reduction of  $\text{NO}_x$  emissions becomes feasible by using lean burn direct injection (LDI) concepts (see right hand side of Figure 16). Such combustors combine the advantages of a lean burn main zone with those of a parallel rich zone. Most fuel is injected into the main zone where stoichiometric peak flame temperatures are never reached [109]. This results in comparably low  $\text{NO}_x$  formation rates. The rich zone (also referred to as pilot zone) ensures optimum low power performance and stability. This zone is fuelled over the entire range of operating conditions while the main zone is active at intermediate and high power settings only. Although the pilot zone degrades the overall  $\text{NO}_x$  characteristics of the engine, the concept has a higher potential for  $\text{NO}_x$  reduction than the RQL process [109]. The General Electric GEnx-1B engine for the Boeing 787 is the first certified engine that applies this concept in its TAPS (Twin Annular Premixing Swirler) combustor. As can be seen in Figure 15, the GEnx-1B family already meets the mid-term technology goal for the year 2016 except for the highest thrust versions. The next generation of LDI combustors is expected to meet the long-term technology goal set by the group of independent experts for the year 2026 [110].



About 90% of all NO<sub>x</sub> emissions from aviation are produced during cruise flight [110]. However, no regulation exists for cruise NO<sub>x</sub> levels of aero engines. For aircraft with RQL combustors, emissions during cruise flight are known to be broadly correlated to emissions in the LTO cycle [109]. It is questionable if the correlation still holds for LDI combustor concepts. Initial evidence presented by General Electric suggests that cruise NO<sub>x</sub> emissions of the company's TAPS combustor are substantially lower compared to a RQL reference design. The NO<sub>x</sub> reduction in cruise flight is claimed to be higher than the benefits in the LTO cycle [110]. As long as no quantitative data on cruise NO<sub>x</sub> emissions from LDI combustors are available, it is difficult to predict their emissions on flight mission level. To a large extent, potential benefits during cruise flight depend on the exact transition point from the combined pilot and main zone operating mode to pilot mode (see Figure 17).

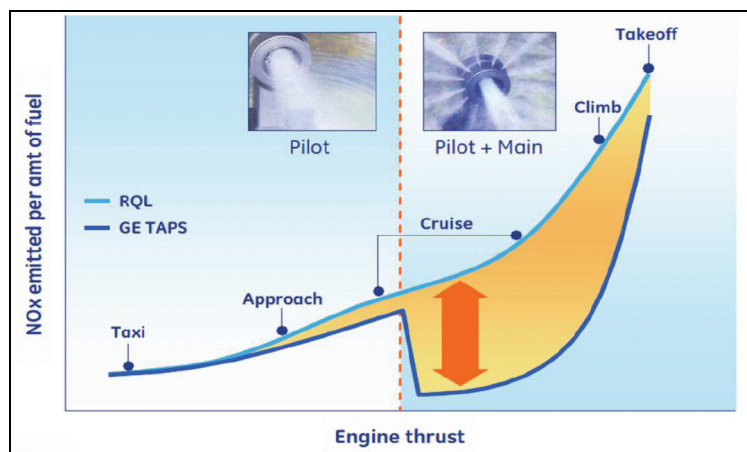


Figure 17: Fuel staging in TAPS combustor [88]



### 2.3.3 OPTIMIZING AIR TRAFFIC MANAGEMENT AND AIRCRAFT OPERATIONS

Besides aircraft and engine technology, constraints resulting from Air Traffic Management (ATM) have a negative influence on air transport emissions. An assessment performed by the Civil Air Navigation Services Organisation (CANSO) found an ATM system efficiency of 92-94% for the year 2005. In the terminology of the assessment this implies a fuel burn penalty of 6-8% on global average [27]. This inefficiency can be broken down into various airborne components (en-route inefficiency from increased flight distances, vertical flight inefficiency from altitude constraints and holdings) and a ground-based component from increased taxi times. Evaluations performed by air traffic service providers from Europe, the US and Australia indicate a fuel burn penalty originating from ground operations in the order of 0.9%-1.4% and a much larger airborne contribution of 5.5%-7.9% [27]. A number of initiatives are under way in order to raise ATM efficiency despite growing traffic volumes. Major projects include the Single European Sky ATM Research (SESAR) and the US Next Generation Air Transportation System (NextGen) programmes. On the global level, CANSO agreed on efficiency goals of 93-95% for 2020 and 95-98% for 2050 [27].

Additional potential to increase the fuel efficiency on air traffic system level lies in aircraft operations. This includes improvements of passenger and cargo load factors, but also optimization in flight planning. According to ICAO statistics, average seat load factors are close to 80% in recent years [77]. As a consequence, potential for improvement exists, but must be regarded as limited. Flight planning includes aspects like choosing optimum trajectories and flight speeds – a topic which is closely linked to ATM. Improved weather forecasts and advanced communication, navigation and surveillance (CNS) equipment will enable improvements in this field. It should be noted that airlines often trade some fuel efficiency against lower flight times to minimize total operating costs and ensure punctuality in their network. The associated fuel burn penalty, however, can be regarded as low [94].

Current research on climate optimized flight planning takes a more integrated approach that is not limited to reducing fuel consumption. Persistent contrails produced by aircraft, amongst other effects, are believed to contribute to global warming. The effects of contrails depend on their location in terms of region and altitude, the season and the time of day. The warming effect of contrails is particularly strong in the winter months and at night time [94]. Contrail formation could be reduced if flights through ice-supersaturated regions were avoided. In many cases slight changes of flight altitudes in the order of 2000 feet were found to be sufficient in order to leave such regions [94]. Changes in altitude, on the other hand, result in a fuel burn penalty. The trade-offs between a short-term benefit from contrail avoidance and longer-term effects of fuel burn, CO<sub>2</sub> and NO<sub>x</sub> emissions need to be understood before climate optimized flight planning becomes feasible. Besides, ATM constraints and airspace capacity need to be taken into account if such strategies are put into practise.

### 2.3.4 ALTERNATIVE FUELS

Alternative fuels are in the focus of the airline industry, mainly due to the potential of biofuels for reducing CO<sub>2</sub> emissions. Besides, alternatives to conventional jet fuel will be required in the longer term in order to reduce aviation's dependency on fossil resources. Considering the short and medium-term options, jet fuel produced from biomass by the Fischer-Tropsch process (F-T) and from hydroprocessed esters and fatty acids (HEFA) are regarded as the most promising options [70]. Both F-T and HEFA fuels are able to meet the certification requirements for use in aviation, can be blended in conventional fuel and typically require no modifications on the aircraft and engine sides. Using biofuels, a reduction of fuel consumption by about 2% can be expected due to their higher energy content per kg fuel<sup>4</sup>. Furthermore, biofuels have a considerable potential for reducing greenhouse gas emissions from a life-cycle perspective, as CO<sub>2</sub> is absorbed while the feedstock is grown.

According to an assessment funded by the Federal Aviation Administration (FAA) [124], life-cycle greenhouse gas (GHG<sup>5</sup>) emissions from biofuels differ widely. Significant benefits in terms of reduced life-cycle emissions are possible, but depend on feedstock and production process. Effects on GHG emissions resulting from land-use change also need to be considered and are surrounded by high uncertainty [124]. F-T fuels produced from biomass were found to deliver GHG reductions in the order of 80-90%, but have a limited production potential at comparably high costs. A considerable GHG reduction of 40-70% is attributed to HEFA fuels produced from jatropha, salicornia or excess rapeseed, soy or palm [124]. On the other hand, large-scale use of such fuels is questionable due to limited availability of cropland and low fuel yield per hectare [124]. The most favourable production potential can be attributed to HEFA fuel produced from algae. However, the GHG reduction of such fuel was estimated as only 42% compared to conventional jet fuel in a baseline scenario, however at high variability depending on details of feedstock recovery [124].

The compatibility of F-T and HEFA fuels with aircraft engines has been demonstrated in a number of military and civil flights. 50% blends of F-T and HEFA fuels in conventional jet fuel have been approved under the American ASTM D7566 standard. Market shares of biofuels in the order of 5-30% for 2030 and up to 100% for 2050 are currently discussed in the aviation community [12], [40]. These numbers appear ambitious in the light of less optimistic forecasts from other institutions. In their BLUE Map scenario, for example, the International Energy Agency predicts a biofuel availability of 200 billion litres in 2050, which corresponds to roughly 30% of the prospective demand of civil aviation [83].

---

<sup>4</sup> For a flight with 100% biofuel, assuming 44.1 MJ/kg for biofuel compared to 43.2 MJ/kg for JET A-1 [66].

A 0.3% reduced energy demand can be assumed on average, as the flight's take-off weight is reduced [66].

<sup>5</sup> Results refer to GHG emissions per unit of energy. The study considers emissions of CO<sub>2</sub>, CH<sub>4</sub> and N<sub>2</sub>O [124].

## 2.4 APPROACH AND FOCUS OF THIS STUDY

A simulation tool has been developed for this study which quantifies fuel consumption and emissions of civil aviation. Based on publicly available data, the model considers current and future air traffic using a bottom-up approach<sup>6</sup>. This report contains a detailed description of the tool and presents initial results from model application. Developed at the DLR Institute of Propulsion Technology, the tool enables a more comprehensive consideration of environmental aspects when evaluating concepts for future aircraft and aircraft engines. It can be regarded as an automated chain of different software covering engine performance and emissions, aircraft flight simulation, current air traffic movements and respective forecast scenarios. A schematic of the tool chain is shown in Figure 18.

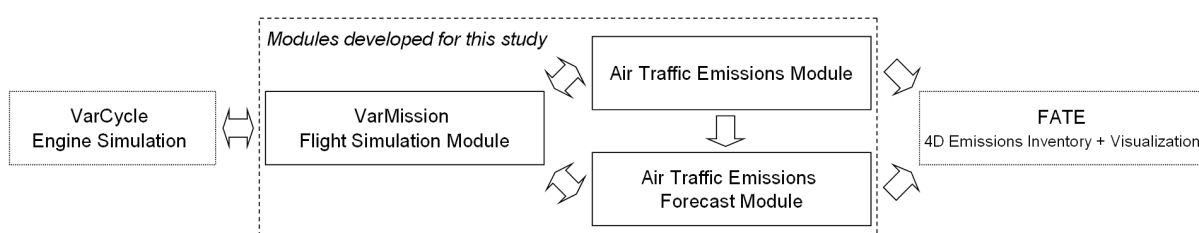


Figure 18: Schematic of tool chain applied in this study

The VarCycle software, the first tool in the chain, is designed to simulate an engine's performance and emissions at different operating conditions. The well-established and validated tool can be linked to a newly developed aircraft performance module named VarMission. Using aircraft data from various sources, VarMission simulates flight missions and calculates fuel burn and emissions along a flight profile. The Air Traffic Emissions Module analyses each flight in a database of worldwide flight movements. It is linked to VarMission, which performs the required fuel burn and emission calculations. Using base year flight movements along with assumptions about traffic growth and aircraft lifetimes, the Air Traffic Emissions Forecast Module predicts future fleet composition as well as future fuel burn and emissions. Models of future aircraft-engine combinations simulated by VarMission and VarCycle can be used. Besides new aircraft and engine technology, efficiency improvements originating from Air Traffic Management and aircraft operations are considered for the forecast. Both the Air Traffic Emissions Module and the Emissions Forecast Module can be linked to the FATE software developed at the DLR Institute of Air Transport and Airport Research. Using this software, the temporal, horizontal and vertical distribution of air traffic emissions can be evaluated in detail. The three core modules developed for this study will be described in chapter 3 of this report.

<sup>6</sup> When creating emission inventories for aviation, a bottom-up approach starts at a database of flight movements. Emissions for each flight are calculated and summed up in order to determine the total emissions amount.

In order to demonstrate the functionality of the Air Traffic Emissions Module, it was applied to determine gaseous and particulate emissions from scheduled aviation for the years 2000 to 2010. The evaluation is based on worldwide flight schedules from the Official Airline Guide (OAG) [100]. Besides global fuel consumption, which is proportional to emissions of carbon dioxide (CO<sub>2</sub>) and water vapour (H<sub>2</sub>O), emissions of nitric oxides (NO<sub>x</sub>), carbon monoxide (CO), hydrocarbons (HC) and black carbon (soot) are calculated for historical aviation. A discussion of results is found in chapter 4.2. In addition, four-dimensional inventories covering air traffic emissions from 2000 until 2010 have been created from the above results by use of the FATE software. The inventories may be used for further analyses of air traffic's climate impact which are beyond the scope of this study.

In a second step of the assessment, the Air Traffic Emissions Forecast Module was applied to predict aviation's fuel consumption and emissions of NO<sub>x</sub> until the year 2030. Regional traffic growth rates from the Airbus global market forecast [4] were used as input data to the model. Furthermore, assumptions about new aircraft and engine types have been made in order to simulate future air traffic. The VarCycle engine simulation was applied to predict performance and NO<sub>x</sub> emissions of future engines types. Characteristics of future aircraft have been estimated and respective VarMission models have been created. Besides, further stringency of regulatory standards for engine NO<sub>x</sub> emissions according to current technology goals is assumed. Emissions of CO, HC and soot are not covered by the forecast due to limited availability of suitable reference data. Model results include traffic volumes, fleet composition, fuel burn and emissions of NO<sub>x</sub> for future aviation and will be presented in chapter 4.3.

Sensitivity analyses regarding certain forecast assumptions are presented in chapter 4.4. This includes an analysis of the assumptions made for future engine combustors and emission standards. Besides, the influence of traffic growth on fuel efficiency and the effects of delivery delays for new aircraft types will be assessed in this chapter. An assessment of potential effects from biofuels and an outlook on future model improvements are finally found in chapter 5.

## 3 METHODOLOGY FOR AVIATION EMISSIONS CALCULATION

### 3.1 MODEL OVERVIEW

A comprehensive model has been developed for this study in order to quantify fuel burn and emissions of global air traffic. Both current and future air traffic are covered by the simulation. Using a bottom-up approach for emissions calculation, the model consists of a chain of software and database tools (see Figure 18 on page 23). The core modules of this tool chain have been specifically developed for this assessment. These core modules are:

- The VarMission Flight Mission and Emissions Module.
- The Air Traffic Emissions Module.
- The Air Traffic Emissions Forecast Module.

The VarMission Flight Mission and Emissions Module is an aircraft performance tool capable of calculating fuel burn and emissions on given flight missions. Built around the BADA database of aircraft models [46] and using reference emissions information from the ICAO engine emissions database [78], VarMission covers a broad range of aircraft-engine combinations. Furthermore, the tool can be coupled to DLR's engine performance software named VarCycle. Aircraft models from various sources and in different formats can be used with this module. VarMission will be described in detail in chapter 3.2.

The Air Traffic Emissions Module is based on worldwide flight schedules compiled by the Official Airline Guide (OAG) [100]. The module consists of several database scripts linking and combining data from various sources. Initially, OAG flight schedule information is converted into a database of flight movements. This movements database is supplemented by fleets information from the ASCEND fleets database [11] and by load factor information from ICAO statistics [77]. The Air Traffic Emissions Module relies on the VarMission module for calculating fuel burn and emissions for each flight. Assumptions are made regarding inefficiencies from Air Traffic Management that influence fuel burn and emissions. More information on the Air Traffic Emissions Module is found in chapter 3.3.

The Air Traffic Emissions Forecast Module described in chapter 3.4 predicts fuel burn and emissions for the short- and medium-term future. The module applies regional traffic growth rates obtained from the Airbus Global Market Forecast (GMF) [4] to given flight movements of a base year. It predicts the future fleet composition based on aircraft lifetime assumptions, entry-into-service dates of new aircraft types and aircraft market shares. VarMission aircraft models are used to determine fuel burn and emissions for each flight. Assumptions about future load factors, ATM efficiencies and NO<sub>x</sub> emission standards are considered for emissions calculation.

### 3.2 VARMISSION – FLIGHT MISSION AND EMISSIONS MODULE

#### 3.2.1 OVERVIEW

An aircraft performance tool named “VarMission” has been developed for this study and can be used to calculate fuel consumption and emissions of NO<sub>x</sub>, CO, HC and soot for a wide range of aircraft-engine combinations. The tool aims at analysing flight missions and, for this purpose, provides a flight mission planner with an easy-to-use interface. The user of the software selects an aircraft and an engine type, specifies the payload to be transported and describes a flight as a sequence of flight phases. Given this information, the tool simulates the flight mission and calculates the required fuel quantities and emissions.

Figure 19 shows a schematic of the VarMission module with input and output data. The BADA database provided by EUROCONTROL [46] serves as the primary source for aircraft models, while ICAO’s engine exhaust emissions databank [78], FOI’s emissions databank for turboprop engines [127] and piston engine information from FOCA [57] are sources for emissions data. As an alternative to BADA, user-defined aircraft can be described by their characteristic masses and aerodynamic drag polars. Furthermore, VarMission can be coupled to external engine simulations like DLR’s VarCycle software. This way, emission calculation methods implemented in engine simulations can be used with VarMission. Historical fleet statistics from the ASCEND Fleets Database [11] are used to identify aircraft-engine combinations in the worldwide fleet. The VarMission tool is written in Microsoft Visual Basic for Applications (VBA) with input and output in Microsoft Excel. A Microsoft Access database contains aircraft and engine data. In the following sections, the approach towards flight modelling and emissions calculation will be described in detail.

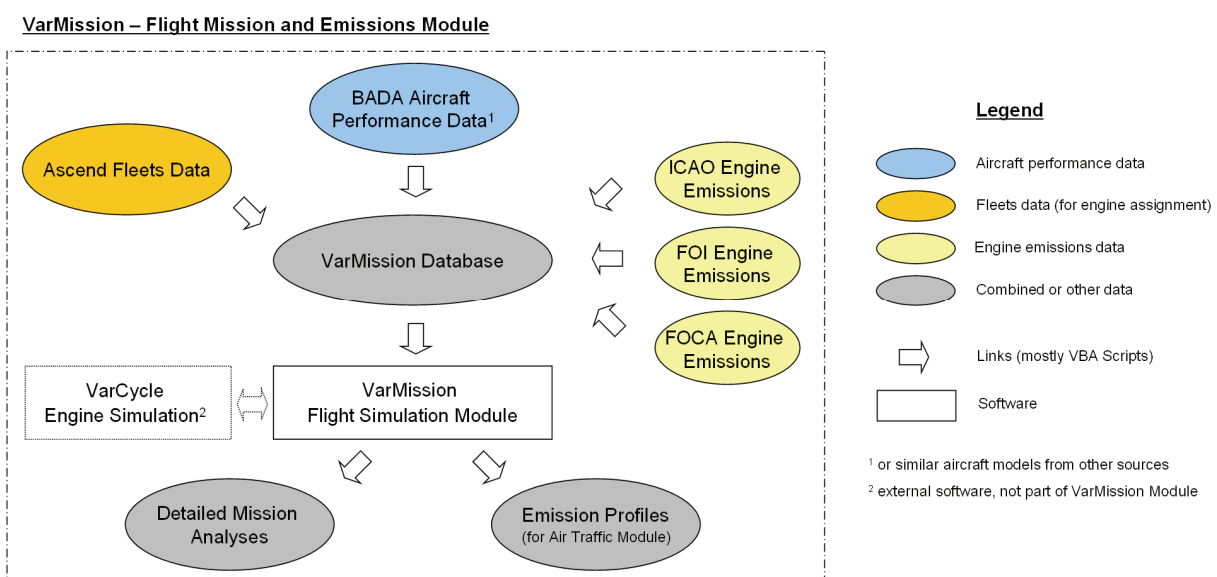


Figure 19: Schematic of the VarMission module



### 3.2.2 THE BADA AIRCRAFT PERFORMANCE MODEL

The Base of Aircraft Data (BADA) is an aircraft performance database maintained by the EUROCONTROL Experimental Centre. BADA is the primary source of aircraft data in VarMission. The BADA version 3.9 is used in this study and contains information on 117 aircraft types, provided by aircraft manufacturers or gathered from reference sources like aircraft manuals [43]. This chapter gives an overview on the database and the underlying performance model. A more detailed description is found in [43] and [46].

The BADA database in its original form consists of ASCII files containing performance and operating parameters for all supported aircraft models. For each aircraft type, the data is stored in the following files:

- Operations Performance Files (\*.OPF) incl. aircraft-specific performance parameters.
- Airline Procedure Files (\*.APF) with aircraft-specific operational data.
- Performance Table Files (\*.PTF) and Performance Table Data Files (\*.PTD) with a summary of an aircraft's performance.

The PTF and PTD files provide look-up tables for instantaneous cruise, climb and descent performance under different flight conditions. For detailed performance calculations, only OPF and APF data are required. Furthermore, a Global Parameter File (BADA.GPF) is provided containing non-aircraft-specific data like maximum accelerations or holding speeds. The OPF files include a total of 55 parameters per aircraft which specify an aircraft's characteristic masses and flight envelope together with its aerodynamic and engine capabilities (see Table 4 on page 28). The APF files supplement the performance data by providing typical speeds or Mach numbers for climb, cruise and descent conditions. BADA data in combination with the underlying performance model can be used to calculate lift and drag as well as thrust and fuel flow at any point of a flight profile.

In principle, the aircraft model behind BADA balances the rate of work done by forces acting on the aircraft and the rate of increase in potential and kinetic energy. This approach, mostly referred to as a Total Energy Model, is represented by the following equation:

$$(1) \quad (T - D) \cdot v_{TAS} = m \cdot g \cdot \frac{dh}{dt} + m \cdot v_{TAS} \cdot \frac{dv_{TAS}}{dt}$$

Equation (1) contains three independent variables which represent typical aircraft control inputs: thrust  $T$ , true airspeed  $v_{TAS}$  and rate-of-climb (or descent)  $dh/dt$ . Controlling any two of these, the third variable can be calculated. When modelling a cruise flight segment, the Total Energy Equation can be used to calculate thrust, while speed and rate-of-climb are usually known. For climb and descent segments, thrust and speed are typically given or can be calculated from BADA-suggested formulae while equation (1) may be used to determine the

resulting rate-of-climb (or rate-of-descent)<sup>7</sup>. As the aerodynamic drag force D is required in equation (1), lift and drag coefficients  $C_L$  and  $C_D$  as well as the respective forces need to be calculated using equations (2) to (5):

$$(2) \quad C_L = \frac{2 \cdot m \cdot g}{\rho \cdot V_{TAS}^2 \cdot S \cdot \cos \phi} \quad (3) \quad C_D = C_{D0} + C_{D2} \cdot C_L^2$$

$$(4) \quad L = \frac{1}{2} \cdot \rho \cdot v_{TAS}^2 \cdot C_L \cdot S \quad (5) \quad D = \frac{1}{2} \cdot \rho \cdot v_{TAS}^2 \cdot C_D \cdot S$$

Equation (2) assumes a flight path angle of zero, while a correction for the bank angle  $\phi$  is applied. The coefficients  $C_{D0}$  and  $C_{D2}$  of a parabolic drag polar are given for up to five configurations (i.e. flaps / slats settings) per aircraft. Landing gear extension is modelled by a  $\Delta C_{D0}$ . Compressibility effects at high Mach numbers and the resulting drag rise are currently not implemented in BADA [43]. Air density  $\rho$  can be obtained from International Standard Atmosphere (ISA) assumptions, unless more precise or measured data is available.

Category	Parameter and Description	Category	Parameter and Description	
aircraft type	$n_{eng}$ – number of engines [-] engine type – Jet/Turboprop/Piston wake category – Heavy/Medium/Light	engine thrust	$C_{Tc,1}$ – 1 <sup>st</sup> max. climb thrust coefficient [N] $C_{Tc,2}$ – 2 <sup>nd</sup> max. climb thrust coefficient [ft] $C_{Tc,3}$ – 3 <sup>rd</sup> max. climb thrust coefficient [1/ft <sup>2</sup> ] $C_{Tc,4}$ – 1 <sup>st</sup> thrust temperature coefficient [°C] $C_{Tc,5}$ – 2 <sup>nd</sup> thrust temperature coefficient [1/°C] $C_{Tdes,low}$ – low alt. descent thrust coefficient [-] $C_{Tdes,high}$ – high altitude descent thrust coef. [-] $h_{des}$ – transition altitude [ft] $C_{Tdes,app}$ – approach thrust coefficient [-] $C_{Tdes,ld}$ – landing thrust coefficient [-] $V_{des,ref}$ – reference descent speed [kt] $M_{des,ref}$ – reference descent Mach number [-]	
	mass		$m_{ref}$ – reference mass [t] $m_{min}$ – minimum mass [t] $m_{max}$ – maximum mass [t] $m_{pyld}$ – maximum payload [t]	
flight envelope	$V_{MO}$ – max. operating speed [kt] $M_{MO}$ – max. operating Mach number [-] $h_{MO}$ – max. operating altitude [ft] $h_{max}$ – max. altitude at MTOW and ISA [ft] $G_w$ – weight gradient on max. altitude [ft/kg] $G_t$ – temp. gradient on max. altitude [ft/C]		fuel flow	$C_{f1}$ – 1 <sup>st</sup> TSFC coefficient [kg/min/kN] $C_{f2}$ – 2 <sup>nd</sup> TSFC coefficient [kt] $C_{f3}$ – 1 <sup>st</sup> descent fuel flow coefficient [kg/min] $C_{f4}$ – 2 <sup>nd</sup> descent fuel flow coefficient [ft] $C_{fcr}$ – cruise fuel flow correction coefficient [-]
	aero-dynamics			ground operation
Some parameters may vary for turboprop and piston aircraft				
			$S$ – reference wing surface area [m <sup>2</sup> ] $C_{D0,i}$ – parasitic drag coefficient for five different flaps / slats settings [-] $C_{D2,i}$ – induced drag coefficient for five different flaps / slats settings [-] $C_{D0,\Delta LDG}$ – delta drag for ext. landing gear [-] $(V_{stall})_i$ – stall speeds for TO,IC,CR,AP,LD [kt] $C_{M16}$ – Mach drag coefficient [-] $C_{Lbo(M=0)}$ – Buffet onset lift coef. [-] *jets only* K – Buffeting gradient [1/M] *jets only*	

Table 4: Operations performance parameters in BADA [46]

<sup>7</sup> For accelerated climb/descent, an energy share factor is assumed to solve equation (1), see Appendix A.



In the BADA model, the thrust specific fuel consumption  $\eta$  of an aircraft is estimated as a function of airspeed. Given the thrust from equation (1),  $\eta$  and hence the fuel flow  $f$  can be calculated based on aircraft-specific fuel flow coefficients<sup>8</sup>:

$$(6) \quad \eta = C_{f1} \cdot \left( 1 + \frac{v_{TAS}}{C_{f2}} \right) \quad (7) \quad f_{cr} = \eta \cdot T \cdot C_{fcr}$$

For simplicity, equation (6) is shown in the version for jet aircraft only, while equation (7) is shown for cruise segments with a cruise fuel flow correction factor  $C_{fcr}$ . The respective formulae for turboprop and piston aircraft as well as more details regarding the BADA data and methodology are found in [46].

As was described above, BADA provides the data and formulae to determine the instantaneous fuel flow of an aircraft at any point of a flight profile. The fuel consumption in a flight segment can be estimated by multiplying fuel flow with time. As the aircraft mass is not constant during a flight, an iterative approach needs to be used for this purpose: starting at a given aircraft mass, the fuel consumption can be calculated for a sufficiently small flight segment. For the following segment, equations (1) through (7) are applied again with the aircraft mass debited by the amount of fuel burnt in the previous segment.

## Mission Analysis

Load defaults for user-def. missions
Load defaults for simplified missions

**Flight profile options**

Constant altitude cruise (default)

Cruise with a single step climb

Continuous climb cruise\*

\* Experimental, but working!

**Step climb options [step climb profile]**

Step climb to final cruise altitude as soon as possible

Step climb after a percentage of total cruise distance (default)

50 % < | | >

Detailed modelling of the "step" (On/Off)

**Climb rate options [step climb & continuous climb profiles]**

Determine climb rate automatically (default)\*\*

Set climb rate manually

300 ft/min < | | >

\*\* The default climb rate for a step climb is set to 300 ft/min!

**Thrust options for climb**

BADA max. climb thrust

BADA red. climb thrust

ICAO max. take-off thrust\*

ICAO max. climb thrust\*

\* ICAO thrust levels only available for engines with entry in ICAO database.

**Type of analysis**

Mission analysis for a given final gross weight (default)

Mission analysis for a given initial gross weight

**Main input parameters**

Initial / final aircraft gross weight:  $m_{mission,1/2} =$  77000 kg < | | >

*Aircraft gross weight is handled automatically, if load planner is activated!*

Initial cruise flight level:  $FL_{cr,1} =$  330 FL < | | >

Final cruise flight level:  $FL_{cr,2} =$  350 FL < | | >

Cruise Mach number:  $M_{cr} =$  0.78 - < | | >

Cruise or mission ground distance:  $d_{cr / mission} =$  4000 km < | | >

A routing factor can be specified in the Mission Planner options on the Right!

**Speed options**

Set min. operating speed limits during climb (On/Off)

Set BADA speed limits below FL140 during cruise (On/Off)

Set min. operating speed limits during descent (On/Off)

**Environmental conditions**

Temperature deviation from ISA:  $\Delta T_{ISA} =$  0 ° < | | >

**Automatic mode**

Do not display uncritical error messages (On/Off)

Maximum TOW

Maximum altitudes

Nominal TOW

Typical altitudes

Low TOW

Default speeds

Figure 20: VarMission main input mask (screenshot)

<sup>8</sup> Note that BADA coefficients are not always dimensionless (see Table 4).

### 3.2.3 FLIGHT MISSION SIMULATION IN VARMISSION

The VarMission software has been developed for fuel burn and emissions calculations of whole flights. Designed as a flight mission calculation tool for BADA aircraft, it can also be used with aircraft and engine models from other sources. VarMission is built around a Microsoft Access database that contains aircraft data from BADA [46] as well as engine emissions data from the ICAO [78], FOI [127] and FOCA [57]. In order to assign engine types to aircraft models, aircraft and engine fleet statistics from the ASCEND Fleets Database [11] are included in the database. The software is written in Microsoft Visual Basic for Applications (VBA) with input and output in Microsoft Excel. It features a graphical user interface that simplifies the selection of an aircraft and an engine type, the specification of an aircraft's initial mass or payload and the description of a flight as a sequence of flight phases. A screenshot of the main input mask is shown in Figure 20.

For compatibility with aircraft models from BADA, all flight phases except the landing and take-off cycle (LTO) are based on the Total Energy Approach described in chapter 3.2.2. When describing a flight mission, every input parameter per flight phase can be specified. The mission analysis functionality has been designed in a way that requires minimum user input. A number of typical missions are pre-defined in the programme. Table 5 lists the available flight phases and summarizes methodologies and input parameters while Table 6 on page 32 presents the standard flight mission used for most analyses in this study. The sequence of flight phases shown in Table 6 is based on the following assumptions:

- For reasons of simplicity, taxi-out and taxi-in modes are based on the ICAO LTO cycle with engines at idle thrust and using given times per mode.
- The departure procedure resembles the so-called modified ATA procedure that is commonly used by many airlines. After lift-off at the origin airport, engine thrust is cut back from take-off thrust to climb thrust at around 1500 ft above ground followed by an acceleration segment at reduced climb rate [64].
- Climb is performed at two different calibrated airspeeds with an acceleration phase on flight level 100. After reaching the transition altitude between high-altitude climb speed and climb Mach number, the climb is continued at constant Mach number.
- Cruise flight is performed at a constant cruise Mach number and may include one or more step climbs. Typical aircraft- and distance-specific cruise altitudes are suggested by VarMission (see Appendix D); user-defined altitudes may also be used.
- Descent is performed at a constant descent Mach number above the transition altitude and two calibrated airspeeds below transition altitude with a deceleration before reaching flight level 100.

	Flight phase	Main input parameters	Methodology
1a	<b>LTO</b> ("landing and take-off cycle")	Time per LTO mode Thrust per LTO mode	LTO cycle as defined by ICAO [78] with user-defined times-in-modes and thrust settings Modes at origin: taxi-out, take-off, initial climb Modes at destination: app./landing, taxi-in
1b	<b>Take-off</b> (may replace LTO take-off mode) <b>Landing</b> (may replace LTO landing mode)	Aircraft gross weight Initial and final airspeed* Thrust	Take-off and landing model considering roll friction and the aircraft's drag characteristics; based on methods from [129]
2	<b>BADA Climb</b> (at given climb thrust and at a given speed schedule) <b>BADA Descent</b> (at given descent thrust and at a given speed schedule)	Aircraft gross weight Initial and final flight levels*	Climb and descent thrust given by BADA CAS/Mach schedule given by BADA Rate-of-climb/descent calculated by Total Energy Equation
3	<b>Cruise / Horizontal</b> (at constant flight level and Mach number)	Aircraft gross weight Flight level CAS or Mach number Cruise distance* or time*	Thrust calculated by Total Energy Equation
4	<b>Acceleration / Deceleration</b> (at constant flight level)	Aircraft gross weight Flight level Initial & final CAS or Mach* Acceleration	Thrust calculated by Total Energy Equation
5	<b>Climb at given thrust</b> (at constant CAS or Mach) <b>Descent at given thrust</b> (at constant CAS or Mach)	Aircraft gross weight Initial and final flight levels* CAS or Mach Number Thrust	Climb and descent thrust given by BADA or other sources, see Appendix B for details Rate-of-climb/descent calculated by Total Energy Equation
6	<b>Climb at given rate-of-climb</b> (at constant CAS or Mach) <b>Descent at given rate-of-descent</b> (at constant CAS or Mach)	Aircraft gross weight Initial and final flight levels* CAS or Mach Number Rate-of-climb/descent or gradient	Thrust calculated by Total Energy Equation
7	<b>Accelerated / decelerated climb at given thrust</b> <b>Accelerated / decelerated descent at given thrust</b>	Aircraft gross weight Initial and final flight levels* Initial & final CAS* Thrust Accel. or energy share factor	Climb and descent thrust given by BADA or other sources, see Appendix B for details Rate-of-climb/descent calculated by Total Energy Equation
8	<b>Accelerated / decelerated climb at given rate-of-climb</b> <b>Accelerated / decelerated descent at given rate-of-descent</b>	Aircraft gross weight Initial and final flight levels* Initial & final CAS* Rate-of-climb/descent or gradient Accel. or energy share factor	Thrust calculated by Total Energy Equation
* Target parameter for the iteration. In case of multiple target parameters, the iteration stops if one of the targets is reached.			

Table 5: Available flight phases in VarMission

- The approach procedure resembles the so-called low-drag-low-power procedure. Speed is reduced and configuration is changed in a horizontal flight segment at about 3000 ft above ground, before starting final approach at a 3° gradient [64].
- Additional flight phases R1-R3 are necessary in order to estimate the reserve fuel on board. Typical reserve fuel policies from [53] for short-range and long-range flights are suggested by the software and can be modified by the user if necessary.

More details regarding characteristic speeds and assumptions about accelerations are found in Appendix A. The thrust levels available for take-off, climb and descent are explained in Appendix B.

Flight phase		Description
1	LTO (taxi-out mode only)	Engine start (2 min) and taxi-out (9 min) at idle thrust
2	Take-off	Acceleration on runway at take-off thrust until take-off speed is reached
3	Climb at given thrust	Climb at take-off thrust and constant CAS to 1500 ft above ground
4	Accelerated climb at given thrust	Accelerated climb at climb thrust until low-altitude climb CAS is reached
5	Climb at given thrust	Climb at climb thrust and constant CAS to flight level 100
6	Acceleration	Acceleration from low-altitude climb CAS to high-altitude climb CAS
7	Climb at given thrust	Climb at climb thrust and constant CAS / Mach to Initial Cruise Altitude
8	Cruise	Cruise flight at constant Mach number (with step climbs if necessary)
9	Descent at given thrust	Descent at descent thrust and constant CAS / Mach to flight level 120
10	Decelerated descent at given thrust	Decelerated descent at descent thrust until low-altitude descent CAS is reached
11	Descent at given thrust	Descent at descent thrust and constant CAS to 3000 ft above ground
12	Horizontal	Horizontal flight segment while preparing for approach
13	Deceleration	Deceleration to approach speed
14	Decelerated descent at given rate-of-descent	Decelerated descent at 3° gradient until landing CAS is reached
15	Descent at given rate-of-descent	Descent at 3° gradient and at constant CAS until ground level
16	Landing	Deceleration on runway at idle thrust
17	LTO (taxi-in mode only)	Taxi-in (5 min) at idle thrust
R1	Missed approach	Missed approach at destination airport.
R2	Alternate	Cruise flight to alternate airport at constant altitude and Mach number.
R3	Holding	Low-altitude holding phase at alternate airport.
<p><b>Remarks:</b></p> <ol style="list-style-type: none"> <li>1. Flaps/slats configuration can be set manually for each flight phase or automatically using an altitude-dependent configuration schedule. Each configuration is assigned its own drag polar.</li> <li>2. Take-off and climb thrust can be calculated according to [129] and [46]. Descent thrust is calculated according to [46]. More details are found in Appendix B.</li> <li>3. Missed approach fuel can be specified by the user or may be neglected. Alternate and Holding phases are, in principle, modified cruise phases with given distance to the alternate airport and given holding time respectively. During the Holding phase, a standard racetrack holding pattern is simulated.</li> </ol>		

Table 6: Default flight mission as sequence of flight phases

VarMission analyses each flight mission from taxi-out to taxi-in and determines fuel burn and emissions along the flight profile. As fuel is burnt during the flight, the aircraft mass is recalculated every time step  $\Delta t$ . A time step in the order of 1-5 minutes is typically assumed for cruise flight while smaller intervals in the order of 10-20 seconds are used for climb and descent. An iterative algorithm is required in order to determine a flight's cruise distance, which is initially unknown. As an option, the flight's payload or load factor can be specified instead of the aircraft's initial mass. In this mode, a flight is analysed "backwards": starting at the aircraft's empty mass plus payload, reserve fuel quantities can be calculated and are added to the aircraft's gross weight. Hence, all flight phases are analysed in reverse order from taxi-in at the destination airport to taxi-out at the origin airport.

An example flight profile of an Airbus A319 on a 1500 km mission is shown in Figure 21. The aircraft's flaps and slats configuration can be set manually for each flight phase or by an altitude- and airspeed-dependent configuration schedule as shown in the figure. International Standard Atmosphere (ISA) and no wind are assumed in this example, although a temperature delta to ISA and a headwind component can be specified in VarMission.

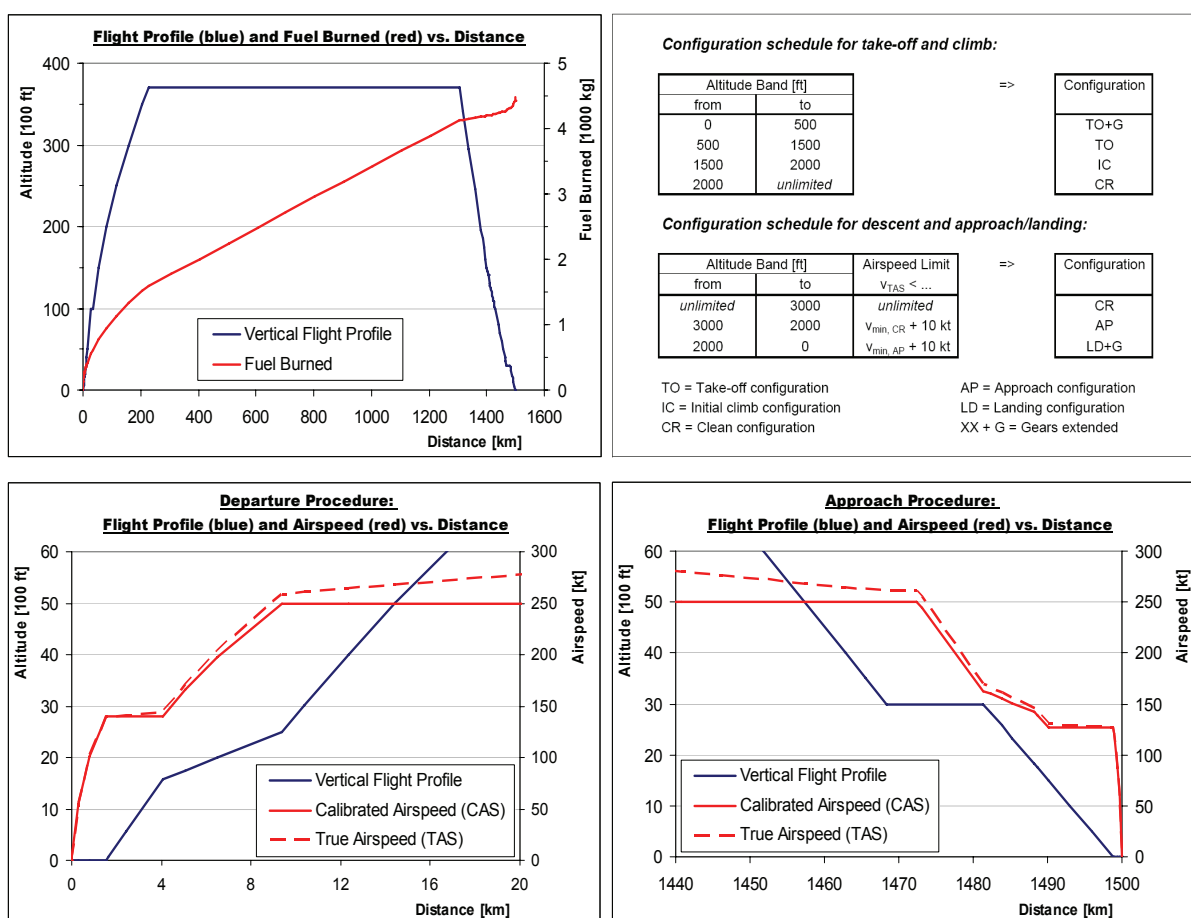


Figure 21: Typical flight profile, flaps/slats schedule, departure and approach procedures for an Airbus A319 example mission

### 3.2.4 EMISSION CALCULATION IN VARMISSION

#### 3.2.4.1 OVERVIEW ON CALCULATION METHODS

As was described in the previous chapter, VarMission is capable of simulating flight missions and predicting the corresponding fuel consumption. Furthermore, gaseous and particulate emissions can be calculated. Figure 22 shows common methods to compute in-flight emissions from aircraft engines. Carbon dioxide ( $\text{CO}_2$ ) and water vapour ( $\text{H}_2\text{O}$ ) are the main combustion products of hydrocarbon fuels and can be assumed to be proportional to fuel consumption. Emissions of nitric oxides ( $\text{NO}_x$ ), carbon monoxide (CO), hydrocarbons (HC) and soot are influenced by a number of parameters, most prominently the engine type, its power setting, current flight speed, altitude and ambient atmospheric conditions.

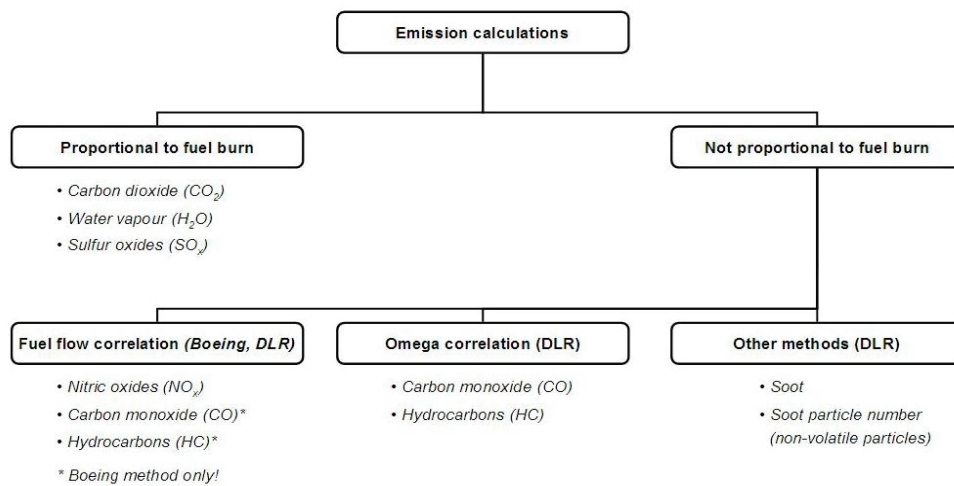


Figure 22: Overview on methods for emission calculation used in this study

For  $\text{NO}_x$ , CO, HC and soot, correlation methods exist that can be used to predict in-flight emissions based on reference emissions for sea-level static conditions. The fuel flow correlation methods for  $\text{NO}_x$  developed by DLR [31] and Boeing [14] as well as the fuel flow correlations for CO and HC developed by Boeing [14] have been implemented into VarMission. The Omega correlation for CO and HC and DLR's soot prediction method are more difficult to integrate into aircraft performance software as they require internal engine parameters as input data. These methods are implemented in DLR's engine simulation software VarCycle. For flight mission simulations, VarCycle can be coupled to VarMission in order to provide the respective in-flight emission indices.

#### 3.2.4.2 EMISSIONS OF $\text{CO}_2$ AND $\text{H}_2\text{O}$

Jet fuel is typically used for transport aircraft with turbofan and turboprop engines. The main products resulting from the combustion of jet fuel are carbon dioxide ( $\text{CO}_2$ ) and water vapour ( $\text{H}_2\text{O}$ ). The relation of  $\text{CO}_2$  to  $\text{H}_2\text{O}$  in the engine exhaust depends on the carbon to hydrogen

ratio of the fuel. Given a chemical mean formula for jet fuel and assuming complete oxidation, the mass of CO<sub>2</sub> and H<sub>2</sub>O in the exhaust can be calculated. Assuming ideal combustion, emissions of these gases are proportional to fuel burn. Emission indices in gram per kilogram fuel were determined in studies on jet fuel properties as summarized in Table 7. The values from Hadaller and Momenthy are used by VarMission to calculate emissions of CO<sub>2</sub>, H<sub>2</sub>O (and also SO<sub>x</sub>) for all aircraft powered by turbofan or turboprop engines.

Aircraft with piston engines use aviation gasoline (AVGAS) instead of jet fuel. AVGAS fuel properties were examined by FOCA [57] and emission indices for CO<sub>2</sub> (3170 g/kg) and H<sub>2</sub>O (1210 g/kg) were suggested to be used for emission calculations. Consequently, VarMission assumes the aforementioned values for piston-powered aircraft.

Emitted substance	Emission index [g/kg] [Rachner (1998)]	Emission index [g/kg] [Nüßer and Schmitt (1990)]	Emission index [g/kg] [Hadaller and Momenthy (1989)]
Carbon Dioxide (CO <sub>2</sub> )	3156	3154	3155
Water (H <sub>2</sub> O)	1237	1239	1237
Sulphur oxides (SO <sub>x</sub> )	-	-	~ 0.8 depending on sulphur content

Table 7: Emission indices for CO<sub>2</sub>, H<sub>2</sub>O and SO<sub>x</sub> from various studies (quoted in [113])

### 3.2.4.3 EMISSIONS OF NO<sub>x</sub>, CO AND HC

Engine emissions of NO<sub>x</sub> depend mainly on pressure, temperature and residence time of the reacting species in the hot flame region of a combustor. Consequently, NO<sub>x</sub> emission indices vary with engine type, the power setting of the engine and ambient atmospheric conditions. While emissions of NO<sub>x</sub> are mainly produced at high engine power settings, products of incomplete combustion like CO and HC are mostly emitted at low power levels, when fuel/air mixing processes are rather inefficient [67].

A number of semi-empirical methods exist which predict in-flight emissions of NO<sub>x</sub>, CO and HC based on reference emission indices for sea level static conditions. Such reference data are available from the ICAO engine emissions databank for jet engines [78] and the FOI emissions databank for turboprop engines [127]. Given the exact engine identification from one of these sources, in-flight emissions can be calculated. For aircraft with piston engines, emission measurements were performed by FOCA [57] both for sea-level and cruise conditions. The FOCA data is included in the VarMission database and can be used for flight mission simulation. Given the limited amount of piston engine data and aircraft data, piston engine emissions other than CO<sub>2</sub> and H<sub>2</sub>O were not evaluated in this study.

Calculation methods for NO<sub>x</sub> emissions typically concentrate on pressure and temperature in the combustion zone as the most influential parameters. The so-called  $p_3T_3$  approach [119] is commonly used by engine manufacturers, yet it requires the knowledge of combustor inlet



pressures and temperatures. In order to simplify emission calculations, fuel flow correlation methods were developed by DLR [31] or Boeing [14]. These methods calculate in-flight emissions of NO<sub>x</sub> as function of engine fuel flow, ambient atmospheric conditions and flight speed. Fuel flow correlations are based on the idea that emission indices under various conditions are correctable to reference conditions and may collapse into a single function of corrected fuel flow. A common principle of these methods is to determine a ratio of emission indices at flight conditions versus reference conditions, which eliminates the influence of internal engine parameters. This scheme is represented by the following formula:

$$(8) \quad \frac{EINO_x}{EINO_{x,ref}} = f\left(\frac{p}{p_{ref}}, \frac{T}{T_{ref}}, \frac{w_{fuel}}{w_{fuel,ref}}\right) \cdot F(H)$$

While the Boeing method and the equivalent DLR approach share the above principle, they differ in the way the parameters are manipulated. Both methods have been implemented into VarMission and can be used to calculate emissions of NO<sub>x</sub> on flight missions. In the following paragraphs, the DLR fuel flow method and its implementation in VarMission is described in more detail. A description of the Boeing-developed fuel flow methods for NO<sub>x</sub>, CO and HC emissions are found in [14].

*The DLR Fuel Flow Method*

When using fuel flow correlation methods to calculate in-flight emissions of NO<sub>x</sub>, a reference function of NO<sub>x</sub> emission index (EINO<sub>x</sub>) versus fuel flow needs to be established for reference conditions. In the ICAO and FOI engine emissions databases, four data points of fuel flow and EINO<sub>x</sub> are published for each engine that represent different thrust settings at sea level static and International Standard Atmospheric (ISA) conditions. VarMission typically assumes a parabolic fit through the four data points as a reference function. Figure 23 shows an example for a CFM56-5A3 engine.

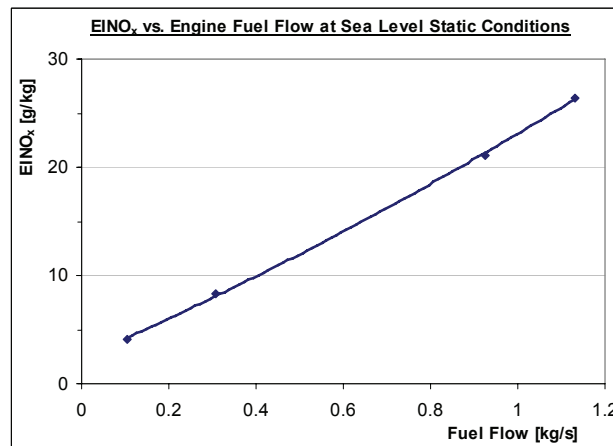


Figure 23: EINO<sub>x</sub> vs. fuel flow at sea level static conditions for a CFM56-5A3 engine



Given the reference function, the engine fuel flow  $w_{fuel}$  for current flight conditions needs to be corrected (or “reduced”) to reference conditions:

$$(9) \quad w_{fuel,red} = \frac{w_{fuel}}{\delta_{total} \cdot \sqrt{\theta_{total}}} \quad \text{with} \quad \delta_{total} = \frac{P_{total}}{101325 Pa} \quad \text{and} \quad \theta_{total} = \frac{T_{total}}{288.15 K}$$

The reduced fuel flow  $w_{fuel, red}$  calculated by formula (9) can be used in order to determine the  $EINOx_{red}$  for reference conditions from the function plotted in Figure 23. In the following step, the emission index for reference conditions needs to be re-corrected for flight conditions. This is done in equations (10)-(11):

$$(10) \quad EINOx = EINOx_{red} \cdot \delta_{total}^{0.4} \cdot \theta_{total}^3 \cdot e^H \quad \text{with} \quad H = -19.0 \cdot (\omega - 0.00634)$$

H represents a humidity correction factor that can be calculated as function of the specific humidity  $\omega$ . The specific humidity depends on altitude and is approximated as follows:

$$(11) \quad \omega = 10^{-3} \cdot e^{-0.0001426 \cdot (h-12900)} \quad \text{with} \quad h = \text{altitude in feet}$$

Details regarding theory and validation of the DLR fuel flow method can be found in [31]. The direct implementation of the fuel flow correlation methods enables VarMission to calculate  $NO_x$  emissions of turbofan and turboprop powered aircraft without the need for a detailed engine model. CO and HC emissions can be estimated using Boeing’s fuel flow method.

Emission indices can also be imported from external engine simulation software: DLR’s VarCycle tool for turbofan simulation and its equivalent for turboprop engines named TPVar can be linked to VarMission. Additional correlation methods for  $NO_x$  like e.g. the  $p_3T_3$  method [119] are implemented in this software. VarCycle and TPVar calculate emissions of CO and HC by DLR’s Omega correlation method [31], which can be regarded as more accurate than respective fuel flow correlations. More importantly, the software provides the opportunity to model advanced combustion technology like e.g. lean burn combustors. The GENx engine equipped with such technology is currently being introduced into the fleet. At the time of writing, quantification of  $NO_x$  emissions from lean burn combustors is difficult due to lack of reliable data. Fuel flow correlations are believed to overestimate  $NO_x$  emissions during cruise flight for engines equipped with such technology. The VarCycle model of the GENx [106] uses a manually defined reference function describing the  $NO_x$  emission index vs. combustor inlet temperature  $T_3$  for sea level static conditions. The switching point from pilot mode to the combined pilot/main mode is assumed to occur at a constant temperature  $T_3$ . Given this reference function, a  $p_3T_3$  approach [119] is applied to estimate emissions of  $NO_x$  during cruise flight. The switching point is selected such that the engine is operated in the combined pilot/main mode during cruise. While this assumption reflects one of the design targets of lean burn combustors (see Figure 17 on page 20), it is also a source of uncertainty.

#### 3.2.4.4 EMISSIONS OF SOOT / BLACK CARBON

Emissions from aircraft engines include particulate emissions of soot, also referred to as black carbon. The formation of soot is a complex process and influenced by various engine parameters including the fuel injection system and combustor technology. Only few measurements of soot emissions for in-flight conditions are publicly available. Furthermore, the ICAO engine emissions database contains the smoke number instead of an emission index for soot.<sup>9</sup> No suitable data are available from the FOI emissions database for turboprop engines, but DLR has obtained smoke number information for a small number of turboprop engines from engine manufacturers.

A semi-empirical correlation method with variable reference functions was developed at DLR that determines the in-flight emission index of soot from smoke number measurements at sea level static conditions [33]. This method is implemented in DLR's VarCycle and TPVar engine simulation software. In principle, the following tasks are performed:

- The soot concentration  $C_{\text{Soot}}$  in  $\text{mg}/\text{m}^3$  is estimated from smoke number measurements at sea level static conditions.
- A reference function of  $C_{\text{Soot}}$  versus combustor inlet temperature  $T_3$  is determined for sea level static conditions (separately for each engine type considered).
- Emission indices are calculated from the reference functions using corrections for combustor inlet pressure  $p_3$ , flame temperature  $T_{\text{fl}}$  and equivalence ratio  $\Phi$ .

A more detailed description and validation of this method is found in [31] and [33]. By coupling VarMission to engine simulation software, emissions of soot on flight mission level can be calculated (by mass). This requires, of course, the availability of suitable engine models.

Besides calculating soot emissions by mass, an estimation of the soot particle number can be provided. However, current knowledge regarding the number of soot particles emitted by aircraft engines must be regarded as low. Very few detailed measurements of particle size distributions are available. In [33], average characteristics of particle number per kilogram soot vs. altitude could be developed. VarMission uses a relation from [33] in order to provide an estimation of soot particle numbers. More details are found in Appendix E. It should be noted that the accuracy of this method for soot particle estimation is unknown and probably low. Consequently, results for soot particle numbers presented in chapter 4.2 should be regarded as rough estimates only.

---

<sup>9</sup> The smoke number (SN) is determined from collecting soot on white filter paper and evaluating the intensity of light reflection, see [78].

### 3.2.5 VARMISSION VALIDATION

#### 3.2.5.1 MISSION FUEL BURN VALIDATION

The accuracy of mission fuel burn results produced by VarMission depends on the quality of available input data. Aircraft models from the BADA database – the main source of aircraft data in VarMission – are created by EUROCONTROL. The implementation of the BADA methodology in VarMission was validated against EUROCONTROL’s reference implementation by comparing point performance data tables from the BADA Performance Table Files (\*.PTF) and Performance Table Data Files (\*.PTD) with VarMission calculations. VarMission is able to reproduce the data in the aforementioned files, which indicates a correct implementation of the BADA methodology in the software. The BADA aircraft models themselves are validated by EUROCONTROL and a Model Accuracy Summary Report [45] is released with each BADA version. The report contains a comparison of BADA model output for each aircraft and the reference performance data the aircraft model is based on. For each aircraft type, vertical speed and fuel flow of climb, cruise and descent trajectories are analysed and a statistical evaluation is presented. The accuracy summary reports are plausibility checks for BADA aircraft models, but have limited value for conditions other than those of the reference data.

In the course of this study, mission fuel burn results from VarMission were compared to fuel burn data provided by two European airlines: Airline A provided high-quality FDR (flight data recorder) information on 14 flights performed by Airbus A310 and Boeing 747-300 aircraft [61]. The data from airline B include mission simulation results by the airline’s performance software for two Boeing 747-400 transatlantic flights [32]. ISA standard atmospheric conditions with no wind were assumed for these simulations. The aircraft’s take-off mass, flight profile and Mach number were matched to the reference data. As can be seen from Figure 24, the delta in fuel burn between VarMission and the airline software is less than 2%.

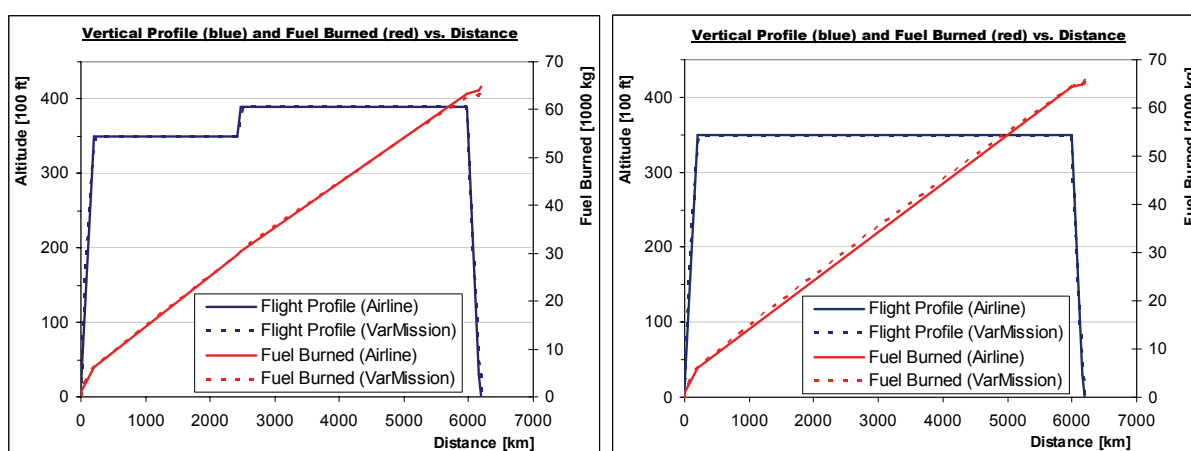


Figure 24: Comparison of mission fuel burn (B747-400, VarMission vs. Airline Software)

While the comparison in Figure 24 covers generic flight missions at standard atmospheric conditions, the FDR data provided by airline A allows for analyses at realistic conditions. Figure 25 shows vertical flight profiles and corresponding fuel burn of two transatlantic flights performed by airline A. Take-off weight, flight profile, Mach number and ambient conditions (i.e. temperature) were matched to the reference data. Average head- or tailwind components were computed for each flight phase based on Mach number and ground distance information from FDR data. As can be seen from Figure 25, VarMission is able to reproduce the fuel burn of these flights at a good level of accuracy (in the order of +2%).

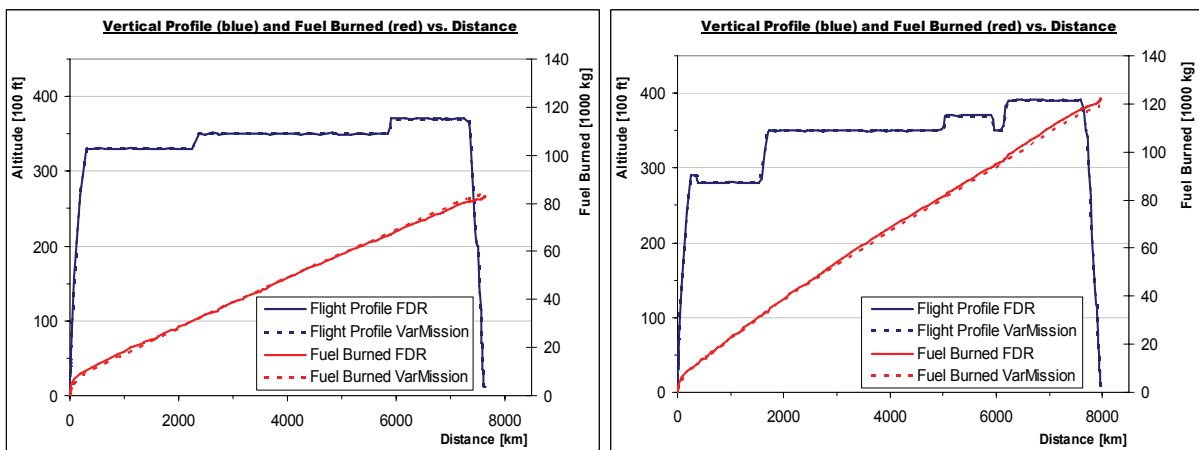


Figure 25: Comparison of mission fuel burn (B747-300, VarMission vs. FDR data)

A comparison between the available FDR data and VarMission calculations is presented in Table 8. The Boeing 747-300 model is able to reproduce the FDR fuel consumption quite well: The mean fuel burn error per flight is -0.2% for this aircraft at a standard deviation of 2.8%. The Airbus A310 model from VarMission / BADA underestimates total fuel burn from the reference source by 6.4% on average at a standard deviation of 1.8%.

Flight	Aircraft	Ground Distance [km]	FDR total fuel [kg]	VarMission total fuel [kg]	Delta fuel [%]
1	B747-300	7620	83000	84454	+1.75
2	B747-300	7961	122200	119601	-2.13
3	B747-300	7483	107600	111311	+3.45
4	B747-300	7382	87800	87508	-0.33
5	B747-300	6886	88300	88546	+0.28
6	B747-300	4500	54500	55766	+2.32
7	B747-300	1170	17100	16649	-2.64
8	B747-300	1229	17700	16745	-5.40
9	B747-300	4853	71800	70418	-1.92
10	B747-300	6901	109000	111521	+2.31
11	A310	4329	26127	24357	-6.77
12	A310	4233	25946	23654	-8.83
13	A310	5498	29719	28205	-5.09
14	A310	5467	37195	35375	-4.89

Table 8: Summary of fuel burn comparison with FDR data

Unfortunately, high-quality reference data like flight data recordings are rare and not publicly available. The large number of aircraft and engine types in the world fleet and the limited availability of aircraft performance reference data make a systematic validation of aircraft models difficult. Additional validation exercises were performed in a diploma thesis [1] including flight-phase-by-flight-phase validation of VarMission simulations and analyses of specific range data in cruise flight for an Airbus A330-200 aircraft. The author shows that the BADA model implementation in VarMission is able to reproduce the aircraft's specific range given in Airbus reference charts at good accuracy for operating points near the typical (BADA-suggested) cruise Mach number. Deviations occur at lower and especially at higher Mach numbers, as compressibility effects are currently not modelled by BADA (see chapter 3.2.2). Besides, payload range diagrams that were calculated with VarMission for both an Airbus A330-200 and a Boeing 737-800 match given reference data except for very low payload and very long range missions [1].

The aforementioned results indicate that the accuracy of VarMission's fuel burn calculations may vary with aircraft type, but should be sufficient for the purpose of global aviation studies. A number of third-party studies confirm these indications by comparing BADA model results with (mostly confidential) reference data. In a validation study for the inventory model SAGE, the Federal Aviation Administration (FAA) concludes:

- Point-by-point comparison of BADA-calculated fuel flows with FDR data for 10 flights and five different aircraft types resulted in a mean error of 6.95% at a standard deviation of 36.7%. Analysing additional FDR data for one more aircraft type and two flights, a mean fuel flow error of -0.24% at a standard deviation of 37.3% was found.
- Flight-by-flight comparisons of mission fuel burn between the SAGE model and airline statistics were conducted for two large samples of flights resulting in an error of <5% on average with no noticeable bias in any direction. The SAGE model uses BADA as main input for aircraft performance modelling [56].

Similar findings result from validation studies for the EUROCONTROL inventory tool AEM3, which also relies on BADA as the main source of aircraft performance data [41], [42], [44]. Analysing FDR information of more than 6500 flights of 14 aircraft types, EUROCONTROL studies find a mean fuel burn error on mission level of -6% to -3% if detailed trajectory information is available for all flights [44]. Standard atmospheric conditions and no winds are assumed in both the AEM3 and SAGE simulations. While BADA release version, model implementation and assumptions in the above mentioned publications vary, all studies indicate that the BADA methodology is suitable for modelling fuel burn and emissions of global aviation. The fuel burn error for individual flights varies with operating conditions and aircraft type, but can be expected to be within +/-10% on average if environmental conditions and trajectory information are available.

**3.2.5.2 VALIDATION OF EMISSIONS CALCULATIONS**

Well established correlation methods for the calculation of NO<sub>x</sub>, CO and HC emissions have been implemented in VarMission (see chapter 3.2.4). While the fuel burn model could be validated by comparing simulation results with flight data recordings, no such reference is available for emission calculations. Given the lack of real-world reference data on mission level, VarMission results can only be compared to results from other software, e.g. DLR’s VarCycle engine performance tool. This way, a correct implementation of the methods for NO<sub>x</sub>, CO and HC calculation can be assured.

Figure 26 presents NO<sub>x</sub> calculations obtained by use of the DLR fuel flow correlation for a Boeing 747-400 transatlantic flight with CF6-80C2B1F engines. The fuel burn calculated for this mission has already been validated (see Figure 24 on page 39). As can be seen in Figure 26, VarMission delivers in-flight emission indices for NO<sub>x</sub> that are well in line with results calculated by VarCycle. The VarCycle data are obtained by using VarCycle-produced look-up tables of emission index versus fuel flow, Mach number and altitude together with the VarMission aircraft performance model. Fuel flow and environmental conditions are calculated by VarMission while emission indices are obtained from the look-up tables. This way, deviations in the results of the two programs are only due to differences in the implementations of the emission correlation methods. As can be seen in Figure 26, total NO<sub>x</sub> emissions on mission level deviate by less than 0.1% between VarMission and VarCycle, which indicates a correct implementation of the DLR fuel flow method in VarMission.

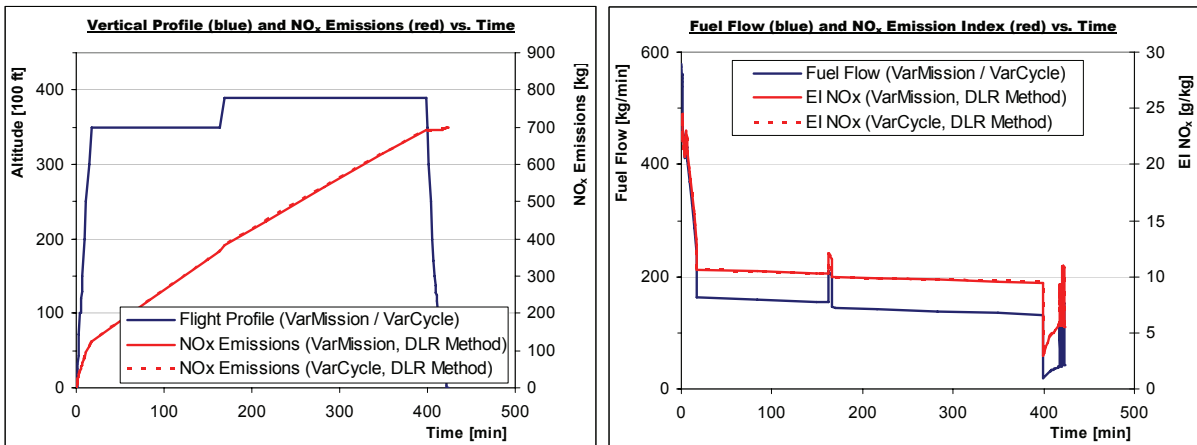


*Figure 26: Comparison of NO<sub>x</sub> emissions between VarMission and VarCycle (DLR method)*

While the DLR fuel flow correlation is the default method for NO<sub>x</sub> calculation in VarMission, the implementation of the Boeing fuel flow correlation for NO<sub>x</sub> emissions can also be validated against results from VarCycle. Total NO<sub>x</sub> emissions on mission level calculated by use of the Boeing fuel flow correlation also deviate by less than +/-0.1% between the two programs (see Figure 27).

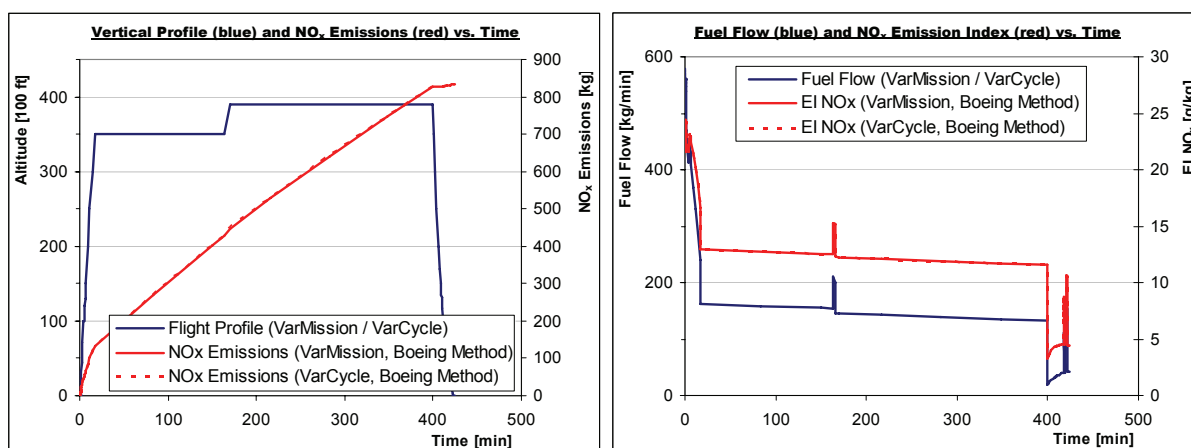


Figure 27: Comparison of NO<sub>x</sub> emissions between VarMission and VarCycle (Boeing method)

When comparing Figure 26 and Figure 27 it becomes obvious that a considerable delta exists between results of the DLR correlation and the Boeing method for NO<sub>x</sub> calculation. Both methods are supposed to predict NO<sub>x</sub> emissions at an accuracy of +/-10% [67]. In the example mission discussed above, total emissions calculated by use of the Boeing method are nearly 16% higher than results obtained by the DLR method. Calculations for global aviation described in chapter 4.2.4 find deltas between the DLR and Boeing methods in the order of 6-8% on average. As a consequence, any results for gaseous emissions of aviation are to be treated with care and should only be compared when obtained by the same method.

Unlike NO<sub>x</sub> emissions, which are mostly produced during take-off, climb and cruise flight, CO and HC emissions are emitted predominantly during descent, where engine thrust is low. Table 9 presents results for CO and HC emissions calculated for the aforementioned flight mission by both the VarMission and VarCycle implementations of the Boeing fuel flow method. Both the VarMission and VarCycle implementations of the Boeing fuel flow methods follow the original write-up of the method from [14] supplemented by corrections for some special cases described in [54] and [41]. As can be seen from the table, the results obtained by both tools are very close to each other (within +/-1%). This indicates a correct implementation of the Boeing fuel flow method for CO and HC emissions in VarMission.

	Fuel [kg]	NO <sub>x</sub> [kg] (DLR correlation)	NO <sub>x</sub> [kg] (Boeing correlation)	CO [kg]	HC [kg]
VarMission	63 800	699.6	834.2	95.3	7.24
VarMission+VarCycle*		700.2	834.4	95.6	7.24

\* Fuel Flow and environmental conditions from VarMission, calculation of emission indices by VarCycle.

Table 9: Comparison of emission calculations between VarMission and VarCycle on a Boeing 747-400 example flight mission



### 3.2.6 “EMISSION PROFILES” – LOOK-UP TABLES OF AIRCRAFT EMISSIONS

Given the large number of flights in the worldwide flight schedules, any microscopic simulation of global aviation requires low processing times per flight. The simulation of a flight by VarMission may take 5-10 seconds on a common personal computer. As a consequence, the use of look-up tables and interpolation methods is recommended in order to speed up calculations. For applications like global air transport studies, tabulated “emission profiles” can be created by VarMission for each aircraft-engine combination. The look-up data contain pre-calculated protocols of typical missions for several flight distances and load factors. Stored in text files these protocols are used by the Air Traffic Emissions Module described in chapter 3.3 and can also be used by DLR’s FATE software [26] for the production of global emission inventories (see chapter 3.3.7).

The file format used by FATE was extended for the VarMission-produced profiles in order to provide mission results as function of mission distance and load factor. For reasons of compatibility, the file structure used by FATE was retained. For each aircraft-engine combination, a set of emission profiles consists of the following files:

- An information file containing aircraft and engine names, the aircraft’s payload-range-capabilities and its characteristic masses (MTOW, MLW, OEW, Fuel Capacity). The file also lists the distances and load factors for which profile files are available.
- A number of profile files representing flight mission protocols. There is one profile file per simulated flight, i.e. for each mission distance and load factor. A profile file contains tabulated data of altitude, distance, fuel burn and emissions versus time.

A more detailed description of the file formats is found in Appendix C. For the purpose of this study, profile sets were produced for more than 500 aircraft-engine combinations. Each of these data sets comprises profile files for four different weight load factors (0%, 33%, 67% and 100% of the aircraft’s maximum payload) and 3-13 mission distances, depending on the aircraft’s maximum range. In total, more than 18,000 mission look-up tables for fuel burn and emissions were produced.

For calculating fuel burn, NO<sub>x</sub>, CO and HC emissions in world-wide emission inventories, profile sets were created for all BADA aircraft in combination with the engine types from the ICAO/FOI databases that can be attributed to the respective aircraft. Typical mission rules and flight profiles were assumed based on the mission description shown in Table 6 on page 31. VarMission’s default settings were applied for speeds, Mach numbers, cruise altitudes and thrust levels as described earlier in chapter 3.2.3. For simplicity, the International Standard Atmosphere (ISA) and no winds were assumed for the emission profiles. NO<sub>x</sub> emissions were calculated by both the DLR and Boeing fuel flow correlation methods while emissions of CO and HC were calculated by the Boeing fuel flow approach.



For the calculation of soot emissions, detailed engine models from the VarCycle software need to be used. Given the limited number of available VarCycle models, one representative engine model (with respect to soot emissions) was selected per aircraft type for which soot emissions were calculated. The selection of the representative engines was performed during DLR's PAZI-2 project [86] and will not be covered in this study.

Given a set of emission profiles for an aircraft-engine combination, mission fuel burn and emissions can be calculated for any flight distance and load factor by simple interpolation methods. Similarly, an average emission profile can be interpolated, including the vertical flight profile as well as fuel burn and emissions along this profile. For this purpose, each flight phase needs to be analysed separately. A VarMission module was created that performs such calculations using both linear and spline interpolation methods. The module can be run independently from VarMission's core routines and is used in the global air traffic module presented in the following chapter.

In addition to emission profiles intended for the analysis of flight missions, interpolation tables of holding fuel flow and emissions were created for each aircraft-engine combination. These tables contain fuel flow and emission indices during a holding flight segment as function of aircraft gross weight and flight level. The holding tables assume that an aircraft is flying racetrack holding patterns (4-minute circles) at the default holding speed suggested by BADA [43]. Using these tables and interpolation methods, fuel burn and emissions during the holding flight segments can be estimated. The tables are applied by the Air Traffic Emissions Module when considering inefficiencies in the Air Traffic System. More details will be described later in chapters 3.3.4 and 3.3.5.

### 3.3 AIR TRAFFIC EMISSIONS MODULE

#### 3.3.1 OVERVIEW

The air traffic module is required in order to calculate transport performance and emissions of global air traffic. The model focusses on commercial scheduled aviation, whereas military flights and general aviation are not considered. The approach chosen for this study supplements worldwide flight schedules by load factor data and combines them with fuel burn and emission calculations. Results are stored in a Flight Movements and Emissions Database in Microsoft Access format. A schematic of the air traffic model is shown in Figure 28. All database operations are automated using Visual Basic for Applications (VBA).

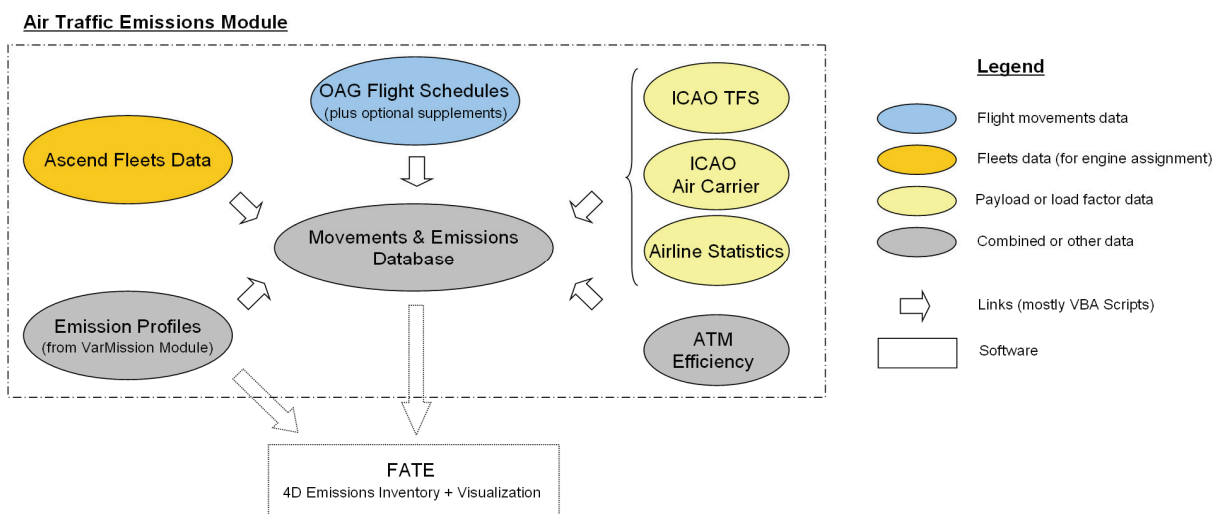


Figure 28: Schematic of Air Traffic Emissions Module with optional link to the FATE software

OAG flight schedules for the years 2000-2010 [100] are the core of the Movements and Emissions Database. Worldwide flight plans compiled by OAG contain information on all scheduled civil flights including – amongst other data – departure and destination airports, aircraft types, great-circle distances between the airport pairs as well as seat- and payload capacities for each flight. By linking ICAO statistics [77] to the OAG schedules, average load factors can be assigned to each flight. Combining these load factors with seat- and payload capacities from OAG, aviation's transport performance in terms of passenger- or ton-kilometres can be estimated.

For emission calculation, an engine type needs to be assigned to each flight. This is done stochastically based on historical aircraft and engine in-service numbers from the ASCEND Fleets Database [11]. Emissions are calculated for each flight based on the emission profiles generated by the VarMission module. Inefficiencies in the Air Traffic Management (ATM) system are accounted for by simulating increased taxi times, increased flight distances and additional holding phases compared to ideal conditions represented by the emission profiles.

The resulting Movements and Emissions Database contains information on flight movements, passengers and payload transported as well as fuel burn and emissions of NO<sub>x</sub>, CO, HC and soot for each flight. Database queries can be run easily using the Microsoft Access interface. As an option, the DLR's global emissions inventory software FATE can be linked to the Air Traffic Emissions Module to create four-dimensional emissions inventories<sup>10</sup>.

### 3.3.2 OAG SCHEDULES AND FLIGHT MOVEMENTS

The Flight Movements and Emissions Database is based on worldwide flight schedules collected in The Official Airline Guide (OAG) [100]. Schedules from OAG were selected for this study since information on actual aircraft movements from filed flight plans or radar trajectories are not publicly available. OAG schedules are used extensively in the field of aviation and airport research and can be regarded as a reference data source for such purposes. The OAG flight schedule for September 2000 was used in this study while no schedules were available for 2001-2002. For the years 2003-2005, OAG data for January and July could be analysed in cooperation with the DLR Institute of Air Transport and Airport Research. For 2006 to 2010, all twelve months are covered by available OAG data. Selected contents of the OAG flight schedules are shown in Figure 29.



Figure 29: Contents of OAG flight schedule data files

The flight schedules are converted into flight movements by filtering out ground services and helicopter flights and by splitting up entries with one or more intermediate stop(s) into single-leg operations. In a second step of the filtering process, duplicate entries in the database were identified and removed. All processes are automated using Microsoft Access and Visual Basic for Applications (VBA).

OAG data contain virtually all scheduled passenger flights, including services provided by most low-cost and leisure carriers. Some charter services operated on behalf of tour

<sup>10</sup> A 4D emissions inventory contains fuel burn and emissions per three-dimensional grid cell around the globe with an additional time code, see [113] for details.

operators and ad-hoc charters are not included in the OAG. Nevertheless, OAG data can be regarded as a good approximation for the air transport volume in the passenger sector [115]:

- According to EUROSTAT figures for 2007, non-scheduled flights account for about 12% of all IFR passenger flights from and to Europe [51]. As OAG data contains all scheduled and some of the unscheduled air traffic, the percentage of non-OAG passenger flights should be smaller than this figure.
- As some flights are typically cancelled, OAG will slightly overestimate the real traffic volumes from scheduled services. This overestimation may partly compensate for the unscheduled passenger flights not included in the schedules.
- A large fraction of non-scheduled passenger flights can supposed to be operated by small aircraft while flights by very large aircraft are mostly scheduled flights. As a consequence, the relative error in terms of passenger-kilometres and fuel burn should be smaller than the relative error for the number of flights.

For the air cargo market, by contrast, OAG's coverage of the worldwide air traffic is less satisfying [115]. While OAG comprises some scheduled cargo services, data on integrator flights and ad-hoc services are not included. These services, however, account for a relatively large part of the all-cargo market. According to EUROSTAT, more than one third of all air cargo shipments (measured in tonnes transported on flights from and to airports in the EU27 countries) were carried on non-scheduled flights in the year 2007 [51]. Consequently, OAG data for cargo air traffic are to be treated with caution. The evaluations presented in this study focus on passenger traffic, where the OAG coverage is much higher<sup>11</sup>.

### 3.3.3 LOAD FACTORS AND PAYLOAD

Analyses of aircraft emissions and transport performance require payload data. A flight's transport performance can be measured in passenger-kilometres or tonne-kilometres and is usually calculated by multiplying the payload transported by the great-circle distance between origin and destination airports. While flight schedules from OAG contain the great-circle distance as well as information on seat- and freight capacities, actual passenger numbers and the total payload need to be calculated. For this purpose, seat load factors and weight load factors need to be known. By definition, a weight load factor (WLF) is obtained by dividing the tonne-kilometres transported by the tonne-kilometres available. Similarly, the seat load factor (SLF) is calculated by dividing passenger-kilometres transported by available

---

<sup>11</sup> An experimental flight schedule containing all-cargo flights from and to Europe for the year 2010 has been compiled at the DLR Institute of Air Transport and Airport Research. Due to the limited regional scope of the schedule it was not used in this study.

seat-kilometres. For a given city pair the distances cancel out. As a result, the number of passengers and the total payload of a flight in kg are given by the following equations:

$$(12) \text{ Number of Passenger} = \text{SLF} \cdot \text{Number of Seats}$$

$$(13) \text{ Total Payload} = \text{WLF} \cdot \text{Payload Capacity}$$

While the number of seats and the freight capacity are given for each flight in the schedules, the (total) payload capacity in kg is not available from OAG. As a consequence, the following simplification is introduced:

$$(14) \text{ Payload Capacity} = \text{Number of Seats} \cdot \text{Passenger Weight} + \text{Freight Capacity}$$

The assumed passenger weight may vary with airline and type of service. An average passenger weight of 90 kg (incl. baggage) is used as a default value in ICAO statistics [77], [80]. For reasons of consistency, this value is also assumed in this study. SLF and WLF can be assigned to each flight in the OAG schedules using the data sources shown in Figure 30.

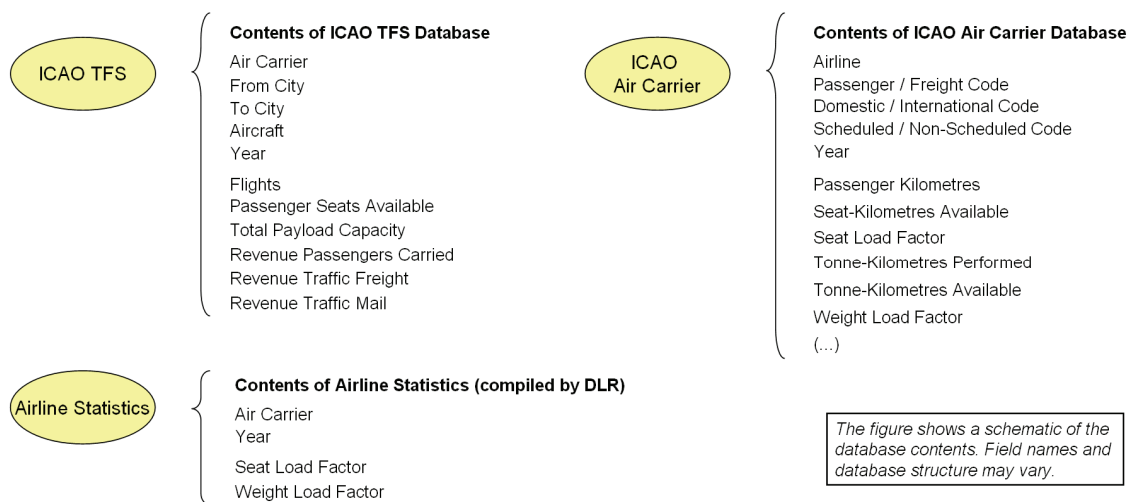


Figure 30: Contents of data sources for load factor assignment

The preferred source of load factor data is the ICAO Traffic by Flight Stage (TFS) database [77], which provides yearly statistics on passenger numbers, freight and mail carried per city-pair, airline and aircraft type. Since the number of seats and the total payload capacities are also available from this database, yearly averaged seat- and weight load factors can be calculated as follows:

$$(15) \text{ SLF}_{\text{TFS}} = \frac{\text{Revenue Passengers Carried}}{\text{Passenger Seats Available}}$$

$$(16) \text{ WLF}_{\text{TFS}} = \frac{\text{Rev. Passengers Carried} \cdot \text{Passenger Weight} + \text{Rev. Traffic Freight} + \text{Rev. Traffic Mail}}{\text{Total Payload Capacity}}$$

When assigning a TFS load factor to an OAG flight, the assignment function matches year, airline code, city pair and aircraft type from OAG to respective entries in the TFS database. In case no matching entry is found for the lowest level of data aggregation, the process is repeated for a higher level of aggregation (e.g. matching year, airline and city pair only). A schematic of the load factor assignment is shown in Figure 31. Due to different identifiers used for airlines, cities and aircraft in the OAG and ICAO databases, tables defining equivalencies between the identifiers from different sources have been created and are used for the automation of the load factor assignment.

**Principle of Load Factor Assignment**

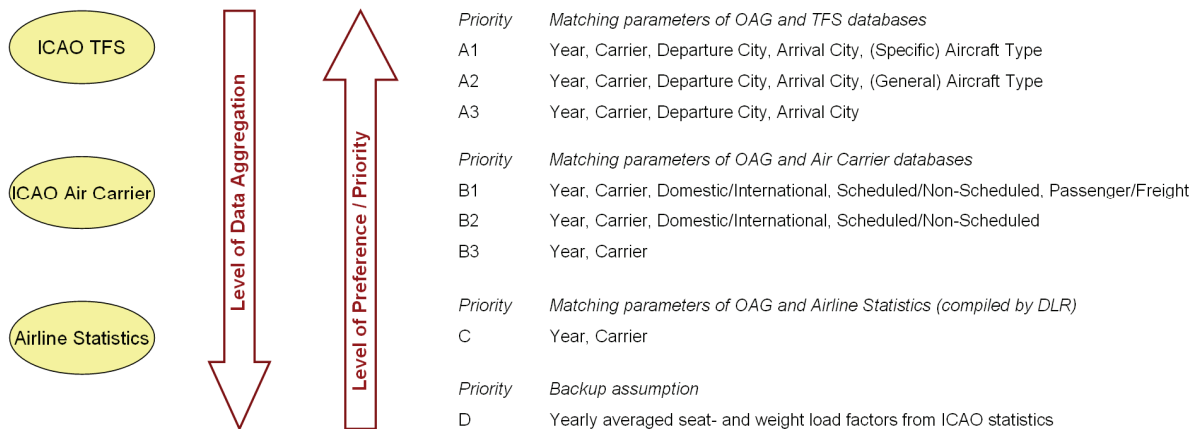


*Figure 31: Principle of load factor assignment*

Unfortunately, ICAO TFS information only includes data for international air traffic reported to ICAO by many (but not all) airlines. For flights with no suitable information in TFS, the ICAO Air Carrier statistics [77] are used as second-best data source. This database contains yearly averaged seat and weight load factors for a large number of airlines specified separately for passenger and cargo flights, domestic and international air traffic and scheduled or unscheduled operations. When assigning load factors from the ICAO Air Carrier statistics to an OAG flight, the assignment function tries to match year, airline, and types of service (i.e. domestic/international, passenger/freight, scheduled/unscheduled). Similar to the approach for TFS data, the load factors from the lowest available level of aggregation are chosen in the assignment process (see Figure 31).

As a third-best solution for flights with no matching entry in both ICAO statistics, yearly averaged airline-specific load factors from a DLR-compiled load factor database are used in the model. The information in this database was looked up manually in airline corporate reports or websites. Such load factor data was compiled for around 20 large airlines with no entry in the ICAO databases, mostly low-cost and holiday carriers like e.g. Ryanair or EasyJet. If no entry is found in this look-up table, average load factors for world-wide air traffic from ICAO statistics are assumed.

### 3.3.4 ATM EFFICIENCY

As radar trajectories of global aviation are not publicly available, generic flight profiles are used when calculating fuel burn and emissions of global air traffic. In addition, assumptions about inefficiencies due to Air Traffic Management (ATM) are required. ATM inefficiencies include ground-based delays as well as horizontal and vertical flight inefficiencies due to routing, holdings or altitude restrictions.

A recent assessment of global ATM efficiency performed by the Civil Air Navigation Services Organisation (CANSO) estimates an ATM system efficiency of 92-94% for the year 2005 [27]. In this report, 100% efficiency corresponds to an ideal system with all aircraft flying at the optimum trajectory and at the most fuel-efficient altitudes and speeds. A system efficiency of 92-94% implies a fuel burn penalty due to ATM measures of 6-8% on average compared to the ideal system. The total ATM inefficiency can be broken down as shown in Figure 32. Unfortunately, the individual contributions to system inefficiency are difficult to quantify on a worldwide level. So far, no comprehensive study on this matter exists. The CANSO reports quotes evaluations of regional air traffic service providers from Europe, the US and Australia, which indicate a total fuel burn penalty caused by ground operations in the order of 0.9%-1.4% and an airborne contribution of 5.5-7.9% [27].

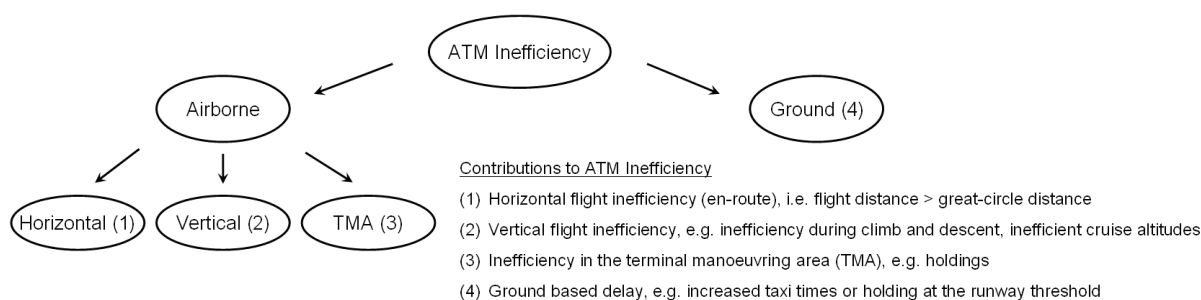


*Figure 32: Flight inefficiency due to Air Traffic Management (ATM)*

The following assumptions and simplifications are made when modelling ATM inefficiencies for the purpose of this study:

- An average ATM inefficiency of 7% is assumed for the year 2005. This figure, which is consistent with the CANSO report [27], is modified as function of time: A linear improvement of ATM inefficiency from 8% to 7% between 1999 and 2005 is assumed. Improvements for the years 2005-2050 according to industry goals [27] are simulated in the baseline forecast. More details will be described in chapter 3.4.6.
- Based roughly on the numbers quoted in the CANSO report [27], the overall ATM inefficiency is broken down into a component for taxiing on the ground (formula 17a) and an airborne component (formula 17b) as follows:



$$(17a) \quad \text{Inefficiency}_{ATM,ground} = 0.15 \cdot \text{Inefficiency}_{ATM}$$

$$(17b) \quad \text{Inefficiency}_{ATM,air} = 0.85 \cdot \text{Inefficiency}_{ATM}$$

- The airborne inefficiency is broken down further into horizontal (en-route), vertical and terminal area (TMA) components. A EUROCONTROL study from 2008 [50] estimates the vertical flight inefficiency as around 0.6% of total fuel consumption compared to 3.8% for the horizontal en-route inefficiency and 2.5%.-6.0% for TMA inefficiencies including holdings. Although this data is valid for the European airspace (with a slightly higher total inefficiency compared to the global average [27]), the value for the vertical inefficiency and the approximately equal shares of horizontal inefficiency and TMA contribution are assumed in the model:

$$(18a) \quad \text{Inefficiency}_{ATM,air,vertical} \approx 0.6\% = \text{const.}$$

$$(18b) \quad \text{Inefficiency}_{ATM,air,horizontal} = 0.5 \cdot (\text{Inefficiency}_{ATM,air} - \text{Inefficiency}_{ATM,air,vertical})$$

$$(18c) \quad \text{Inefficiency}_{ATM,air,TMA} = 0.5 \cdot (\text{Inefficiency}_{ATM,air} - \text{Inefficiency}_{ATM,air,vertical})$$

As can be seen from formula (18a), the vertical inefficiency component is assumed to be constant and is not affected by improvements of the ATM system efficiency with time. This simplification is due to model limitations: The emission profiles used for fuel burn and emission calculations simulate typical departure and arrival procedures and assume typical cruise altitudes derived from historical radar data (see Appendix D). As a consequence, the vertical ATM inefficiency is assumed to be included in the standard missions described by the emission profiles. Changing these procedures and parameters would require new sets of emission profiles. Considering the relatively small contribution of the vertical ATM inefficiency compared to the total system inefficiency, the improvement of the vertical component with time can be neglected. All other components that contribute to ATM inefficiency are modelled explicitly for the purpose of fuel burn and emission calculations. In principle, the following approach is taken:

- Taxi times of all flights are increased uniformly in order to reflect the given ground-based ATM inefficiency.
- Similarly, flight distances larger than the great-circle distances between origin and destination airports are assumed in order to model the horizontal flight inefficiency.
- Holding flight segments are created for all flights in the movements database in order to cover inefficiency due to TMA delays.

The details about the above approach will be described in the following chapter.



### 3.3.5 FUEL BURN AND EMISSIONS OF GLOBAL AIR TRAFFIC

#### 3.3.5.1 PROCEDURE FOR CALCULATING FUEL BURN AND EMISSIONS

Fuel burn and emissions of NO<sub>x</sub>, CO, HC and soot are calculated for each flight in the Flight Movements and Emissions Database. The calculations are based on look-up tables of aircraft emissions for standardized flight missions. These tabulated emission profiles are produced by the VarMission Flight Mission and Emissions Module for a large number of aircraft-engine combinations (see chapter 3.2.6). Using emission profiles and interpolation methods, fuel burn and emissions of global air traffic can be calculated at low processing times<sup>12</sup>. Initially, fuel burn and emissions are calculated for an ideal air traffic system without inefficiencies. In a second step, Air Traffic Management (ATM) inefficiencies are accounted for in order to determine corrected fuel burn and emission results. As a simplification, standard atmospheric conditions and no wind are currently assumed for these calculations.

Flight schedules from OAG contain information on aircraft types as well as the great-circle distances for each flight. Some additional data are required for emissions calculations:

- Aircraft Model Assignment: Each aircraft type from the OAG flight schedules needs to be assigned to a representative aircraft model from the VarMission module.
- Engine Type Assignment: In this study, engine types are assigned stochastically to a given aircraft type according to actual engine shares by airline and in the global fleet. The engine type is required for emission calculations.
- ATM Inefficiency: ATM inefficiency is considered by modelling increased taxi times, cruise distance extensions and additional holding flight segments. This way, the emissions impact of ATM can be estimated.

Flight schedules from OAG contain more than 200 specific aircraft types while the VarMission Flight Mission and Emissions module is based on 117 aircraft models from the EUROCONTROL BADA database. A table of equivalencies was created, which assigns a VarMission aircraft model to each aircraft type from OAG. It should be noted that most large civil aircraft are available as VarMission / BADA models whereas the broad spectrum of small aircraft (with less than 30 seats) cannot fully be covered by the BADA database. In case no aircraft model is matching an OAG aircraft, a model with similar fuel burn and emissions characteristics needs to be selected as representative model. While the selection of a representative aircraft is not a fully deterministic choice (and leaves some scope for expert judgement), criteria for the selection include the following aspects:

---

<sup>12</sup> Processing times are in the order of few minutes for a month of flight schedules. See chapter 3.2.6 for details.

- Take-off weight, year of entry into service.
- Number of seats and payload capacity, payload-range characteristics.
- Aerodynamic and engine configuration (i.e. number and type of engines).

The complete list of aircraft equivalencies is found in Appendix F. Moreover, the engine type from the ICAO [78] or FOI engine emissions databases [127] is required for emission calculations. A database of the global fleet of aircraft compiled by ASCEND Worldwide Ltd [11] was used to assign an engine type to each flight in the OAG schedules. By the use of this database, the relative shares of all engines in service on a given aircraft can be obtained. An excerpt of the database contents is shown in Figure 33.

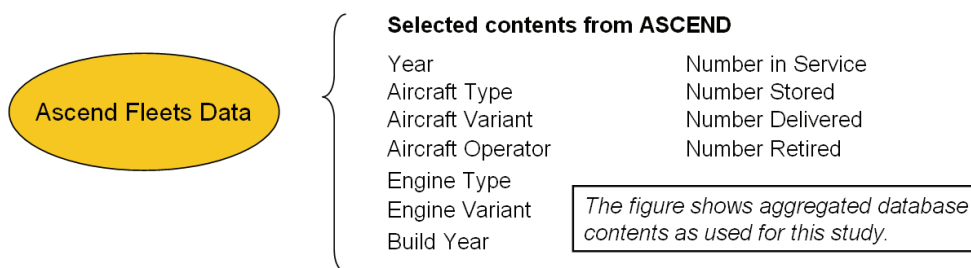


Figure 33: Selected contents of the ASCEND Fleets Database

In principle, the engine assignment to an OAG flight is performed in four steps:

- Step 1: The VarMission / BADA aircraft model used for the simulation of the flight is matched to one or more equivalent aircraft types or aircraft variants in the ASCEND Fleets Database using an equivalence table created for this purpose. Similarly, the airline code from OAG is matched to an aircraft operator from ASCEND.
- Step 2: Given the aircraft identifier(s) and the operator from the ASCEND Database as well as the year for which the flight schedule is valid, engine variants and their market shares on the aircraft type are obtained by a database query.
- Step 3: One of the engines obtained from step 2 is selected stochastically based on the respective market shares<sup>13</sup>.
- Step 4: The ASCEND engine identifier selected in step 3 is matched to an entry in the ICAO or FOI engine emissions databases by use of another equivalence table<sup>14</sup>.

The engine ID from the ICAO or FOI database is finally assigned to the given flight.

<sup>13</sup> A Monte Carlo simulation could be performed, but is currently omitted. Test runs of the assignment process lead to deltas of total aircraft emissions that are well below 1%.

<sup>14</sup> Sometimes more than one ICAO/FOI entry is matching the engine variant from the Ascend database; In these cases, an ICAO/FOI entry is selected randomly amongst the matching identifiers.

A slightly modified approach is followed for flight schedules of the year 2010, which are used as base year flight schedules for the Emissions Forecast Module. In order to simulate the future fleet rollover, the build year of the aircraft is required in addition to its engine type (see chapter 3.4.4). As a consequence, a build year is assigned stochastically to each flight depending on aircraft type and airline information from OAG. In a following step, the engine assignment process is performed separately by aircraft type, airline and build year.

Given aircraft and engine identifiers as well as great-circle distance and payload information, fuel burn and emissions of NO<sub>x</sub>, CO, HC and soot can be calculated for each flight. Emission profiles produced by the VarMission module are applied for this purpose. As the emission profiles are produced for a discrete number of flight distances and load factors, interpolation methods are used in order to calculate a flight's fuel burn and emissions. The results are also written to the Flight Movements and Emissions Database.

In an additional analysis step, inefficiencies due to ATM are accounted for. Inefficiency components are given as fraction of aviation's total fuel consumption in an ideal air traffic system. As was described in chapter 3.3.4, a vertical flight inefficiency of small magnitude is implicitly included in the precalculated emission profiles. For reference, the total fuel consumption for ideal conditions, i.e. without inefficiencies, can be estimated as follows:

$$(19) \quad TotalFuel_{ideal} = \frac{1}{1 + Inefficiency_{ATM,air,vertical}} \cdot \sum_{Flights} (FuelConsumption_{profiles} \cdot Frequency)$$

Apart from the vertical flight inefficiency, the following contributions to ATM inefficiency are considered in the model:

- A ground-based inefficiency component.
- A terminal manoeuvring area (TMA) flight inefficiency.
- A horizontal flight inefficiency component (en-route).

The above inefficiencies are modelled explicitly by simulating increased taxi times (ground-based inefficiency), holding flight segments at the destination airports (TMA inefficiency) and by extended flight distances compared to the great-circle distance between departure and arrival airports (horizontal flight inefficiency). This way, the corresponding emissions impacts can be estimated. Given the total fuel consumption for ideal conditions from formula (19), the fuel impact caused by the inefficiencies can be calculated as follows:

$$(20a) \quad AdditionalTaxiFuel_{ATM} = Inefficiency_{ATM,Ground} \cdot TotalFuel_{ideal}$$

$$(20b) \quad HoldingFuel_{ATM} = Inefficiency_{ATM,air,TMA} \cdot TotalFuel_{ideal}$$

$$(20c) \quad AdditionalCruiseFuel_{ATM} = Inefficiency_{ATM,Air,horizontal} \cdot TotalFuel_{ideal}$$

In order to simulate the horizontal flight inefficiency and to determine its effects on emissions, flight distances are extended such that the additional fuel burn given by formula (20c) is met. In an interim step, flight distances are extended as function of each flight's great-circle distance (see Figure 34). The average distance-dependency shown in Figure 34 was developed from EUROCONTROL and FAA statistics for the year 2008 (see Appendix G). After re-calculating fuel burn and emissions and evaluating the additional fuel burn from the interim assumptions, a correction factor can be applied uniformly to the en-route extensions of all flights in order to reach the fuel burn target set by formula (20c). This way, the distance-dependency of the en-route extension is maintained while at the same time an inefficiency level can be set as an input parameter.

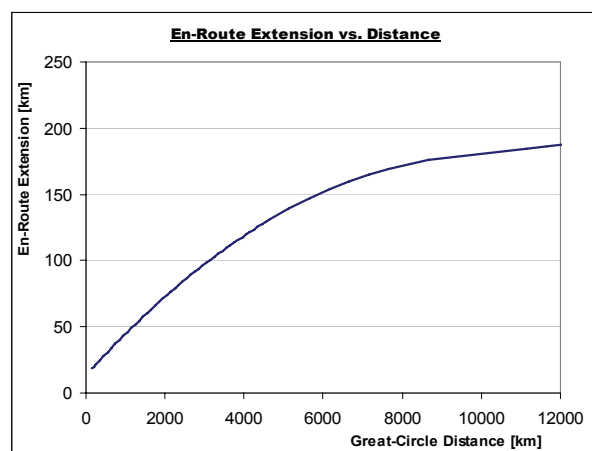


Figure 34: En-route extension vs. great-circle distance from EUROCONTROL statistics [48]

A similar approach is followed when modelling ground-based ATM inefficiency and TMA delays. As was described earlier in chapter 3.2.3, the flight mission represented by the emission profiles includes 16 minutes of ground operations with engines in idle. The 16 minutes are estimated to be an average timeframe required for engine start, taxi-out and taxi-in at airports in a system without inefficiencies. To consider ground-based inefficiencies, the taxi times of all flights are increased uniformly such that the additional fuel burn given by formula (20a) is reached. Furthermore, delays in the terminal area airspace are modelled by holding flight segments that are created for all flights from the movements database. The average holding time assumed uniformly for all flights can be chosen such that the fuel burn penalty described by formula (20b) is met. Fuel burn and emissions of the holding flight segments can be estimated by use of the holding data tables described in chapter 3.2.6.

In summary, corrected mission fuel consumption and emissions including average ATM inefficiencies can be estimated for each flight. The results are written to the Flight Movements and Emissions Database. More details regarding the consideration of ATM inefficiencies for calculating fuel burn and emissions are found in Appendix H.

### 3.3.5.2 SIMPLIFICATIONS AND UNCERTAINTIES

This section summarizes model simplifications for calculating fuel burn and emissions of global air traffic. Similar assumptions are used in other publications on global aviation emissions (e.g. [14], [53], [55], [90]) and include the following aspects:

- No consideration of wind and actual atmospheric conditions.
- Assumption of standardized (simplified) flight trajectories.
- No simulation of fuel tankering.
- No consideration of airframe and engine deterioration.

Head- or tailwinds alter the ground speed of an aircraft and influence fuel burn and emissions. If meteorological information is available, wind speed and actual atmospheric conditions can be considered by aircraft performance software in order to simulate the effects on fuel burn and emissions. Table 10 shows results of a parametric study performed by Boeing [14], which evaluates the influence of typical meteorological conditions in different seasons on the fuel consumption of long-range flights. According to this data, the fuel burn increase caused by wind amounts to less than 2% for typical weather conditions. Assuming actual air temperatures instead of ISA (International Standard Atmosphere) conditions leads to additional fuel burn of less than 1% for the examined flights. The error from neglecting wind and actual atmospheric conditions is considerably higher for individual flights in less favourable weather conditions. Considering the aforementioned results, an underprediction of fuel burn and emissions of well below 5% is expected on global average.

Changes to assumptions	Average fuel burn increase	Maximum fuel burn increase
No winds to actual winds	1.89% [B747, Route A] 1.15% [B747, Route B] 0.44% [B747, Route C] <i>four seasons average</i>	2.62% [B747, Route A] <i>autumn winds</i>
Standard temperature to actual temperatures	0.46% [B747, Route A] 0.29% [B747, Route B] 0.67% [B747, Route C] <i>four seasons average</i>	0.72% [B747, Route A] <i>summer temperatures</i>
No fuel tankering to actual practice	4.04% [B737, Route D] <i>averaged over a four-leg mission</i>	8.15% [B737, Route D] <i>first leg of a four-leg mission</i>
<i>Note: All missions are round-trips on the following routes: Route A = Los Angeles – Tokyo, Route B = New York – London, Route C = New York – Rio de Janeiro, Route D = Los Angeles – San Francisco.</i>		

*Table 10: Estimation of errors from model assumptions [14]*

Simplified flight trajectories based on a standardized flight mission description are assumed in this study. As was described in the previous chapter, a flight distance extension and other

inefficiency components caused by Air Traffic Management (ATM) are considered. Additional fuel burn resulting from operational airline decisions is not accounted for. Airlines often trade some fuel-efficiency against lower flight time in order to reduce delays or minimize their total cost of operation. The resulting fuel burn penalty is difficult to quantify for global aviation, but may be in the order of a few percent [94]. Furthermore, airlines tanker fuel on certain routes, i.e. carry more fuel than necessary in order to take advantage of fuel price differences between origin and destination airports. Fuel tankering may also be used to avoid refuelling at the destination airport and reduce the turn-around time for short-range flights. As the additional fuel carried on board increases the aircraft's weight, fuel tankering leads to additional fuel burn and emissions. In an evaluation by Boeing [14], the additional fuel burn resulting from such practice was quantified as 4% on an example route where fuel tankering is performed (see Table 10). As fuel tankering is mostly performed on short- and medium-range flights and, for economical reasons, is only attractive on certain airports, the total effect on aviation emissions is regarded as low. The Aero2k project report estimates the additional fuel burn due to fuel tankering as 0.5% of the fuel consumption by civil air traffic [53].

According to Airbus, the fuel-efficiency of an aircraft degrades by up to 5-7% after some years in operation [62]. Although maintenance reduces the impact on fuel consumption and emissions, such effects cannot fully be eliminated. Deterioration of the engine (by distortion or erosion of parts, buildup of deposits etc.) is regarded as more influential than airframe-related effects (e.g. surface misrigging, rough or deformed surfaces) [62], [53]. In addition to its influence on fuel consumption, aging of engine components may affect NO<sub>x</sub> emissions. According to Lukachko and Waitz, degradation of high-pressure combustor and high-pressure turbine have the largest impact on NO<sub>x</sub> production [91]. In a simulated aging scenario leading to an increase of engine SFC by 3%, NO<sub>x</sub> output during cruise flight was found to change by -1% to +4% depending on engine type [91]<sup>15</sup>. Such effects are not considered explicitly in the current publication. Aircraft performance models from the BADA database [46], which are used in this study, are not necessarily simulating new aircraft and may partly include aging effects. Considering the uncertainty regarding aircraft performance models and taking into account the mix of new and old aircraft in the global fleet, a 0-3% underprediction [53] of total fuel burn and emissions from neglecting aging effects seems plausible.

In total, simplifications in the model lead to a systematic underestimation of fuel use and emissions in the order of 5-10%. As will be discussed in chapter 4.2, additional uncertainty is caused by the incomplete coverage of air traffic in the OAG flight schedules [100].

---

<sup>15</sup> The -1% to +4% change of NO<sub>x</sub> emissions is caused by the opposing influence of turbine and compressor degradation on combustor inlet temperature (and hence NO<sub>x</sub> emission index, see [91] for details).

### 3.3.6 CONTENTS OF THE FLIGHT MOVEMENTS AND EMISSIONS DATABASE

As was described in the previous chapters, the Air Traffic Emissions Module consists of several database files in Microsoft Access format. These files include most prominently:

- The Flight Movements and Emissions Database.
- The VarMission Database including ASCEND Fleets data.
- The load factor data file including ICAO Traffic by Flight Stage (TFS), ICAO Air Carrier statistics and other load factor data.

Visual Basic for Applications (VBA) in combination with SQL database queries are used for linking database contents and for data operations in general. More information on structure and contents of the VarMission Database, the load factor databases from ICAO and the OAG flight schedules are found in Appendix I.

The Flight Movements and Emissions Database is built around OAG schedules and is the main database of the Air Traffic Emissions Module. It contains data from OAG supplemented by engine types, load factors and payloads for each flight. Furthermore, fuel burn and emissions calculated for each flight are collected in this database. In order to reduce the database file size, the original flight schedule tables delivered by OAG are split up into flight plan tables, carrier information, airports data and aircraft information. In accordance with the relational database model, unique identifiers are used in each table. Non-OAG data, i.e. supplements required for flight simulation and calculation results like fuel burn and emissions, are stored in a Mission Analysis Table. Figure 35 shows a schematic of the Flight Movements and Emissions Database. More detailed information is found in Appendix I.

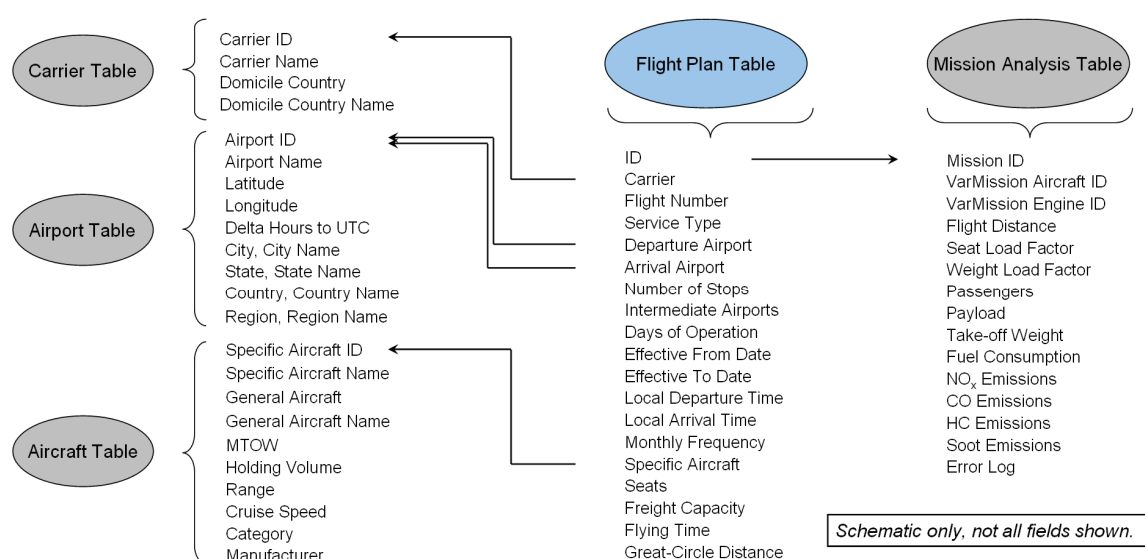


Figure 35: Contents and structure of the Movements and Emissions Database



### 3.3.7 LINK TO THE FATE GLOBAL INVENTORY SOFTWARE

The emissions inventory software FATE of the DLR Institute of Air Transport and Airport Research can be linked to the Air Traffic Emissions Module in order to create four-dimensional emissions inventories for global aviation. An emissions inventory contains fuel burn and emissions per three-dimensional grid cell around the globe, sometimes supplemented by an additional time code. Emission inventories for aviation are used for research on air transport's potential impact on climate change. More details about purpose and methodologies of emission inventories have been summarized in [113].

FATE uses the emission profiles produced by the VarMission module in order to calculate fuel burn and emissions of aviation (see chapter 3.2.6). Apart from emission profiles, flight movements stored in a text file are the main input to the FATE software. The movements file may also contain detailed radar trajectory information if such data is available. As an alternative, flight schedules from the Movements and Emissions Database of the Air Traffic Emissions Module can be used with FATE. In this case, FATE assumes each flight trajectory along the great-circle between departure and arrival airports, while assumed cruise altitudes correspond to those from the emission profiles. An export function has been developed as part of the Air Traffic Emissions Module that writes all necessary information from the Movements and Emissions Database to a FATE-compatible text file. The following information is required in order to create the flight movements input file for FATE:

- Airport coordinates, i.e. latitude and longitude for departure and destination airports: The airport coordinates of each departure and arrival airport can be obtained from data tables in The Official Airline Guide (OAG) [100].
- Universal Time Coordinates for departure and arrival times: For this purpose, the delta in hours between local time and UTC is determined for each airport in the movements database. Given the airport coordinates from OAG, the online webservice <http://ws.geonames.org/timezone> is used in order to obtain such data<sup>16</sup>.

While climate research is the main focus of the FATE software, it can also be used to visualize the regional and temporal variation of aviation's emissions. Figure 36 shows the regional distribution of scheduled aviation's CO<sub>2</sub> and NO<sub>x</sub> emissions in the year 2010. As can be seen in the figure, the majority of CO<sub>2</sub> and NO<sub>x</sub> is released in the Northern Hemisphere, mostly between 30° and 60° North latitude. Emissions of CO<sub>2</sub> are proportional to fuel burn. More diagrams showing the regional distribution of air traffic fuel consumption and emissions in the years 2000 and 2010 are found in Appendix V.

---

<sup>16</sup> The delta in hours between local time and UTC is returned by the webservice for both standard time and daylight saving time. The information is stored locally in the Movements and Emissions Database.



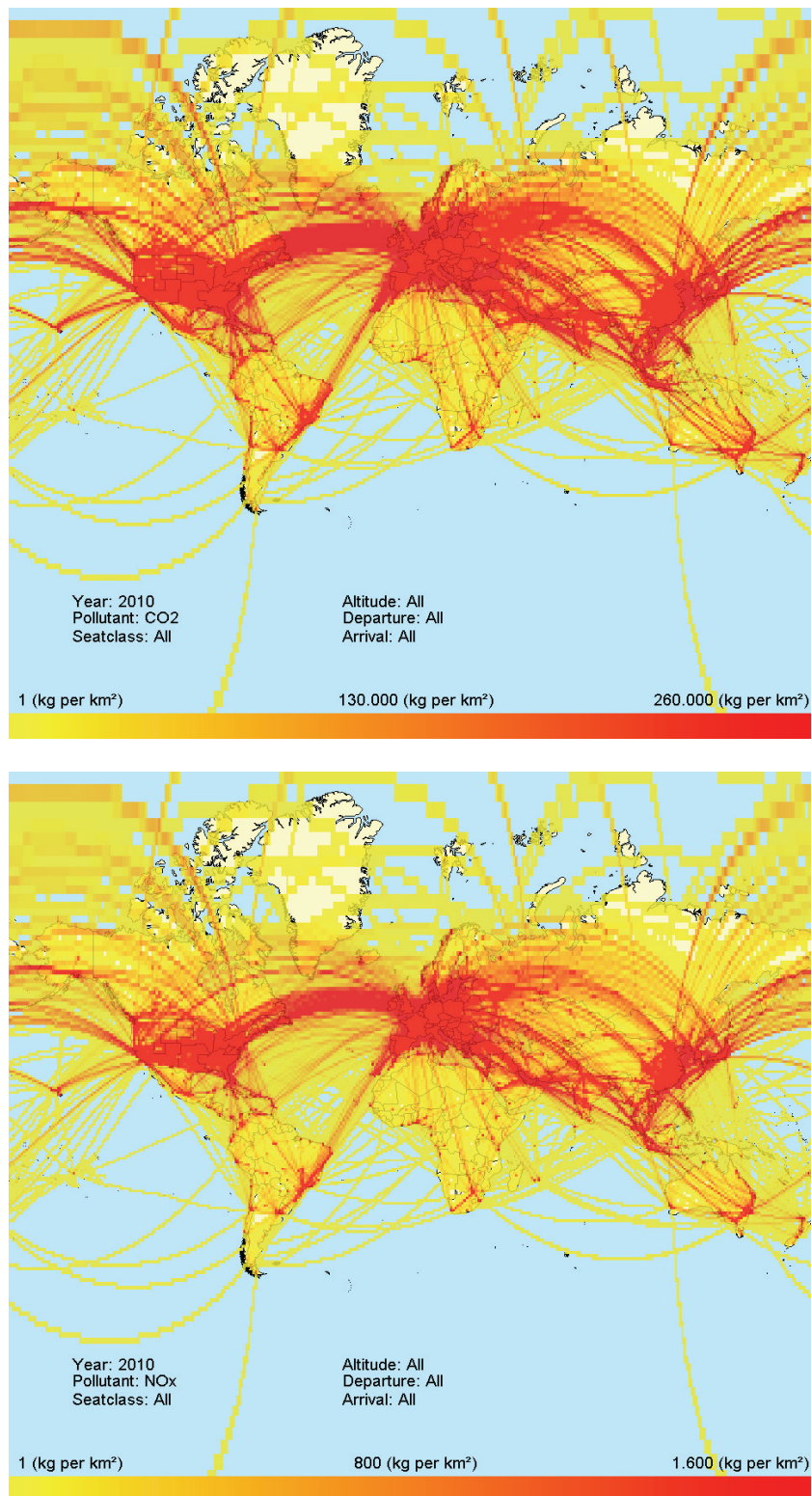


Figure 36: Visualization of scheduled aviation's CO<sub>2</sub> and NO<sub>x</sub> emissions (January - December 2010. Source: DLR-FW)

## 3.4 AIR TRAFFIC EMISSIONS FORECAST MODULE

### 3.4.1 OVERVIEW

The Air Traffic Emissions Forecast Module creates a Flight Movements and Emissions Database for a forecast year from given movements data for a base year. The module, which is fully automated, aims at simulating effects of new aircraft and engines on aviation's fuel burn and emissions. Traffic growth and fleet rollover are simulated and the base year flight movements are modified accordingly. Emission profiles for current and future aircraft-engine combinations have been produced by the VarMission Module (see chapter 3.2.6) and can be used to estimate air traffic's future fuel burn and emissions. Figure 37 shows a schematic of the Forecast Module.

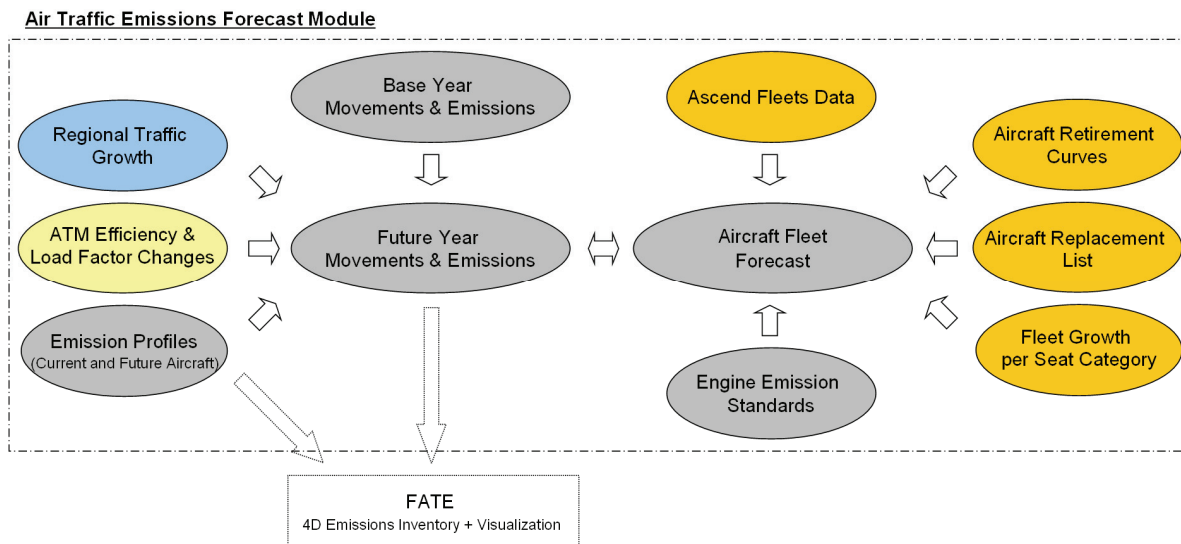


Figure 37: Schematic of the Forecast Module with optional link to the FATE software

In principle, the following tasks are performed by the Forecast Module:

- Regional traffic growth rates are applied to the monthly frequencies of flights in the base year Movements and Emissions Database.
- A fleet rollover model assigns new aircraft to flights from the movements database to account for the delivery of new aircraft and the retirement of older types. Emission standards for NO<sub>x</sub> and assumptions about future engine combustors are considered.
- Fuel burn and emissions of each flight are calculated by the use of emissions profiles for current and future aircraft-engine combinations.
- Non-aircraft related effects with influence on fuel burn and emissions, e.g. improved ATM procedures or load factor changes, are also considered by the Forecast Module.

The fleet rollover model implemented in the Air Traffic Emissions Forecast Module requires a year-by-year analysis until the final year of the forecast. In this study, aviation's fuel burn and emissions are forecasted for the years 2011-2030. A flight movements sample of one month is used for the traffic forecast (instead of a full year) in order to keep the database size within limits that can be processed by Microsoft Access. The flight movements of September 2010 were chosen as representative for the base year. Regional growth rates for passenger traffic and assumptions about the distribution of newly delivered passenger aircraft amongst seat categories are obtained from the Airbus Global Market Forecast (GMF) 2011-2030 [4]. As traffic growth rates and fleet information for cargo traffic are not contained in the latest GMF, this information is obtained from the Airbus GMF 2010-2029 [3]. Using a common database format with the Air Traffic Emissions Module described in the previous chapter, the Forecast Module can be coupled to DLR's FATE software in order to create global emissions inventories.

### **3.4.2 SIMPLIFYING ASSUMPTIONS FOR THE FORECAST**

While the database format of the Forecast Module is the same as for the Air Traffic Emissions Module, simplifications have been introduced in order to reduce the complexity of the model. These simplifications, which will be briefly covered below, include the following aspects:

- A reduction of the number of aircraft codes in the flight movements data compared to historical OAG flight schedules.
- A standardization of seat capacities and payload capacities per aircraft type.
- The use of a limited number of newly developed aircraft and engine models representing the most common commercial aircraft types of the near future.

More than 200 aircraft codes are found in the OAG schedules for the base year 2010. While most of these are specific aircraft codes which identify aircraft type and aircraft variant, for some flights only a general aircraft code is given. In this case, only the aircraft type (but not the aircraft variant) is known. In order to simplify the fleet forecast, about 30 aircraft codes were removed from the flight schedules: Flights with large commercial aircraft identified by a general aircraft code had the aircraft code replaced by one of the specific aircraft codes that can be attributed to the given general type. The replacement process was performed stochastically, based on the variants' actual fleet shares according to the ASCEND Fleets Database [11]. Furthermore, about 20 specific aircraft codes were replaced by other specific or general aircraft codes. This includes variants of older cargo aircraft and small aircraft types with piston engines, which were replaced by the respective general aircraft codes. A full list of the aircraft types that are used in the forecast model is found in Appendix N.

In the original flight schedules compiled by OAG, each flight has given seat- and freight capacities. Depending on airline policy, available seat- and freight capacities of an aircraft type may vary considerably. Comfortable seating configurations are often used on longer flights while high seat densities are typically found on short-haul flights. Furthermore, the most modern aircraft types are often used in more comfortable seating configurations than older aircraft of the same size and range category.

As future airline policies are difficult to predict and in order to reduce the complexity of the model, a simplified approach was chosen for modelling seat and freight capacities in the Air Traffic Forecast module. A flight's seat capacity is modelled as function of aircraft type and great-circle distance between origin and destination airports. Baseline seat capacities have been defined for each passenger aircraft type based on standardized seating configurations described by the manufacturers. The baseline seat capacities are corrected as function of aircraft category and great-circle distance based on a systematic evaluation of seat capacities from OAG flight schedules (see Figure 38). After estimating the actual seat capacity on a flight mission, the respective freight capacity is calculated considering aircraft-specific limits with respect to cargo volume and maximum structural payload. Following recommendations described in [77] and [80], a passenger weight of 90 kg (incl. 14kg of checked baggage), a baggage and cargo density of 161 kg/m<sup>3</sup> and a maximum loadability of 85% for baggage and cargo are assumed for this purpose. More details regarding aircraft capacities in the Air Traffic Emissions Forecast Module are found in Appendix K.

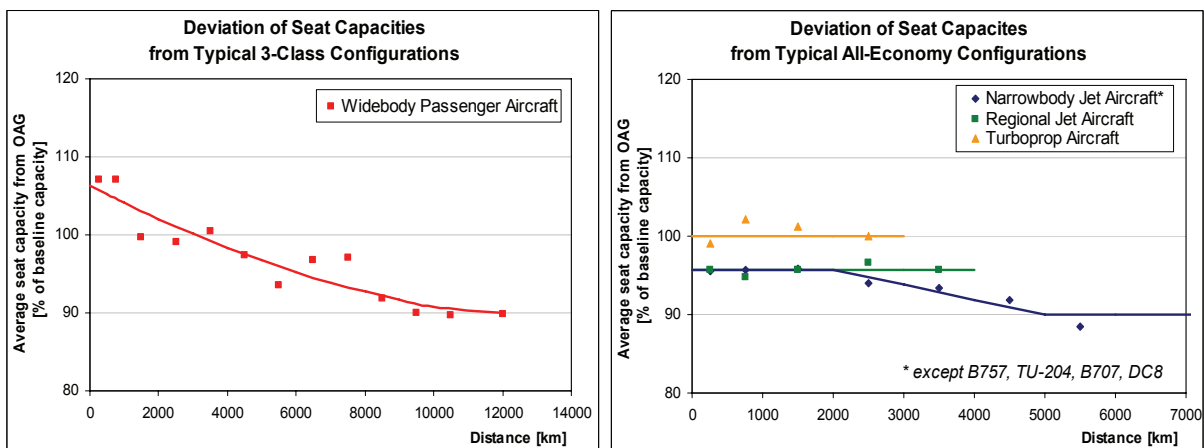


Figure 38: Deviation of OAG seat capacities from baseline seating configurations

Assumptions about future aircraft and engine types and their expected entry into service have been made, which are in accordance with announcements by aircraft manufacturers until December 2011. Only a limited number of new aircraft types are considered, with a focus on western-built commercial transport aircraft with more than 100 seats. Generic aircraft types like a future turboprop aircraft with 90 seats may represent two or more similar types from different manufacturers. Table 11 gives an overview on future aircraft for

passenger transport that are considered for the fleet forecast. Future cargo aircraft in the model include the Boeing 777F, 747-8F, 787F and 737-700C as well as the Airbus A330-200F, A380-800F and A350-900F. Considering the limited coverage of flight movements for cargo traffic, forecast results for the cargo sector will not be evaluated in detail. More information on the baseline fleet scenario will be described later in chapter 3.4.4.4.

	Aircraft Type and Variants	Seat Capacity	First Deliveries	Last Deliveries
Turboprops	ATR-42 / 72 Successor	50 / 70	2023 / 2017	> End of Forecast
	Bombardier DHC-8 Successor	70	2018	> End of Forecast
	Future Generic Turboprop (90 seats)	90	2020	> End of Forecast
Regional Jets	Bombardier CRJ1000	100	2011	2020
	Suchoi Superjet SSJ100-75 / 95	78 / 98	2015 / 2012	> End of Forecast
	Bombardier CSeries 100 / 300	110 / 130	2013 / 2014	> End of Forecast
	Mitsubishi MRJ 70 / 90	72 / 88	2017 / 2014	> End of Forecast
	Embraer ERJ/E-Jet Successor	50 / 70 / 98	2025 / 2018 / 2019	> End of Forecast
	Bombardier CRJ Successor	70 / 90	2020 / 2022	> End of Forecast
	Comac ARJ-21-700 / 900	90 / 105	2012 / 2015	> End of Forecast
Narrowbody Aircraft	Airbus A319 / A320 / A321 NEO	134 / 164 / 199	2017 / 2016 / 2018	> End of Forecast
	Boeing 737 MAX 7 / 8 / 9	140 / 175 / 187	2018 / 2017 / 2019	> End of Forecast
	Comac C919	134 / 164 / 199	2018 / 2016 / 2019	> End of Forecast
Widebody Aircraft	Boeing 787-8 / 9	237 / 280	2011 / 2013	> End of Forecast
	Airbus A350 XWB-800 / 900 / 1000	270 / 314 / 350	2016 / 2014 / 2017	> End of Forecast
	Boeing 747-8I	467	2012	2030
	Airbus A380-800 / 900	525 / 650	2008 / 2019	> End of Forecast
	Boeing 777 Successor	305 / 368	2019 / 2020	> End of Forecast

*New aircraft types and their year of introduction consider available information from industry until December 2011.*

*Table 11: Future passenger aircraft assumed in a baseline fleet scenario*

Simulation models for emissions calculation covering some of the most important aircraft types of the near future have been developed by the author. This includes a generic future regional jet similar to the Mitsubishi MRJ 90, models of the Boeing 787-8 and 747-8 as well as the Airbus A350 XWB-900. In addition, models of a family of narrowbody aircraft similar to the Airbus A320 NEO have been developed. Simple methods for preliminary aircraft design were used in order to create the aircraft models. Simulations of future aircraft engines were performed by DLR's VarCycle engine performance software based on available performance models. The engines' emission characteristics are based on information from literature (as far as available), supplemented by assumptions. Comparable to the approach in the Air Traffic Emissions Module, emission profiles have been created by the VarMission module for all aircraft-engine-combinations for which simulation models exist. The emission profiles are applied by the Forecast Module in order to calculate fuel burn and emissions for each flight. Aircraft types with no available simulation model need to be represented by similar types. Corrections are applied to results from existing models in order to estimate the emissions from such aircraft (see chapter 3.4.5). Furthermore, simplifying assumptions are made regarding gradual improvements of aircraft and engine types during their production periods. This aspect will be described later in chapter 3.4.6.



### 3.4.3 TRAFFIC GROWTH MODEL

A simple traffic growth model is used to estimate traffic volumes for a forecast year given the Flight Movements and Emissions Database for a base year. Average annual growth rates from the Airbus Global Market Forecast (GMF) 2011-2030 are used in this study, which are specified for different time periods and traffic flows [4], [24]. As cargo traffic is not covered in this edition of the GMF, growth rates for the cargo sector are obtained from the GMF 2010-2029 [3]. Growth rates for passenger traffic relate to aviation’s transport performance in revenue passenger-kilometres (RPK) while traffic growth in the cargo sector is measured in terms of freight tonne-kilometres transported (FTKT). An excerpt of the growth rates for passenger traffic is shown in Table 12. The full data tables are found in Appendix J.

From Region	Region Codes	Country Codes	To Region	Region Codes	Country Codes	Dom / Int	Average Annual Growth Rate		
							2011-2015	2016-2020	2021-2030
Western Europe	EU1		Western Europe	EU1		D	2.7%	2.9%	2.7%
Western Europe	EU1		Western Europe	EU1		I	3.8%	3.4%	2.8%
Western Europe	EU1		Africa Sub Sahara	AF2,AF3,AF4			5.3%	4.5%	3.9%
Western Europe	EU1		Asia	AS2,AS3,AS4			5.3%	4.5%	3.8%
Western Europe	EU1		Australia / New Zealand		AU,NZ		3.0%	3.4%	3.1%
Western Europe	EU1		Canada		CA		3.6%	4.6%	4.4%
Western Europe	EU1		Caribbean	LA1			3.8%	3.4%	2.8%
Western Europe	EU1		Central America	LA2			4.5%	4.3%	3.3%
Western Europe	EU1		Central Europe	EU2			7.3%	6.2%	4.7%
Western Europe	EU1		CIS		AM,AZ,BY,KZ,GE,KG,MD,TJ,TM,UA,UZ		5.6%	5.3%	4.5%
Western Europe	EU1		Indian Sub	AS1			7.9%	5.8%	5.7%
Western Europe	EU1		Japan		JP		2.0%	3.5%	2.8%
Western Europe	EU1		Middle East	ME1			7.9%	5.8%	4.6%
Western Europe	EU1		North Africa	AF1			6.1%	4.7%	3.9%
Western Europe	EU1		Pacific	SW1			5.1%	4.0%	3.2%
Western Europe	EU1		China		CN		7.4%	6.5%	5.4%
Western Europe	EU1		Russia		RU		5.8%	5.0%	4.4%
Western Europe	EU1		South Africa		ZA		3.5%	4.6%	4.9%
Western Europe	EU1		South America	LA3,LA4			5.8%	5.3%	4.6%
Western Europe	EU1		United States		US		4.5%	3.9%	3.6%

Table 12: Excerpt of regional growth rates for passenger air traffic [4], [24]

As can be seen in Table 12, country and region codes from the OAG flight schedules have been added to the original growth rate information from the Airbus GMF. The ‘Domestic / International’ field shown in the table can be utilized to specify growth rates between regions separately for domestic and international traffic. In principle, any growth rates defined by country pairs or region pairs can be used by the model. Given regional growth rates for both passenger and freight traffic, the growth rate assignment consists of three steps: Initially, growth rates are applied to passenger flights only. The service type information from the Movements and Emissions Database is used to identify the corresponding flight schedule entries. In order to identify the most appropriate growth rate for each flight, the departure and arrival countries are obtained from the flight schedules and are matched to available entries in the growth rate table. In case no match is reached for the lowest level of data aggregation, the process is repeated for a higher level of aggregation (e.g. matching departure and arrival regions instead of countries). Figure 39 presents a schematic with more details about the growth rate assignment.

## Principle of Growth Rate Assignment

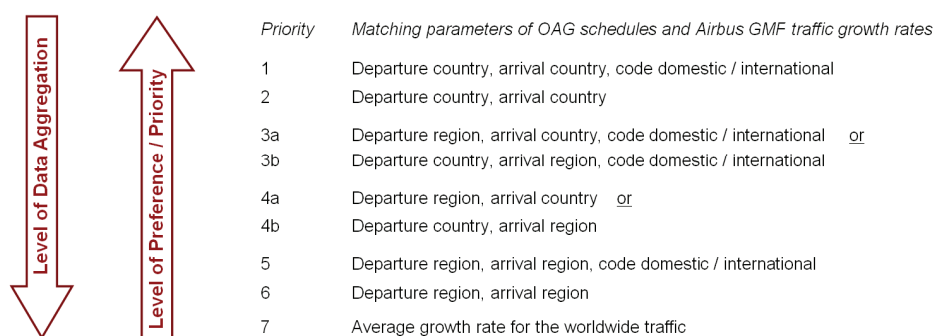


Figure 39: Schematic of traffic growth rate assignment

In a second step, freight traffic needs to be considered. As freight is transported on passenger and cargo flights, the freight tonne-kilometres transported (FTKT) have already increased after modelling traffic growth for the passenger segment<sup>17</sup>. Cargo flights need to take over the remaining FTKT that are required to reach the predicted growth. In a region-by-region analysis, regional growth rates for cargo flights are calculated such that the FTKT growth specified in the Airbus GMF are met. The newly calculated growth rates are applied to the frequency of cargo flights only.

The worldwide average growth of passenger-kilometres and freight tonne-kilometres resulting from the aforementioned steps is finally calculated and compared to the worldwide average growth rates for passenger and freight traffic given by the Airbus GMF. Due to differences in the regional coverage of flights movements between this study and the Airbus GMF, deviations of small magnitude may occur. These deviations are eliminated in the third step by applying correction factors on the frequencies of passenger and cargo flights. This way, the worldwide traffic growth in the model matches the growth in the Airbus GMF while, at the same time, regional differences in terms of growth rates are considered.

It is obvious that the use of regional growth rates in combination with flight movements data based on OAG flight schedules is a simple approach towards forecasting future air traffic. The air traffic growth model modifies the number of flights on existing routes, while new city pair connections or potential capacity constraints at airports are not considered. Internationally, a number of studies apply a similar model (e.g. [102]). The approach is not suitable for analyses that require a high granularity of the forecasted movements data, e.g. evaluations on city pair level. In combination with the fleet forecast model described in the following chapter, however, the approach should be sufficient to estimate aviation's fuel burn and emissions on global or regional levels.

<sup>17</sup> Assuming that passenger and weight load factors do not change. See chapter 3.4.6.3 for load factor changes.

### 3.4.4 FLEET ROLLOVER MODEL

#### 3.4.4.1 APPROACH AND ASSUMPTIONS

A fleet rollover model has been developed in order to simulate the modernization of the global aircraft fleet with time. New aircraft are introduced into the fleet in order to cope with traffic growth and to replace aircraft that are retired.

The modelling approach is based on the assumption that the yearly (or monthly) transport performance covered by an aircraft type is proportional to the number of aircraft in service  $n_{ac}$  of the given type. This simplification implies a constant average utilization of an aircraft type with time and at least similar operation patterns. Using capacity tonne-kilometres (often referred to as tonne-kilometres offered, TKO) as a measure of transport performance, the basic assumption can be written as follows:

$$(18) \quad TKO_{perAircraft_{ac}} = \frac{TKO_{ac}}{n_{ac}} = \text{constant for a given aircraft type}$$

The Air Traffic Emissions Forecast Module uses a base year Flight Movements and Emissions Database that is transformed into a database of forecasted flight movements by modelling traffic growth and fleet changes on a year-by-year basis (see Figure 37 on page 62).  $TKO_{ac, \text{ base year}}$  can be calculated for each aircraft type in service by a simple database query. On the other hand, the number in service  $n_{ac, \text{ base year}}$  of each aircraft type can be obtained from the ASCEND Fleets Database [11] and is known for the base year of the forecast<sup>18</sup>. Combining the information from movements data and fleet statistics, the transport performance per aircraft described by formula (18) can be calculated for each aircraft type that is in service in the base year.

For each run of the year-by-year forecast process, the fleet forecast modifies the aircrafts' fleet shares after the traffic growth model described in chapter 3.4.3 was applied to the base year movements data. After introducing traffic growth, the aircraft types' distribution in the forecasted flight movements are temporarily the same as in the base year. In case of (positive) traffic growth, this implies for each aircraft type a larger transport performance  $TKO_{ac, \text{ temp}}$  in the forecast year compared to the base year – even for aircraft that are no longer in production. This is corrected by the fleet forecast model in four steps:

- Step 1: The traffic growth  $TKO_{Growth, ac, \text{ temp}}$  between base year and forecast year is determined for each aircraft type.

---

<sup>18</sup> The original base year is the first base year of the year-by-year forecast, for which historical fleet statistics are available. During the forecast, the historical data is supplemented by forecasted aircraft numbers.



- Step 2: Using a fleets database in combination with assumptions about aircraft lifetimes, the number of aircraft that are retired between base year and forecast year are predicted for each aircraft type. By the use of formula (18), the retirement number can be converted into an equivalent transport performance  $TKO_{\text{Retirement, ac}}$ .
- Step 3: To simulate the delivery of new aircraft due to traffic growth and retirements of older aircraft, new aircraft need to be assigned to flights with a total transport performance of  $\sum_{ac} (TKO_{\text{Growth, ac, temp}} + TKO_{\text{Retirement, ac}})$ .  
In principle, flights of each aircraft type with a total transport performance of  $TKO_{\text{Growth, ac, temp}} + TKO_{\text{Retirement, ac}}$  are selected from all flights of the given type and have the aircraft replaced by in-production aircraft types of the same category.
- Step 4: Flights with newly assigned aircraft from step 3 may have their aircraft types changed again to in-production aircraft of a different capacity category. This is an optional step, which enables the definition of target delivery shares by category.

The four-step approach assumes that new aircraft are produced in numbers that are required to take over the transport performance assigned to retiring aircraft and, additionally, to cope with the forecasted traffic growth. For reasons of simplicity, limits regarding aircraft production rates are currently not considered. The ASCEND Fleets Database [11] provides reference statistics for the retirement analysis in steps 2-3 of the fleet forecast. Retirement curves, which specify an aircraft's fleet attrition rate as function of time, have been derived from historical fleet statistics and are applied by the forecast model. The details regarding aircraft retirements will be described in chapter 3.4.4.2.

The selection of suitable in-production aircraft for the aircraft assignment in steps 3 and 4 requires the definition of production or delivery periods for each aircraft type as well as the introduction of categories for aircraft with similar characteristics, e.g. with respect to range capabilities and payload capacities. In step 3 of the fleet forecast, a flight's original aircraft type can be replaced by in-production aircraft types of the same category while in step 4 the replacement aircraft is from a different category. In both cases, all in-production aircraft types of one category are considered as potential replacement candidates. The selection of a replacement aircraft type amongst the candidate types is performed stochastically and is based on given replacement probabilities (i.e. market shares of competing aircraft within a category). As different aircraft types may have different seat and payload capacities, each aircraft re-assignment to a flight schedule entry requires an adjustment of the flight's monthly frequency: When assigning a larger aircraft to a flight schedule entry, for example, the flight's frequency needs to be reduced such that the transport performance covered by the flight schedule entry remains unchanged. More details regarding the aircraft assignment in steps 3 and 4 of the forecast model will be described in chapter 3.4.4.3.

For aircraft types that are in production, the transport performance  $TKO_{ac}$  attributed to each type after steps 3 and 4 of the fleet forecast can be converted to forecasted delivery numbers assuming a given  $TKOperAircraft_{ac}$  value.  $TKOperAircraft_{ac}$  can be calculated for most aircraft types by use of formula (18) with data from the base year. For new aircraft types that are not yet in service in the base year of the forecast,  $TKOperAircraft_{ac}$  is initially unknown and needs to be estimated from data for existing aircraft types with similar size, range and operating pattern (see Appendix M). The forecasted delivery numbers and in-service numbers supplement historical fleet statistics from the ASCEND Fleets Database [11] and, consequently, are used for retirement analyses in later years of the forecast.

### 3.4.4.2 AIRCRAFT RETIREMENTS

In the forecast model, new aircraft are delivered in numbers that are required to replace retired aircraft and to cope with the assumed traffic growth. As a consequence, retirement numbers need to be predicted in each step of the year-by-year forecast. A set of functions has been developed in Visual Basic for Applications (VBA), which forecast the number of units in service of an aircraft type provided that no additional aircraft of this type are delivered. Referring to this forecasted number as  $n_{ac, Forecast Year, Temp}$ , the retirement number between base year and a forecast year is given by the following formula:

$$(19) \quad n_{Retirement, ac} = n_{ac, Base Year} - n_{ac, Forecast Year, Temp}$$

The ASCEND Fleets Database [11] provides historical fleet statistics, which are required for retirement analyses. The data used for the model consist of aircraft in-service numbers, deliveries and retirements by aircraft type and build year from 1945 to 2010<sup>19</sup>. Furthermore, the number of aircraft that are temporarily in storage is also given for each year. Depending on the aircraft type, one of the following methods is used to model the fleet attrition with time:

- Method 1: Linear projection of in-service numbers into the future, assumed for comparably old aircraft types with less than 15% of the originally produced units still in service in the year 2010.
- Method 2: Lifetime assumptions (retirement curves) are used for all other aircraft types. In principle, retirement curves specify an individual aircraft's "in-service probability" as function of aircraft age.

Method 1 is a simplified approach for a small number of aircraft types at the end of their operational lives. For such aircraft, historical in-service numbers from the ASCEND database cover nearly the complete in-service period of the aircraft type. As a consequence, trends are fairly easy to identify and in-service numbers can be projected into the future. Aircraft types with less than 15% of the originally produced number still in service in the year 2010 are classified into three groups, which are treated slightly differently: For aircraft of group 1, in-service numbers are linearly extrapolated from historical data. As a constraint for the fleet attrition rate it is assumed that all such aircraft are retired in the year 2015 or earlier. For aircraft of groups 2 and 3, a linear decrease of in-service numbers from 2010 onwards is assumed with all aircraft retired by 2018 and 2021 respectively. The classification into groups 1-3 was performed by personal judgement, based on trends determined from historical in-service numbers. Figure 40 shows two graphs with historical and forecasted in-service numbers obtained by Method 1.

<sup>19</sup> The numbers given for each year are end-of-year numbers, i.e. refer to the 31<sup>st</sup> of December.

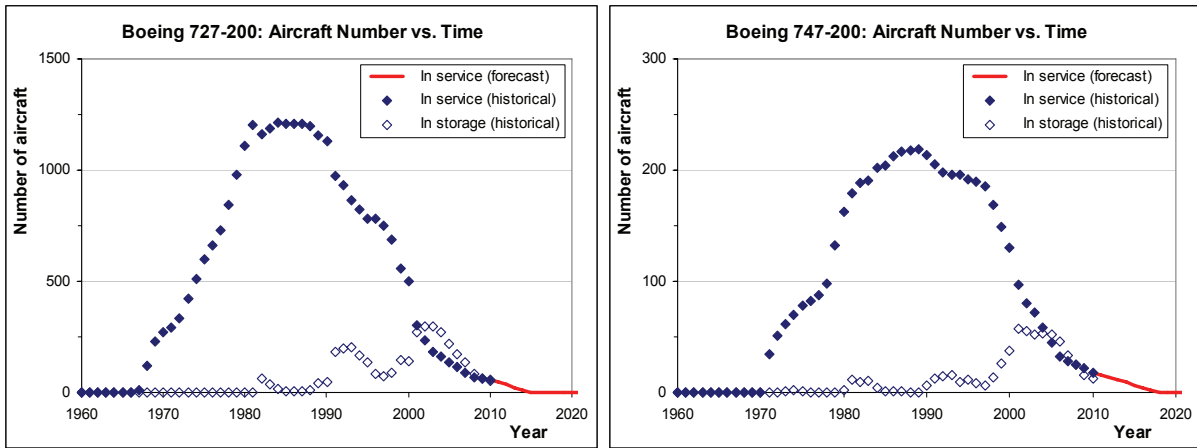


Figure 40: Examples of historical and forecasted aircraft numbers vs. time (method 1) [11]

Method 2 is the standard method to forecast aircraft retirements. Retirement curves specify an individual aircraft’s “in-service probability” or “survival fraction” as function of age and are used e.g. in the fleet forecast by ICAO CAEP [76]. Evaluations of historical fleet statistics have been performed for this study in order to derive typical retirement curves for widebody and narrowbody aircraft as well as for aircraft with turboprop engines. Figure 41 shows the resulting graphs and compares them to the retirement curves applied by ICAO CAEP.

While both diagrams indicate longer in-service times of narrowbody aircraft compared to widebodies, the newly developed curves seem to specify shorter lifetimes than the curves used by ICAO. This is particularly visible for narrowbody aircraft. The differences are most probably due to different definitions of the “survival fraction”: While ICAO considers passenger aircraft as out-of-service if they are either retired or converted to a freighter, the curves derived for this study additionally consider any (temporary) storage of aircraft. The probability of such storage events typically increases with aircraft age. More details about the statistical evaluation behind the newly developed curves are found in Appendix L.

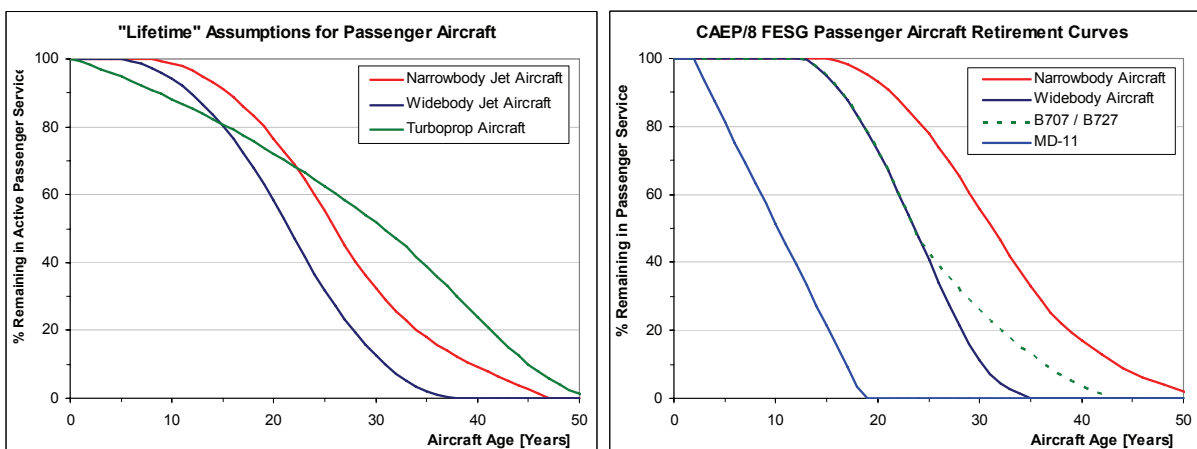


Figure 41: Typical retirement curves from this study (left) and ICAO CAEP (right) [76]

In this study, retirement curves are applied to predict the number of active aircraft by aircraft type and build year<sup>20</sup>. Given historical fleet statistics in combination with a retirement curve, the number of aircraft that remain in service in any future year is calculated as follows: for each build year, the aircrafts' age in the forecast year is known. In a second step, the corresponding "survival" percentage is obtained from the retirement curve. The total in-service number in the forecast year can finally be calculated as the sum of the "survivors" from all build years.

The retirement curves shown on the left hand side of Figure 41 reflect average lifetimes for three categories of aircraft and will be referred to as "reference curves" in the following paragraphs. It is obvious that aircraft life-spans not only vary between these categories, but may also differ by aircraft type. The equation of a reference curve is obtained by approximating its characteristic shape using linear, parabolic and cubic functions<sup>21</sup>. In order to consider differences between aircraft types, the following characteristic points of each reference curve can be modified:

1. The point at which (nearly) 100% of all aircraft are still in service.
2. The point at which 50% of all aircraft are in service.
3. The point at which (nearly) all aircraft are out of service.

Examples of derivative curves obtained by variation of the aforementioned three points are shown in Figure 42. This way, a broad range of aircraft lifetimes can be covered while, at the same time, the characteristic shape of a reference curve is maintained.

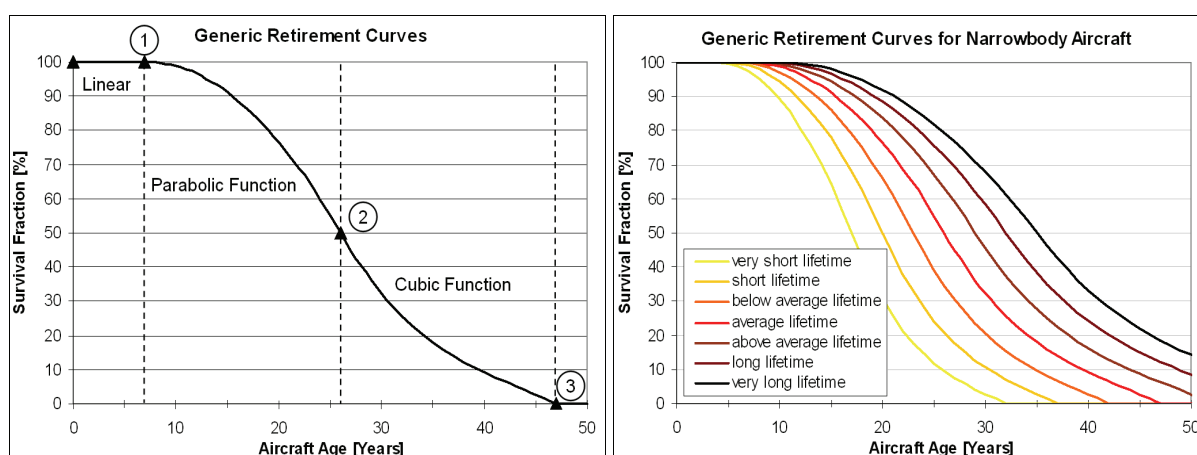


Figure 42: Example of reference retirement curve (left) and parameter variation (right)

<sup>20</sup> Unlike in ICAO studies [76], where retirement curves are applied to predict retirements of individual aircraft.

<sup>21</sup> In addition, the slopes of the parabolic and cubic segments at points 1 and 3 (see Figure 42) need to be given to fully describe the retirement curve. These parameters are assumed as constants.

Similar to the example shown in Figure 42, six variants have been derived from each reference curve by means of parameter variation. One of these curves is assigned to each aircraft type in the forecast model. The “best-fitting” curve was selected for comparably old aircraft types where available fleet statistics are covering both the full production periods plus at least ten years after production end. The ASCEND Fleets Database [11] was used to provide such statistics. In order to select the best curve for an aircraft type, all available retirement curves were initially applied to predict in-service numbers of the aircraft type up to the year 2010. Comparing the predicted numbers with the historical number of active aircraft from ASCEND, the curve which leads to the best fit can be identified by use of the least squares method.

Passenger aircraft with a production period ending in the year 2000 or later – this includes the current generation of aircraft and all future types – are assigned to the reference curves from Figure 41. Only few of these aircraft types had their retirement curve replaced after manual checks, if actual in-service numbers up to the year 2010 showed fundamentally different trends than obtained by use of the reference curves. For such aircraft types, retirement curves leading to more plausible results have been selected. A full list of all aircraft types and the associated retirement curves are found in Appendix N. Figure 43 shows example graphs of historical and forecasted in-service numbers obtained by the use of retirement curves.

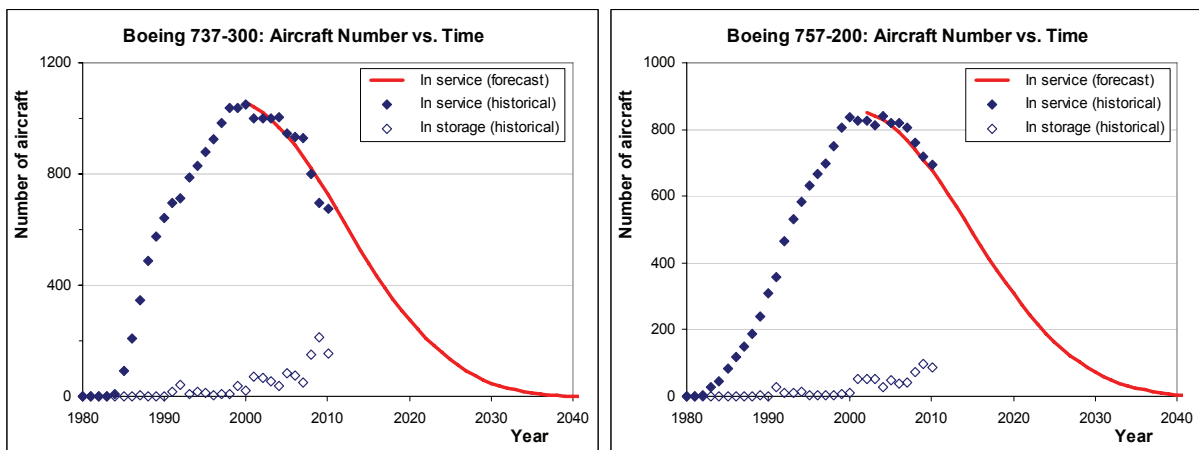


Figure 43: Examples of historical and forecasted aircraft numbers vs. time (method 2) [11]

A simplified approach is followed for cargo aircraft with a production period ending in the year 2000 or later. It is difficult to establish retirement curves for cargo aircraft from statistics due to rather heterogeneous lifetimes. As an approximation, a constant lifetime of 30 years is assumed for most widebody cargo aircraft and 25 years for narrowbody aircraft. Aircraft types with no available fleet statistics require additional assumptions for retirement analyses. Information on these special cases are compiled in Appendix M.

### 3.4.4.3 AIRCRAFT DELIVERIES AND ASSIGNMENT TO FLIGHT MOVEMENTS

#### *Modelling Aircraft Deliveries*

In each run of the year-by-year forecast, the number of aircraft deliveries is determined by the number of new aircraft required to cope with the forecasted traffic. The traffic growth model, which was described in chapter 3.4.3, increases the frequencies of flights from the base year flight schedule according to given traffic growth rates. In the temporary forecast flight schedule created by this module, aircraft types and their respective fleet shares are the same as in the base year. In case of (positive) traffic growth, this implies a larger transport performance in the forecast year than in the base year for each aircraft type. This is changed by the fleet rollover model, which partly re-assigns aircraft types to flights from the movements database. This way, aircraft retirements and the introduction of new aircraft-engine combinations can be considered by the model.

In the temporary forecast schedule, the expected traffic growth is distributed amongst all aircraft types from the base year. Newly delivered aircraft need to take over the transport performance in tonne-kilometres that reflects the assumed traffic growth as well as the transport performance of aircraft that retire. The total tonne-kilometres that need to be assigned to newly delivered aircraft can be described by the following formula:

$$(20) \quad TKO_{NewlyDelivered, Total} = \sum_{ac} (TKO_{Growth, ac, temp} + TKO_{Retirement, ac})$$

For each aircraft type, the transport performance growth  $TKO_{Growth, ac, temp}$  between base year and forecast year and the transport performance  $TKO_{Retirement, ac}$  corresponding to the number of aircraft that retire during this timeframe can be calculated as follows:

$$(21) \quad TKO_{Growth, ac, temp} = TKO_{Forecast, ac, temp} - TKO_{BaseYear, ac}$$

$$(22) \quad TKO_{Retirement, ac} = n_{Retirement, ac} \cdot TKO_{perAircraft, ac}$$

The transport performance in available tonne-kilometres (TKO) that can be covered by an aircraft type is assumed to be proportional to the aircraft number. The number of aircraft  $n_{Retirement, ac}$  that retire between base year and forecast year can be calculated as described previously in chapter 3.4.4.2.

As different aircraft types may have different seat and payload capacities, each re-assignment of an aircraft type to a flight schedule entry requires an adjustment of the flight's monthly frequency. The frequency needs to be corrected such that the available transport performance of the flight schedule entry remains unchanged. The frequency correction for replacing an old aircraft by a new type is calculated as follows:

$$(23) \text{ Frequency}_{new} = \text{Frequency}_{old} \cdot k_{\text{Frequency}}$$

$$\text{with } k_{\text{Frequency}} = \frac{\text{Seats}_{old}}{\text{Seats}_{new}} \quad \text{for passenger flights and}$$

$$k_{\text{Frequency}} = \frac{\text{PayloadCapacity}_{old}}{\text{PayloadCapacity}_{new}} \quad \text{for cargo flights.}$$

Formula (23) assumes that seat load factors and weight load factors are unaffected by an aircraft change. Chapter 3.4.6.3 will describe the methodology to deal with load factor changes during the forecast. Details regarding the aircraft re-assignment process to flights from the movements database are found in the following section. After completion of this process, delivery numbers per aircraft type can be estimated as described by formula (24):

$$(24) \ n_{\text{NewlyDelivered},ac} = \frac{\text{TKO}_{\text{NewlyAssigned},ac}}{\text{TKO}_{\text{perAircraft},ac}}$$

#### *Assignment of Newly Delivered Aircraft to Flight Movements*

In the Fleet Forecast Module, the introduction of newly delivered aircraft to the forecasted flight movements is performed in two consecutive steps:

- For each aircraft type from the temporary flight schedule (after traffic growth), flights with a total transport performance of  $\text{TKO}_{\text{Growth},ac,temp} + \text{TKO}_{\text{Retirement},ac}$  are selected randomly amongst all flights of the given aircraft type and have the original aircraft type replaced by newly delivered aircraft with similar characteristics.
- Flights with newly assigned aircraft from the previous step may have their aircraft types changed to in-production types of a different capacity category such that the total delivery numbers reflect expected delivery shares by category.

For aircraft types with an assigned retirement curve, the first step of the replacement procedure is performed separately not only by aircraft type, but also by aircraft build year. This way, the age distribution of the “surviving” fleet remains consistent with the assumed retirement curve. The redistribution of aircraft types in the second assignment step is optional and enables a more flexible evaluation of different aircraft fleet mixes in the forecast model. In both steps of the assignment, the selection of suitable aircraft types requires the definition of delivery periods per aircraft type. The delivery periods of older aircraft types are given by information from the ASCEND Fleets Database [11] and – for aircraft types with no such information available – by Jane’s All The World’s Aircraft [85]. For aircraft types that are in production in the base year of the forecast and for new aircraft types that are in development, assumptions for the first and last years of delivery are required.



The initial assignment of in-production aircraft types to flights from the movements database aims at replacing the original aircraft type by aircraft with similar characteristics in terms of seat capacity (or payload capacity for cargo aircraft) and range capability. The definition of groups of aircraft with similar characteristics is helpful to simplify such analyses. In order to select a suitable replacement aircraft in the model, each aircraft type is assigned to:

- One technology generation A-D: The generations are roughly defined by the aircrafts' production periods. Aircraft types of generations A-B are no longer in production in the first forecast year while generations C-D are in production or in development.
- A group of aircraft of the same generation and with similar characteristics in terms of payload and range capabilities. These aircraft types are treated as competing models in the same market segment.
- One or more groups of aircraft of the following generation, which can be expected to replace the given aircraft type. This does not apply to aircraft of generation D, which are typically assumed to remain in production until the last year of the forecast.

Figure 44 shows a schematic of the relations described above. By using these relations, aircraft replacement schemes as shown in Figure 45 can be simulated. When assigning a new aircraft type to a flight schedule entry, all competing aircraft types of the flight's original aircraft and all aircraft from the replacement groups are treated as potential replacement candidates. Replacement candidates of subsequent generations ("replacement candidates of replacement candidates") are also considered by the algorithm in the model.

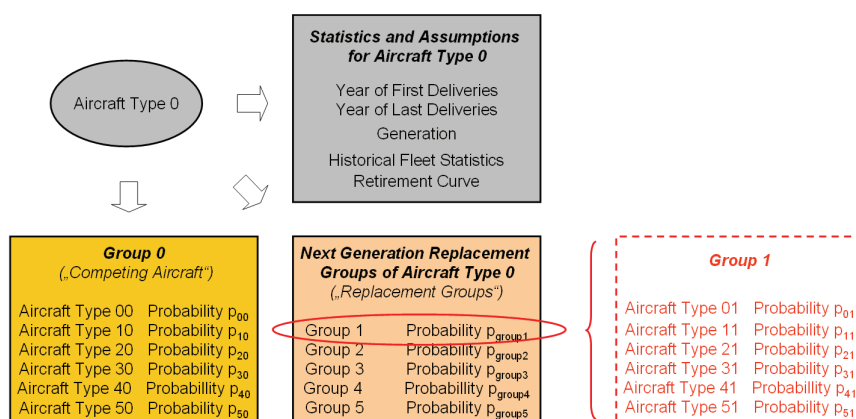


Figure 44: Schematic of relations between aircraft types

The new aircraft type for an individual flight schedule entry is selected stochastically from the replacement candidates. User-defined replacement probabilities are applied for this purpose. Within its group, each aircraft type is assigned to a replacement probability (or market share)  $p_{\text{Acft,Group}}$ . The next generation of potential replacement aircraft may consist of several groups. These groups are assigned to user-defined probabilities  $p_{\text{group}}$ .

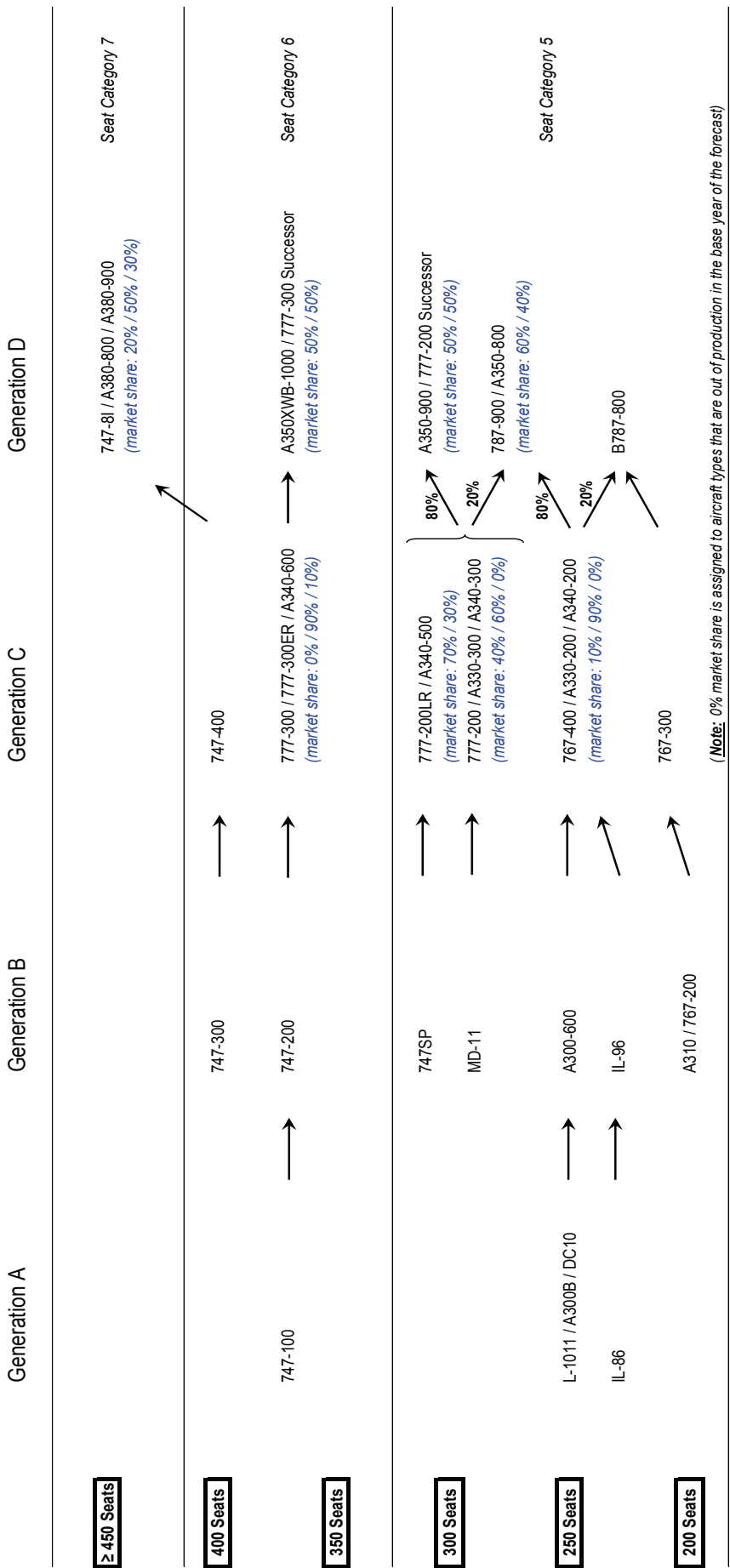


Figure 45: Example of an aircraft replacement scheme for widebody passenger aircraft

As a consequence, potential replacement aircraft of one generation have the following market shares:

$$(25) \quad P_{Acft,Gen} = P_{Group} \cdot P_{Acft,Group} \quad \text{with} \quad \sum_{Acft} P_{Acft,Gen} = 1$$

Formula (25) also applies to candidate aircraft of the same generation as the original aircraft type, i.e. from group 0. In this particular case,  $p_{Group}$  is equal to one.

Not all candidates of a given generation may be in production in a given forecast year. This needs to be checked by comparing the current forecast year with the aircrafts' delivery periods. The availability of a generation of replacement aircraft can be expressed as:

$$(26) \quad Availability_{Gen} = \sum_{AvailableAcft} P_{Acft,Gen} \leq 1$$

Considering aircraft availability, the replacement probabilities within one generation of replacement candidates need to be corrected as follows:

$$(27) \quad P_{Acft,Gen\_Corrected} = 0 \quad \text{for aircraft not available in the year of the forecast;}$$

$$P_{Acft,Gen\_Corrected} = \frac{P_{Acft,Gen}}{Availability_{Gen}} \quad \text{for all other aircraft.}$$

If replacement candidates of more than one generation are in production in the forecast year, the probability that the replacement aircraft is from a given generation is estimated as:

$$(28) \quad P_{Gen} = \frac{Availability_{Gen}}{\sum_{Gen} Availability}$$

Formula (28) is a rough simplification, but it should be sufficient to model (short) transition periods between different generations of aircraft. In summary, the probability of any candidate aircraft to be selected as a replacement aircraft can be expressed as:

$$(29) \quad P_{Acft} = P_{Gen} \cdot P_{Acft,Gen\_Corrected}$$

In order to estimate future market shares for in-production aircraft types, both the actual aircraft numbers in-service and the order backlog according to ASCEND fleets data [11] have been analysed (as far as available). If no market shares are available from ASCEND, all candidate aircraft types from one group have the same probability to be selected as a replacement aircraft. This simplification seems adequate, particularly for aircraft that are still in the development phase, considering the focus of this study on emissions (rather than manufacturers' market shares). An overview on the assumed groups of aircraft, market shares and replacement schemes by aircraft category are found in Appendix P.

During the initial aircraft assignment, base year aircraft types are replaced by new aircraft with similar characteristics. In a second step, flight schedule entries with newly assigned aircraft types may have their aircraft types changed again to in-production aircraft of a different aircraft category. This way, target delivery shares per aircraft category can be set as input parameters. The aircraft categories used for the re-distribution of aircraft types need not be identical with the groups of aircraft defined for the initial assignment. Expected delivery shares per seat category have been derived from the Airbus Global Market Forecast (GMF) 2011-2030 [4] and the Embraer Market Outlook 2011-2030 [38]. While the focus of the Airbus GMF is on large passenger aircraft, the Embraer Market Outlook is dealing mainly with regional aircraft. The seat categories applied in both publications are roughly compatible. Assuming the demand for aircraft above 100 seats as predicted by Airbus combined with the demand for smaller aircraft as forecasted in the Embraer Outlook, relative delivery shares per seat category have been determined (see Table 13). The respective shares for cargo aircraft are based on the Airbus GMF 2010-2029 [3].

All passenger aircraft types above 30 seats and all cargo aircraft types are assigned to one of the categories shown in Table 13. Given the delivery numbers per aircraft type resulting from the initial aircraft assignment process, deliveries per seat category can be calculated and deviations from the target delivery shares can be detected. In an iterative algorithm, flight schedule entries with newly assigned aircraft from the initial assignment have their aircraft types changed to aircraft of the next higher or lower seat category until the target distribution regarding aircraft deliveries is reached. Separate analyses are performed for passenger and cargo aircraft. When re-assigning aircraft types in this step of the simulation, all types of the “target category” that are in production are treated as potential replacement candidates. The specific aircraft type within the target category is selected stochastically, based on the candidates’ market shares in the initial assignment process.

No.	Seat / Capacity Category	Delivery Share 2011-2020	Delivery Share 2021-2030
1	30-60 seats*	1.2%	3.6%
2	61-90 seats*	13.4%	13.4%
3	91-120 seats*	11.5%	12.1%
4	121-210 seats**	51.4%	48.8%
5	Small twin aisle**	14.4%	11.7%
6	Intermediate twin aisle**	4.9%	6.0%
7	Very large aircraft**	3.2%	4.4%
101	Small freighter**	22.6%	
102	Medium / regional freighter**	46.6%	
103	Large freighter**	30.8%	
<i>* category from Embraer Market Outlook; ** category from Airbus GMF</i>			

Table 13: Aircraft deliveries by seat category derived from [3], [4] and [38]

### 3.4.4.4 AIRCRAFT PRODUCTION PERIODS

As was described in the previous paragraphs, new aircraft are delivered in order to replace retiring aircraft and to cope with the forecasted traffic growth. As a consequence, aircraft production- or delivery periods need to be defined for each aircraft type that is included in the fleet forecast. Figure 46 summarizes the delivery periods for the most important aircraft types as assumed in the baseline scenario of the forecast. In this scenario, the entry into service (EIS) of new aircraft types corresponds to published time schedules of aircraft manufacturers in December 2011 (see e.g. [6], [20]). For some aircraft types of the more distant future the EIS has been estimated by the author. As new aircraft types are introduced into the fleet, their predecessors are going out of production. A three years overlap of deliveries between old and new aircraft types with similar size and range characteristics is assumed. A full list of aircraft types and their delivery periods is found in Appendix N.

In addition to the baseline scenario shown in Figure 46, alternative fleet scenarios will be assessed in this study. These alternative scenarios, which include variations with respect to available aircraft types and their EIS, will be described later in chapter 4.4.



Figure 46: Aircraft delivery periods in the baseline scenario of the forecast

### 3.4.5 MODELS OF FUTURE AIRCRAFT-ENGINE COMBINATIONS

#### 3.4.5.1 APPROACH AND OVERVIEW

Performance and emission models of future aircraft-engine combinations are required in order to predict aviation's future emissions. Unfortunately, no performance models are currently available from the BADA database for aircraft types expected to be introduced in the near future (e.g. the Airbus A350 XWB or the Boeing 737 MAX). For such aircraft, predictions of fuel efficiency and limited information on other characteristic parameters are found in literature. At the time of writing, only preliminary estimates of engine performance and emission characteristics are available. The situation is even more difficult for aircraft and engines expected for the more distant future. Most prominently, a successor (or major update) of the Boeing 777 family can be expected to be introduced around the year 2020. As such aircraft and their engines are in an early phase of development, only estimates of fuel efficiency and emissions can be made.

In order to forecast aviation emissions, simulation models have been created covering selected aircraft-engine combinations of the near future. Simple aircraft models based on characteristic aircraft masses, drag polars and engine models provided by the DLR Institute of Propulsion Technology are used for this purpose. This approach is applied for the following aircraft:

- Models of the Boeing 787-8 and 747-8 as well as the Airbus A350-900 have been created. Using these simulation models, the development of fuel efficiency and specific NO<sub>x</sub> emissions is estimated for the widebody fleet.
- From the narrowbody segment, the Airbus A320 NEO family and a generic regional jet similar to the Mitsubishi MRJ-90 have been simulated. The A320 NEO models are also used to represent the Boeing 737 MAX for fuel burn and emissions calculation.
- Handbook methods for preliminary aircraft design have been applied to simulate a family of narrowbody aircraft similar in size and range to the Airbus A320. These aircraft are powered by an advanced turbofan engine and represent a technology level expected for the early 2020s. These aircraft models are used in a hypothetical fleet scenario only, which will be described later in chapter 4.4.4.

The aforementioned models will be discussed in chapters 3.4.5.2 to 3.4.5.4. For other aircraft types in the forecast, fuel efficiency and NO<sub>x</sub> emissions are estimated based on existing models for similar aircraft (or their predecessors). Assumptions about the effects of technological improvements compared to the reference models can be used to predict fuel efficiency and NO<sub>x</sub> emissions of such aircraft. This simplified approach, which will be described in chapter 3.4.5.5, is also used for aircraft of the more distant future.

### 3.4.5.2 WIDEBODY AIRCRAFT OF THE NEAR FUTURE

Some of the most important aircraft types that are expected to be introduced in the near future are simulated by newly created models. These comparably simple models, which are based on publicly available data, are intended to predict fuel consumption and NO<sub>x</sub> emissions on flight mission level and air traffic system level. Model parameters for which no information is found in literature are estimated by engineering judgement or using handbook methods for preliminary aircraft design described by Roskam [111] and Torenbeek [130]. Engine performance and emission models provided by the DLR Institute of Propulsion Technology [106] are used with the aircraft models to predict fuel burn and NO<sub>x</sub> emissions.

Three components determine fuel efficiency and specific emissions of the newly created aircraft-engine models: characteristic aircraft weights, aircraft aerodynamics and engine characteristics. Table 14 summarizes the characteristic weights assumed for widebody passenger aircraft of the near future. At the time of writing, no information on operating empty weight and maximum payload were available for the Boeing 787-8 and the Airbus A350 XWB-900. As a consequence, these parameters have been estimated. Assumptions for the cargo version of the Boeing 747-8 are found in Appendix S.

	Boeing 787-8	Airbus A350 XWB-900	Boeing 747-8I
Maximum take-off weight (MTOW) [kg]	219 539	268 000	442 253
Operating empty weight (OEW) [kg]	112 000 (est.)	132 000 (est.)	214 503
Maximum payload (MPL) [kg]	45 400 (est.)	60 000 (est.)	76 703
Maximum fuel capacity (MFC) [kg]	101 894	108 330	194 659
Source of data	Preliminary airplane characteristics [17]	Airbus specifications [6]	Preliminary airplane characteristics [17], [18]

*Table 14: Characteristic weights of future widebody aircraft*

Drag polars approximated by polynomials are used to reflect the lift-to-drag characteristics of the aircraft types. Mach-number dependent lift-to-drag ratios for the Boeing 787-8 could be obtained from a freely available model of this aircraft developed by Lyssis Ltd [93]. A parabolic drag polar for cruise flight at Mach 0.85 was estimated for the Boeing 747-8 by use of handbook methods for preliminary aircraft design [111], [130]. Figure 47 shows the lift-to-drag ratios assumed for the 787 in clean configuration, i.e. with gears, flaps and slats retracted. As an approximation, the drag polars of the 787 model are equally assumed for the Airbus A350 XWB. More information regarding the aerodynamic properties of the aircraft models is found in Appendix Q.

Two engine options are currently offered for the 787-8 consisting of the Rolls-Royce Trent 1000 and the General Electric GENx-1B. The Rolls-Royce Trent XWB engine is assumed for the A350 XWB-900. Performance models of engines similar to the GENx-1B and Trent XWB have been developed at the DLR Institute of Propulsion Technology [106]. These models are simulated by the VarCycle engine performance software based on preliminary performance



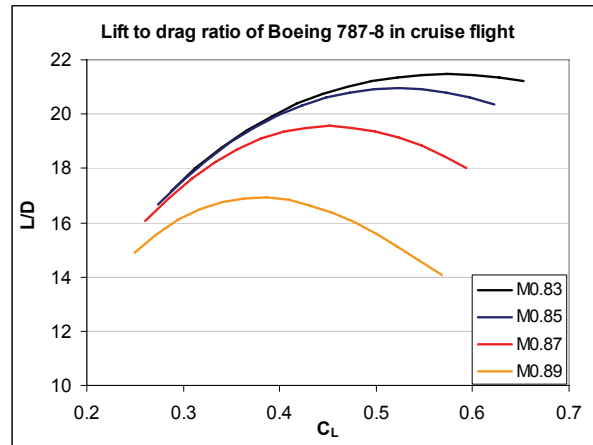


Figure 47: Lift-to-drag characteristics assumed for a model of the Boeing 787-8 [93]

data for the engine types mainly from [29] and [110]. No detailed performance models are available for the GENx-2B engine of the Boeing 747-8 and the Trent 1000 for the 787. Assuming a similar technological level for the Trent 1000 as for the GENx-1B, the fuel burn of a 787 with Rolls-Royce engines is assumed to be equal to the GENx powered aircraft variant. Differences in the NO<sub>x</sub> emissions between GENx and Trent 1000 are accounted for, as will be described below. A modified version of the GENx-1B model is applied to provide engine performance and NO<sub>x</sub> emissions for the 747-8<sup>22</sup>. Table 15 shows selected engine parameters according to the models created for this study.

Using sea level emissions of NO<sub>x</sub> as a reference, in-flight emissions from the engines are calculated by use of emission correlation methods. At the time of writing, the engines' emission indices of NO<sub>x</sub> have not yet been published in the ICAO emissions database [78]. Instead, NO<sub>x</sub> emission indices for sea-level static (SLS) conditions have been estimated based on the characteristic NO<sub>x</sub> levels that are predicted by engine manufacturers (see Figure 48). For the Rolls-Royce engines, NO<sub>x</sub> emissions in cruise flight are calculated by use of the DLR fuel flow correlation [31] assuming a single stage combustor. A combustor with TAPS (twin annular premixing swirler) technology is simulated for the GENx model using a

Flight phase	GENx-1B		Trent XWB	
	Cruise <sup>1</sup>	Take-off <sup>2</sup>	Cruise <sup>1</sup>	Take-off <sup>2</sup>
Thrust F [kN]	45	298	55	373
Overall pressure ratio π	37.5	42.6	39.5	43.9
Bypass ratio μ	10.2	9.2	13.6	12.1
Turbine entry temperature TET [K]	1486	1805	1522	1835
SFC [g/kN/s]	15.1	7.6	14.7	7.0

<sup>1</sup> Typical cruise at FL350, M0.85, installed engine; <sup>2</sup> Max. thrust for SLS conditions, uninstalled.

Table 15: Engine parameters of simulated engines for widebody aircraft [106]

<sup>22</sup> Assuming a 2% increase in SFC for the GENx-2B due to its lower fan diameter (see Appendix Q).

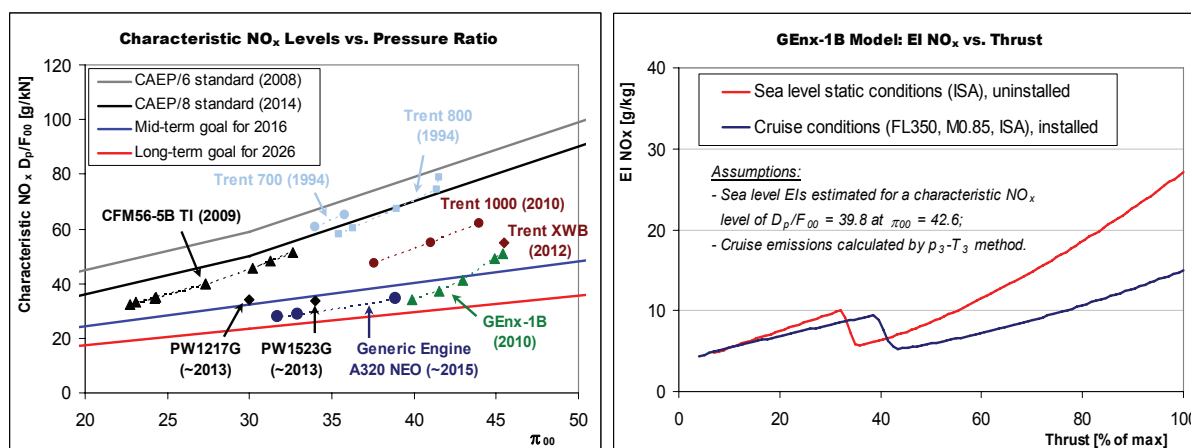


Figure 48: Characteristic NO<sub>x</sub> levels assumed for engines of the near future (left) [78], [110] and NO<sub>x</sub> emissions as function of thrust assumed for the GEnx-1B model (right) [106]

p<sub>3</sub>T<sub>3</sub> approach [119]. The switching point from pilot mode to the combined pilot/main mode is assumed to occur at a constant temperature T<sub>3</sub>. During cruise, the model is operating in the pilot/main mode resulting in comparably low NO<sub>x</sub> emissions. The emission characteristics assumed for the GEnx-1B model are shown in the right diagram of Figure 48. Emission indices assumed for the Trent 1000 and Trent XWB models are found in Appendix Q.

Given characteristic aircraft weights, drag polars and engine models, fuel consumption and NO<sub>x</sub> emissions can be calculated by the VarMission software. Figure 49 compares fuel efficiency and NO<sub>x</sub> emissions of the aircraft models to results for similarly sized reference aircraft [46]. Engine types with average NO<sub>x</sub> emissions (i.e. average D<sub>p</sub>/F<sub>00</sub> according to year 2010 fleet statistics) are assumed for the reference aircraft if more than one engine option is in service on the aircraft type. The graphs refer to flight missions performed at the aircrafts' maximum payload and assuming typical mission rules described earlier in chapter 3.2.3. Considering the limited and preliminary input data for the aircraft and engine models, the results shown in Figure 49 should be seen as estimates.

For flights between 3000 and 8000 km, the Boeing 787 model has a specific fuel consumption that is 16% lower than for the Airbus A330-200. This number compares well to claims by Boeing predicting fuel efficiency improvements near 20% compared to existing aircraft [22]. Specific NO<sub>x</sub> emissions were found to be 33-35% lower for a 787-8 with GEnx-1B engines compared to the A330-200 powered by Trent 772 engines. For the 787-8 with Trent 1000 engine model, however, specific NO<sub>x</sub> emissions are calculated to be about 23% higher than for the reference aircraft. Considering the single stage combustor of the Trent 1000 in combination with its high pressure ratio and bypass ratio, comparably high NO<sub>x</sub> emissions on mission level seem plausible. The high bypass ratio of the Trent 1000 leads to a strong decline of maximum thrust with altitude. As a consequence, operating temperatures in cruise flight and hence NO<sub>x</sub> emissions are higher than for engines with lower bypass ratio.

The model representing the Airbus A350 XWB-900 with Trent XWB engines is found to be 25% more fuel-efficient than the Boeing 777-200ER with Trent 892 engines while the difference in terms of specific NO<sub>x</sub> emissions is in the order of 38-40%. When comparing the Boeing 747-8I with GENx-2B engines to its predecessor, the new aircraft's fuel efficiency is 14% better on average. The deltas are in line with predictions by the manufacturers (see [7], [21]). According to the models, specific NO<sub>x</sub> emissions of the 747-8I are 35% lower than for the 747-400 with PW 4056 engines.

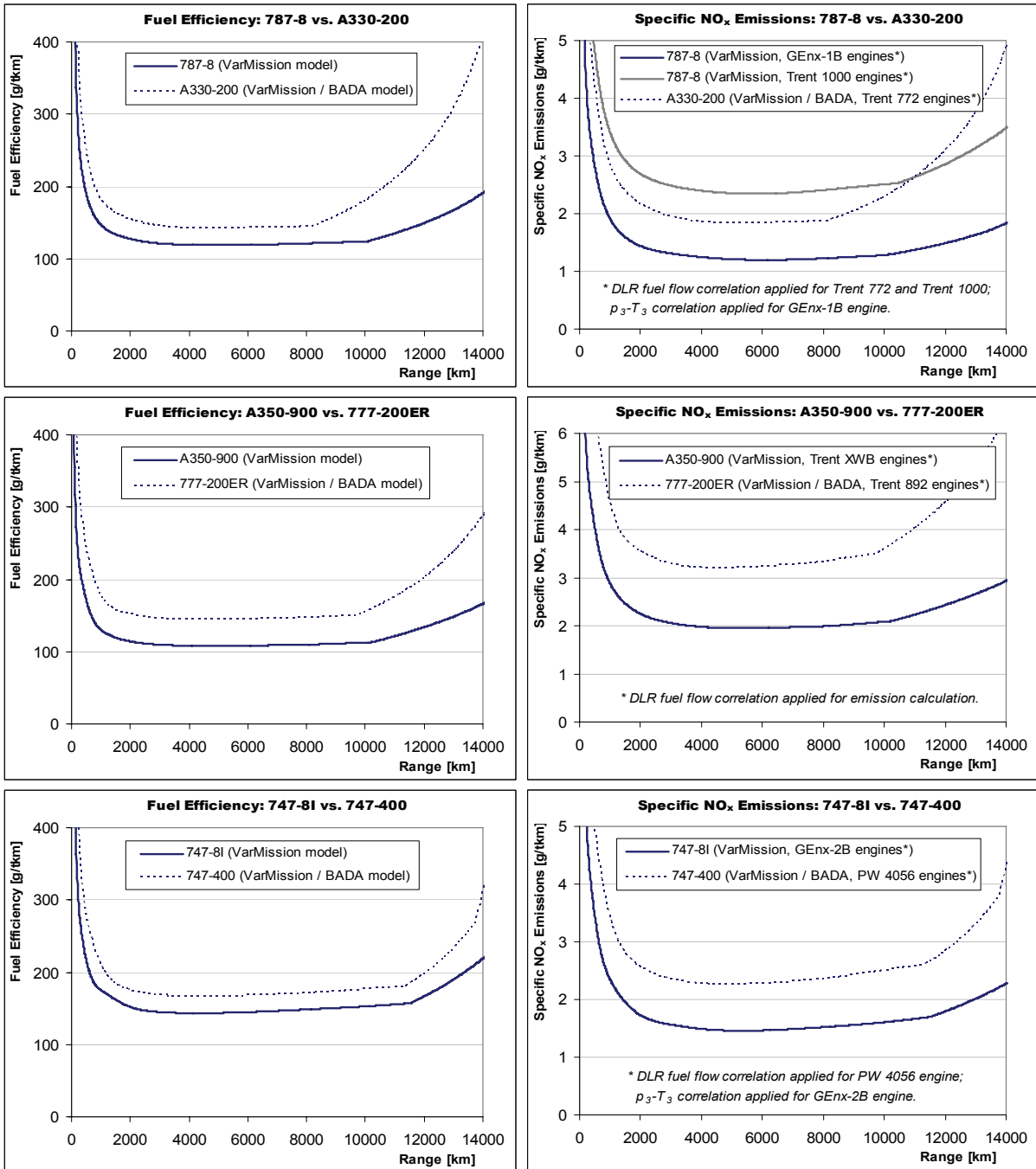


Figure 49: Fuel efficiency and specific NO<sub>x</sub> emissions of future widebody aircraft

### 3.4.5.3 NARROWBODY AIRCRAFT OF THE NEAR FUTURE

Airbus A320 and Boeing 737 currently dominate the market for narrowbody aircraft. New engine types are planned to be introduced for both aircraft families, resulting in considerable improvements of fuel efficiency and emissions. The A320 NEO (new engine option) will be delivered from 2016 onwards, whereas the recently announced 737 MAX will be introduced in 2017. The CFM International LEAP-X engine and a geared turbofan based on the Pratt & Whitney PW1000G family are being developed for the A320 NEO. The Boeing 737 MAX will be powered by a derivative of the LEAP-X.

In order to consider this new generation of aircraft in the emissions forecast, aircraft and engine models for the A320 NEO family have been developed. At the time of writing, available information on the 737 MAX and on its engine were not sufficient to create a simulation model. As a workaround, the A320 NEO models are used to represent the Boeing 737 MAX for fuel burn and emissions calculation. A generic regional jet resembling the Mitsubishi MRJ-90ER has also been simulated and is used to represent a number of similar aircraft types expected for the near future. This includes the Mitsubishi MRJ family as well as the Suchoi SSJ100<sup>23</sup>. The aircraft models are based on characteristic weights, drag polars and representative engine models simulated by DLR's engine performance software VarCycle. Table 16 presents the characteristic weights assumed for the generic regional jet and the A320 NEO family. The NEO models are based on data for the A320 family, but with modified empty weights and increased MTOW [60].

	Generic RJ	A319 NEO	A320 NEO	A321 NEO
Maximum take-off weight (MTOW) [kg]	40 995	76 500 (est.)	79 000	94 000 (est.)
Operating empty weight (OEW) [kg]	24 900	42 300 (est.)	44 100	49 900 (est.)
Maximum payload (MPL) [kg]	11 000	17 900	20 100	24 640
Maximum fuel capacity (MFC) [kg]	8 000	18 729	18 729	23 300
Source of data	Similar to MRJ90 [96], [105]	Based on A319 [2], [60]	Based on A320 [2], [60]	Based on A321 [2], [60]

*Table 16: Characteristic weights of future regional jet and A320 NEO models*

For the A320 NEO family, the lift-to-drag characteristics are based on an existing model of the Airbus A320 from Lyssis Ltd [92], which was modified by a delta  $C_{D0}$  for the stretch and shrink variants obtained by use of handbook methods. Aerodynamic improvements of the NEO aircraft (e.g. by improved winglets) are assumed to compensate for the new engine's larger dimensions. Handbook methods for preliminary aircraft design from [111] and [130] have been used to estimate a parabolic drag polar for the generic regional jet in cruise configuration. More information about the aircrafts' aerodynamics is found in Appendix Q.

<sup>23</sup> Bombardier CSeries aircraft are represented by the A319 NEO model for fuel burn and emissions calculations.

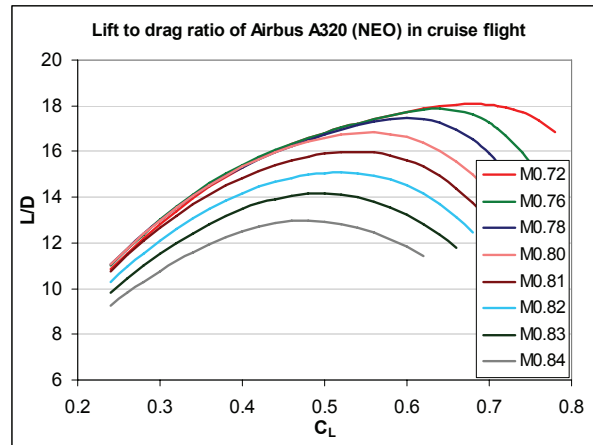


Figure 50: Lift-to-drag characteristics assumed for the A320 NEO [92] in cruise flight

The regional jet is assumed to be powered by the Pratt & Whitney PW1217G engine developed for the Mitsubishi MRJ. A VarCycle model [106] of an engine with similar characteristics was available for this study based on preliminary engine specifications from [85] and [110]. As certification data are not yet published for the PW1217G, sea-level  $NO_x$  emission indices have been estimated as function of thrust based on the characteristic  $NO_x$  level used as design target (see Figure 48 on page 85). A derivative of the PW1000G series with insertion of new technology is in development for the re-engined A320 family. At the time of writing, detailed characteristics are not yet available for this engine nor for the competing LEAP-X. For this study, the engine model used for the regional jet has been up-scaled to provide a take-off thrust of up to 150 kN (for the A321 NEO). The up-scaled model has been tweaked slightly for improved fuel efficiency and is assumed as representative engine for the A320 NEO family. Derated versions are used for the A320 NEO and A319 NEO.  $NO_x$  emission characteristics for these engines have been estimated as 55% below the CAEP/6 limit (see Figure 48). Emissions in cruise flight are calculated by use of the DLR fuel flow method [31] assuming a conventional RQL combustor. While these emissions are assumed as representative for PW1000G-powered aircraft, the potential of the TAPS combustor of the LEAP-X engine is assumed to result in reduced emissions in cruise flight: A 20% reduction of the EI  $NO_x$  is therefore assumed for the NEO variant powered by LEAP-X.

Flight phase	PW 1217G		Generic Eng. (A321 NEO)*	
	Cruise <sup>1</sup>	Take-off <sup>2</sup>	Cruise <sup>1</sup>	Take-off <sup>2</sup>
Thrust F [kN]	12	77	23	150
Overall pressure ratio $\pi$	28.8	30.1	-	-
Bypass ratio $\mu$	14.8	12.9	-	-
Turbine entry temperature TET [K]	1482	1755	-	-
SFC [g/kN/s]	15.3	7.4	14.6	6.7

\* Scaled version of the PW1217G model; no detailed performance model available.  
<sup>1</sup> Typical cruise at FL350, M0.77 (RJ) or M0.78 (A321); <sup>2</sup> Max. thrust for SLS conditions, uninstalled.

Table 17: Engine parameters of simulated engines for narrowbody aircraft

Figure 51 shows fuel efficiency and specific  $\text{NO}_x$  emissions of the newly created models. Engine types with average  $\text{NO}_x$  emissions (i.e. average  $D_p/F_{00}$  according to year 2010 fleet statistics) are assumed for the reference aircraft if more than one engine option is in service for this aircraft type. The graphs refer to flight missions performed at the aircrafts' maximum payload and assuming typical mission rules described earlier in chapter 3.2.3. Considering the limited and mostly preliminary input data for aircraft and engine models, the results should be seen as initial estimates. According to the models, the new regional jet delivers a fuel efficiency improvement of 25% over the similarly sized Bombardier CRJ-900 on flights between 500km and 1500km. In accordance with predictions by Airbus [5], the A320 NEO is found to be 15% more fuel efficient than the A320 reference aircraft. Similar improvements are found for the A319 NEO and A321 NEO models compared to their predecessors. Specific  $\text{NO}_x$  emissions of the A320 NEO model in the version with RQL combustor are roughly 23% below those of an A320 with CFM56-5A3 engines. As mentioned before, an additional 20% reduction is assumed for the version with TAPS combustor. In the fleet forecast, equal market shares are assumed for both engine options.  $\text{NO}_x$  emissions of the generic regional jet are found to be of comparable magnitude as for the CRJ-900. This can be explained by higher temperatures of the PW1000G engine in cruise flight.

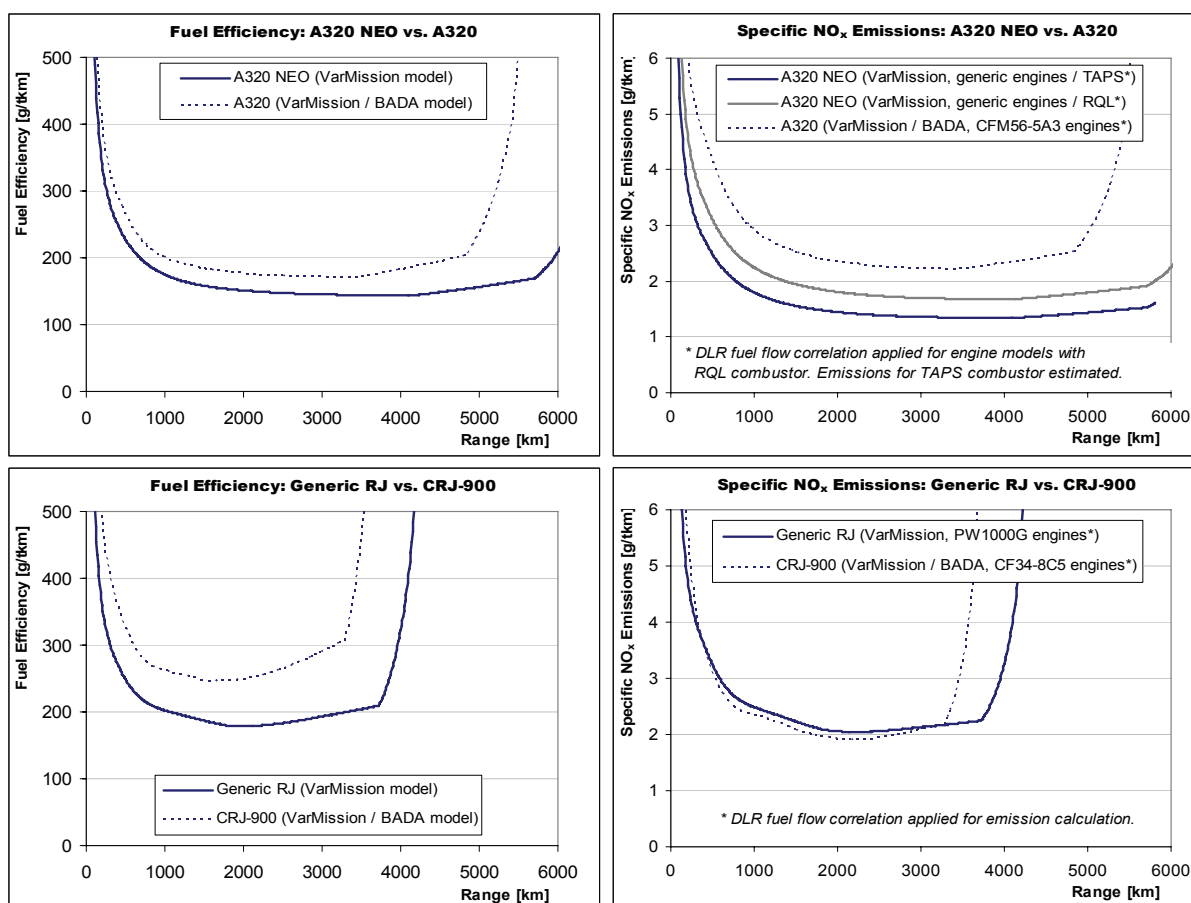


Figure 51: Fuel efficiency and specific  $\text{NO}_x$  emissions of future narrowbody aircraft

### 3.4.5.4 A GENERIC NARROWBODY AIRCRAFT FAMILY OF THE 2020S

Models of a generic narrowbody aircraft have been developed for this study. The new aircraft are assumed to be comparable in size and range to the Airbus A320 family while making use of more advanced technologies, particularly in the fields of engine systems and materials. The aircraft represent a technology level that can be expected for the early 2020s. Following recent decisions by Airbus and Boeing to re-engine the existing generation of narrowbody aircraft instead of developing new aircraft and assuming that new aircraft in this segment will not be developed until the late 2020s, these aircraft models are used in an alternative and hypothetical fleet scenario only (see chapter 4.4.4).

Different concepts are being discussed for a new single-aisle aircraft, ranging from aircraft powered by advanced turbofans (e.g. geared turbofans with ultra high bypass ratio) to more revolutionary designs with open rotor engines. While open rotors may lead to a better fuel efficiency than advanced turbofans, this option is likely to have drawbacks in terms of noise emissions and flight speed and may require more radical changes in the fields of aircraft configuration and aircraft design. For the current study, a thermodynamic engine model with ultra-high bypass ratio (UHBR) based on a design from the CLAIRE 2 project by DLR and MTU [35] was available for the propulsion of the new aircraft. Table 18 summarizes the most important design specifications of the baseline aircraft.

Specifications of an Airbus A320 successor	
Entry into service	approx. 2021
Number of seats	150 in a 3-class configuration
Design range	2300 NM (4260 km)
Design payload / max. payload	18,000 kg / 20,100 kg
Typical cruise Mach number	0.78
Typical cruise altitude	35,000 ft
Engine	2x ultra high bypass ratio turbofans
Derivative aircraft	stretched variant with 199 seats shrink variant with 134 seats

*Table 18: Design specification for a future narrowbody aircraft family*

Handbook methods for preliminary aircraft design by Roskam [111] and Torenbeek [130] have been used in order to provide estimations of characteristic weights and aerodynamic properties of the new aircraft. Moderate technological improvements compared to the current state-of-the-art are assumed in these fields. The advanced UHBR engine was simulated in DLR's VarCycle engine performance software and has been scaled during the design process in order to match the aircrafts' thrust requirements. Assuming a family concept, both a stretch and a shrink version have been derived from the baseline aircraft. An overview on the preliminary design process and major assumptions made during this process are given in Appendix R.



The resulting characteristics of the future aircraft family will be described briefly in the following paragraphs. More details are found in a separate report [131]. Three components determine fuel efficiency and emissions of the aircraft-engine models used in this study: characteristic aircraft weights, aircraft aerodynamics and engine characteristics. These components have been matched during the preliminary design process. Table 19 summarizes the resulting weights of the aircraft family. The operating empty weight of the baseline aircraft is approximately 10% lower than the empty weight of the similarly sized Airbus A320 due to new materials and improvements in the field of lightweight construction.

	Future Narrowbody (Shrink)	Future Narrowbody (Baseline)	Future Narrowbody (Stretch)
Maximum take-off weight (MTOW) [kg]	65 750	68 600	81 900
Maximum zero fuel weight (MZFW) [kg]	54 420	58 240	68 000
Operating empty weight (OEW) [kg]	36 520	38 140	43 360
Maximum payload (MPL) [kg]	17 900	20 100	24 640
Maximum fuel capacity (MFC) [kg]	15 200	15 200	18 770 incl. center tanks

Table 19: Characteristic weights of future narrowbody aircraft

The aerodynamic properties required for flight mission simulation are approximated by a parabolic drag polar. Figure 52 shows the drag polars of the future narrowbody family in clean configuration (with gears, flaps and slats retracted). Only a moderate improvement of the lift-to-drag ratios compared to aircraft of the current generation is assumed. This is based on the assumption that revolutionary improvements in aerodynamics, e.g. the use of laminar flow control, are not yet ready to be applied on these aircraft [65].

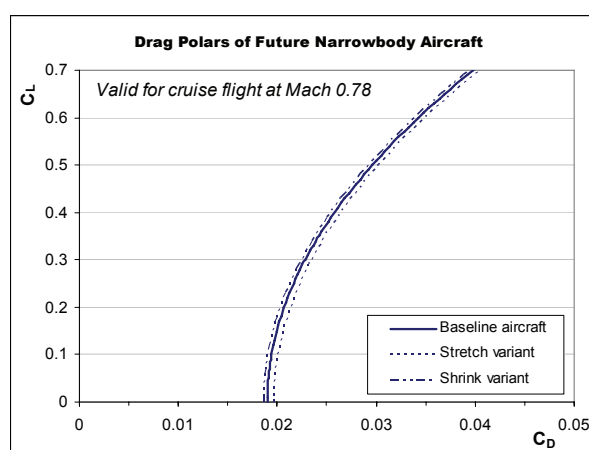


Figure 52: Parabolic drag polars assumed for future narrowbody aircraft in cruise flight

The engine type chosen for the new aircraft family is based on an engine model with ultra-high bypass ratio (UHBR) originating from the CLAIRE 2 project by DLR and MTU [35]. The engine model is simulated in VarCycle and has been scaled to meet the thrust requirements of the heaviest (i.e. the stretched) aircraft version. Top-of-climb conditions were identified as

the dimensioning case for the engines. The main engine characteristics are summarized in Table 20. Derated versions of this engine with 118-113kN take-off thrust are assumed to power the baseline and shrink variants of the aircraft family.

	Cruise <sup>1</sup>	Top-of-climb <sup>2</sup>	Take-off <sup>3</sup>
Thrust F [kN]	18.8	25	140
Overall pressure ratio $\pi$	40.5	50.0	42.8
Bypass ratio $\mu$	15.7	14.0	13.2
Turbine entry temperature TET [K]	1499	1750	1820
SFC [g/kN/s]	14.0	14.9	6.4
<sup>1</sup> Engine design point, FL350, M0.78, ISA; <sup>2</sup> FL350, M0.78, ISA; <sup>3</sup> Max. thrust for SLS conditions, ISA			

Table 20: Engine parameters of future narrowbody aircraft (highest thrust version)

Engine emissions of NO<sub>x</sub> have been estimated based on mid-term and long-term technology goals and taking into account certification NO<sub>x</sub> levels of the most recent aircraft engines [78], [110]. This includes most notably the GENx-1B engine with TAPS (twin annular premixing swirler) combustor technology intended for the Boeing 787 aircraft. The TAPS technology delivers a comparably large reduction of NO<sub>x</sub> emissions compared to single annular combustors. As can be seen on the left hand side of Figure 53, the GENx-1B engines already reach the mid-term technology goal for engine NO<sub>x</sub> emissions forecasted by a group of independent experts for the year 2016 [110]. Until the assumed entry into service of the UHBR engine around 2020, further maturation of the TAPS technology can be expected. Considering the recent progress in the field of TAPS combustors and assuming evolutionary improvements of combustor technology until 2020, characteristic NO<sub>x</sub> levels of 21-29 g/kN seem plausible for the UHBR engine, depending on the actual thrust rating<sup>24</sup>. These NO<sub>x</sub> levels, which are also visualized in Figure 53, are below those predicted for the GENx family and also below the level of the CFM56-5B engines used on the Airbus A320 – despite the much higher pressure ratios of the UHBR engines.

In order to simulate engine emissions at different operating conditions, a model of the TAPS combustor has been created in DLR's VarCycle software [106]. Given the characteristic NO<sub>x</sub> levels described above and assuming a staged reference function of NO<sub>x</sub> emission index versus combustor inlet temperature ( $T_3$ ), in-flight emissions of NO<sub>x</sub> can be calculated. The  $p_3T_3$  correlation [119] was applied for this purpose assuming that the switching point from pilot mode to the combined pilot/main mode occurs at a constant temperature  $T_3$ . Figure 53 shows the emission index of NO<sub>x</sub> versus thrust as simulated by the software. During cruise flight the engines are operated in the combined pilot/main mode resulting in NO<sub>x</sub> emissions which are considerably lower than for a comparable engine with RQL combustor.

<sup>24</sup> The characteristic NO<sub>x</sub> level  $D_p/F_{00}$  is used by ICAO for engine certification (see chapter 2.3.2).

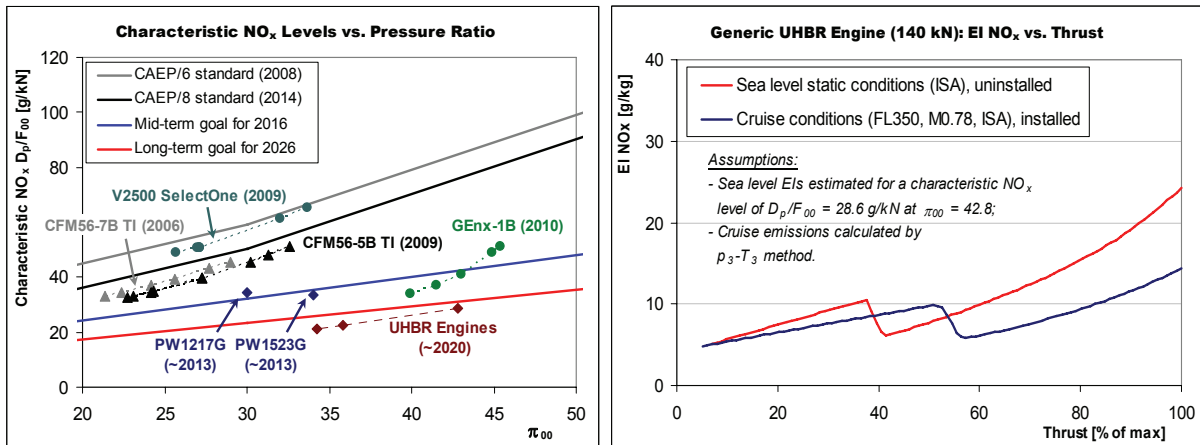


Figure 53: NO<sub>x</sub> emission characteristics assumed for future UHBR engines [106]

For flight mission simulation, VarCycle has been coupled to VarMission. Figure 54 visualizes fuel efficiency and specific NO<sub>x</sub> emissions of the future aircraft in baseline configuration compared to a simulated Airbus A320 with the latest CFM56-5B4/3 engines. The graphs refer to flight missions performed at the maximum payload for each range. At mission distances between 500 and 4500 km the fuel efficiency of the new aircraft is 27-30% better than for the similarly sized A320. This delta represents a conservative, but realistic estimate compared e.g. to a 25-35% fuel burn reduction potential identified by the International Air Transport Association (IATA) for a newly developed aircraft before 2020 [71]. Specific NO<sub>x</sub> emissions are 36-45% lower than for the reference aircraft. The payload-range performance and further details about the new aircraft family are found in Appendix R.

Considering the large number of design parameters, it is difficult to predict future aircraft and engine characteristics. The generic narrowbody aircraft designed for this study reflect the author’s view of future aircraft and engine development. An engine with lower pressure ratio and lower combustion temperature, for instance, can be expected to deliver even lower NO<sub>x</sub> emissions – but at the cost of a fuel burn penalty.

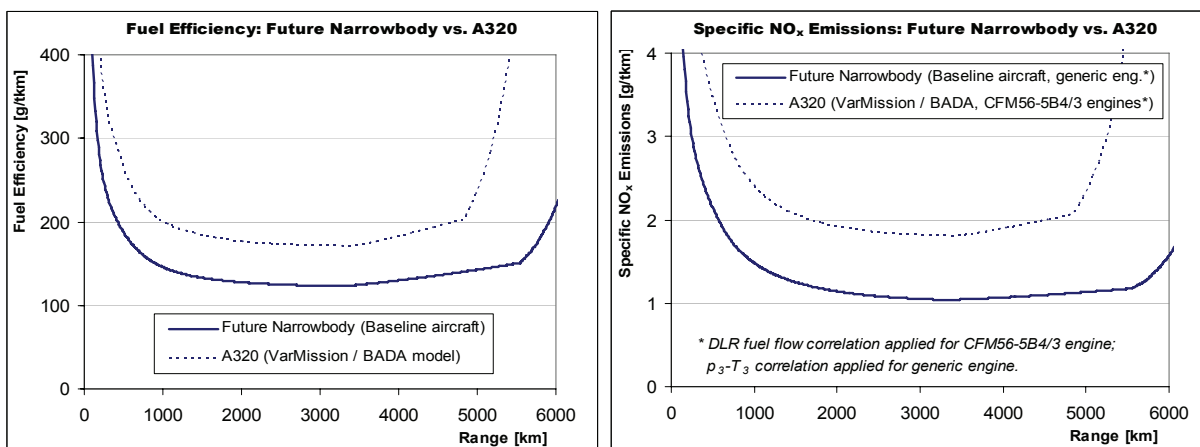


Figure 54: Fuel efficiency and specific NO<sub>x</sub> emissions of future narrowbody aircraft

### 3.4.5.5 AIRCRAFT REPRESENTATION FOR FUEL BURN AND EMISSIONS CALCULATION

In the Air Traffic Emissions Module, fuel burn and emissions of aircraft types with no available performance model are estimated by assuming a representative aircraft model with similar characteristics. In this approach, the absolute fuel burn and emissions calculated for the representative model are equally assumed for the original aircraft type (see chapter 3.3.5). For simulations of present civil aviation, performance models from the EUROCONTROL BADA database are available for nearly all major aircraft types. As a consequence, the error associated with this approach can be expected to be rather small.

In the Air Traffic Emissions Forecast Module, only a limited number of performance models are available for aircraft types of the short-term and medium-term future. For the Airbus A350 XWB family, for example, a model of the -900 version has been created while no performance models are currently available for the -800 and -1000 variants. Consequently, representative aircraft models are to be used for fuel burn and emissions calculation. Given the presumably high significance of the aforementioned aircraft types for future aviation, a modified approach is followed in order to reduce the potential error associated with aircraft representation: In the Air Traffic Emissions Forecast Module, any representative aircraft's fuel burn and emissions can be altered in order to better reflect the expected characteristics of the aircraft type it represents. Table 21 shows the assumptions used in this study.

Aircraft type*	Representative model	Assumption for aircraft representation
Boeing 737 MAX 7 / 8 / 9	A319 / A320 / A321 NEO (TAPS)	equal fuel burn and emissions per kg payload
Boeing 787-9	Boeing 787-8	equal fuel burn and emissions per kg payload
Airbus A350 XWB-800 / -1000	Airbus A350 XWB-900	equal fuel burn and emissions per kg payload
Boeing 777-200 / -300 Successor	Airbus A350 XWB-900	equal fuel burn per kg payload and 30% reduction of NO <sub>x</sub> emissions per kg payload**
E-Jet Successor (98 seats)	Generic Regional Jet (similar to MRJ-90ER)	equal fuel burn per kg payload and 30% reduction of NO <sub>x</sub> emissions per kg payload**
CRJ Successor (90 seats)		
CRJ & E-Jet Successor (70 seats)	E170	20% red. of fuel burn and emissions per kg payload
ERJ Successor (50 seats)	E145	25% red. of fuel burn and emissions per kg payload
Future Turboprop (90 seats)	ATR 72	25% red. of fuel burn and emissions per kg payload
ATR / DHC Succ. (50 / 70 seats)	ATR 42 / ATR 72	20% red. of fuel burn and emissions per kg payload
* Passenger aircraft only; see Appendix S for cargo aircraft. ** Assuming TAPS combustor technology.		

Table 21: Assumptions for passenger aircraft without available simulation model

The A350 XWB-800 and -1000 are represented by the -900 version assuming the same fuel efficiency and emissions per kg payload. Equal fuel burn per kg payload and a 30% reduction of NO<sub>x</sub> emissions compared to the A350 XWB-900 are assumed for a Boeing 777 successor expected to be introduced around 2020. To account for the trend towards re-engining existing airframes instead of developing all-new aircraft, these performance assumptions represent conservative estimates. Further assumptions about the development of engine NO<sub>x</sub> emissions will be described in the following chapter.

### 3.4.6 OTHER ASSUMPTIONS

Besides modelling air traffic growth and aircraft fleet changes over time, other effects that influence fuel efficiency and emissions are accounted for by the Air Traffic Emissions Forecast Module. This includes the following aspects:

- The improvement of aircraft and engine types during their production periods, e.g. by aerodynamic optimization, weight reduction or new combustor technology.
- Load factor changes with time.
- Improvements of Air Traffic Management procedures.

The assumptions with respect to the aforementioned effects are shortly summarized in the following paragraphs.

#### 3.4.6.1 FUEL EFFICIENCY IMPROVEMENT BY SERIAL MODIFICATION

Commercial aircraft types are often optimized during their production periods, e.g. by weight reduction, minor aerodynamic modifications or updated engine revisions. Such modifications have a positive influence on fuel efficiency, although the (comparably small) effect is difficult to quantify. In the Air Traffic Emissions Forecast Module, an aircraft type's fuel efficiency is assumed to improve by 0.4% per year during its production period. This assumption was adopted from the Aero2k emissions forecast [53]. A correction factor for fuel consumption and emissions on flight mission level can be calculated as follows:

$$(30) \text{ EfficiencyFactor} = (1 - 0.4\%)^{\text{DeltaYears}}$$

For aircraft types that are in production in the first year of the forecast, DeltaYears is the number of years between the delivery of the individual aircraft and the base year of the forecast. For aircraft types introduced during the forecast period, DeltaYears is the delta between the delivery year of an aircraft and the aircraft type's year of introduction. It should be noted that the efficiency correction is only applied to aircraft that are newly delivered during the forecast, whereas the fuel efficiency of older aircraft is assumed to remain constant. Given the above assumption, a newly delivered Boeing 777-300ER in 2020 would be around 4% more fuel-efficient than an aircraft of the same type delivered in 2010. The efficiency factor is applied on mission fuel consumption and emissions as calculated by use of the emission profiles (see chapter 3.2.6):

$$(31a) \text{ FuelConsumption}_{\text{corrected,efficiency}} = \text{FuelConsumption}_{\text{profiles}} \cdot \text{EfficiencyFactor}$$

$$(31b) \text{ Emissions}_{\text{corrected,efficiency}} = \text{Emissions}_{\text{profiles}} \cdot \text{EfficiencyFactor}$$

### 3.4.6.2 REDUCTION OF NO<sub>x</sub> EMISSIONS BY IMPROVED ENGINE COMBUSTORS

Fuel efficiency improvement by serial modification, as described in the previous paragraphs, has only a minor effect on NO<sub>x</sub> emissions. Considerably higher savings of NO<sub>x</sub> may result from new combustor technology, which potentially influences NO<sub>x</sub> emission indices (EI) measured in gram emissions per kilogram fuel. In the past, improved combustors with reduced emission indices of NO<sub>x</sub> have been implemented as part of engine revision updates, for example for the PW4000 and GE90 engine families. The recent certification of lean-burn “TAPS” combustors with the GENx-1B engines gives rise to hopes that low-NO<sub>x</sub> combustor technology will also be implemented into new revisions of other engine types.

It is difficult to predict whether or when such engine updates will be introduced. No information on entry into service (EIS), performance or emissions of future combustors are currently available from engine manufacturers. Assumptions have to be made to consider potential effects from improved combustors in an emissions forecast until 2030. Two methodologies have been implemented into the Forecast Module that can be used to simulate improvements of an engine type’s NO<sub>x</sub> emissions during its production period:

- Method 1: The EIS of improved engine revisions can be specified manually for each engine type. For aircraft delivered after this date and equipped with such engines, a correction factor for NO<sub>x</sub> emissions on flight mission level is used to account for an improved emission index.
- Method 2: Emission standards as those set by ICAO can be defined for the forecasting period. In each year of the forecast, compliance with effective emission standards is checked for all newly delivered aircraft-engine-combinations. Non-compliant engines have their emission characteristics modified such that compliance to the standards is reached.

A combination of the two methods is used for the emissions forecast presented in this study. Method 1 is applied for the most recent large turbofan engines with a presumably high contribution to aviation’s NO<sub>x</sub> emissions in the medium term future. Table 22 summarizes the respective assumptions. By the year 2020, the 30% reduction targets shown in Table 22 should be well within the capabilities of both lean burn and optimized RQL combustors.

Engine family	Corresponding aircraft family	EIS improved combustor	Effect of improved combustor*
Trent 1000 (EIS 2011)	Boeing 787	2020	EI NO <sub>x</sub> as for competing GENx-1B
Trent XWB (EIS 2013)	Airbus A350	2022	30% reduction of EI NO <sub>x</sub>
Trent 900 (EIS 2007)	Airbus A380	2024	30% reduction of EI NO <sub>x</sub>
GP 7200 (EIS 2007)	Airbus A380	2026	30% reduction of EI NO <sub>x</sub>

\* For simplicity, effects are considered on flight mission level by use of a correction factor on calculated NO<sub>x</sub> emissions.

Table 22: Assumptions for future combustor updates in aircraft engines (baseline scenario)



For engine types not listed in Table 22, method 2 ensures that regulatory standards for engine  $\text{NO}_x$  emissions are met. This approach requires the prediction of future emission standards until the end of the forecasting period. Emission standards for  $\text{NO}_x$  are set by ICAO and define upper limits for an engine's characteristic value  $D_p/F_{00}$  that is calculated by dividing  $\text{NO}_x$  emissions  $D_p$  during a standardized landing-and-take-off cycle by the engine's maximum take-off thrust  $F_{00}$ . Upper limits for  $D_p/F_{00}$  are defined as function of overall pressure ratio  $\pi_{00}$  at take-off conditions. The left-hand diagram in Figure 55 shows historical and current  $\text{NO}_x$  standards for jet engines with more than 89kN thrust. Since 2008, newly certified engine types need to comply with the CAEP/6 emissions standard. The more stringent CAEP/8 standard for newly certified engines will come into effect in 2014. For the year 2013, a production cut-off was agreed for engines that are not compliant to the CAEP/6 limit [81]. Also shown in the left-hand diagram are technology goals for 2016 and 2026 according to a  $\text{NO}_x$ -review performed for ICAO by a group of independent experts [109].

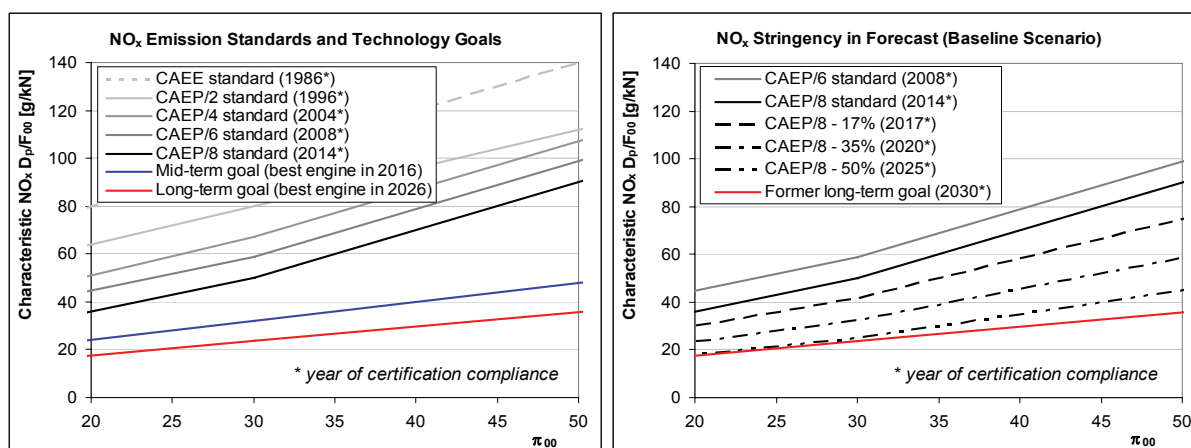


Figure 55:  $\text{NO}_x$  standards and technology goals (left);  $\text{NO}_x$  stringency in forecast (right)

Future stringency of emission standards as assumed in this study is roughly based on the technology goals. The right-hand diagram in Figure 55 shows future  $\text{NO}_x$  limits for newly certified engines that are assumed for the baseline forecast scenario. The predicted emission limits are based on the assumption that the technology goals set by the independent experts group are met. Some of the most recent engine designs like the GENx-1B engines for the Boeing 787 already comply with the mid-term technology goal, at least in their lower-thrust versions [109]. Assuming a quick adoption of the most recent combustor technology by all engine manufacturers, ICAO may be able to set certification limits in 2020 and 2030 that correspond to the former medium-term and long-term goals for 2016 and 2026. Agreements limiting the  $\text{NO}_x$  emissions of in-production engines are assumed to be reached in 2020 (CAEP/8 standard) and in 2030 (CAEP/8-35%). The details regarding assumed  $\text{NO}_x$  limits are summarized in Table 23. A scenario without further stringency of  $\text{NO}_x$  limits after 2014 has also been evaluated and will be discussed later in chapter 4.4.2.



Year	NO <sub>x</sub> regulatory limit for newly certified engines	NO <sub>x</sub> regulatory limit for in-production engines
2004	CAEP/4	CAEP/2
2008	CAEP/6	CAEP/2
2014	CAEP/8	CAEP/6 (from 2013)
2017	CAEP/8 – 17%	CAEP/6
2020	CAEP/8 – 35% (~Mid-term goal from [109] for low $\pi_{00}^*$ )	CAEP/8
2025	CAEP/8 – 50%	CAEP/8
2030	Long-term goal from [109]	CAEP/8 – 35% (~ Mid-term goal from [109] for low $\pi_{00}^*$ )
* higher slope compared to mid-term technology goal for $\pi_{00} > 30$ , see Figure 55.		

Table 23: NO<sub>x</sub> stringency assumptions in the baseline scenario of the forecast

Given the emission standards from Table 23, the Air Traffic Emissions Forecast Module ensures that limits for in-production engines are met for all aircraft-engine combinations that are newly delivered during the forecast. In the model, this task is implemented as part of the engine assignment process to newly delivered aircraft. Similar to the approach described in chapter 3.3.5 for the Air Traffic Emissions Module, engine types for newly delivered aircraft are chosen stochastically according to the engines' relative shares in the aircraft manufacturer's order backlog. The ASCEND fleets database contains this information [11] while engine emissions including the characteristic  $D_p/F_{00}$  levels are available from the ICAO Engine Exhaust Emissions Databank [78]. If an engine type assigned to a newly delivered aircraft does not meet the emission limit for in-production engines, this engine type is assumed to be equipped with new combustor technology.

In the model, combustor updates are introduced in the year in which a new limit for in-production engines becomes obligatory. In reality, updated combustor revisions can be expected to be certified some time before a new limit comes into effect. Any such upgrade is likely to be designed not only to meet the upcoming NO<sub>x</sub> standard, but any limit for in-production engines within the expected production period. For simplicity, the model assumes new combustors leading to target values of  $D_p/F_{00}$  that are 25% (for engines < 200kN thrust) or 15% (for engines  $\geq$  200kN thrust) below the certification limit from the previous year. These percentages are rough estimates for NO<sub>x</sub> characteristics of upgraded engine revisions, based on recent certification data [78]. To reach the target value for  $D_p/F_{00}$ , an engine's emission indices of NO<sub>x</sub> are reduced uniformly in all four ICAO certification points while all other engine parameters including thrust, pressure ratio and fuel flow are assumed to remain unchanged. The relative change of the average emission index of NO<sub>x</sub> on flight missions is assumed to be equal to the relative change of the  $D_p/F_{00}$  value when reducing the LTO emission indices as described above. Similar simplifications were used in the Aero2k emissions inventory for the year 2025 [53].

### 3.4.6.3 LOAD FACTOR DEVELOPMENT

Figure 56 shows the historical development of load factors from 1970 to 2010. Moderate improvements of the average load factors are assumed in the baseline forecast of this study to account for progress in the fields of reservation systems and airline yield management. Linear improvements of load factors from 2010 onwards until 2030 are assumed. An average seat load factor of 81% and a weight load factor of 68% are assumed as targets for the year 2030 – compared to 78% and 65% in preliminary figures for 2010 [8]. The seat load factor development in the model is roughly in line with the 80% load factor assumed for the year 2025 in the ICAO Outlook for Air Transport [79].

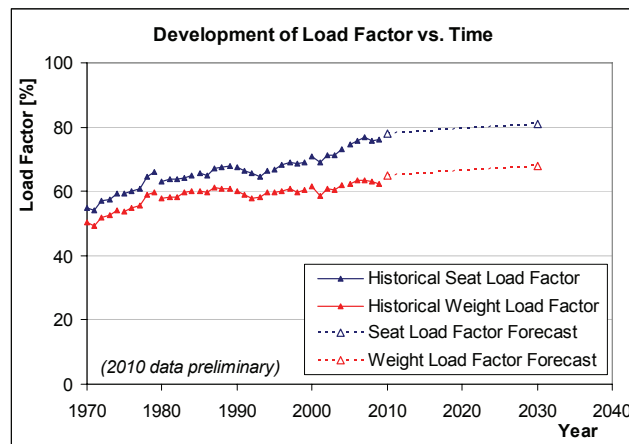


Figure 56: Load factors according to ICAO [77], [8] and forecast assumptions

During the forecast, load factors are modified after the Air Traffic Growth model has been applied to the Flight Movements and Emissions Database. As the base year flight movements are assigned to city-pair-specific or airline-specific load factors from ICAO statistics, year-by-year deltas of the average load factors are calculated from the input assumptions and are applied to all flights from the movements database. This way, the average load factors assumed as targets for the forecast years are met while load factor differences between city-pairs or airlines are retained. In the forecast model, traffic growth is modelled by increasing flight frequencies (see chapter 3.4.3) whereas load factor improvements imply a reduction of flight frequencies. A frequency correction is required in order to keep the revenue transport performance of each flight schedule entry unchanged:

$$(32) \quad Frequency_{new} = Frequency_{old} \cdot k_{Frequency}$$

$$\text{with} \quad k_{Frequency} = \frac{SLF_{old}}{SLF_{new}} \quad \text{for passenger flights and}$$

$$k_{Frequency} = \frac{WLF_{old}}{WLF_{new}} \quad \text{for cargo flights.}$$

### 3.4.6.4 IMPROVEMENT OF ATM EFFICIENCY

Potential improvement in the field of Air Traffic Management (ATM) can be simulated by modifying ATM efficiency with time. In the emission forecasts of this study, efficiency goals set by the Civil Air Navigation Services Organization (CANSO) are assumed to be met. Figure 57 shows the efficiency goals for the years 2005-2050 originating from a recent CANSO report [27]. In this report, 100% efficiency corresponds to an ideal system with all aircraft flying at the optimum trajectory and at the most fuel-efficient altitudes and speeds. The global efficiency of the ATM system is expected to increase from around 93% in 2005 to 97% in 2050. A system efficiency of 93% implies a fuel burn penalty due to ATM measures of 7% on average compared to the ideal air traffic system.

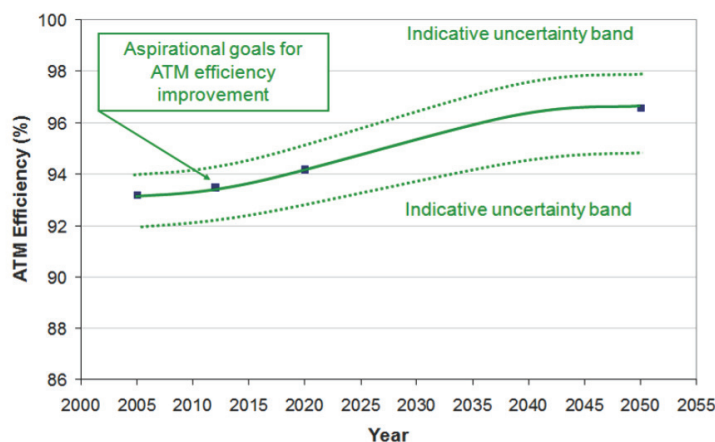


Figure 57: ATM efficiency goals from the CANSO report [27]

The graph shown in Figure 57 can be approximated by a polynomial function that is used to determine the ATM efficiency in every year of the forecast. Of course, any other function describing the development of ATM efficiency as function of time could also be used by the model. Applying the same approach as in Air Traffic Emissions Module, the remaining inefficiency is split up into a ground-based component, a terminal area component as well as horizontal and vertical en-route components. The relative shares of the individual components are assumed to remain constant. Except for the vertical en-route inefficiency<sup>25</sup>, all the aforementioned components can be considered when calculating fuel burn and emissions. As was described earlier for the Air Traffic Emissions Module, increased taxi times, additional holding flight phases and an extension of the flight distance compared to ideal conditions are simulated. The details about ATM efficiency and the associated fuel burn and emissions calculations were described earlier in chapter 3.3.4 and 3.3.5.

<sup>25</sup> The vertical en-route efficiency is not modelled explicitly, but assumed to be included in the pre-calculated emission profiles, see chapter 3.3.4.

## 4 AIR TRAFFIC EMISSIONS 2000-2030

### 4.1 OVERVIEW ON APPLICATION STUDIES

This chapter presents results from an initial application of the Air Traffic Emissions Module and the Air Traffic Emissions Forecast Module, which were described in chapter 3. Emission profiles produced by the VarMission Flight Mission and Emissions tool are used by these modules in order to calculate fuel burn and emissions in the application studies. The following studies have been performed:

- An analysis of transport performance, fuel burn and emissions of scheduled aviation for the years 2000-2010.
- A forecast of transport performance, fuel burn and NO<sub>x</sub> emissions of scheduled aviation for the years 2011-2030.
- Sensitivity analyses regarding selected forecast assumptions including traffic growth rates, assumptions about future engine combustors and the entry into service date of future aircraft types.

Chapter 4.2 presents calculation results for historical aviation from the year 2000 until 2010. Transport performance and emissions determined by the simulation model are analysed and compared to results from reference sources like ICAO air transport statistics [74], the IEA statistics on sold aviation fuels [84], the Aero2k study [53] and the FAA's SAGE inventories [55]. The assessment regarding historical aviation covers transport performance, fuel burn and emissions of NO<sub>x</sub>, CO, HC and black carbon.

Forecast results for 2011-2030 are presented in chapter 4.3 and are compared to studies like the ICAO Outlook for Air Transport [79], the Airbus and Boeing market forecasts [4], [19], the Aero2k inventory for 2025 [53] and ICAO CAEP forecasts of fuel burn and NO<sub>x</sub> emissions until 2036 [82]. Forecast results cover transport performance, fuel consumption, fleet composition and emissions of NO<sub>x</sub>. Emissions of CO, HC and black carbon are not predicted by the forecast module, as reliable input data for such evaluations are currently not available.

Sensitivities of selected forecast assumptions and their influence on air traffic emissions are evaluated in chapter 4.4. This includes assumptions regarding the introduction of improved low-NO<sub>x</sub> combustors for future aircraft engines. Besides, the effects of traffic growth on fuel efficiency and the effects of delays in the introduction of future aircraft types on global emissions are discussed. In an additional case study, a hypothetical scenario with all-new single aisle aircraft types instead of the re-engined 737 MAX and A320 NEO families is assessed in this chapter.

## 4.2 AIR TRAFFIC EMISSIONS 2000-2010

### 4.2.1 RESULTS SUMMARY

The Air Traffic Emissions Module has been used to calculate transport performance, fuel burn and emissions of NO<sub>x</sub>, CO, HC and soot for scheduled aviation. Flight schedules compiled by the Official Airline Guide (OAG) for the years 2000 and 2003-2010 have served as the primary source of flight movements data. The main results are summarized in Table 24, more detailed tabulated data is found in Appendix U.

Year	RPK [10 <sup>12</sup> Pkm]	TKT [10 <sup>9</sup> tkm]	Fuel [10 <sup>9</sup> kg]	NO <sub>x</sub> [10 <sup>9</sup> kg]	CO [10 <sup>6</sup> kg]	HC [10 <sup>6</sup> kg]	Soot [10 <sup>6</sup> kg]	Soot Particle Number Est.
2000*	3.24	412	155	1.95	630	1073	6.78	6.67·10 <sup>25</sup>
2003**	3.20	399	145	1.83	554	804	5.62	5.72·10 <sup>25</sup>
2004**	3.60	451	156	1.99	582	795	5.83	6.01·10 <sup>25</sup>
2005**	3.92	495	168	2.14	600	804	6.01	6.25·10 <sup>25</sup>
2006	4.15	519	172	2.21	603	771	6.02	6.25·10 <sup>25</sup>
2007	4.48	557	181	2.34	615	740	6.08	6.34·10 <sup>25</sup>
2008	4.58	567	185	2.40	621	713	6.17	6.46·10 <sup>25</sup>
2009	4.53	549	178	2.33	583	622	5.75	6.02·10 <sup>25</sup>
2010	4.95	603	188	2.47	604	622	6.09	6.40·10 <sup>25</sup>

\* September 2000 schedules available only. Results have been scaled for the estimation of yearly values.  
 \*\* January and July schedules available for 2003-2005. Results have been scaled to estimate yearly values.

*Table 24: Historical transport performance, fuel burn and emissions for scheduled aviation*

According to the model, the transport performance of scheduled aviation measured in revenue passenger-kilometres (RPK) has increased by 53% from  $3.24 \cdot 10^{12}$  Pkm in the year 2000 to  $4.95 \cdot 10^{12}$  Pkm in 2010. Total tonne-kilometres transported (TKT), which include both passenger and (belly-) cargo transport, have increased by 46% from  $412 \cdot 10^9$  tkm to  $603 \cdot 10^9$  tkm. Fuel consumption has grown by 21% from 155 Mt to 188 Mt while NO<sub>x</sub> emissions increased by 27% from 1.95 Mt to 2.47 Mt. HC emissions show a decreasing trend while CO and soot emissions remain approximately constant. It should be noted that the accuracy of the soot emission calculations (and particularly the soot particle number estimation) must be regarded as low and the respective results require careful interpretation.

The relative growth in fuel consumption is lower than the increase in transport performance, which is due to more efficient aircraft, increasing load factors and improved air traffic management procedures in the year 2010 compared to the year 2000. Using fuel burn per tonne-kilometres as a measure of fuel efficiency, efficiency has improved from 376 g/tkm to 313 g/tkm. This corresponds to a 17% efficiency improvement in the timeframe 2000-2010. Specific emissions of NO<sub>x</sub> have decreased from 4.74 g/tkm in the year 2000 to 4.11 g/tkm in 2010 corresponding to a 13% improvement. A more detailed analysis of transport performance, fuel burn and emissions results will be performed in the following chapters.

## 4.2.2 TRANSPORT PERFORMANCE

Figure 58 compares the transport performance calculated in this study to statistics from the International Civil Aviation Organization (ICAO). These statistics cover “scheduled services of airlines of ICAO contracting states” [74], [8] and rely on data reported by ICAO member states. The scope of the ICAO statistics should be roughly comparable to the OAG flight schedules, which are used as the primary data source in this study. Given the rather difficult differentiation between scheduled and unscheduled traffic and considering the potentially incomplete coverage of flights both in ICAO and OAG data, the comparison should be seen as a plausibility check rather than a validation.

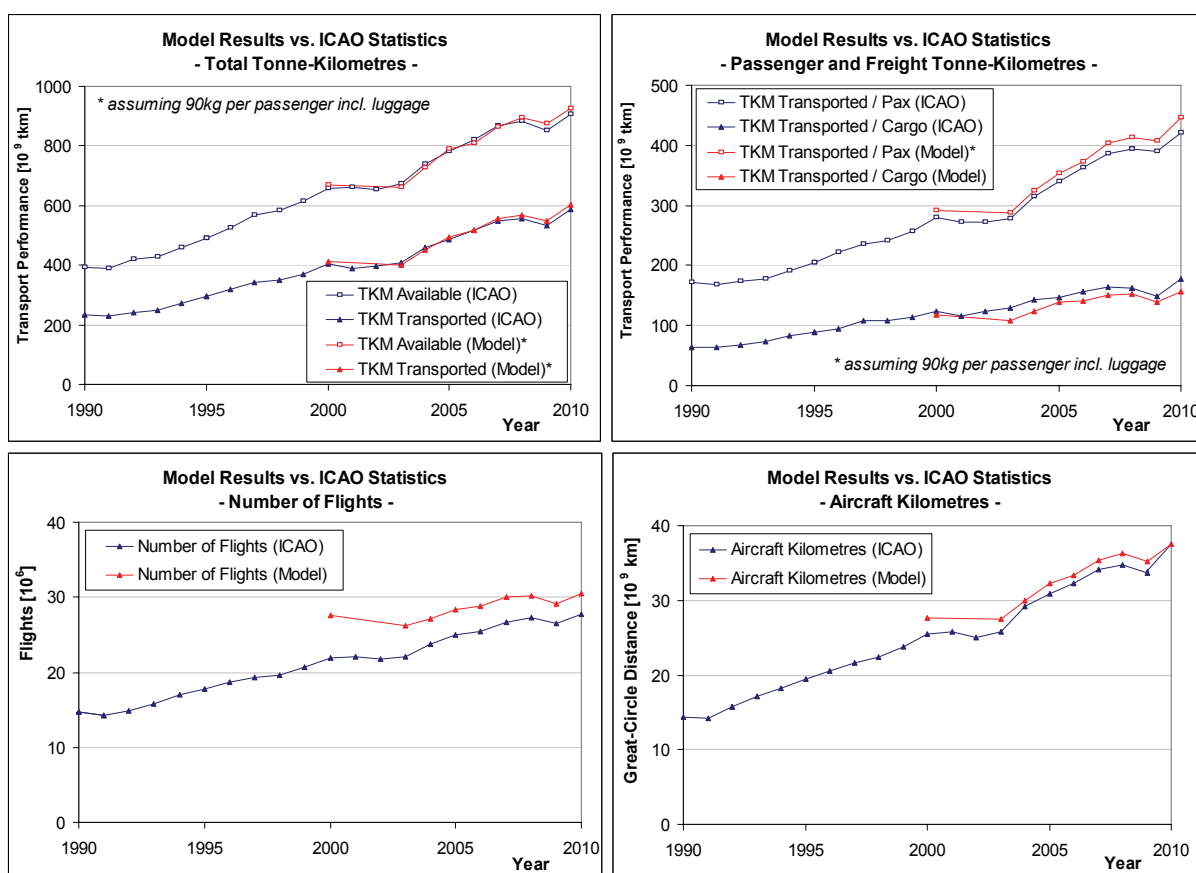


Figure 58: Comparison of model results based on OAG with ICAO statistics [74], [8]

Both the available and the actual transport performance from the model agree well with corresponding ICAO data. This implies comparable average load factors in the model and in the ICAO statistics. The downturn of air traffic after September 11<sup>th</sup> 2001 and the effects of the economic recession starting in mid-2008 are clearly visible in the graphs. When analysing the transport performance contributions from the passenger and freight sectors, it can be seen that the model shows a slightly higher passenger transport performance (3-6%) than ICAO statistics, which is partly compensated by a lower contribution from the freight sector. The higher transport performance in the passenger sector indicates a wider coverage

of passenger flights in the OAG schedules compared to ICAO statistics. The lower transport performance in the freight sector is most likely due to the incomplete coverage of cargo flights in the OAG flight schedules (see chapter 3.3.2).

Differences between the OAG and ICAO data samples become more obvious when analysing the number of flights and aircraft kilometres per year (see Figure 58). The number of flights in the model is 10-20% higher than in the ICAO statistics while aircraft kilometres are only 3-6% higher than reported by ICAO. A possible explanation for these findings is a higher coverage of short-distance flights in the OAG schedules. The explanation is consistent with the transport performance results described above: Given the short distances of the additional flights in the OAG schedules and assuming that such flights are mostly performed by small passenger aircraft, the contribution of these flights to the total transport performance is comparably small.

### 4.2.3 FUEL CONSUMPTION

While ICAO statistics are a reference source for transport performance and traffic volumes, the fuel consumption of scheduled aviation is not available from ICAO. Statistics of aviation fuel sold compiled by the International Energy Agency (IEA) may provide a rough guidance for the validation of fuel burn results and will be evaluated below. Furthermore, fuel burn calculations from aviation emission inventories created in US and European projects will be discussed and compared to results from this study.

Figure 59 visualizes the fuel burn results and compares them to the aviation fuel sold according to IEA [84]. The figure also includes the total fuel burn for civil and military aviation calculated in NASA ([13], [14], [126]), DLR ([26], [118]) and ANCAT [63] emission inventories, by the AERO modelling system [95] as well as in the AERO2k project [53]<sup>26</sup>. Calculations for civil commercial aviation (excluding general aviation and military flights) are presented separately and are also available from the FAA's SAGE inventories ([55], [87]) and the AEDT [133]. As this study focuses on scheduled aviation, results for scheduled aviation are shown as far as such data is available<sup>27</sup>. As can be seen from the figure, all emission inventories find smaller values of aviation fuel burn compared to IEA statistics. Explanations for this issue are found in literature: An underestimation of fuel consumption can be expected for emission inventories due to incomplete movements data, particularly for military aviation, and inherent model simplifications (see chapter 3.3.5.2). The accuracy of IEA statistics, which are compilations of fuel production data collected from different sources and countries, is unknown [67]. However, the fuel amount sold is not necessarily consumed in flight.

---

<sup>26</sup> The DLR and ANCAT results are nearly identical and presented as DLR/ANCAT in the diagram.

<sup>27</sup> Results for scheduled aviation are not available from Aero2k, SAGE and AEDT.



Aviation fuel may be used for ground vehicles and engine testing or can be mixed with fuel oils or diesel fuel in order to lower the freezing point. Jet fuel may also be reclassified and sold as kerosene [14]. In summary, it seems reasonable that the IEA values may slightly overestimate aviation fuel consumption while inventories underestimate fuel burn. Reference statistics that are better suited for validating fuel burn calculations for commercial aviation could be gathered from airline data or reported data by airlines to governments (as performed in the United States). Unfortunately, such data is not available on a global basis.

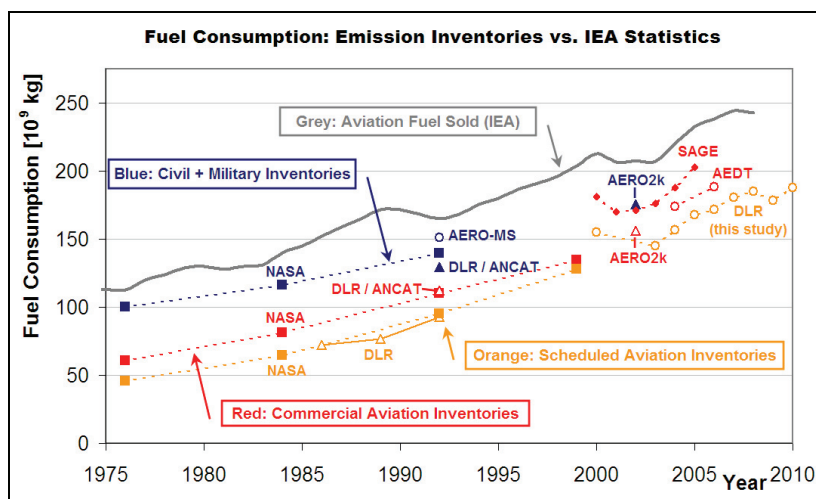


Figure 59: Comparison of fuel consumption in IEA statistics and emission inventories

Differences in the emission inventories are either due to the calculation methodologies or result from different coverage of the worldwide flight movements. A detailed comparison of methodologies and results of emission inventories can be found in [113]. The results from the current study seem to follow the trend of the IEA statistics and fit reasonably well to the Aero2k and AEDT results for commercial aviation. Both the Aero2k and the AEDT studies consider unscheduled air traffic, which should explain the 7-10% higher fuel burn in these inventories. The SAGE inventories, on the other hand, show a fuel consumption that is roughly 8-10% higher than in the Aero2k and AEDT studies. This must be blamed on differences in the simulation of flight routings and, more importantly, on erroneous double counting of flights in SAGE when merging movements data from different sources [133]. The error was fixed in the AEDT model, which can be regarded as the successor of SAGE.

Comparing scheduled aviation inventories and considering the fuel consumption trend from the IEA statistics, the fuel burn from the current study is slightly higher than the fuel consumption calculated by the older NASA and DLR inventories. This may be partly attributable to a wider coverage of scheduled flights in the latest editions of the OAG flight schedules. Furthermore, inefficiencies in the ATM system that lead to higher fuel burn were not modelled in the older emission inventories, but are considered in the more recent studies.

### 4.2.4 NO<sub>x</sub> EMISSIONS

Figure 60 compares the obtained NO<sub>x</sub> emissions to global total emissions of NO<sub>x</sub> according to the emission inventories for aviation described in the previous chapter. The results for NO<sub>x</sub> show a similar pattern as observed for fuel consumption. A trend towards higher NO<sub>x</sub> output is visible, although specific NO<sub>x</sub> emissions (in gram emissions per tonne-kilometre) are going down. The outcome of this study goes well with the older NASA and DLR inventories for scheduled aviation and also fits to the Aero2k results that include unscheduled air traffic.

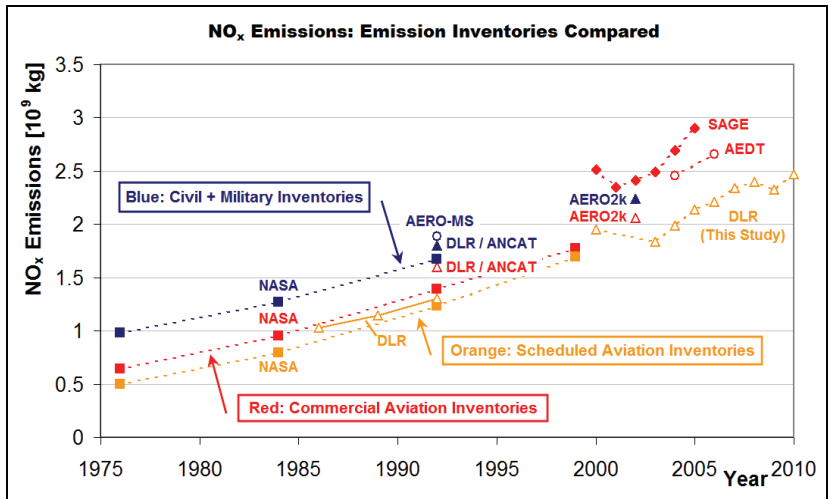


Figure 60: Comparison of NO<sub>x</sub> emissions in emission inventories

The AEDT and SAGE inventories deliver NO<sub>x</sub> totals that are higher than both the results from this study and the Aero2k inventory – even when considering the fuel burn differences discussed in the previous chapter. The average emission index (EI) for NO<sub>x</sub> in gram emissions per kilogram fuel is evaluated in Figure 61. As can be seen from the figure, the EIs from SAGE and AEDT are higher than the average EIs calculated in this study.

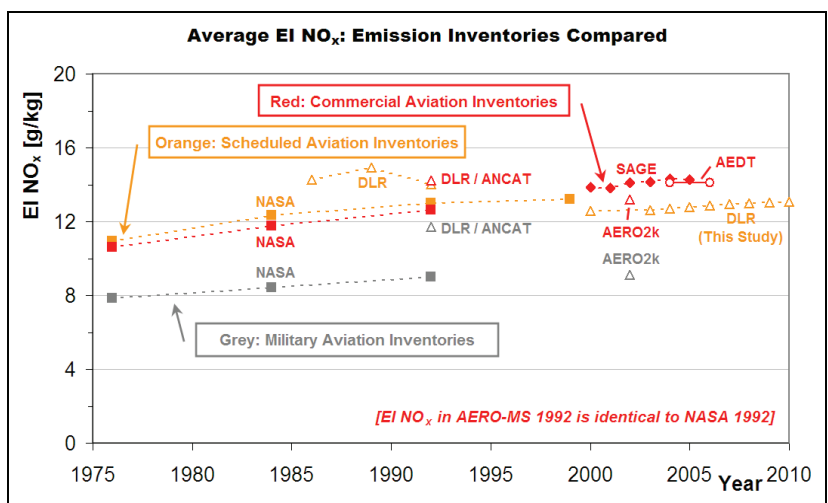


Figure 61: Comparison of the average NO<sub>x</sub> emission index in emission inventories

An increase of the NO<sub>x</sub> emission index since the 1970s is visible in Figure 61, which corresponds to the introduction of high bypass engines with turbine inlet temperatures in the 1970s and 80s. More recently, this tendency has slowed down, as progress has been made in the field of NO<sub>x</sub> reduction technologies. The average emission index for NO<sub>x</sub> determined in this study is approximately 13 g/kg – and has increased slightly from 12.6 to 13.1 between 2000 and 2010. In the AEDT and SAGE inventories, the average EI NO<sub>x</sub> lies around 14 g/kg whereas in Aero2k it equals 13.2 g/kg. Such deviations may be caused by differences in the aircraft and engine representation, the aircraft performance models or the emission calculation methods applied for NO<sub>x</sub> prediction. While the first two aspects are difficult to evaluate without an in-depth analysis of the respective methodologies, the influence of the emission calculation method is briefly assessed below.

Both the SAGE and AEDT inventories as well as the older NASA inventories apply the Boeing fuel flow correlation method for the calculation of NO<sub>x</sub> emissions [14]. The Aero2k and DLR studies, on the other hand, use a DLR-developed fuel flow correlation [31] described earlier in chapter 3.2.4.3. Both methods are well established and can be expected to predict NO<sub>x</sub> emission indices at an accuracy of +/-10% [67]. As a consequence, the deviation in the average EIs described above is still within the error bars of the methods.

The influence of the NO<sub>x</sub> calculation method on the outcome of this study can be quantified by recalculating aviation's NO<sub>x</sub> emissions and applying the Boeing fuel flow approach instead of the DLR method. Results are summarized in Table 25. The Boeing method leads to average emission indices that are 6-8% higher than the EIs calculated by use of the DLR correlation. These findings seem to explain – at least to a large extent – the deltas in the average EIs between the current study and Aero2k on the one hand and the SAGE and AEDT inventories on the other hand. Further analyses regarding the differences between NO<sub>x</sub> calculation methods will not be performed at this point. Investigations on the issue and particularly on the increasing delta in the EI NO<sub>x</sub> between the 2000 and 2010 inventories (see Table 25) are being prepared at DLR, but are beyond the scope of this study.

Year	NO <sub>x</sub> (DLR method) [10 <sup>9</sup> kg]	NO <sub>x</sub> (Boeing method) [10 <sup>9</sup> kg]	EI NO <sub>x</sub> (DLR method) [g/kg]	EI NO <sub>x</sub> (Boeing method) [g/kg]	Delta EI NO <sub>x</sub> [%]
2000	1.95	2.06	12.59	13.31	5.71%
2003	1.83	1.96	12.61	13.49	6.93%
2004	1.99	2.13	12.71	13.62	7.14%
2005	2.14	2.30	12.76	13.71	7.44%
2006	2.21	2.38	12.87	13.84	7.56%
2007	2.34	2.52	12.95	13.96	7.73%
2008	2.40	2.59	12.97	14.01	7.96%
2009	2.33	2.52	13.04	14.11	8.15%
2010	2.47	2.67	13.09	14.17	8.26%

Table 25: Influence of calculation method on global NO<sub>x</sub> emissions and average EI NO<sub>x</sub>

### 4.2.5 CO AND HC EMISSIONS

While emissions of CO and HC may influence air quality in the surroundings of airports, their importance regarding the climate impact of aviation is limited. Nevertheless, emissions of CO and HC are calculated in most of the emission inventories described in chapter 4.2.3. Figure 62 compares the total CO emissions obtained for scheduled aviation to results from the NASA and DLR inventories as well as to the more recent Aero2k, SAGE and AEDT studies.

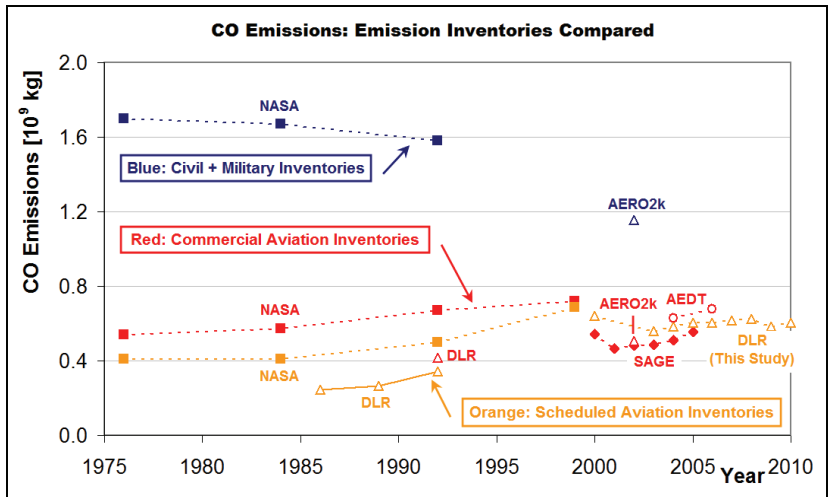


Figure 62: Comparison of CO emissions in emission inventories

As can be seen in the above figure, CO emissions from civil commercial aviation show only a slight increase since the 1970s (when comparing data produced by the same methodology). Emissions from general aviation and military aviation contribute a much larger percentage towards aviation CO emissions than to fuel consumption. The total CO emissions calculated for scheduled aviation in this study fit well to the most recent AEDT results for commercial aviation and are slightly higher than calculated in Aero2k and SAGE.

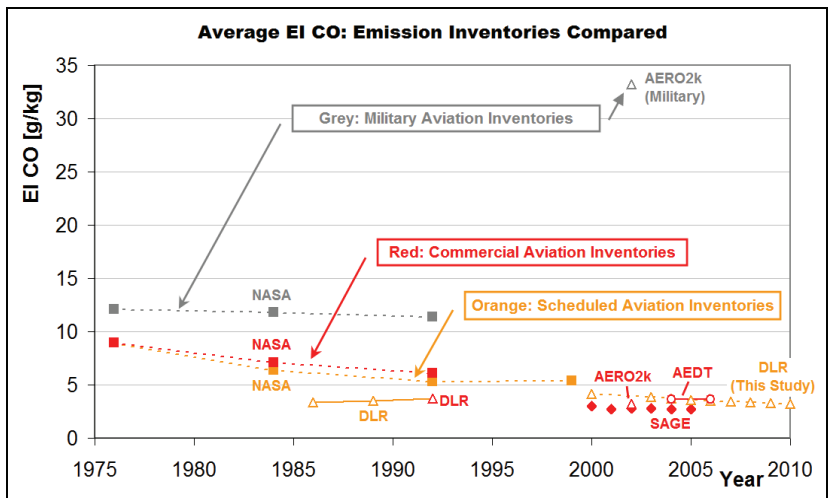


Figure 63: Comparison of the average CO emission index in emission inventories

Figure 63 shows the average emission indices (EI) in grams of emissions per kg fuel. In commercial and scheduled aviation, a trend towards lower CO emission indices is visible. This corresponds to considerable improvements in the combustion efficiency of aircraft engines. As can be seen from Figure 63, the average emission indices for CO from this study are nearly identical to the emission indices from the AEDT inventories. For the military sector, AERO2k found a much higher emission index for CO than the older NASA inventories. It is obvious that this development does not reflect a trend in real-world military aviation, but may largely be attributable to different assumptions about the use of reheat and afterburning operations [53].

Emissions of hydrocarbons (HC) from different studies are compared in Figure 64. As can be seen from the diagram, the older DLR and NASA-determined HC emissions for commercial aviation differ almost by a factor of two. The more recent AERO2k and SAGE results seem to confirm the DLR values. The results of the current study are between the AEDT and SAGE results and show a decreasing trend in total HC emissions.

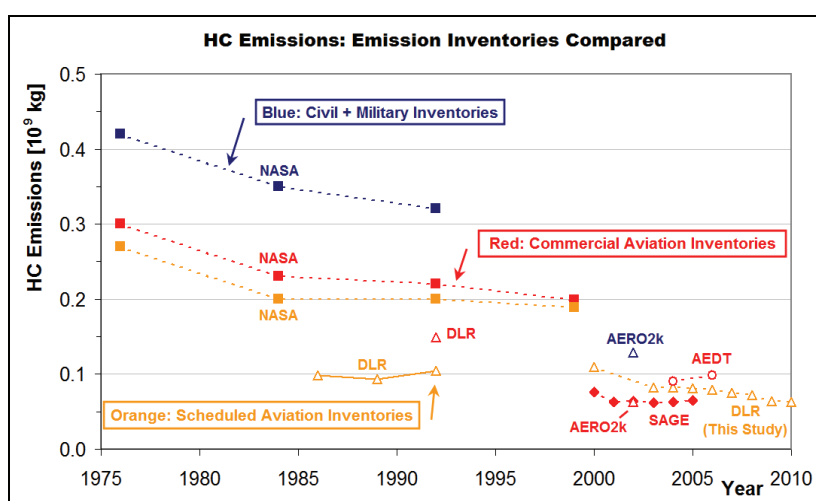


Figure 64: Comparison of HC emissions in emission inventories

Figure 65 displays the average emission indices for HC emissions. A clear trend towards lower emission indices is visible, caused by improvements in the field of combustion technology that were already mentioned above. Differences between the compared studies are likely due to differences in aircraft performance modelling, particularly in the descent and taxi phases, where engine thrust is low and where most CO and HC emissions are produced. Emissions of CO and HC are very sensible to small variations in fuel flow, which may explain the comparably large delta between the NASA inventories and the most recent studies. Two different calculation methods for CO and HC emissions are applied in the inventories: the older DLR inventories and the Aero2k study use the DLR-developed Omega correlation for CO and HC calculation [31]. The current study as well as the NASA, SAGE and AEDT inventories apply the Boeing fuel flow correlation [14].

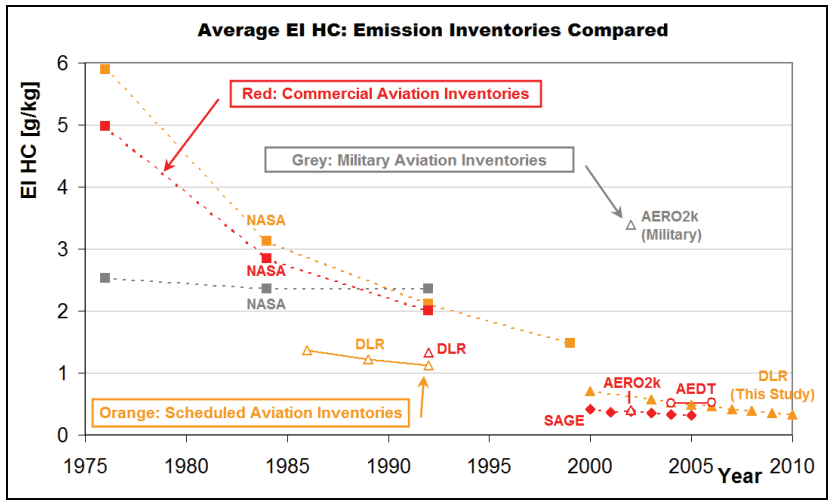


Figure 65: Comparison of the average HC emission index in emission inventories

#### 4.2.6 EMISSIONS OF SOOT / BLACK CARBON

The prediction of soot emissions<sup>28</sup> from aircraft engines in flight conditions must still be regarded as difficult. The accuracy of the available calculation methods is low compared to fuel burn or NO<sub>x</sub> emissions. Soot emissions have been determined in this study by considering a limited number of aircraft-engine combinations that were chosen to be representative for the worldwide fleet of aircraft. The DLR soot method [33] implemented into the VarCycle engine performance software has been applied for the calculation of emission indices (see chapter 3.2.4.4 and 3.2.6 for more details). The resulting soot emissions for scheduled aviation can be compared to results from Aero2k [53] and AEDT [133].

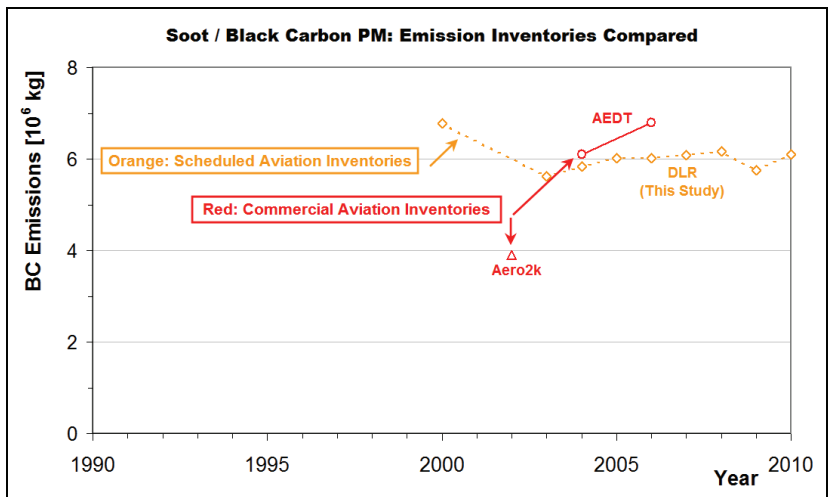


Figure 66: Comparison of soot emissions in emission inventories

<sup>28</sup> Soot emissions from aviation are also referred to as black carbon (particle) emissions.

As can be seen in Figure 66, the Aero2k soot estimate is considerably lower than both the results from this study and from AEDT. In principle, the Aero2k emissions inventory applied a similar methodology for soot calculation as the current study: An earlier version of DLR's VarCycle software was used for the calculation of the emission indices. On the other hand, soot emissions were not considered explicitly in Aero2k when selecting the representative engine types for which performance models were created [53]. It is likely that this explains to a large extent the deviation between the current results and Aero2k.

The AEDT results for total soot emissions are close to the values from this study. It should be noted, however, that the AEDT totals refer to scheduled and unscheduled air traffic while only scheduled traffic is considered for the purpose of this study. Unlike in the current study, where detailed soot prediction methods implemented in engine performance models are applied, the AEDT results assume a constant emission index for soot of 0.035 g/kg. This value was estimated to reflect typical cruise conditions [133] and fits well to the average EIs calculated in this study. Figure 67 shows the emission indices resulting from this study and the aforementioned inventories. A decreasing trend of the average EI for soot can be identified from the current results due to the modernization of the worldwide aircraft fleet.

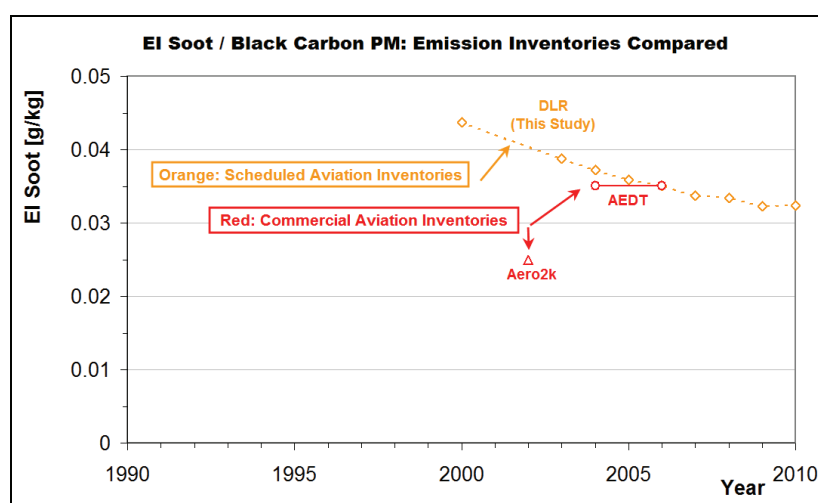


Figure 67: Comparison of the average soot emission index in emission inventories

Besides a calculation of soot emissions by mass, the number of soot particles emitted by aircraft engines can be estimated. A relation from [33] approximating the specific soot particle number as function of altitude was applied for this purpose. More details are described in Appendix E. As already shown in Table 24 on page 102, the number of emitted soot particles from scheduled aviation was found to be in the order of  $6 \cdot 10^{25}$  to  $7 \cdot 10^{25}$ . Given the uncertainty that is associated with such estimations, these results are to be treated with care. Previous estimates from Aero2k show a lower particle number of around  $4 \cdot 10^{25}$ . Considering the lower value for emitted soot by mass in Aero2k compared to the current study, the current results appear plausible.



## 4.3 FORECAST OF AIR TRAFFIC EMISSIONS 2011-2030

### 4.3.1 RESULTS SUMMARY

The Air Traffic Emissions Forecast Module was used to estimate scheduled aviation's fuel burn and emissions up to the year 2030. The model applies regional traffic growth rates from the Airbus Global Market Forecast (GMF) to base year flight movements obtained from the Official Airline Guide (OAG). A fleet rollover module accounts for the retirement of old aircraft and the introduction of new aircraft types. Simulation models of newly introduced aircraft-engine combinations are applied for fuel burn and emissions calculations. As was described in chapter 3.4, further assumptions about load factor development, inefficiencies in the Air Traffic Management (ATM) system and stringency of NO<sub>x</sub> emission standards have been made. The Air Traffic Emissions Forecast Module calculates transport performance, fuel burn and NO<sub>x</sub> emissions of scheduled aviation whereas emissions of CO, HC and soot are currently not predicted. As already mentioned before, emissions of CO<sub>2</sub> and H<sub>2</sub>O are proportional to fuel consumption.

Table 26 summarizes the forecast results in a baseline scenario. More detailed tabulated data is found in Appendix U. The transport performance of scheduled air traffic measured in revenue passenger-kilometres (RPK) is forecasted to increase by 157% between 2010 and 2030. According to the model, the tonne-kilometres transported (TKT), which include both passenger and cargo transport, will increase by 172% in the aforementioned timeframe.

Year	Flights [10 <sup>6</sup> ]	Distance [10 <sup>9</sup> km]	RPK [10 <sup>12</sup> Pkm]	TKT [10 <sup>9</sup> tkm]	Fuel [10 <sup>9</sup> kg]	NO <sub>x</sub> [10 <sup>9</sup> kg]
2010*	30.5	37.5	4.95	603	188	2.47
2015	38.1	47.7	6.59	801	241	3.20
2020	46.2	58.8	8.38	1032	293	3.89
2025	54.2	70.1	10.33	1301	344	4.43
2030	64.1	84.0	12.74	1640	405	4.96
* base year of the forecast; flight movements from OAG schedules						

Table 26: Forecasted transport performance, fuel burn and emissions for scheduled aviation

Fuel consumption is forecasted to grow from 188 Mt in the year 2010 to 405 Mt in the year 2030 – a 115% increase – while NO<sub>x</sub> emissions will increase from 2.47 Mt to 4.96 Mt. Using fuel burn per tonne-kilometre as a measure of efficiency, fuel efficiency will improve from 313 g/tkm to 247 g/tkm. This corresponds to a 21% improvement in the timeframe 2010-2030. Specific NO<sub>x</sub> emissions are forecasted to decrease from 4.1 g/tkm in 2010 to 3.0 g/tkm in 2030, which corresponds to a 27% improvement. A more detailed analysis of transport performance, fuel burn and emissions including a comparison to results from third-party studies will be performed in the following chapters.

### 4.3.2 TRANSPORT PERFORMANCE

Figure 68 compares the transport performance as calculated by the Air Traffic Forecast Module to results from the Airbus Global Market Forecast (GMF) 2011-2030 [4] and the Boeing Market Outlook 2011-2030 [19]. The revenue passenger-kilometres (RPK) obtained by the model for the year 2030 are nearly identical to the Airbus GMF and slightly lower than in the Boeing Outlook. As traffic growth rates from the Airbus GMF are used as input data for the model, this outcome could have been expected. The deviation compared to the Airbus forecast is somewhat larger for freight traffic measured in freight tonne-kilometres transported (FTKT). As the latest Airbus GMF does not cover freight traffic, the GMF 2009-2029 edition [3] provides traffic growth rates for the model and is included as a reference in the right hand diagram of Figure 68. The reason for the deviation between model results and reference forecast in terms of FTKT is the incomplete coverage of cargo flights in the base year flight schedules (see chapter 3.3.2). The relative increase of freight traffic, on the other hand, is in accordance with the Airbus GMF. When looking at tonne-kilometres transported (TKT), which include both passenger and cargo traffic, the deviation between model results and the Airbus GMF is less than 2%.

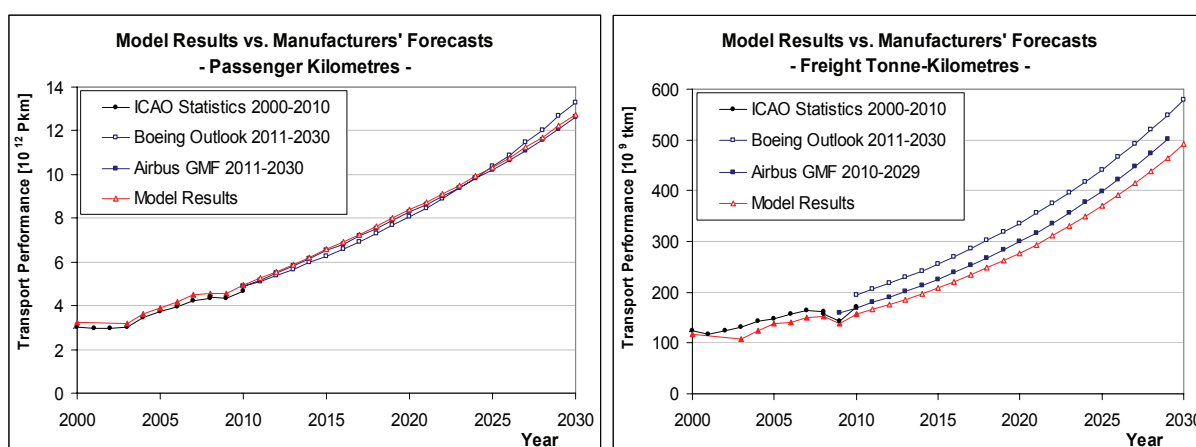


Figure 68: Comparison of model results with Airbus and Boeing forecasts [3], [4], [19]

As can be seen in Figure 68, results from the Airbus and Boeing traffic forecasts are roughly comparable, at least for passenger traffic. The average annual growth rate predicted for passenger traffic is slightly higher in the Boeing Outlook (5.1%) than in the Airbus GMF (4.8%). In the cargo sector, the Airbus GMF 2009-2029 predicts an average annual growth rate for worldwide FTKT of 5.9% whereas the Boeing Market Outlook forecasts 5.6%. As can be seen on the right hand side of Figure 68, the deviation between Airbus and Boeing forecasts in the cargo sector results from different base year values rather than different growth rates. Whereas the base year value of the Airbus GMF is roughly in accordance with ICAO statistics, the value from the Boeing market outlook is about 15% higher.

Besides aircraft manufacturers, the International Civil Aviation Organization (ICAO) also published a forecast of air traffic. Results from the ICAO Outlook for Air Transport 2005-2025 [79] are shown in Figure 69. Compared to the Airbus and Boeing market forecasts, some more parameters are analysed and published in the ICAO study. In addition to the transport performance in terms of RPK and FTKT, the number of flights and aircraft kilometres are predicted in the ICAO forecast.

As can be seen in Figure 69, the total tonne-kilometres transported according to the model (including passenger and freight transport) are nearly identical to the ICAO's "Most Likely" scenario. The traffic growth in terms of passenger-kilometres is higher in the model than in the aforementioned ICAO scenario. This is compensated by lower values for freight tonne-kilometres, which result from a lower base year value in combination with lower growth rates compared to the ICAO study. The simulated number of flights in the model is slightly higher than both in ICAO's historical statistics and its forecast. The discrepancy of the historical number of flights has been discussed earlier in chapter 4.2.2. The relative growth of the number of flights appears plausible. Furthermore, the aircraft kilometres predicted by ICAO fit quite well to the model results.

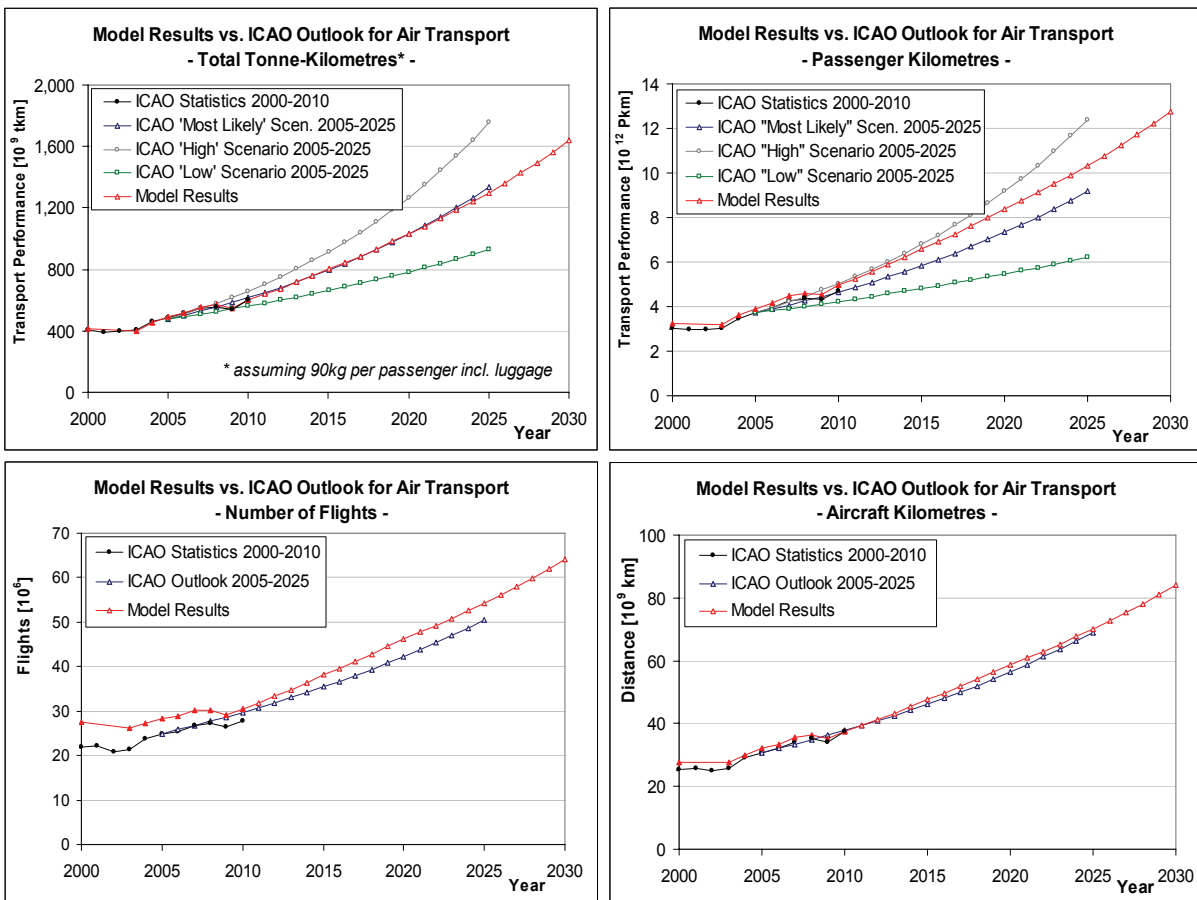


Figure 69: Comparison of model results with ICAO Outlook for Air Transport [79]

### 4.3.3 FLEET COMPOSITION

Changes in the global fleet of aircraft are simulated by a fleet rollover model which considers the retirement of old aircraft and the introduction of new aircraft types: While forecasting the number of active aircraft in a year-by-year analysis, the flight movements data are modified accordingly. The distribution of newly delivered aircraft between seat categories is based on combined results from the Airbus Global Market Forecast (GMF) [4] and – for regional aircraft up to 120 seats – the Embraer Market Outlook [38]. Market shares within each category and the production periods of aircraft types have been estimated by the author. Figure 70 visualizes the results of the fleet forecast for passenger aircraft. Tabulated data by aircraft variant including results for cargo aircraft are found in Appendix U.

As can be seen in Figure 70, the widebody fleet is currently dominated by Boeing 767 and 777 as well as Airbus A330 aircraft. Boeing 787, Airbus A350, Airbus A380 and an assumed successor of the Boeing 777 will gradually take over this role during the 2020s. The Boeing 777 and Airbus A330 families retain important positions in the fleet well beyond the year 2020. The narrowbody segment is dominated by the Boeing 737 and Airbus A320 families. In this study, the Bombardier CSeries and Comac C919 families are not expected to reach high

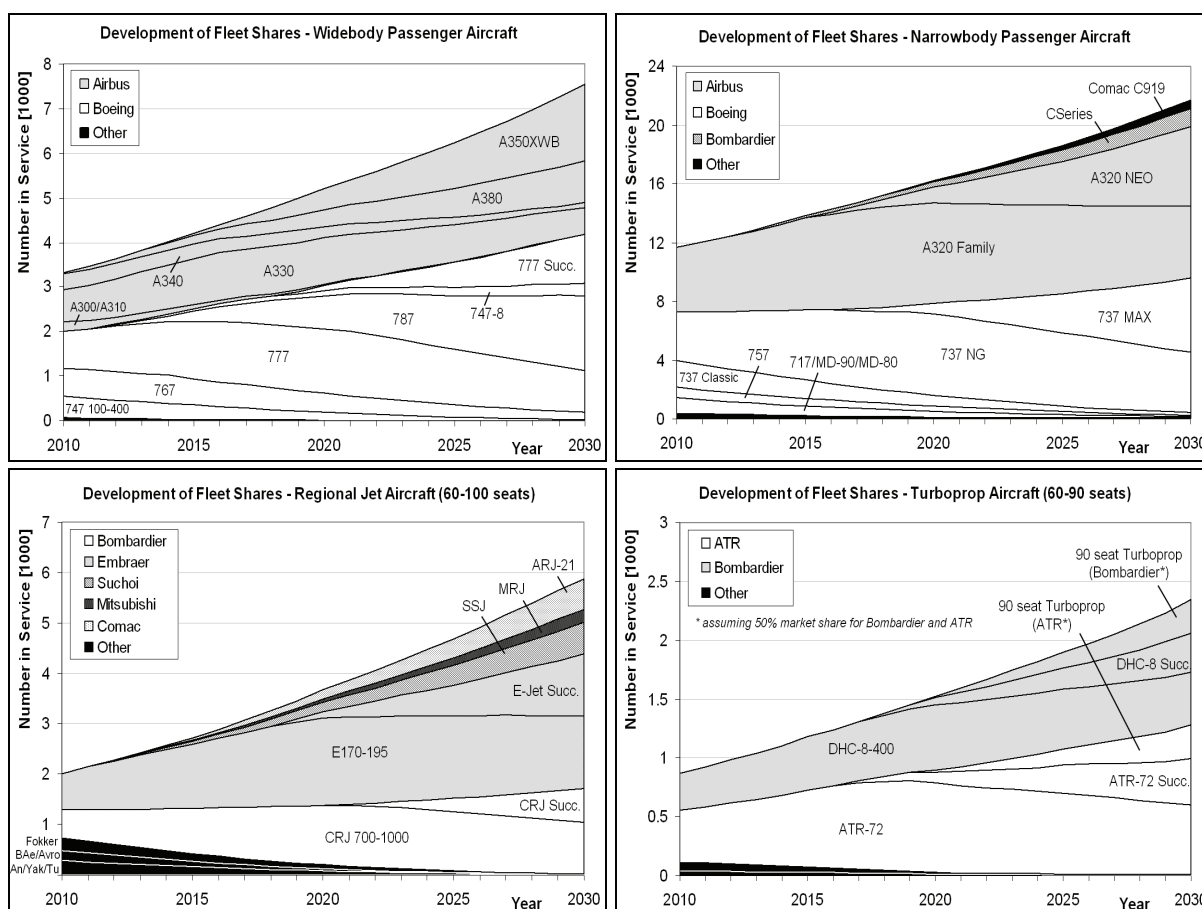


Figure 70: Development of fleet shares for passenger aircraft

market shares in the single-aisle segment. The re-engined Airbus A320 NEO family and the recently announced Boeing 737 MAX gain significant fleet shares in the 2020s and will make up nearly half the fleet in the narrowbody sector by 2030.

Bombardier and Embraer are currently the most important manufacturers for regional jet aircraft and are expected to defend their positions in the market until the year 2030. Competitors like Comac, Suchoi and Mitsubishi have been assigned a combined market share of 30% for newly delivered aircraft, resulting in an increasing share of the active fleet throughout the forecast period. In accordance with estimations by Bombardier [23] and Embraer [38], the turboprop sector accounts for roughly 45% of all deliveries with 30-90 seats. ATR and Bombardier are assumed to remain the only major competitors in the turboprop market. Very low delivery numbers are expected for regional aircraft in the 30-60 seats segment. Consequently, the number of active aircraft in this category is decreasing.

Figure 71 visualizes the significance of different seat categories within the global fleet of passenger aircraft. According to this forecast, widebody aircraft account for only 14% of the passenger fleet in 2010, but are responsible for more than 45% of the available seat-kilometres (ASK). Their contribution in terms of tonne-kilometres (TKO) exceeds 50%<sup>29</sup>. Throughout the forecast, the significance of the widebody segment is increasing: About 19% of the worldwide fleet will be widebodies by 2030 and these aircraft will contribute 53% of the total ASK. Narrowbody aircraft with more than 120 seats are currently responsible for 45% of the fleet both in terms of numbers and ASK. The contribution of such aircraft to the ASK will decrease to 40% in the year 2030 whereas by numbers their share will increase to 51%. Aircraft with 30 to 120 seats account for roughly 40% of the fleet in 2010 and 30% in 2030. Their contribution in ASK remains approximately constant in the order of 7-8%. A trend towards larger aircraft is visible in the diagrams.

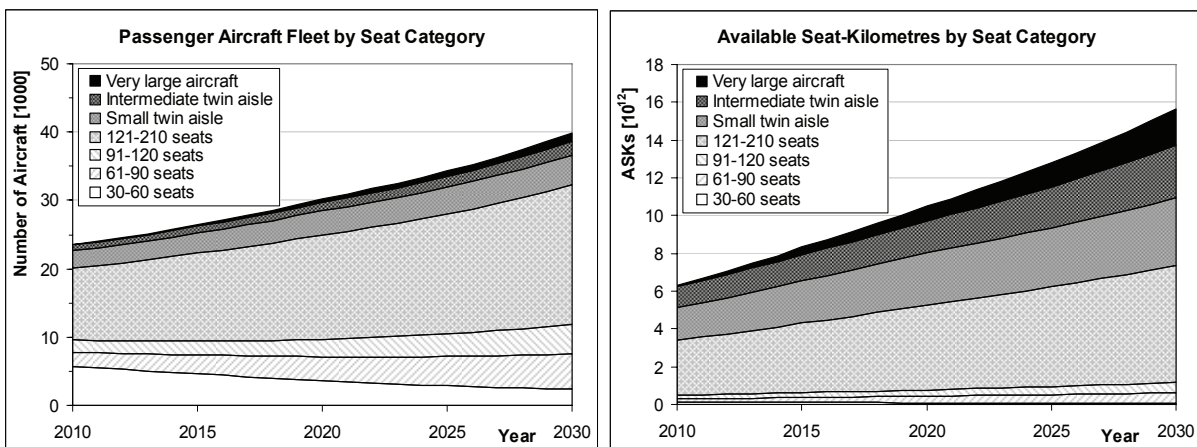


Figure 71: Development of aircraft number and ASK by seat category

<sup>29</sup> For the passenger fleet. Considering passenger and all-cargo aircraft, the share of widebodies is even higher.

Figure 72 compares the fleet composition in the model to results from the Airbus GMF [4]. The fleet forecast by Airbus is based on the same traffic growth rates and uses similar seat categories as the current study. The number of aircraft in the 2010 and 2030 fleets is roughly comparable. Minor deviations for 2010 may be due to differences between the applied database products or in the criteria for identifying seat categories. The number of aircraft in 2030 is slightly higher in the model than predicted by Airbus, mainly due to a higher share of comparably small aircraft around 100 seats. The higher number of 100-seat aircraft is in accordance with the Embraer Market Outlook [38]. In the model, the distribution of newly delivered aircraft between seat categories is based on a combination of data from the Airbus and Embraer forecasts (see chapter 3.4.4.3). As a result, the split between large aircraft above 120 seats and regional aircraft up to 120 seats is in between respective predictions by Airbus and Embraer. The aircraft size distributions within these two segments correspond to the Airbus GMF (for aircraft above 120 seats) and the Embraer Market Outlook (for regional aircraft).

As shown in the lower diagrams of Figure 72, the number of “surviving” aircraft from 2010 in the fleet of 2030 is slightly higher in the simulation than in the Airbus forecast. This deviation can be attributed to differences in the aircraft lifetime assumptions.

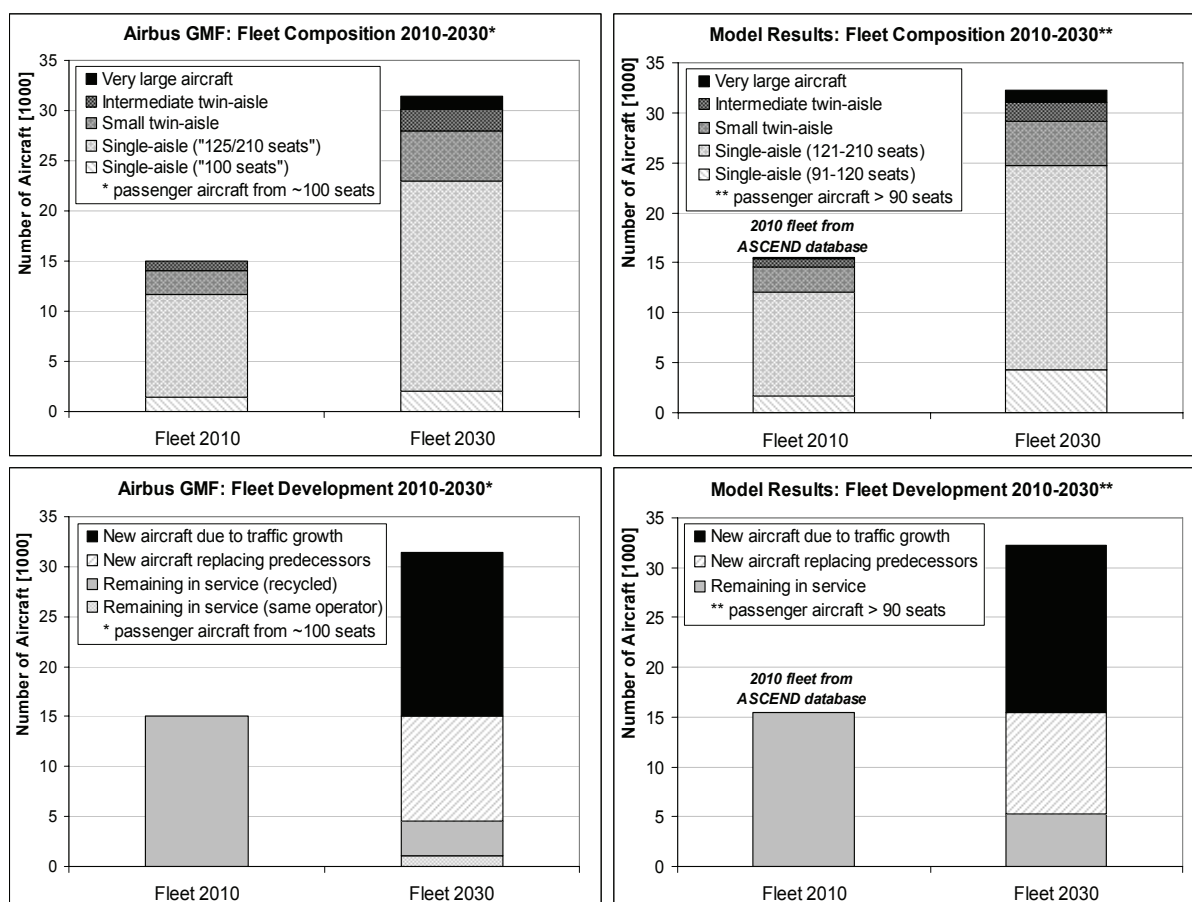


Figure 72: Comparison of simulated fleet development with Airbus GMF [4]



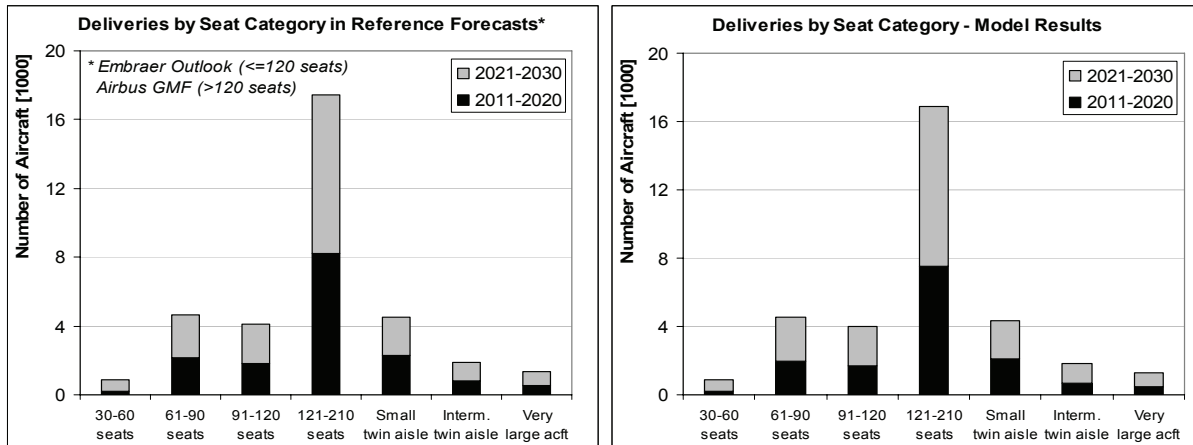


Figure 73: Delivery numbers by seat category in reference forecasts [4], [38] and model

The number of newly delivered aircraft and its distribution on seat categories is presented in Figure 73. The demand for aircraft predicted by Airbus [4] and Embraer [38] is also shown for reference. The simulated number of deliveries during 2011-2020 is lower than in the reference forecasts, whereas for 2021-2030 the model suggests slightly higher delivery numbers. The reasons for these deviations may be differences in the aircraft lifetime assumptions. This study considers a certain retirement or storage probability for aircraft even within the first 15 years after delivery (see chapter 3.4.4.2). As a consequence, the increased number of deliveries in later years may partly be attributable to replacements for retired or stored aircraft that have been delivered in early years of the forecast. In total, the number of newly delivered aircraft throughout the forecasting period is slightly lower in the simulation than in the manufacturers' forecasts. This is in accordance with Figure 72 that is showing a slightly larger "survival" fraction of the base year fleet compared to the Airbus GMF.

The above analysis demonstrates that the fleet rollover model delivers plausible results. Considering the high number of influencing factors, it is not surprising that the demand for new aircraft and the resulting fleet composition varies in forecasts from other sources. Discrepancies in the assumed traffic growth and incompatible seat categories used in different studies make systematic comparisons difficult. A quick look at the most important industry forecasts reveals the following findings: The number of widebody aircraft predicted in this study for the year 2030 is in between the respective forecasts by Airbus [4] and Embraer [38] – and nearly identical to the value from the Boeing Market Outlook [19]. Boeing predicts a higher number of single-aisle aircraft above 90 seats than Airbus and Embraer. In this segment, results from the current study are closer to the Airbus and Embraer estimations. Manufacturers of regional aircraft like Embraer and also Bombardier [23] forecast a higher demand for aircraft up to 90 seats than Airbus and Boeing. In the model, the demand for such small aircraft is slightly below the Embraer prediction. In summary, the forecast from the current study resembles common industry forecasts and can be seen as an exemplary prediction of future fleet composition.



#### 4.3.4 FUEL CONSUMPTION

Figure 74 shows the development of aviation's fuel consumption until 2030 as predicted by the Air Traffic Emissions Forecast Module. The diagram highlights the individual effects that influence fuel consumption and fuel efficiency. Fuel efficiency measured in fuel burn per tonne-kilometre is forecasted to improve by 1.18% per year on average. As can be seen in Figure 74, the fleet rollover process described in the previous chapter has the largest impact on fuel efficiency and is responsible for an annual efficiency improvement of 0.76%. Besides changes of aircraft fleet composition, the model assumes an increase of the average seat load factor from 78% to 81% between 2010 and 2030 and a corresponding change of the weight load factor from 65% to 68%. The load factor assumptions lead to an annual improvement of aviation's fuel efficiency by 0.16%. The efficiency of the Air Traffic Management (ATM) system is assumed to improve from 93% to 95% according to industry goals set by CANSO [27]. The progress in ATM has a comparably small influence on fuel consumption and contributes a yearly efficiency improvement in the order of 0.1%. Further 0.15% efficiency improvement per year result from the above-average growth of the cargo sector and a trend to longer flight distances.

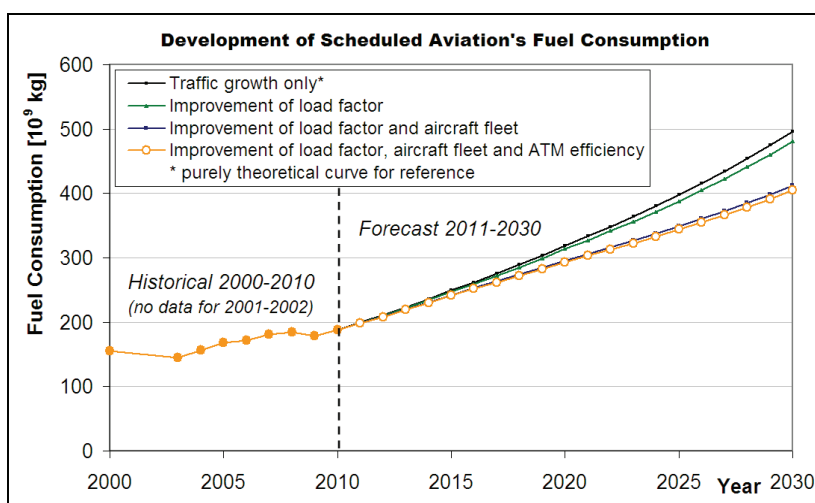


Figure 74: Influence of increased load factors, fleet rollover process and ATM efficiency improvement on fuel consumption

Fuel burn and fuel efficiency can be compared to the latest ICAO fuel burn forecast up to the year 2036 [75]. 2006 is the base year of the ICAO study while forecast results are available for the years 2016, 2026 and 2036. Figure 75 compares calculations from the Air Traffic Emissions Forecast Module to five fuel burn scenarios defined by ICAO. Furthermore, results from the Aero2k project [53], a NASA forecast for 2020 [125] and the AEDT inventories [133] are also shown in the figure. The reference studies consider scheduled and (in parts) unscheduled air traffic while the current study is restricted to scheduled flights only.

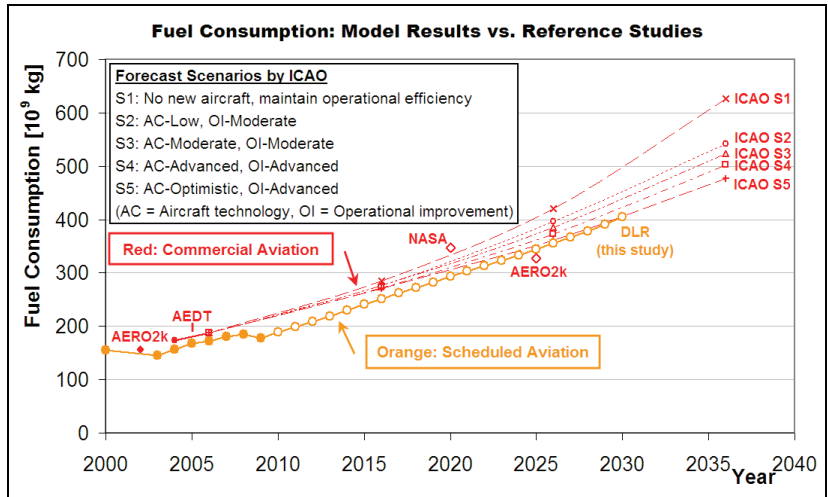


Figure 75: Comparison of fuel burn with reference studies [75], [53], [133]<sup>30</sup>

The fuel burn assumed by ICAO for 2006 is identical to the value from AEDT, which is 9% higher than the 2006 value calculated in this study. The deviation can be blamed on the lack of unscheduled flights in the DLR model. After the recovery of air traffic from the economic recession, the forecasted growth of the fuel consumption seems to follow the ICAO’s intermediate scenario 3. This ICAO scenario assumes a “moderate” improvement of both aircraft technology and operational efficiency [75]. The fuel burn from Aero2k for 2025 is lower than in the more recent forecasts, which is due to lower traffic growth rates assumed in Aero2k in combination with comparable assumptions about future fuel efficiency<sup>31</sup>.

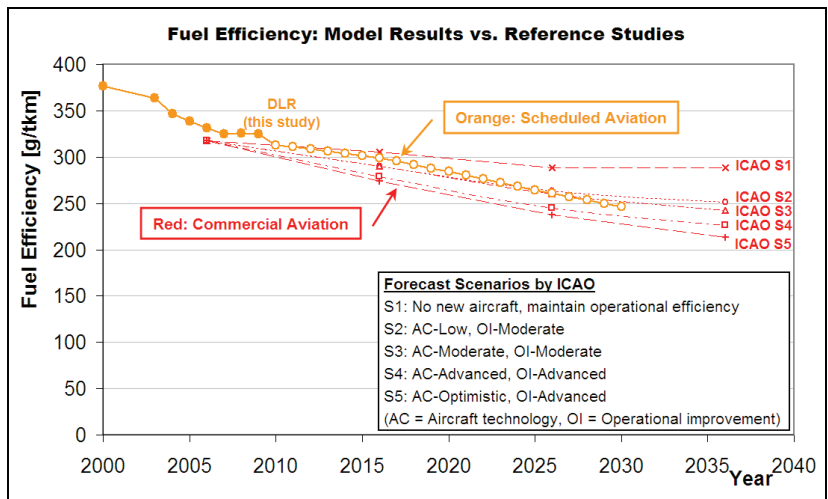


Figure 76: Comparison of fuel efficiency with reference studies [75]

<sup>30</sup> Results for “commercial aviation” cover IFR flights including unscheduled traffic for areas with radar coverage (Europe and the US). Unscheduled traffic outside these areas and VFR flights are not accounted for [75].

<sup>31</sup> In Aero2k capacity was forecasted to increase from  $4.8 \cdot 10^{12}$  to  $12.4 \cdot 10^{12}$  ASK between 2002 and 2025 [53]. This corresponds to an increase of 4.2% per year compared to nearly 5% in the current study.

More precise observations can be made when comparing fuel efficiency, which is not available for the NASA and Aero2k studies (see Figure 76). The efficiency improvement predicted in this study until 2030 is in between the ICAO scenarios 3 and 4 and can therefore be regarded as plausible. In general, the DLR model delivers slightly higher fuel burn per tonne-kilometre than ICAO. The deviation in fuel efficiency between the two studies is in the order of 4% in 2006. As a consequence, it should be within the error bars that are typically expected for any evaluation on air traffic system level<sup>32</sup>. The incomplete coverage of cargo flights, which are often more fuel efficient than passenger flights, may also contribute to the slightly higher fuel burn per tonne-kilometre observed for the DLR model.

Figure 77 shows the distribution of fuel burn and tonne-kilometres amongst different aircraft size categories. Flights by cargo aircraft – as far as covered by OAG flight schedules – consume 7% of the fuel in the base year 2010 and are responsible for 12% of the tonne-kilometres transported. By 2030, their share will increase slightly to 9% of the fuel burn and 16% of the tonne-kilometres. More than 95% of the contributions from cargo aircraft are delivered by widebody aircraft types. For passenger aircraft, trends regarding the distribution of tonne-kilometres between seat categories are similar to those identified earlier for available seat-kilometres. These trends were described in chapter 4.3.3. Widebody passenger aircraft are responsible for 43% of the fuel burn in 2010, a share that is forecasted to increase to 48% by 2030. Narrowbody passenger aircraft above 120 seats are responsible for 40% of the fuel burn with a slightly decreasing share throughout the forecast period. Their share in terms of fuel consumption will decrease to 34% by 2030. The contribution of regional aircraft up to 120 seats to aviation's fuel consumption is in the order of 10% while their contribution to transported tonne-kilometres remains around 5%.

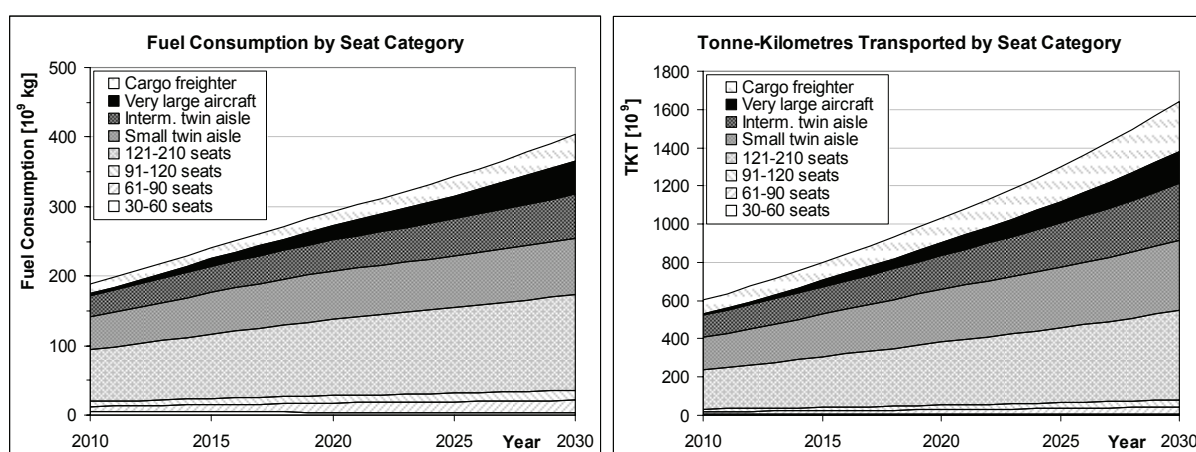


Figure 77: Distribution of fuel consumption and tonne-kilometres amongst seat categories

<sup>32</sup> See for example [67] and [113].

### 4.3.5 NO<sub>x</sub> EMISSIONS

Figure 78 presents results regarding future emissions of nitric oxides (NO<sub>x</sub>) as predicted by the Air Traffic Emissions Forecast Module. Results from reference publications are also shown in the figure including a NASA study for the year 2020 [125], the Aero2k forecast for 2025 [53] and three technology scenarios from an ICAO CAEP evaluation [82] covering the years 2016, 2026 and 2036. Considering the difficult prediction of NO<sub>x</sub> emissions from future aircraft engines on flight mission level, the uncertainty in any such study must be regarded as high. Each study uses different flight movements data, methodologies, traffic growth rates and technology assumptions. The comparison of results in the following paragraphs should therefore be regarded as a plausibility check rather than a systematic validation.

As can be seen in Figure 78, the base year NO<sub>x</sub> emissions of the Aero2k and ICAO evaluations are higher than comparable values from this study. This can partly be explained by the inclusion of unscheduled flights in both the ICAO analysis and in Aero2k. Furthermore, the ICAO and NASA publications use the Boeing fuel flow correlation for NO<sub>x</sub> calculation, which was found to deliver 6-8% higher results on average compared to the DLR fuel flow correlation (see chapter 4.2.4). The DLR fuel flow method was used in the Aero2k project and is also the standard method for NO<sub>x</sub> calculation in this study<sup>33</sup>.

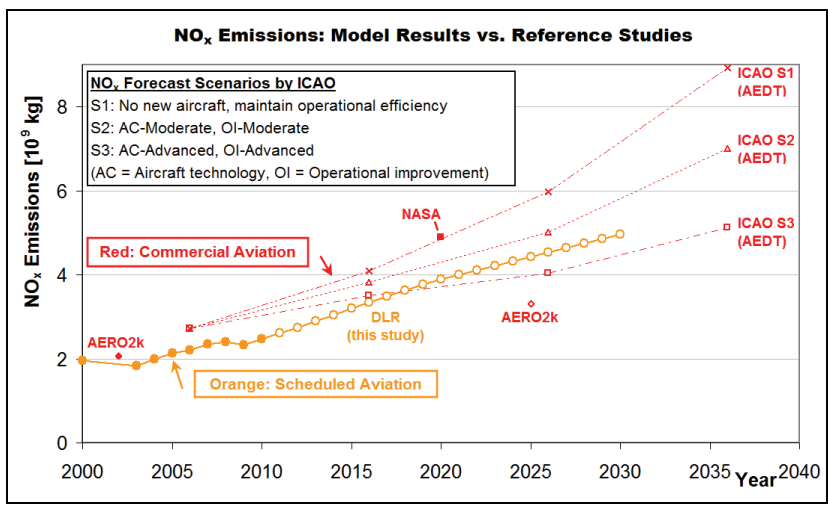


Figure 78: Comparison of NO<sub>x</sub> forecast with reference studies [53], [82], [125]

The relative increase of the forecasted NO<sub>x</sub> emissions from this study is considerably higher than predicted by Aero2k, which is due to higher traffic growth rates and less optimistic technology assumptions compared to Aero2k. Until 2016, the obtained NO<sub>x</sub> increase is higher than in the ICAO S1 scenario, while between 2020 and 2026 the slope resembles

<sup>33</sup> Except for engines with TAPS combustors, for which a p<sub>3</sub>T<sub>3</sub> approach is applied (see chapter 3.4.5). Alternative results using the Boeing method instead of the DLR method are included in Appendix U.

more the S2 scenario. The NASA inventory for 2020, on the other hand, predicts even higher  $\text{NO}_x$  emissions resulting from conservative assumptions about future engine technology.

Specific  $\text{NO}_x$  emissions measured in gram emissions per transported tonne-kilometre are visualized in Figure 79. Reference data for specific  $\text{NO}_x$  emissions are available for the ICAO CAEP scenarios only<sup>34</sup>. The deviation between results from this analysis and the base year value of the ICAO study amounts to 8% and can almost fully be explained by the different  $\text{NO}_x$  calculation methods. Specific  $\text{NO}_x$  emissions from this study show a decreasing trend, which – in early years of the forecasting period – resembles the trend from the ICAO S1 scenario. A more rapid improvement is predicted for the years after 2016, when the trend in specific  $\text{NO}_x$  emissions becomes more similar to the S2 and even S3 scenarios. No technological improvement in the field of  $\text{NO}_x$  reduction is assumed in the ICAO study after 2026 [82], which explains its lower improvement rates after this year.

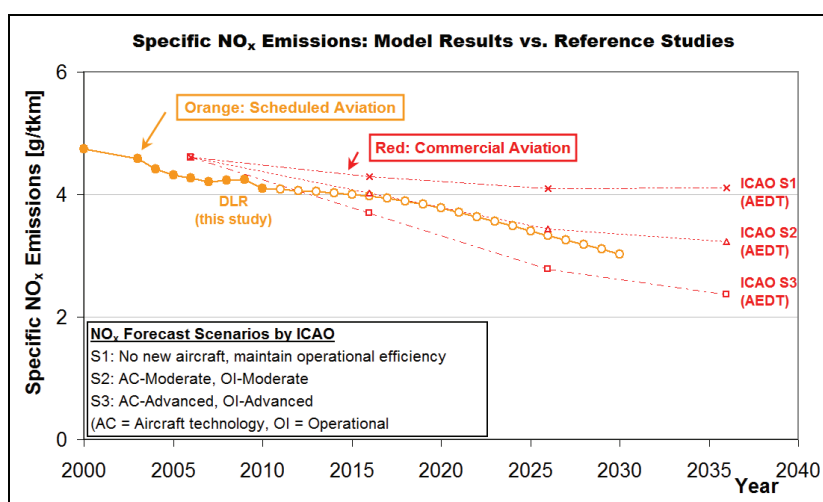


Figure 79: Comparison of specific  $\text{NO}_x$  emissions with reference studies [82]

According to the model, the main drivers behind the improvement of specific  $\text{NO}_x$  emissions until 2020 are better fuel efficiency in combination with only a minor increase of the average emission index (EI). Figure 80 shows the development of the EI  $\text{NO}_x$  measured in gram emissions per kg fuel. The more rapid improvement of specific  $\text{NO}_x$  emissions after 2020 is linked to a reduction of the EI caused by the introduction of low- $\text{NO}_x$  combustors assumed for the timeframe 2020-2025. As the uncertainty regarding developments after 2020 is high, alternative scenarios have been evaluated and will be described in chapter 4.4.2.

The ICAO scenarios S2 and S3 assume a reduction of the average EI  $\text{NO}_x$  from 2006 until 2016 and a further reduction by 2026 (see Figure 80). The higher base year EI in the ICAO

<sup>34</sup> Specific  $\text{NO}_x$  emissions for the ICAO scenarios were calculated by dividing the ICAO  $\text{NO}_x$  results by respective tonne-kilometre information obtained from corresponding ICAO scenarios on fuel efficiency.

study is largely caused by differences in the NO<sub>x</sub> calculation methods. Given the trend of increasing emission indices for NO<sub>x</sub> between 2000 and 2010 – which implies higher EIs for newly delivered aircraft compared to their predecessors – the EI NO<sub>x</sub> development according to the ICAO S2 and S3 scenarios appears rather optimistic<sup>35</sup>.

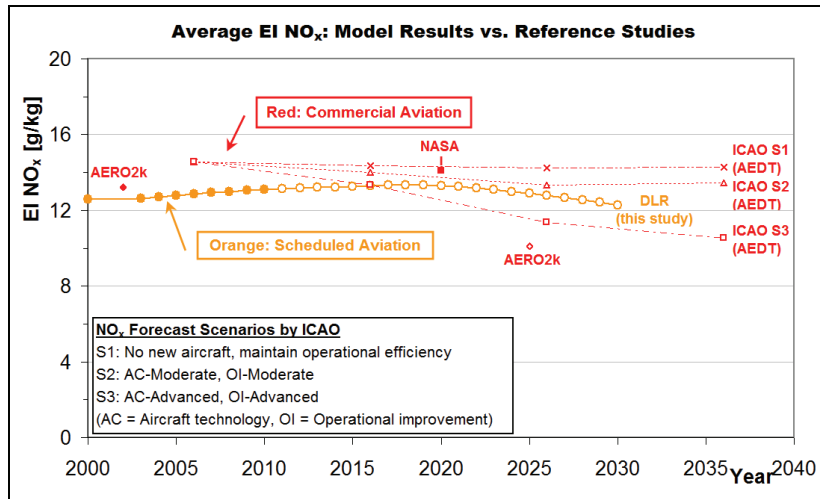


Figure 80: Comparison of forecasted EI NO<sub>x</sub> with reference studies [53], [82], [125]

The distribution of NO<sub>x</sub> emissions amongst aircraft size categories is shown in Figure 81. As can be seen from the figure, the growth of total NO<sub>x</sub> emissions is considerably lower than traffic growth in terms of transport performance (tonne-kilometres). More than half of the NO<sub>x</sub> emissions from scheduled aviation in 2010 can be attributed to widebody passenger aircraft or freighters. Given the trend towards larger aircraft types, which was discussed earlier in chapters 4.3.3 and 4.3.4, this share is forecasted to increase to nearly 60% by 2030.

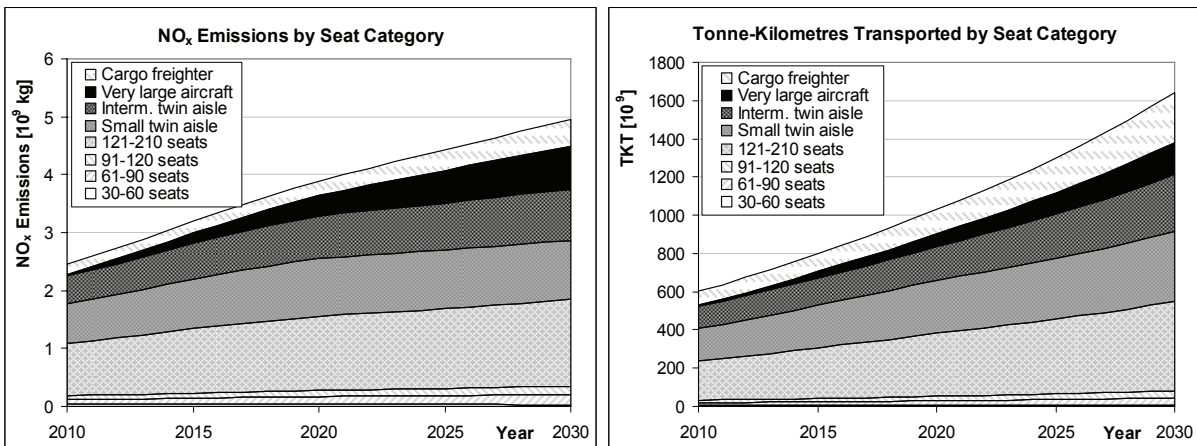


Figure 81: Distribution of NO<sub>x</sub> emissions and tonne-kilometres amongst seat categories

<sup>35</sup> The average EI NO<sub>x</sub> for the ICAO scenarios is calculated by combining scenarios of the fuel burn and NO<sub>x</sub> forecasts with corresponding technology assumptions. This assumes consistency of the respective forecasts.



## 4.4 SELECTED SENSITIVITIES AND CASE STUDIES

### 4.4.1 INFLUENCE OF TRAFFIC GROWTH

Traffic growth rates from the Airbus Global Market Forecast (GMF) [4] are assumed for the baseline forecast of air transport emissions. It is obvious that traffic growth has a major influence on fuel consumption and NO<sub>x</sub> emissions. Higher growth, for example, can be coped with by a combination of the following items:

- Increased flight frequencies, which typically implies a higher demand for new aircraft.
- Increased average load factors.
- Increased average aircraft size.

In the forecast model, traffic growth rates, load factors and the average size of newly delivered aircraft are usually set as input parameters (see chapter 3.4.4.3). In principle, all the aforementioned factors can be modified to evaluate different growth scenarios. Moderate improvements of load factors compared to the year 2010 are already assumed in the baseline scenario of the forecast. Besides, the average size of newly delivered aircraft in the baseline scenario can already be regarded as high compared to the active fleet in 2010<sup>36</sup>.

To evaluate the influence of traffic growth on model results, growth rates for passenger and freight traffic will be varied by +/-20% in a parameter study. For simplicity, load factors, aircraft lifetimes and the size of newly delivered aircraft are assumed to remain unchanged. If traffic growth rates are modified without changing any other parameters, the forecast model adjusts future flight frequencies and recalculates the resulting demand for new aircraft.

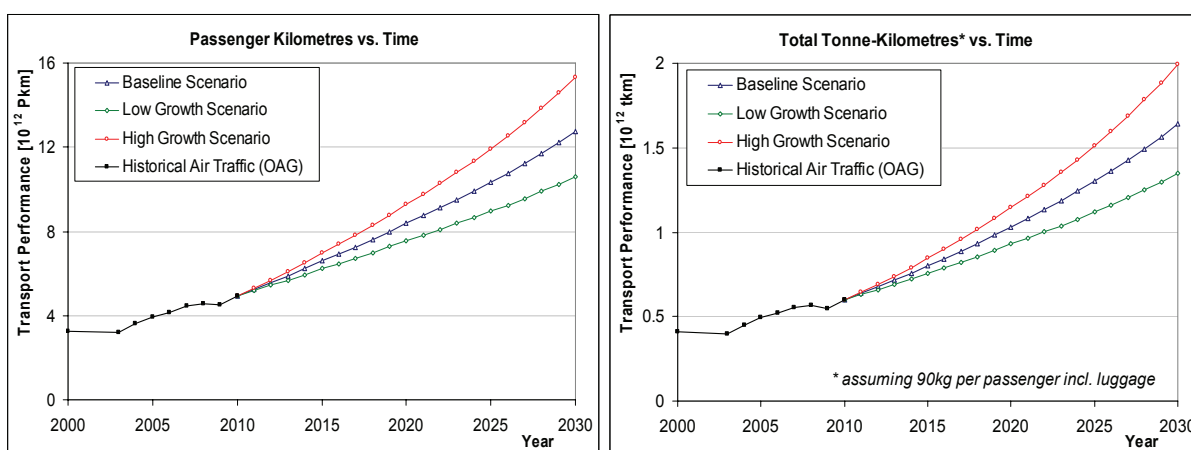


Figure 82: Transport performance in alternative traffic growth scenarios

<sup>36</sup> The distribution of newly delivered aircraft amongst aircraft size categories follows a combination of results from the Airbus GMF and the Embraer Market Outlook. More information is found in chapter 4.3.3.



Figure 82 visualizes the traffic growth scenarios examined in the parameter study, while Figure 83 shows the corresponding effects on model results. Given the aforementioned simplifications, the number of flights and the total distance travelled are roughly proportional to transport performance: By 2030, revenue passenger kilometres (RPK) and tonne-kilometres transported (TKT, including passenger and freight transport) are 20-22% higher in the high growth scenario than in the baseline forecast, while the number of flights and the total distance increase by 19-20%. The minor differences between these numbers results from the larger average size of newly delivered aircraft compared to the global fleet of 2010 and the higher number of new aircraft in the high growth scenario. Similarly, fuel consumption and NO<sub>x</sub> emissions in the high growth case are 20% higher than in the baseline scenario. In the low growth case, on the other hand, RPKs and TKTs in 2030 are 17-18% lower than in the baseline scenario while the number of flights, distance travelled, fuel consumption and NO<sub>x</sub> emissions decrease by 16-17%.

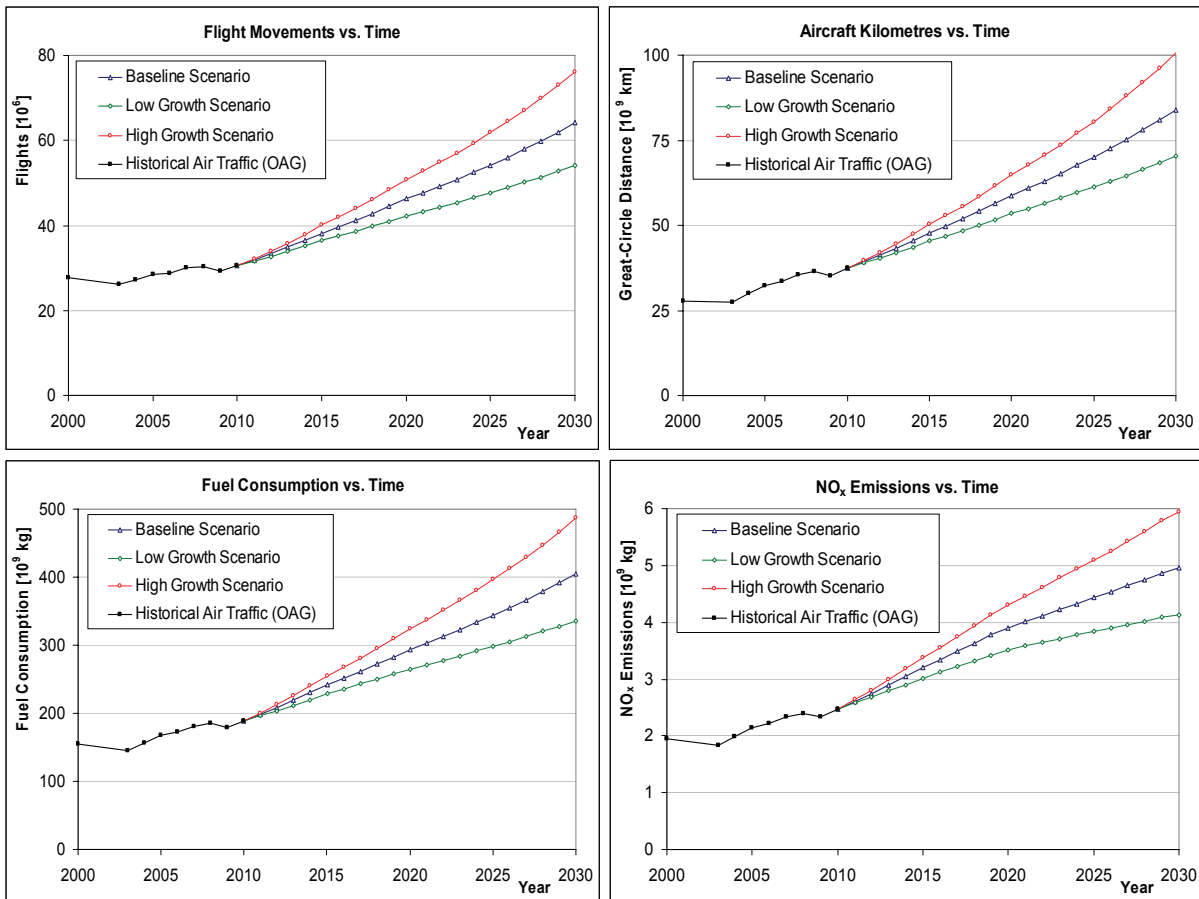


Figure 83: Flight movements, total distance, fuel consumption and NO<sub>x</sub> emissions as function of traffic growth

As can be seen in Figure 84, higher traffic growth leads to an increasing number of new aircraft and hence accelerates the fleet rollover process. The number of aircraft deliveries is roughly 23% higher in the high growth scenario compared to the baseline forecast, which

leads to a 19% increase in the number of active aircraft by 2030. In the low growth case, by contrast, the number of deliveries is 19% lower than in the baseline scenario, while the number of active aircraft decreases by 16%.

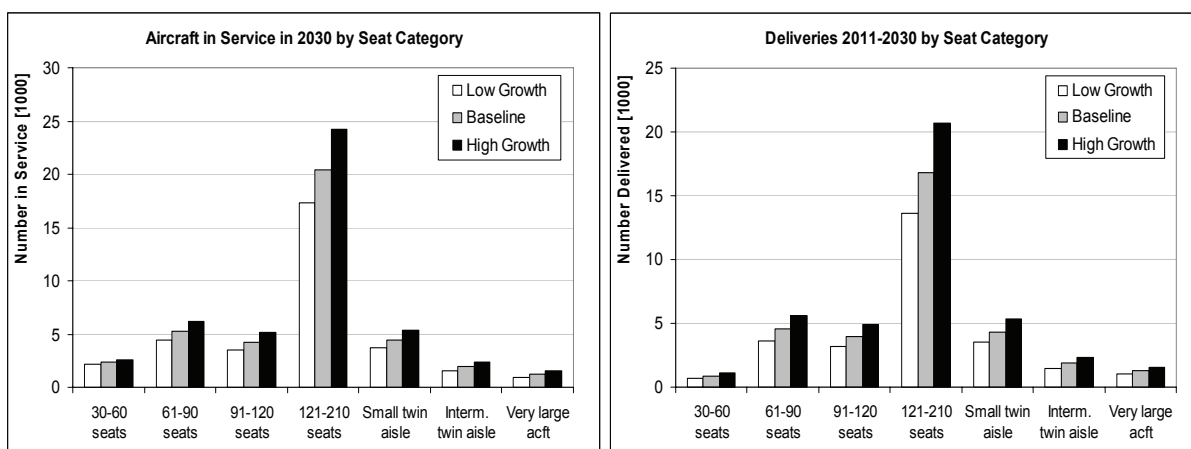


Figure 84: Number of aircraft in service in 2030 and delivered during 2011-2030

The (comparably small) effects resulting from the increasing or decreasing number of new aircraft and engine types on fuel efficiency and specific  $\text{NO}_x$  emissions are shown in Figure 85: In the high growth scenario, fuel efficiency in the year 2030 is 1.1% better than in the baseline scenario while specific  $\text{NO}_x$  emissions are reduced by nearly 1.5%. In the low growth scenario, a fuel efficiency penalty of 1.2% compared to the baseline forecast can be observed in 2030 while specific  $\text{NO}_x$  emissions also increase by 1.2%.

As initially mentioned, the parameter study discussed in this chapter aims at understanding the influence of traffic growth on model results. The Air Traffic Forecast Model developed for this study is capable of evaluating more complex scenarios including changes in the composition of the newly delivered fleet, prolonged service life of existing aircraft or load factor changes. Such detailed scenarios, however, are beyond the scope of this study.

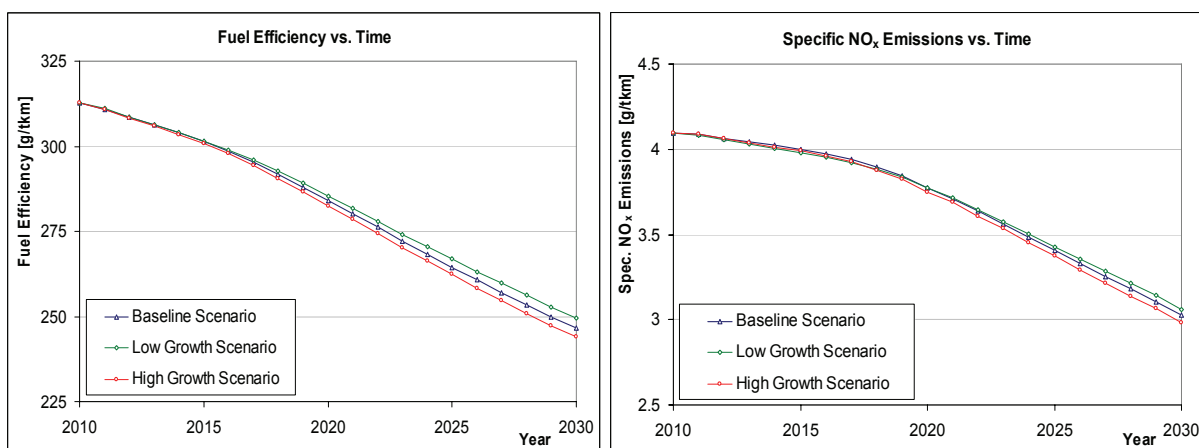


Figure 85: Fuel efficiency and specific  $\text{NO}_x$  emissions as function of traffic growth

#### 4.4.2 INFLUENCE OF ASSUMPTIONS ABOUT FUTURE ENGINE COMBUSTORS

A major source of uncertainty for the emissions forecast is the limited transparency regarding engine NO<sub>x</sub> emissions during cruise flight. Only few information on NO<sub>x</sub> emissions of future aircraft engines during cruise are available today. Simplifying assumptions are required for any forecast of NO<sub>x</sub> emissions on air traffic system level. While a detailed analysis of this uncertainty is beyond the scope of this study, a sensitivity analysis regarding selected model assumptions is presented in this chapter.

The emission models applied for aircraft engines of the near and medium-term future are mostly based on the manufacturers' design targets in terms of  $D_p/F_{00}$ , i.e. the characteristic NO<sub>x</sub> level for landing and take-off emissions used for engine certification (see chapter 3.4.5). While the engine models developed for this study cover the time period until the early 2020s, simplifying assumptions are used to estimate NO<sub>x</sub> emissions in the more distant future. As was described in chapter 3.4.6.2, a combination of two methods is applied for this purpose:

- Method 1: The assumed entry into service (EIS) of improved engine revisions is specified manually for large turbofan engines with a presumably high contribution to future NO<sub>x</sub> emissions. For aircraft delivered after this EIS date and equipped with such engines, a correction factor for NO<sub>x</sub> emissions on flight mission level is used to account for an improved NO<sub>x</sub> emission index.
- Method 2: Further stringency of engine emission standards until 2030 is assumed in this study. In each year of the forecast, compliance with assumed emission standards is checked for all newly delivered aircraft-engine-combinations that are not covered by method 1. Non-compliant engines have their emission characteristics modified automatically such that compliance to the standards is reached.

In the following analysis, the EIS of improved engine revisions will be modified compared to the baseline scenario. Table 27 summarizes the assumptions about future engine revisions for the reference case (also referred to as scenario C) and for a more optimistic scenario D. The 30% reduction targets assumed for the NO<sub>x</sub> emission indices (EI) of new engine revisions should be within the capabilities of both lean-burn and optimized RQL combustors.

Engine family	Corresponding aircraft	EIS improved combustor (Scenario C / Scenario D)	Effect of improved combustor*
Trent 1000 (EIS 2011)	Boeing 787	2020 / 2017	EI NO <sub>x</sub> as for competing GENx-1B
Trent XWB (EIS 2013)	Airbus A350	2022 / 2018	30% reduction of EI NO <sub>x</sub>
Trent 900 (EIS 2007)	Airbus A380	2024 / 2019	30% reduction of EI NO <sub>x</sub>
GP 7200 (EIS 2007)	Airbus A380	2026 / 2020	30% reduction of EI NO <sub>x</sub>
Generic / RQL (EIS 2016)	A320 NEO	- / 2022	30% reduction of EI NO <sub>x</sub>

Table 27: Baseline assumptions and alternative assumptions for future low-NO<sub>x</sub> combustors

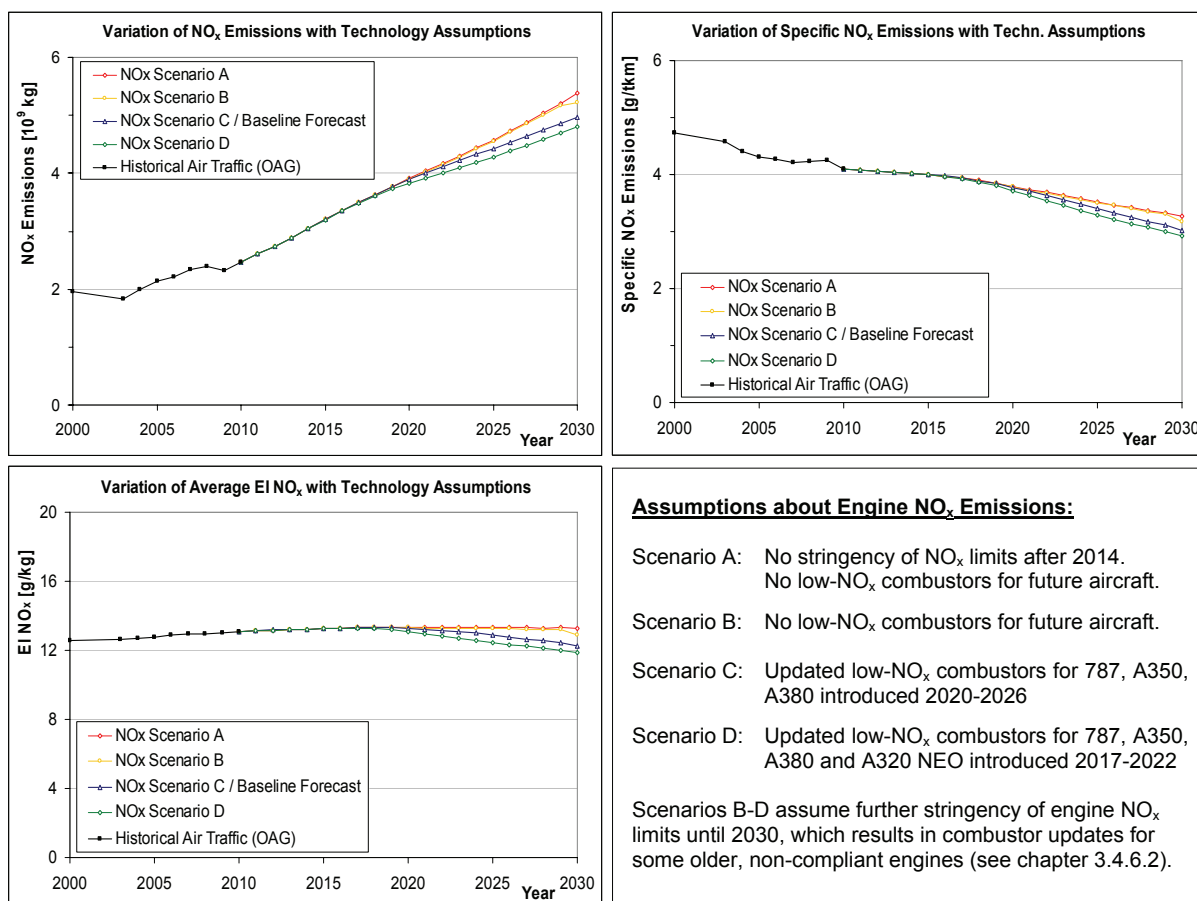


Figure 86: Variation of NO<sub>x</sub> Emissions with Technology Assumptions

Unlike in scenarios C and D, scenarios A and B do not assume an introduction of improved combustors for the aircraft engines shown in Table 27. While the emission standards predicted for the future are still enforced in scenario B, no further stringency of NO<sub>x</sub> limits after 2014 is assumed in scenario A.

Figure 86 presents the results of the sensitivity analysis. As can be seen from this figure, specific NO<sub>x</sub> emissions measured in gram emissions per kg fuel show a decreasing trend in all four scenarios. The NO<sub>x</sub> emission index, on the other hand, is increasing in scenarios A and B until the late 2020s whereas a peak EI is reached in scenarios C and D between 2015 and 2020. Quantitatively, assumptions for low-NO<sub>x</sub> engine combustors have a considerable influence on NO<sub>x</sub> emissions after the year 2020: The earlier introduction of low-NO<sub>x</sub> combustors in scenario D leads to 3.1% lower NO<sub>x</sub> emissions by 2030 compared to the baseline scenario. Without assuming improved combustors for major aircraft types, scenario B delivers NO<sub>x</sub> emissions which are 5.2% higher in 2030 compared to the reference case. On the other hand, the influence of stricter emission standards on simulation results is comparably small: Scenario A leads to 8.2% higher NO<sub>x</sub> emissions than in the baseline forecast, but only 2.9% higher emissions than in scenario B.

The surprisingly low delta between scenarios A and B can be explained as follows:

- Only a selection of new engine types, all of which are assumed to be certified before the year 2022, are simulated explicitly in the model. NO<sub>x</sub> emissions of these engines, which typically represent the baseline variants of an engine family, easily meet the assumed certification limits.
- Derivative versions of these engines (e.g. higher thrust variants certified later than the baseline engine) may be affected by more stringent certification standards in later years of the forecast. Such engine variants are not explicitly included in the model<sup>37</sup>.
- NO<sub>x</sub> standards for engine types that are in production are typically less strict than certification limits. Only few engine types in the model reach the assumed limits and require an update for compliance with the standards during their production periods.

Until 2029, the slightly lower NO<sub>x</sub> emissions in scenario B as against scenario A are mainly caused by a new combustor revision assumed for GE90 engines on the Boeing 777-300ER. In scenario B, the model introduces an improved combustor in 2020 in order to meet the stringency of NO<sub>x</sub> emission standards that is assumed for this year<sup>38</sup>. The following stringency of standards for in-production engines is assumed for 2030, which explains the improvement of specific NO<sub>x</sub> emissions between 2029 and 2030 that can be observed in results for scenario B.

Considering the lack of reliable reference data, assumptions regarding the introduction of future low-NO<sub>x</sub> combustors are difficult to make. In the baseline scenario of this study, new combustor revisions are assumed to be introduced in the early 2020s for selected families of large aircraft engines with a high share of future emissions. Given the potential of lean burn combustors to significantly reduce NO<sub>x</sub> emissions on flight mission level [97], such assumptions have a considerable impact on aviation's NO<sub>x</sub> emissions after the year 2020. By contrast, the consideration of NO<sub>x</sub> emission standards in the model has only a minor influence on model results. This functionality can be seen as an additional check for aircraft and engine production periods that are set as input parameters for a simulation run.

---

<sup>37</sup> But are represented by the baseline engine of the respective family for emissions calculation.

This limitation is the main reason for defining improved engine revisions manually for major engine types.

<sup>38</sup> See chapter 3.4.6.2 for assumptions about emission standards. The 777-300ER is produced until 2021 in the baseline fleet scenario. As a result, only aircraft delivered in 2020 and 2021 are affected by this modification.

### 4.4.3 DELAYED INTRODUCTION OF NEW AIRCRAFT

Changes in the aircraft manufacturers' development plans for future aircraft types affect fuel efficiency and emissions of future air transport. As an exemplary case study and to demonstrate the model's capabilities, delays in the introduction of future aircraft types and the resulting effects on fuel burn and emissions of NO<sub>x</sub> will be evaluated in this chapter. In the past, delays in the development, production and delivery of new aircraft types could be observed for a number of major projects. In October 2011, the first Boeing 787-8 aircraft entered commercial service at All Nippon Airways, more than three years behind the original schedule. The first delivery of an Airbus A380-800 to Singapore Airlines took place in October 2007 instead of June 2006 as originally planned. The development of a stretched A380-900, which was planned to be introduced in 2015, and of the cargo version A380F once scheduled for the year 2009, is currently suspended.

In order to quantify the additional fuel burn and emissions resulting from a delayed introduction of new technology, the entry into service (EIS) of future aircraft types is modified compared to the baseline scenario. The production periods of their predecessors are prolonged accordingly. As development delays may also affect succeeding projects of an aircraft manufacturer (due to limited engineering resources), the assumed delivery delays are higher for aircraft of the more distant future than for aircraft types announced for the near future. Table 28 summarizes the main assumptions in this case study. The introduction of stricter NO<sub>x</sub> emission standards and the EIS of improved (low-NO<sub>x</sub>) engine revisions are assumed to be delayed accordingly. Details regarding the stringency scenario for NO<sub>x</sub> emission standards in this case study are found in Appendix T.

EIS in baseline scenario	Affected large passenger aircraft (and their engine types*)	Assumed EIS delay in sensitivity analysis*
2011-2013	787-8, 747-8	+1 year
2014-2015	787-9, A350-900, CSeries	+2 years
2016-2018	A350-800/1000, A320 NEO family, 737 MAX 7/8, C919-200	+3 years
> 2018	A380-900, 777-200/300 Successors, 737 MAX 9, C919-300	+5 years
* Delayed EIS of an aircraft type equally delays the EIS of improved engine revisions for this aircraft (see chapter 3.4.6.2).		

*Table 28: Assumptions about delivery delays of future aircraft types in sensitivity study*

Figure 87 compares the fleet composition of large passenger aircraft in the baseline forecast of this study and in the sensitivity scenario described above. In the sensitivity scenario, the number e.g. of Airbus A350 aircraft or of the assumed 777 successor are lower throughout the forecast, while the share of the current generation of aircraft (e.g. the Boeing 777) is higher than in the baseline forecast. In the narrowbody sector the delayed introduction of the Airbus A320 NEO and 737 MAX families is clearly visible in the diagrams – and is compensated by additional deliveries of A320 and 737 aircraft from the previous generation.

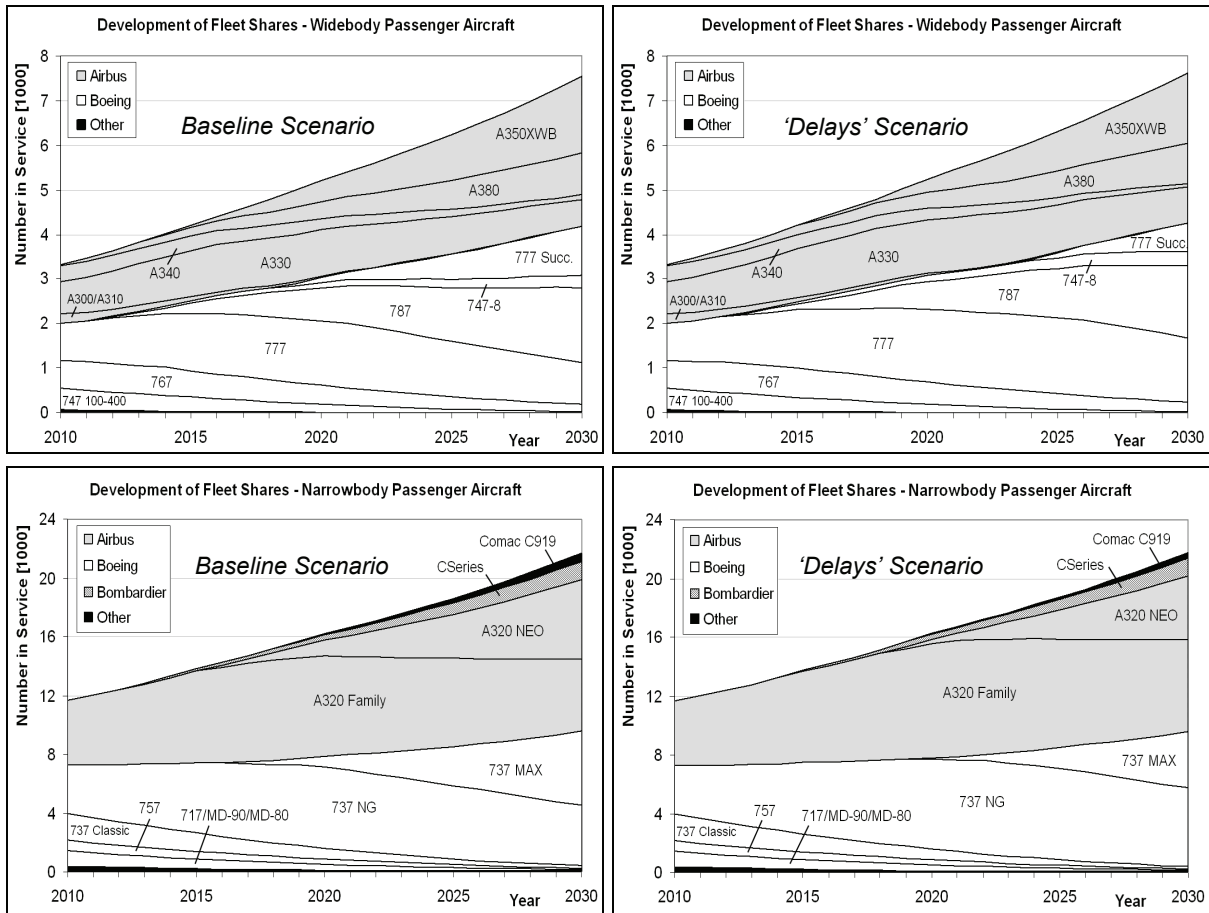


Figure 87: Fleet shares of large passenger aircraft in baseline scenario (left) and in scenario with delivery delays (right)

The effects of the delayed introduction of new technology on total fuel burn and NO<sub>x</sub> emissions are shown in Figure 88. A third scenario is also included in the figure: in this hypothetical scenario, no new aircraft types and engine revisions are introduced throughout the forecast while aircraft types that are in production in 2010 will continue to be delivered until 2030<sup>39</sup>. Taking this scenario as a reference, the newly introduced technology assumed in the baseline forecast leads to 9.6% lower fuel burn and 19.3% lower NO<sub>x</sub> emissions by 2030. About 2.5% more fuel is consumed in the “delays” scenario in 2030 while total NO<sub>x</sub> emissions are 4.1% higher than in the baseline forecast.

As the observed deltas of fuel burn and emissions are small, in-depth analyses of results can be performed to highlight differences between the scenarios. The left diagram in Figure 89 shows the fuel efficiency measured in gram fuel per transported tonne-kilometre in the aforementioned scenarios. For comparison, the right diagram presents the fuel efficiency of newly delivered aircraft in their first year of service. As expected, the efficiency of the newly

<sup>39</sup> Except aircraft types with a recently launched successor that go out of production in early years of the forecast.



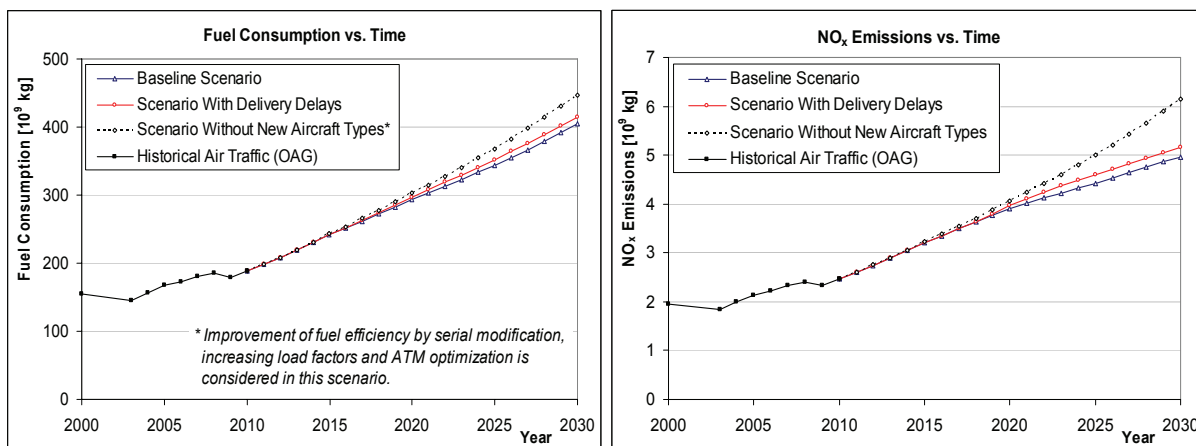


Figure 88: Effects of delivery delays on fuel burn and emissions of air traffic

delivered fleet is better than the fuel efficiency of the total fleet. More interesting is the step-by-step improvement of the new fleet's fuel efficiency e.g. in the baseline forecast, which is due to the introduction of new aircraft types. Additional components that are contributing to efficiency changes are a moderate increase of load factors, higher efficiency of future air traffic management and minor modification of aircraft types by serial modification. These secondary factors, which are simulated as continuous (year-by-year) improvements, are responsible for the efficiency change of the newly delivered fleet in the scenario without new aircraft types. Some fluctuation in the efficiency of the newly delivered fleet is observable in Figure 89 due to the comparably low number of flights performed by newly delivered aircraft and the stochastic selection of these flights when simulating the fleet rollover process.

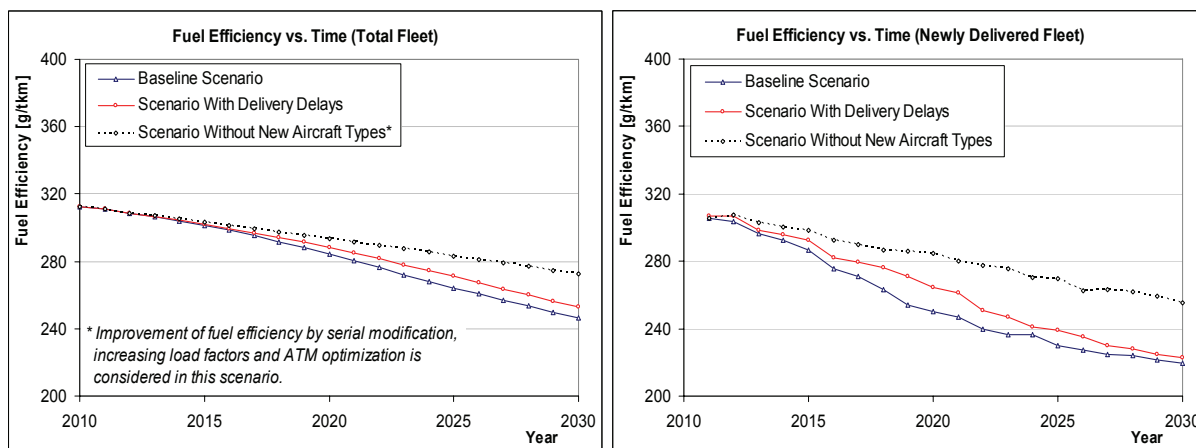


Figure 89: Effects of delivery delays on fuel efficiency

Considering the large number of aircraft types in the simulation and secondary effects on fuel efficiency mentioned above, it is difficult to identify the individual contributions leading to year-by-year efficiency improvements. Figure 90 shows an exemplary analysis for the fleet segment with 121-210 seats. The influence of a delayed introduction of new aircraft types is

clearly visible in the diagram. For the evaluated fleet segment, improvements in the efficiency of the newly delivered fleet as well as improvements in its specific NO<sub>x</sub> emissions can be traced back to the introduction of the A320 NEO and 737 MAX families. Other new aircraft types (e.g. the Comac C919 family and the Bombardier CS300) also belong to this seat category, but have only minor market shares and a much more limited influence on average fuel efficiency and emissions.

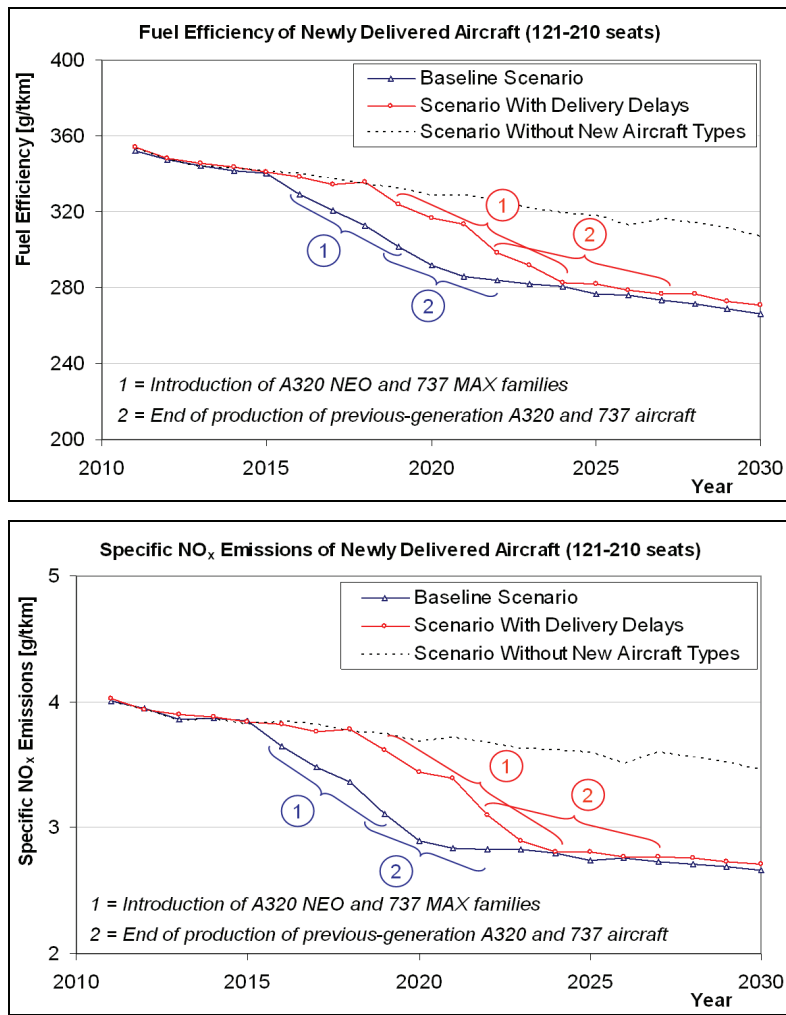
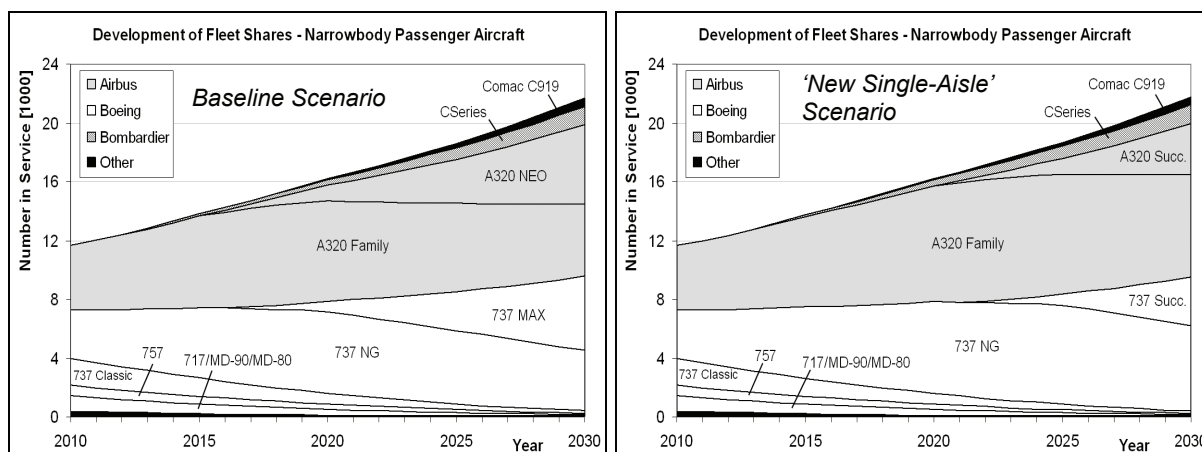


Figure 90: Effects of delivery delays on fuel efficiency and specific NO<sub>x</sub> emissions - exemplary analysis for the fleet segment with 121-210 seats

#### 4.4.4 NEW SINGLE-AISLE AIRCRAFT INSTEAD OF RE-ENGINEED A320 AND 737

In an additional case study, new single-aisle aircraft are assumed to be introduced by Airbus and Boeing instead of the re-engineed A320 NEO and 737 MAX families. The considerably higher development effort for a new single-aisle aircraft is expected to result in a later entry into service (EIS) of the new aircraft compared to the re-engineed A320 and 737 variants. Simulation models for a generic single-aisle aircraft family powered by an advanced turbofan engine have been created and are used as representative models for successors of the A320 and 737 aircraft. Assuming an EIS in the early 2020s, the new aircraft are estimated to be 27-30% more fuel efficient than the A320 and 737 and about 15% more fuel efficient than the A320 NEO and 737 MAX (see chapter 3.4.5). In the following assessment, the new aircraft types are introduced from 2021 onwards, five years later than the A320 NEO and 737 MAX families in the baseline forecast. The production periods of A320 and 737 from the previous generation are prolonged accordingly. Details regarding the assumed production periods of all aircraft variants are found in Appendix O.

Figure 91 shows the fleet composition in the narrowbody segment for the baseline scenario and for the alternative scenario with the newly developed aircraft. The later introduction of these aircraft types compared to the A320 NEO and 737 MAX families in the baseline scenario is visible in the charts below.



*Figure 91: Fleet shares of large single-aisle passenger aircraft in baseline scenario (left) and in scenario with new single-aisle aircraft types (right)*

The difference between the baseline forecast and the alternative scenario regarding fuel efficiency and specific NO<sub>x</sub> emissions is shown in Figure 92 for the fleet segment with 121-210 seats. The A320 and 737 families (and their successors) dominate this category and are responsible for 80-90% of its fuel consumption. The improved fuel efficiency and lower NO<sub>x</sub> emissions of the newly developed aircraft compared to the A320 NEO and 737 MAX are visible in the lower diagrams of Figure 92, which refer to newly delivered aircraft only.

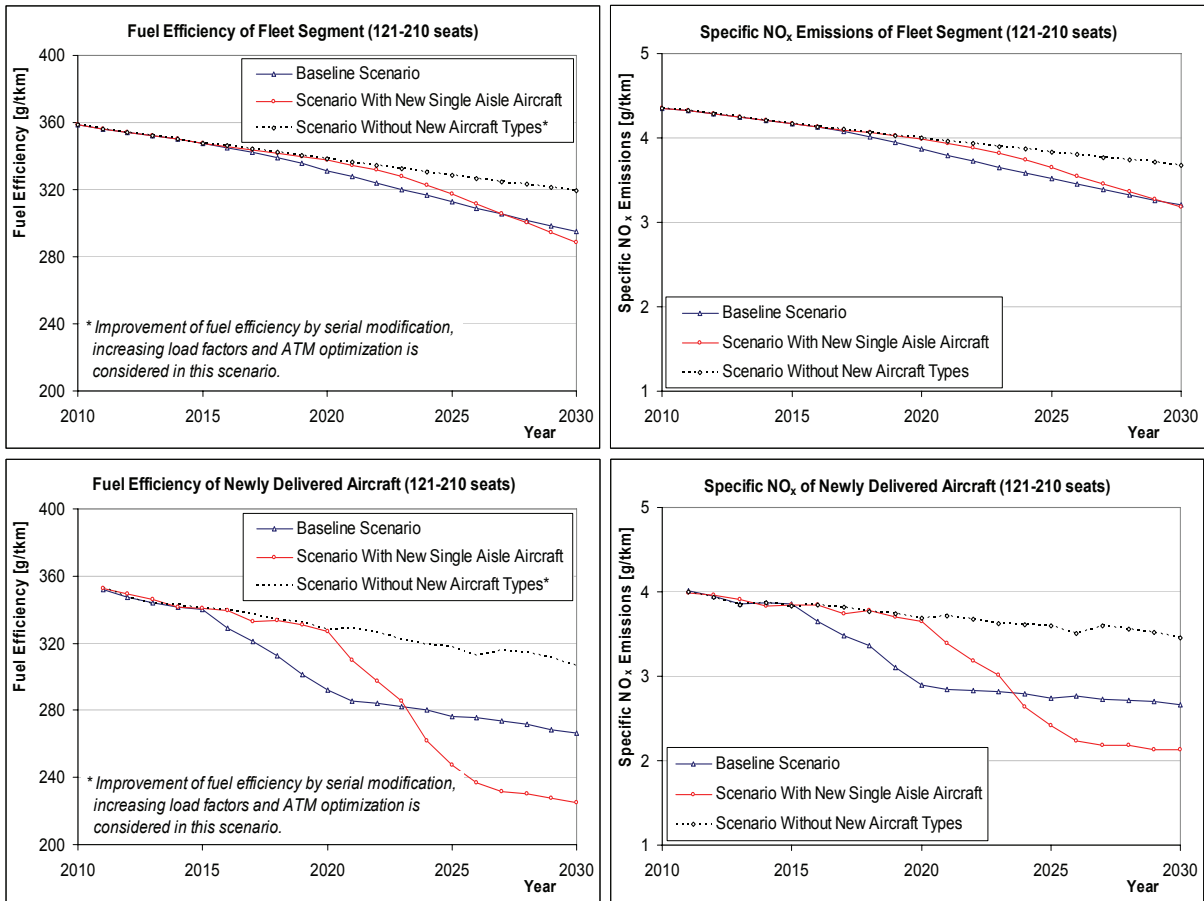


Figure 92: Comparison of fuel efficiency and specific NO<sub>x</sub> emissions in different scenarios

The upper diagrams in Figure 92 cover all aircraft in the fleet segment and show the effect of the fleet rollover process on average fuel efficiency and specific NO<sub>x</sub> emissions. As can be seen in the above charts, the fleet rollover requires time and delays the effects of any new aircraft types. The new single aisle aircraft, which are gradually introduced between 2021 and 2024, account for 33% of the fleet segment in the last year of the forecast. In the baseline scenario, for comparison, A320 NEO and 737 MAX account for 51% of the fleet segment in 2030 due to their earlier EIS. As a consequence, the delta in fuel efficiency between the baseline and the alternative scenario is of small magnitude (<1%). Until 2030, the improved fuel efficiency of the all-new aircraft types is largely compensated by their later introduction.

While advanced combustor technology used in the new single-aisle aircraft leads to lower NO<sub>x</sub> emissions than for the A320 NEO and 737 MAX, a similar effect can be observed for global NO<sub>x</sub> emissions. The aircrafts' improved characteristics are compensated by their later introduction and will not lead to lower NO<sub>x</sub> emissions until the year 2030. However, the uncertainty regarding NO<sub>x</sub> emissions for both the re-engined and the new single-aisle aircraft should be regarded as high. At the time of writing, only limited information is available on NO<sub>x</sub> emissions of the engines for A320 NEO and 737 MAX. Consequently, as was discussed

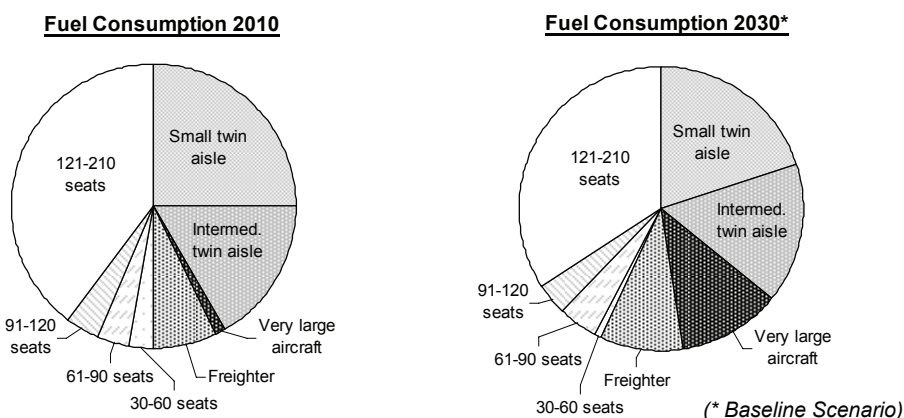


Figure 93: Distribution of fuel consumption between aircraft size categories

in chapter 3.4.5, the emission characteristics assumed for the simulated engine models are estimations only and may deviate from those of the real engines.

The significance of the fleet segment with 121-210 seats for global fuel consumption and emissions is visualized in Figure 93. Aircraft from this segment are responsible for 40% of air traffic's fuel consumption in 2010. According to the baseline forecast from this study, their share will decrease slightly throughout the forecasting period to about 33% in 2030. Despite this decrease, which is caused by the above average growth of the widebody segment, the share is still higher than for any other seat category used in this study. Total fuel consumption and  $\text{NO}_x$  emissions from air traffic are finally presented in Figure 94. The delta in fuel consumption between the baseline forecast and the alternative scenario with new single-aisle aircraft remains within 1%. Results for  $\text{NO}_x$  show a similar pattern as for fuel consumption. Considering the small deltas observed in the single-aisle segment alone, which were discussed in the previous paragraphs, the comparably low effects on global fuel burn and emissions are plausible.

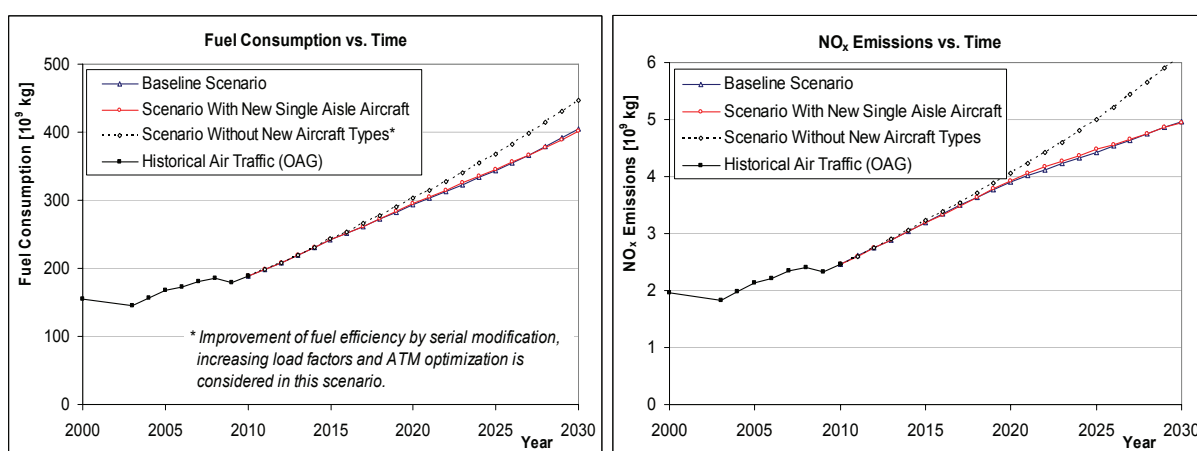


Figure 94: Comparison of global fuel burn and  $\text{NO}_x$  emissions in different scenarios

## 5 PERSPECTIVES

### 5.1 OUTLOOK ON FUTURE AIR TRAFFIC

While aviation contributes to economic growth, environmental balance is becoming a decisive requirement for the air transport sector. Increased awareness for environmental aspects both in the public and in the political community have lead to regulatory measures to reduce air traffic noise and emissions. This includes the recent stringency of NO<sub>x</sub> emission standards for aircraft engines from 2014 onwards [81] and the planned inclusion of aviation into the EU emissions trading scheme in 2012 [28], [115]. Current discussions on ICAO level regarding a future CO<sub>2</sub> standard for aircraft indicate growing political pressure on airline and aircraft industries.

Aircraft emissions of carbon dioxide (CO<sub>2</sub>) are proportional to fuel burn and contribute to climate change. From an ecological point of view, uncoupling traffic growth and fuel consumption is desirable. This is reflected by current technology goals: The International Civil Aviation Organization (ICAO) aims at a 2% annual improvement of fuel efficiency through 2050 [75] while the International Air Transport Association (IATA) targets a 1.5% efficiency improvement per year until 2020, and carbon-neutral growth afterwards [68]. Results from the current study are summarized in Figure 95 and consider available information about aircraft and engine developments of the short-term and medium-term future. Using fuel burn per tonne-kilometre as a measure of fuel efficiency, this study predicts an efficiency improvement of 1.2% per year on average between 2010 and 2030. The forecasted improvement of fuel efficiency is higher in the 2020s (around 1.4% p.a.) than in the first decade of the forecast (1.0% p.a.). In the light of these findings, the aforementioned targets by ICAO and IATA must be regarded as ambitious.

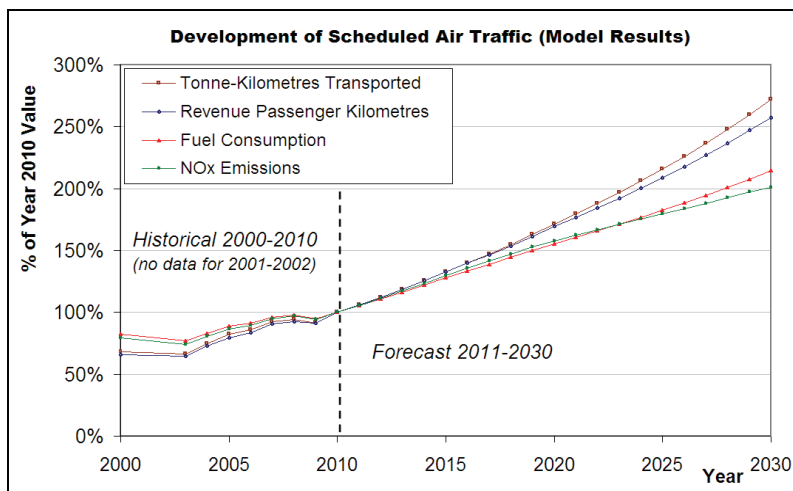


Figure 95: Development of transport performance, fuel burn and NO<sub>x</sub> emissions 2000-2030

To close the gap between the targeted improvement of CO<sub>2</sub> emissions and progress on the aircraft and engine sides, alternative fuels and economic measures are increasingly in the focus of the airline industry. As was described in chapter 2.3.4, alternative (drop-in) fuels have a considerable potential for reducing CO<sub>2</sub> emissions from a life-cycle perspective. Fischer-Tropsch fuel produced from biomass (biomass to liquid, BTL) enables reductions of life-cycle greenhouse gas (GHG) emissions in the order of 80-90% compared to conventional jet fuel [124]. The GHG reduction potential for jet fuel obtained from hydroprocessed esters and fatty acids (HEFA) is typically lower and currently estimated as 40-70% [124].

Figure 96 compares IATA's environmental targets to the life-cycle CO<sub>2</sub> emissions from aviation fuels. The diagram visualizes the influencing factors on CO<sub>2</sub> emissions that were discussed in earlier chapters. In addition, effects of alternative fuels are assessed for the year 2030. Assuming biofuels with 80% reduced GHG emissions (on average) compared to conventional jet fuel, a biofuel market share of nearly 40% would be required in 2030 in order to meet the IATA targets mentioned before. In the aviation community, market shares of 5-30% are currently discussed for the year 2030 [12], [40], the higher estimates being difficult to achieve. In the longer term until 2050, IATA aims at reducing GHG emissions to 50% of the emissions from the year 2005 [68]. This target is visualized in Figure 97, using the optimistic ICAO S5 scenario [75] as a reference for fuel consumption in 2050<sup>40</sup>. Figure 97 indicates that under the assumptions mentioned above, the long-term target cannot be met by means of alternative fuels alone. Forecasted biofuel market shares for 2050 are highly

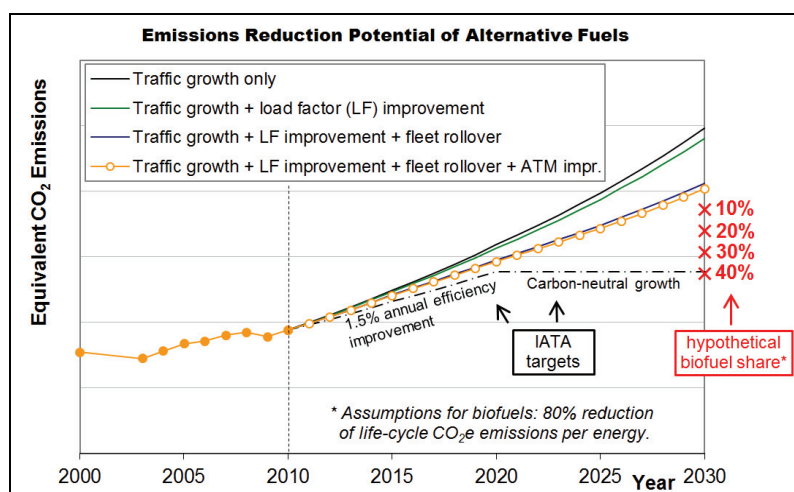


Figure 96: IATA environmental targets and potential effects of alternative fuels<sup>41</sup>

<sup>40</sup> Using the ICAO S5 prediction of fuel burn in 2050 implies a higher annual improvement of fuel efficiency in 2030-2050 than obtained in this study for 2010-2030. See chapter 4.3.4 for information on ICAO S5.

<sup>41</sup> Life-cycle equivalent CO<sub>2</sub> (CO<sub>2</sub>e) emissions include GHG emissions from fuel production, distribution and combustion. They are here assumed to be proportional to fuel consumption for a given type of fuel.



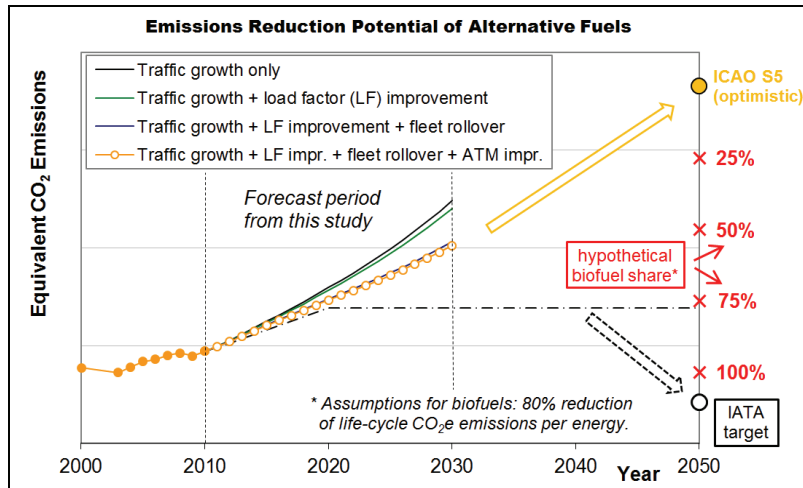


Figure 97: Analysis of IATA's long term target for CO<sub>2</sub> emissions

speculative and range from 30% [83] to 100% [12]. However, it is hard to tell if the barriers that are preventing large-scale use of alternative fuels can be overcome. The cost of sustainable fuel is an important issue: neither BTL nor HEFA fuels are currently cost competitive. According to results from the SWAFEA project [99], cost competitiveness with conventional jet fuel cannot be expected before 2030 for BTL fuels and around 2040 for HEFA solutions – even in a scenario assuming a large-scale production ramp-up, abundant availability of capital and cheap feedstock resources. Capital expenditure to establish production facilities is seen as the number one barrier for BTL fuels while HEFA fuels are more constrained by the feedstock price [99]. New processes may emerge until 2020, but are currently in an early stage of development. Besides fuel costs, the availability of production capacities and of feedstock resources are potential bottlenecks that need to be addressed [99], [124]. According to SWAFEA, more than 50% of all available biomass from agriculture, forestry and waste would be required in 2050 in order to reduce projected greenhouse gas emissions from aviation to levels of the year 2020 [99]. While this is regarded as technologically feasible, it requires considerable effort and investment in agriculture [99]. The use of alternative feedstock resources like algae appears promising, but respective production pathways are not yet mature. Furthermore, the GHG reduction by use of HEFA fuels from algae is estimated as only 42% compared to conventional jet fuel in a baseline scenario, however at high variability depending on details of feedstock recovery [124].

In addition to alternative fuels, political and economic measures are required in order to reach the ambitious industry goals. Economic measures include carbon offset mechanisms or emissions trading, which provide means to allow traffic growth while limiting GHG emissions at the same time. In the European Union, aviation is planned to be included into the EU Emissions Trading Scheme (ETS), which has already been established for stationary emission sources [28]. In a cap-and-trade approach, airlines are obliged to hold allowances for their CO<sub>2</sub> emissions from 2012 onwards. With few exceptions, commercial flights

departing from or arriving at EU airports will be subject to the trading scheme [28]. An emissions cap will be in force, which is intended to be lowered in the future. In order to enable further growth, airlines need to purchase emission allowances from other operators or other industry sectors, where CO<sub>2</sub> reductions may be easier (and cheaper) to achieve.

Non-CO<sub>2</sub> emissions of air traffic are more difficult to deal with, as they are not proportional to fuel burn. It is essential to consider these emissions and their potential impact on climate: Emissions of NO<sub>x</sub> from aircraft engines influence atmospheric chemistry and indirectly contribute to global warming [89], [112]. Aircraft emissions of soot are believed to influence cloud formation, which may also affect climate [121]. The difficulty in forecasting non-CO<sub>2</sub> emissions is caused by the complexity of the combustion process in aircraft engines, the large number of aircraft and engine types, limited availability of reference data from industry and technological trade-offs to be considered for future aircraft and engine development. In this study, soot emissions were assessed for historical aviation from the year 2000 until 2010, while a forecast of future soot emissions was omitted due to lack of reference data. Limited information is provided by engine manufacturers on NO<sub>x</sub> emissions of future aircraft engines, although the comprehensiveness and quality of this data are not satisfactory: Emission standards for NO<sub>x</sub> and respective technology targets are mostly defined on engine level and refer to the ICAO's standardized landing and take-off (LTO) cycle. Emission targets for future engines are often specified relative to an emission standard, which is a function of the engine's pressure ratio. Without knowing the engine's pressure ratio at maximum thrust, this information is of limited value for emissions quantification. More importantly, no information is published by engine manufacturers on engine emissions during cruise flight. Given current trends towards higher engine bypass ratios and pressure ratios, and considering the recent introduction of staged lean-burn combustors, the relation between NO<sub>x</sub> output in the LTO cycle and NO<sub>x</sub> emitted during cruise flight is getting increasingly complex. Detailed engine models and flight simulations are required in order to predict NO<sub>x</sub> emissions at cruise altitude and on flight mission level. As a consequence, emission calculations on air traffic system level result in a considerable modelling effort. An additional certification requirement for aircraft or aircraft engines covering NO<sub>x</sub> emissions during cruise flight would help to improve transparency with respect to NO<sub>x</sub> emissions of global air traffic.

In the emissions forecast developed for this study, specific NO<sub>x</sub> emissions measured in gram NO<sub>x</sub> per transported tonne-kilometre are predicted to decrease by 27% between 2010 and 2030. In this forecast, advanced low-NO<sub>x</sub> combustors using lean burn technology are assumed to gain significant market shares in the 2020s. Alternative scenarios have also been evaluated and were discussed in chapter 4.4.2. The reduction of specific NO<sub>x</sub> emissions in the baseline scenario of the forecast exceeds the expected improvement of fuel efficiency and can be seen as a result of the high investments into low-NO<sub>x</sub> combustion technology that were made by the engine industry in the past two decades.

## 5.2 PAST AND FUTURE MODEL APPLICATION

The software modules presented in this study have been used in a number of European and DLR research projects. Developed at the DLR Institute of Propulsion Technology, future use of the tool chain will focus on effects of future engine technology on global aviation emissions.

The VarMission module for flight mission and emissions calculation can be seen as a replacement for the former VarFlight tool of the DLR Institute of Propulsion Technology. VarMission was initially applied in a DLR research project on particle emissions named PAZI-2 [86]. In this activity, VarMission and the VarCycle engine simulation were used to calculate emission profiles including soot emissions for a number of aircraft-engine combinations. Flight mission analyses were also conducted in the CLAIRE 2 project of the DLR Institute of Propulsion Technology and MTU Aero Engines [35] and in a study on climate optimized flight planning sponsored by the German Federal Ministry of the Environment [94]. Current applications of VarMission include the European Alfa-Bird project on alternative fuels and a DLR activity on integrated air traffic modelling named IML 2 (“Integrierte Modellierung des Luftverkehrssystems 2”).

The Air Traffic Emissions Module determines flight movements, transport performance and emissions of air traffic and automates a number of tasks that had to be done manually in the past. This includes the creation of input data for DLR’s FATE software, which produces four-dimensional inventories of aviation emissions. The Air Traffic Emissions Module and FATE were applied in the IML 1 project lead by the DLR Institute of Air Transport and Airport Research [103]. Both modules will also be used in the work package on technology evaluation of the European 7<sup>th</sup> framework Joint Technology Initiative (JTI) / Clean Sky. Emission inventories for aviation in 2000 and 2020 will be produced in this work package<sup>42</sup>.

The tool chain consisting of VarCycle and VarMission, the Air Traffic Emissions Module and earlier versions of the Air Traffic Emissions Forecast Module was used for joint publications of the DLR Institute of Propulsion Technology and the DLR Institute of Air Transport and Airport Research on potential effects of the planned inclusion of aviation into the EU Emissions Trading Scheme (EU-ETS) [115], [116]. In the future, the existing tool chain will be used to monitor emissions from air traffic and to assess forecast scenarios considering various technology scenarios. Furthermore, the tool chain can be regarded as a prototype for a more comprehensive forecast model that is being developed in the ongoing IML 2 project mentioned above.

---

<sup>42</sup> The inventory for the year 2020 in JTI / Clean Sky is based on a flight movements forecast produced by Airbus.

As a consequence, the Air Traffic Emissions Forecast Module will not be applied in this project.

---

### 5.3 PROSPECTIVE MODEL IMPROVEMENTS

Future model improvements are mostly linked to newly available input data and software. This includes input information for aircraft and engine models as well as more detailed flight movements including trajectory information.

Future versions of the ICAO engine emissions database [78] will provide more information on NO<sub>x</sub> emissions of future aircraft engines. This includes information on the GEnx and LeapX engines for the Boeing 787 and A320 NEO family using TAPS combustor technology. In addition, more detailed information on such engines including emission characteristics during cruise flight may become available from engine manufacturers or publications. Such data can be used in simulation models of the engines and will help to reduce the uncertainty regarding NO<sub>x</sub> emissions of future air traffic. Similarly, emission characteristics of alternative fuels gathered by measurement will help to improve the accuracy of emission forecasts for the medium-term and long-term future.

The VarMission module developed for this study is mainly used with aircraft models from the BADA database [46]. This database is maintained by EUROCONTROL and is typically updated every year providing newly added or modified aircraft models. As such updates may include changes in methodology, VarMission needs to be adapted to reflect these changes. Besides, a new interface has been established between VarMission and a new software for engine simulation named GTlab. GTlab is being developed at the DLR Institute of Propulsion Technology and will replace the existing VarCycle software for the purpose of engine simulation [15]. A re-programming of VarMission using the C++ programming language is under consideration, mainly to improve software performance<sup>43</sup> and to harmonize the software architecture between GTlab and VarMission.

The Air Traffic Emissions Module is based on worldwide flight schedules. More detailed flight plan information or flight trajectories from radar data are currently not available for global air traffic. Access to information from air traffic service providers is usually restricted. An alternative source of flight movements are position broadcasts of aircraft equipped with ADS-B transponders (Automatic Dependent Surveillance Broadcast). The majority of large transport aircraft are already equipped with ADS-B technology and broadcast their position periodically. Such broadcasts can be received by other aircraft or ground stations within range. Online communities like flightradar24.com collect position information from ADS-B receivers all over the world and provide “virtual radar screens” to the public. While the regional coverage of these communities is still limited, the use of ADS-B information for air traffic models is a promising option for the future.

---

<sup>43</sup> i.e. to reduce calculation times for flight simulation.

The Air Traffic Forecast Model, which was developed for this study, provides a possibility to predict future emissions of the air transport sector based on traffic forecasts from external sources like e.g. the Airbus Global Market Forecast. Results from this model will be used to assess aviation's impact on climate change. A more comprehensive forecast model is currently being developed in the IML 2 project ("Integrierte Modellierung des Luftverkehrssystems 2") lead by the DLR Institute of Air Transport and Airport Research. In this forecast it is planned to use aircraft models and the fleet rollover methodology from this study in combination with a new model predicting future flight movements. The new traffic forecast will consider constraints in airport capacities, which are not evaluated explicitly in today's air traffic forecasts. The modular structure of the model developed for this study allows the gradual introduction of improvements and the implementation of new modules or sub-modules for future applications.

---

## REFERENCES

- [1] Ahlefelder, S.: Weiterentwicklung und Validierung des DLR-Tools zur Triebwerks- und Flugleistungsrechnung, Diplomarbeit an der Hochschule für Angewandte Wissenschaften Hamburg / Department Fahrzeugtechnik und Flugzeugbau, 2008
- [2] Airbus S.A.S.: A319 Airplane Characteristics for Airport Planning, Blagnac Cedex, July 1995  
(Airbus airplane characteristics were used for the following aircraft types: A300, A310, A318, A319, A320, A321, A330, A340, A380)
- [3] Airbus S.A.S.: Global Market Forecast 2010-2029, Presentation by John Leahy, Toulouse, December 2010
- [4] Airbus S.A.S.: Delivering The Future / Global Market Forecast 2011-2030, Blagnac Cedex, September 2011
- [5] Airbus S.A.S: Website on Airbus A320 NEO, retrieved June 15<sup>th</sup> 2011, [www.airbus.com/aircraftfamilies/passengeraircraft/a320family/spotlight-on-a320neo/](http://www.airbus.com/aircraftfamilies/passengeraircraft/a320family/spotlight-on-a320neo/)
- [6] Airbus S.A.S: Website on A350 specifications, retrieved November 9<sup>th</sup> 2010, [www.airbus.com/en/aircraftfamilies/a350/efficiency/specifications/a350-900\\_specifications/](http://www.airbus.com/en/aircraftfamilies/a350/efficiency/specifications/a350-900_specifications/)
- [7] Airbus S.A.S: Website on A350 efficiency, retrieved June 15<sup>th</sup> 2011, [www.airbus.com/aircraftfamilies/passengeraircraft/a350xwbfamily/](http://www.airbus.com/aircraftfamilies/passengeraircraft/a350xwbfamily/)
- [8] Air Transport Association, Traffic and Operations Statistics 1929-Present (based on ICAO data), retrieved July 20<sup>th</sup> 2011, [www.airlines.org/Economics/DataAnalysis/Pages/AnnualResultsWorldAirlines.aspx](http://www.airlines.org/Economics/DataAnalysis/Pages/AnnualResultsWorldAirlines.aspx)
- [9] Apffelstaedt, A. / Langhans, S. / Gollnick, V.: Identifying Carbon Dioxide Reducing Aircraft Technologies and Estimating their Impact on Global CO<sub>2</sub> Emissions, Deutscher Luft- und Raumfahrtkongress 2009, DocumentID: 121282, 2009
- [10] Argüelles et al.: European Aeronautics: A vision for 2020 – Meeting society's needs and winning global leadership, Report of the group of personalities, January 2001
- [11] ASCEND Worldwide Limited, ASCEND Online Fleets, Online Database Product obtained from 2008 to 2011, [www.ascendworldwide.com](http://www.ascendworldwide.com)
- [12] Bauen, A. / Howes, J. / Bertuccioli, L. / Chudziak, C.: Review of the potential for biofuels in aviation, E4tech, final report for CCC, August 2009
- [13] Baughcum, S. L. / Henderson, S. C. / Tritz, T. G.: Scheduled Civil Aircraft Emission Inventories for 1976 and 1984: Database Development and Analysis, NASA Contractor Report 4722, June 1996
- [14] Baughcum, S. L. / Tritz, T. G. / Henderson, S. C. / Pickett, D. C.: Scheduled Civil Aircraft Emission Inventories for 1992: Database Development and Analysis, NASA Contractor Report 4700, April 1996

- [15] Becker, R. / Wolters, F. / Nauroz, M. / Otten, T.: Development of a gas turbine performance code and its application to preliminary engine design, DLRK2011-241485, Deutscher Luft- und Raumfahrtkongress, 27.-29. September 2011
- [16] Berghof, R. / Schmitt, A. / Eyers, C. / Haag, K.-H. / Middel, J. / Hepting, M. / Grübler, A. / Hancox, R.: CONSAVE 2050 Final Technical Report, July 2005
- [17] Boeing Commercial Airplanes: 767 / Airplane Characteristics for Airport Planning, D6-58328, September 2005  
(Boeing airplane characteristics were used for the following aircraft types: 707, 717, 727, 737, 747-400, 747-8, 757, 767, 777, 787-800, DC3, DC9, DC10, MD11, MD80, MD90)
- [18] Boeing Commercial Airplanes: 747-8 Airport Compatibility, Preliminary Document, Seattle, January 2008
- [19] Boeing Commercial Airplanes: Current Market Outlook 2011-2030, Seattle, September 2011
- [20] Boeing Commercial Airplanes: Company website retrieved June 15<sup>th</sup> 2011, [www.boeing.com/commercial/](http://www.boeing.com/commercial/)
- [21] Boeing Commercial Airplanes: Website on 747-8, retrieved June 15<sup>th</sup> 2011, [http://www.boeing.com/commercial/747family/747-8\\_background.html](http://www.boeing.com/commercial/747family/747-8_background.html)
- [22] Boeing Commercial Airplanes: Website on 787 family, retrieved June 15<sup>th</sup> 2011, <http://www.boeing.com/commercial/787family/background.html>
- [23] Bombardier Aerospace: Bombardier Commercial Aircraft, Market Forecast 2011-2030, Bombardier Inc, June 2011
- [24] Bonnbau, P.: Detailed Passenger Traffic Growth Rates from Airbus GMF 2011-2030, email conversation, November 2011
- [25] Bresson, J.: Cost-Benefit Analysis of NOx Regulation in Air Transport, GAMMA / AIR-NOx, ENAC, June 2009
- [26] Brunner, B. / Lenic, J. / Schmitt, A. / Deidewig, F. / Döpelheuer, A. / Lecht, M.: Die zeitliche Entwicklung der Luftverkehrsemissionen, DLR Köln, 1998
- [27] Civil air navigation services organisation CANSO: ATM Global Environment Efficiency Goals for 2050, December 2008
- [28] Council of the European Union: Directive 2008/101/EC of the European Parliament and the Council of 19 November 2008 amending Directive 2003/87/EC so as to include aviation activities in the scheme for greenhouse gas emission allowance trading within the Community, in: Official Journal of the European Union L 8/3, Brussels, 13 January 2009
- [29] Daly, M. (ed.) / Gunston, B. (ed.): Jane's Aero-Engines, Issue Twenty-seven, IHS Global Limited, March 2010
- [30] Deidewig, F.: Ermittlung der Schadstoffemissionen im Unter- und Überschallflug, DLR Forschungsbericht 98-10, DLR Institut für Antriebstechnik, Köln, 1998



- 
- [31] Deidewig, F. / Döpelheuer, A. / Lecht, M.: Methods to Assess Aircraft Engine Emissions in Flight, in: ICAS Proceedings 1996, Volume 1, ICAS-96-4.1.2, 1996
- [32] Deutsche Lufthansa, personal communication
- [33] Döpelheuer, A.: Anwendungsorientierte Verfahren zur Bestimmung von CO, HC und Ruß aus Luftfahrttriebwerken, DLR Forschungsbericht 2002-10, DLR Institut für Antriebstechnik, Köln, 2002
- [34] Döpelheuer, A.: Quantities, Characteristics and Reduction Potentials of Aircraft Engine Emissions, Society of Automotive Engineers (SAE) 2001-02-3008, 2001
- [35] Döpelheuer, A. / Guérin, S. / Hemmer, H. / Lengyel, T. / Moreau, A. / Nicke, E. / Otten, T.: Abschlussbericht CLAIRE 2, internal DLR report IB 325-11-10, August 2010
- [36] Döpelheuer, A. / Lecht, M.: Influence of engine performance on emission characteristics, RTO-Symposium of AVT on Gas Turbine Engine Combustion, Emissions and Alternative Fuels, published in: RTO MP-14, pp. 20-1 to 20-12, ISBN 92-837-0009-0, Lisbon 1999
- [37] Embraer S.A.: Embraer 170 / Airport Planning Manual, APM-1346, December 2003 / Revision 10, October 2008  
(Embraer airport planning manuals were used for the following aircraft types: E120, E135, E140, E145, E145XR, E170, E175, E190, E195)
- [38] Embraer S.A.: Embraer Market Outlook 2011-2030, 2011
- [39] Epstein, A.: Aircraft Propulsion Considerations for the 21<sup>st</sup> Century: Delivering Value Thru Innovation, Pratt & Whitney Presentation, Hampton VA, 2010
- [40] EQ<sup>2</sup>: Sustainable Flying – Biofuels as an Economic and Environmental Salve for the Airline Industry, February 2010
- [41] EUROCONTROL Experimental Centre: Advanced Emission Model (AEM3) v1.5, Validation Report + Appendices, EEC/SEE/2004/004, June 2004
- [42] EUROCONTROL Experimental Centre: Advanced Emission Model (AEM3) v1.5, Validation Exercise #2, EEC/SEE/2004/012, January 2005
- [43] EUROCONTROL Experimental Centre: Base of Aircraft Data (BADA), Performance Modelling Report, EEC Technical/Scientific Report No. 2009-009, March 2009
- [44] EUROCONTROL Experimental Centre: GAES / Advanced Emissions Model v1.5, Validation Exercise 3, EEC/SEE/2006/005, 2006
- [45] EUROCONTROL Experimental Centre: Model Accuracy Summary Report for the Base of Aircraft Data (BADA) Revision 3.9, EEC Technical/Scientific Report No. 11/03/08-011, April 2011
- [46] EUROCONTROL Experimental Centre: User Manual for the Base of Aircraft Data (BADA) Revision 3.9, EEC Technical/Scientific Report No. 11/03/08-08, April 2011

- [47] EUROCONTROL Performance Review Commission: PRR 2007, Performance Review Report, An Assessment of Air Traffic Management in Europe during the Calendar Year 2007, May 2008
- [48] EUROCONTROL Performance Review Commission: PRR 2008, Performance Review Report, An Assessment of Air Traffic Management in Europe during the Calendar Year 2008, May 2009
- [49] EUROCONTROL Performance Review Commission: PRR 2009, Performance Review Report, An Assessment of Air Traffic Management in Europe during the Calendar Year 2009, May 2010
- [50] EUROCONTROL Performance Review Commission: Vertical Flight Efficiency, Technical note prepared by the Performance Review Unit, Final Report, March 2008
- [51] EUROSTAT (2009): EUROSTAT data, retrieved April 1<sup>st</sup> 2009, <http://epp.eurostat.ec.europa.eu/portal/page/portal/transport/data/database>
- [52] European Commission: Flightpath 2050 – Europe’s Vision for Aviation, Report of the High Level Group on Aviation Research, Luxembourg, 2011
- [53] Eyers, C. J. / Norman, P. / Middel, J. / Plohr, M. / Michot, S. / Atkinson, K. / Christeou, R. A.: AERO2k Global Aviation Emissions Inventories for 2002 and 2025, QinetiQ Ltd, December 2004
- [54] Federal Aviation Administration FAA: SAGE – System for assessing Aviation's Global Emissions, Version 1.5, Technical Manual, FAA-EE-2005-01, September 2005
- [55] Federal Aviation Administration FAA: SAGE – System for assessing Aviation’s Global Emissions, Version 1.5, Global Aviation Emissions Inventories for 2000 through 2004, FAA-EE-2005-02, September 2005
- [56] Federal Aviation Administration / Office of Environment and Energy: SAGE Version 1.5, Validation Assessment, Model Assumptions and Uncertainties, FAA-EE-2005-03, September 2005
- [57] Federal Office of Civil Aviation FOCA: Aircraft Piston Engine Emissions / Summary Report, Reference: 0/3/33/33-05-003.022, March 2007
- [58] Fichter, C.: personal communication, DLR Institute of Atmospheric Physics, 2008
- [59] Flightglobal.com: website, retrieved November 9<sup>th</sup> 2010, [www.flightglobal.com/articles/2009/12/10/336055/boeing-ups-787-weights-shrinks-9-wing.html](http://www.flightglobal.com/articles/2009/12/10/336055/boeing-ups-787-weights-shrinks-9-wing.html)
- [60] Flightglobal.com: website, retrieved June 15<sup>th</sup> 2011, [www.flightglobal.com/articles/2010/12/07/350465/airbus-a320neo-will-be-heavier-than-existing-a320-models.html](http://www.flightglobal.com/articles/2010/12/07/350465/airbus-a320neo-will-be-heavier-than-existing-a320-models.html)
- [61] Förtsch, W.: personal communication, 1994
- [62] Fueri, M.: Aircraft performance degradation, presentation by the Airbus Director Performance at the 16<sup>th</sup> Performance and Operations conference, May 2009

- 
- [63] Gardner, R. M. (ed.): ANCAT/EC2 Global Aircraft Emissions Inventories for 1991/1992 and 2015: Final Report, EUR-18179, ANCAT/EC Working Group, 1998
- [64] Hemmer, H. / Schaefer, M. / Otten, T.: Einfluss lärmarmen An- und Abflugverfahren auf NO<sub>x</sub>- und CO<sub>2</sub>-Emissionen im Flughafennahbereich, Deutscher Luft- und Raumfahrtkongress 2008
- [65] Hepperle, M.: personal communication, DLR Institute of Aerodynamics and Flow Technology, 2009
- [66] Hileman, J. I. / Stratton, R. W. / Donohoo, P. E.: Energy Content and Alternative Jet Fuel Viability, *Journal of Propulsion and Power*, Vol. 26, No. 6, doi: 10.2514/1.46232, November-December 2010
- [67] Intergovernmental Panel on Climate Change IPCC: Aviation and the Global Atmosphere, Cambridge University Press 1999
- [68] International Air Transport Association IATA: Aviation and Climate Change / Pathway to carbon-neutral growth in 2020, July 2009
- [69] International Air Transport Association IATA: Beginner's Guide to Aviation Biofuels, Air Transport Action Group, May 2009
- [70] International Air Transport Association IATA: IATA 2010 Report on Alternative Fuels, 5<sup>th</sup> Edition, Montreal – Geneva, December 2010
- [71] International Air Transport Association IATA: The IATA Technology Roadmap Report, 3<sup>rd</sup> Edition, June 2009
- [72] International Air Transport Association IATA: The IATA Technology Roadmap / Technical Annex, June 2009
- [73] International Civil Aviation Organization ICAO: Annex 16 to the Convention on International Civil Aviation, Volume II Aircraft Engine Emissions, Second Edition, July 1993
- [74] International Civil Aviation Organization ICAO: Civil Aviation Statistics of the World, ICAO Statistical Yearbook, Various Editions
- [75] International Civil Aviation Organization ICAO: Environmental Report 2010, Montreal, 2010
- [76] International Civil Aviation Organization ICAO: FESG CAEP/8 Traffic and fleet forecasts, CAEP-SG/2/20082-IP/08, Committee on aviation environmental protection (CAEP), Steering Group Meeting, Seattle, 22 to 26 September 2008
- [77] International Civil Aviation Organization ICAO: ICAO data, retrieved June 8th 2011, [www.icaodata.com](http://www.icaodata.com)
- [78] International Civil Aviation Organization ICAO: ICAO Engine Exhaust Emissions Databank, ICAO Doc 9646-AN/943, First Edition 1995 (plus revisions available at [www.caa.co.uk](http://www.caa.co.uk). Issue 17A is the version used for this study)

- 
- [79] International Civil Aviation Organization ICAO: Outlook for Air Transport to the Year 2025, September 2007
- [80] International Civil Aviation Organization ICAO: Working Paper / Tenth Session of the Statistics Division, STA/10-WP/5, Montreal, 23-27 November 2009
- [81] International Civil Aviation Organization ICAO / Committee on Aviation Environmental Protection CAEP: Eighth Meeting, Montréal, 1 to 12 February 2010: CAEP/8-WP/80 and Appendices
- [82] International Civil Aviation Organization ICAO / Committee on Aviation Environmental Protection CAEP: Environmental Goals Assessment, CAEP/8-IP/8, 7 December 2009
- [83] International Energy Agency IEA: Energy Technology Perspectives 2010 – Scenarios & Strategies to 2050, OECD/IEA, Paris, 2010
- [84] International Energy Agency IEA: Oil Information, Editions 1993-2010
- [85] Jackson, P. / Munson, K. / Peacock, L.: Jane's all the worlds Aircraft 2008-2009, Jane's Information Group, 2008
- [86] Kärcher, B. (ed.): Particles and Cirrus Clouds (PAZI-2) / Final Report (2004-2007), DLR Mitteilung 2008-01, 2008
- [87] Kim, B. Y. / Fleming, G. G. / Lee, J. J. / Waitz, I. A. / Clarke, J.-P. / Balasubramanian, S. / Malwitz, A. / Klima, K. / Locke, M. / Holsclaw, C. A. / Maurice, L. Q. / Gupta, M. L.: System for assessing Aviation's Global Emissions (SAGE), Part 1: Model description and inventory results, Transportation Research Part D, December 2007
- [88] Lee, Chi-Ming: NASA Low NO<sub>x</sub> Fuel Flexible Combustor / Technical Challenges, Presentation at NASA Green Aviation Summit, NASA AMES, September 8-9, 2010
- [89] Lee, D. S. / Fahey, D. W. / Forster, P. M. / Newton, P. J. / Wit, R. C. N. / Lim, L. L. / Owen, B. / Sausen, R.: Aviation and global climate change in the 21<sup>st</sup> century, Atmospheric Environment (2009), doi: 10.1016/j.atmosenv.2009.04.024, 2009
- [90] Lee, D. S. / Owen, B. / Graham, A. / Fichter, C. / Lim, L. L. / Dimitriu, D.: Study on the Allocation of Emissions from International Aviation to the UK Inventory – CPEG7 / Final Report to DEFRA Global Atmosphere Division, Report 2 of 3, Manchester Metropolitan University, December 2005
- [91] Lukachko, S. P. / Waitz, I. A.: Effects of Engine Aging on Aircraft NO<sub>x</sub> Emissions, ASME paper 97-GT-386, June 1997
- [92] Lyssis Ltd: PIANO User's Guide, Online html version, retrieved November 11<sup>th</sup> 2010, [www.piano.aero](http://www.piano.aero)
- [93] Lyssis Ltd: PIANO-X aircraft performance and emissions software (including some freely available aircraft models), retrieved November 11<sup>th</sup> 2010, [www.piano.aero](http://www.piano.aero)
-

- 
- [94] Matthes, S. / Gierens, K. / Grewe, V. / Mannstein, H. / Sausen, R. / Mollwitz, V. / Schaefer, M. / Weiss, M.: Climate optimized flight planning, BMU Vorhaben 300/2008, Draft of final report, DLR, March 2011
- [95] Middel, J. / de Witte, T. D.: Aviation Emissions and Evaluation of Reduction Options (AERO), Flights and Emissions Model (FLEM), NLR-CR-2001-100, March 2001
- [96] Mitsubishi: Website on Mitsubishi Regional Jet / Principal Characteristics, retrieved November 11<sup>th</sup> 2010, [www.mri-japan.com/characteristics.html](http://www.mri-japan.com/characteristics.html)
- [97] Mongia, H. / Dodds, W.: Low Emissions Propulsion Engine Combustor Technology Evolution – Past, Present and Future, ICAS paper 2004-6.9.2, 2004
- [98] MTU Aero Engines: PurePower PW 1000G Engine, online brochure, retrieved April 8<sup>th</sup> 2011, [www.mtu.de/de/products\\_services/new\\_business\\_commercial/programs/pw1000g/PW1000G\\_brochure.pdf](http://www.mtu.de/de/products_services/new_business_commercial/programs/pw1000g/PW1000G_brochure.pdf)
- [99] Novelli, P. (ed.): SWAFEA / Sustainable Way for Alternative Fuels and Energy in Aviation, Final Report, April 2011
- [100] OAG Aviation Solutions: OAG MAX flight schedules on CD-ROM, monthly editions covering the years 2000 and 2003-2010
- [101] Owen, B. / Lee, D. S.: Study on the Allocation of Emissions from International Aviation to the UK Inventory – CPEG7 / Final Report to DEFRA Global Atmosphere Division, Report 1 of 3, Manchester Metropolitan University, November 2005
- [102] Owen, B. / Lee, D. S.: Study on the Allocation of Emissions from International Aviation to the UK Inventory – CPEG7 / Final Report to DEFRA Global Atmosphere Division, Report 3 of 3, Manchester Metropolitan University, March 2006
- [103] Pak, H. / Berster, P. / Dahlmann, K. / Gelhausen, M. / Grimme, W. / Grunewald, E. / Hepting, M. / Hoffmann, E. / Leipold, A. / Sausen, R. / Schaefer, M. / Schlauch, T.: Integrierte Modellierung des Luftverkehrsberichts 1 – Abschlussbericht, DLR ID: IB 326-2010/1, Mai 2010
- [104] Peeters, P. M. / Middel, J. / Hoolhorst, A.: Fuel efficiency of commercial aircraft – An overview of historical and future trends, NLR-CR-2005-669, November 2005
- [105] Perrett, B.: Mitsubishi Spec to Rival Embraer, Bombardier RJs, in: Aviation Week and Space Technology, June 18<sup>th</sup> 2007, available online at [www.aviationweek.com/aw/generic/story\\_channel.jsp?channel=busav&id=news/aw061807p3.xml&headline=null&next=20](http://www.aviationweek.com/aw/generic/story_channel.jsp?channel=busav&id=news/aw061807p3.xml&headline=null&next=20)
- [106] Plohr, M.: DLR engine models simulated by use of the VarCycle software, personal communication, 2010-2011

- [107] Ponater, M. / Marquart, S. / Sausen, R.: Contrails in a comprehensive global climate model: parameterisation and radiative forcing results, *Journal of Geophysical Research*, vol. D107, S ACL 2-1-ACL 2-15, 2002
- [108] Rachner, M.: Die Stoffeigenschaften von Kerosin JET A-1, DLR-Mitteilung 98-01, Deutsches Zentrum für Luft- und Raumfahrt (DLR), 1998
- [109] Ralph, M. et al.: Report of the Independent Experts to the Long Term Technology Task Group on the 2006 LTTG NO<sub>x</sub> Review and the Establishment of Medium and Long Term Technology Goals for NO<sub>x</sub>, 2006
- [110] Ralph, M. / Kuentzmann, P. / Maurice, L. / Tilston, J.: Report of the Independent Experts to CAEP 8 on the Second NO<sub>x</sub> Review & Long Term Technology Goals, London, March 2009
- [111] Roskam, J.: *Airplane Design – Part I: Preliminary Sizing of Airplanes*, DARcorporation, 3<sup>rd</sup> edition, 2003
- [112] Sausen, R. / Isaksen, I. / Greve, V. / Hauglustaine, D. / Lee, D. / Myhre, G. / Köhler, M. / Pitari, G. / Schumann, U. / Stordal, F. / Zerefos, C.: Aviation radiative forcing in 2000: An update on IPCC (1999), in: *Meteorologische Zeitschrift*, Vol. 14, No. 4, pp. 555-561, August 2005
- [113] Schaefer, M.: *Methodologies for Aviation Emission Calculation – A comparison of alternative approaches towards 4D global inventories*, master thesis presented to TU Berlin, May 2006
- [114] Schaefer, M. / Grimme, W.: *The Variability of Air Transport's Specific Emissions and Implications for Airline Strategies*, 1<sup>st</sup> CEAS European Air and Space Conference / Deutscher Luft- und Raumfahrtkongress 2007
- [115] Schaefer, M. / Scheelhaase, J. / Grimme, W. / Maertens, S.: *Modelling Air Transport's CO<sub>2</sub>-Emissions and Evaluating the Impact of the Upcoming EU Emissions Trading System*, DGLR Congress Paper, 2009
- [116] Schaefer, M. / Scheelhaase, J. / Grimme, W. / Maertens, S.: *Ökonomische Effekte des EU-Emissionshandelssystems auf Fluggesellschaften und EU-Mitgliedstaaten – ein innovativer Modellierungsansatz*, in: *DIW Vierteljahreshefte zur Wirtschaftsforschung*, Duncker & Humblot Berlin, Band 02.2010, ISSN 0340-1707, 2010
- [117] Scheelhaase, J. / Grimme, W. / Schaefer, M.: *The inclusion of aviation into the EU emission trading scheme – Impacts on competition between European and non-European network airlines*, *Transportation Research Part D* (2009), doi: 10.1016/j.trd.2009.07.003
- [118] Schmitt, A.: *Berechnung der Emissionsverteilung und deren Trends, Teil I – Sachbericht*, DLR Köln, 1996
- [119] Schumann, U. (ed.): *AERONOX / The Impact of NO<sub>x</sub> Emissions from Aircraft Upon the Atmosphere at Flight Altitudes 8-15 km*, Final report to the Commission of European Communities, August 1995



- 
- [120] Schumann, U.: Aircraft Emissions, in: Nunn, Ted (ed.): Encyclopedia of Global Environmental Change (Volume 3, pp. 178-186), John Wiley & Sons 2002
- [121] Schumann, U.: Formation, properties and climatic effects of contrails, in: Comptes Rendus Physique (Volume 6, pp. 549-565), 2005
- [122] Seebach, O.: Entwicklung einer GUI-gestützten Datenbankanwendung zu Abfrage, Visualisierung und Reporting von Emissionsstudien Daten aus dem Luftverkehr, Bachelorarbeit an der Dualen Hochschule Baden-Württemberg Mannheim, September 2010
- [123] Stern, N.: The Economics of Climate Change / The Stern Review, Cambridge University Press, 2007
- [124] Stratton, R. W. / Wong, H. M. / Hileman, J. I.: Life Cycle Greenhouse Gas Emissions from Alternative Jet Fuels, PARTNER Project 28 report, Version 1.2, Report No. PARTNER-COE-2010-001, June 2010
- [125] Sutkus D. J. Jr. / Baughcum S. L. / DuBois D. P.: Commercial Aircraft Emission Scenario for 2020: Database Development and Analysis, NASA/CR-2003-212331, May 2003
- [126] Sutkus D. J. Jr. / Baughcum S. L. / DuBois D. P.: Scheduled Civil Aircraft Emission Inventories for 1999: Database Development and Analysis, NASA/CR-2001-211216, October 2001
- [127] Swedish Defence Research Agency FOI: Confidential database for Turboprop Engine Emissions, see [www.foi.se/FOI/templates/Page\\_4618.aspx](http://www.foi.se/FOI/templates/Page_4618.aspx)
- [128] Teresko, John: Boeing 787: A Matter of Materials – Special Report: Anatomy of a Supply Chain, December 2007, available online at: [www.industryweek.com/articles/boeing\\_787\\_a\\_matter\\_of\\_materials\\_-\\_special\\_report\\_anatomy\\_of\\_a\\_supply\\_chain\\_15339.aspx](http://www.industryweek.com/articles/boeing_787_a_matter_of_materials_-_special_report_anatomy_of_a_supply_chain_15339.aspx)
- [129] Thorbeck, J.: Manuskript zur integrierten Lehrveranstaltung Flugzeugentwurf I und II, TU Berlin, Oktober 2003
- [130] Torenbeek, E.: Synthesis of Subsonic Airplane Design, Delft University Press, 1972
- [131] Waldowski, A.: Vorentwurf einer Narrow-Body-Flugzeugfamilie der nächsten Generation auf Basis des A320, Deutsches Zentrum für Luft- und Raumfahrt, internes Dokument DLR-AT-TW, November 2009
- [132] Wiedemann, M.: CFK-Entwicklungskette für den Flugzeugbau – Organisation der CFK-Produktentwicklung, Powerpoint Präsentation, DLR-Institut für Faserverbundleichtbau und Adaptronik, May 2009
- [133] Wilkerson, J. T. / Jacobson, M. Z. / Malwitz, A. / Balasubramanian, S. / Wayson, R. / Fleming, G. / Naiman, A. D. / Lele, S. J.: Analysis of emission data from global commercial aviation: 2004 and 2006, in: Atmospheric Chemistry and Physics, doi: 10.5194/acp-10-6391-2010, 5 February 2010



---

---

---

## **APPENDICES**

---

## Appendix A AIRCRAFT SPEEDS AND ACCELERATIONS

### Take-off speed:

In the standard flight mission, the aircraft accelerates to take-off speed on the runway. The airspeed at take-off can be estimated as incremented stall speed in take-off configuration. A reference stall speed is given by BADA [46] for take-off configuration, see chapter 3.2.2:

$$(1) \quad v_{\text{stall,ref}} = \text{from BADA OPF file}$$

The reference stall speed can be corrected for the aircraft's actual take-off mass. For reasons of simplicity, the aircraft's maximum take-off mass is assumed by default:

$$(2) \quad v_{\text{stall,MTOW}} = v_{\text{stall,ref}} \cdot \sqrt{\frac{m_{\text{max}}}{m_{\text{ref}}}}$$

Hence, the take-off speed  $v_{\text{take-off}}$  is estimated as incremented stall speed following a BADA recommendation [46]:

$$(3) \quad v_{\text{take-off}} = C_{V_{\text{min,TO}}} \cdot v_{\text{stall,MTOW}} + V_{d,TO} \quad \text{with } C_{V_{\text{min,TO}}} = 1.2 \quad \text{and } V_{d,TO} = 5 \text{ kt}$$

### Climb speeds:

The calibrated airspeeds for climb are obtained from BADA airline procedure information. BADA provides a typical low-altitude climb speed, a high-altitude climb speed and a climb Mach number for each aircraft model [46]. While the BADA user manual suggests a speed schedule of constant speed segments during climb and descent, VarMission uses explicit acceleration and deceleration flight phases.

In the modified ATA departure that is assumed as default procedure by VarMission, the aircraft accelerates from take-off speed to low-altitude climb speed after reaching an altitude of 1500 feet above ground. An energy share factor of 0.3 is assumed for the accelerated climb segment<sup>44</sup>. A speed limit of 250 kt CAS can be applied below flight level 100 if selected by the user. After reaching flight level 100, the aircraft accelerates from low-altitude climb speed to high-altitude climb speed in a constant-altitude acceleration segment<sup>45</sup>. An acceleration of 0.6 m/s<sup>2</sup> is assumed in this segment. When reaching the transition altitude between high-altitude climb speed and climb Mach number, climb is continued at constant Mach number until the initial cruise altitude is reached.

<sup>44</sup> See BADA manual [46] for a definition of the energy share factor.

<sup>45</sup> Following procedures described in aircraft performance documentation. Procedures used in reality may vary.

**Cruise speeds:**

After reaching initial cruise altitude, the aircraft is accelerated or decelerated to the aircraft's typical cruise Mach number as suggested by BADA [46]. An acceleration of  $0.2 \text{ m/s}^2$  is assumed for this purpose. It should be noted that for many aircraft models, the climb Mach number equals the cruise Mach number. In these cases, no acceleration is required. After the cruise phase, the aircraft is accelerated or decelerated to the descent Mach number (if required). Again, an acceleration of  $0.2 \text{ m/s}^2$  is assumed for this purpose.

**Descent speeds:**

BADA provides an aircraft-specific descent Mach number and typical calibrated airspeeds for descent at high altitudes and low altitudes. When descending from final cruise altitude, the given descent Mach number is assumed. Descent is performed at constant Mach number until the transition altitude between Mach number and high-altitude descent CAS is reached. A decelerated descent phase is assumed before reaching flight level 100. An energy share factor of 0.7 is used for modelling this segment. A speed limit of 250 kt CAS can be applied below flight level 100 if selected by the user.

**Approach and landing speeds:**

In the simulated approach procedure, the aircraft is decelerated from low-altitude descent speed to approach speed in a horizontal deceleration segment at an altitude of 3000 feet. The approach speed is estimated by formula (4):

$$(4) \quad v_{\text{approach}} = v_{\text{landing}} + \frac{12}{100} \cdot (v_{\text{Descent,low}} - v_{\text{landing}})$$

$v_{\text{Descent,low}}$  is the low-altitude descent speed from BADA. The aircraft's landing speed  $v_{\text{landing}}$  is calculated as incremented stall speed in landing configuration. A reference stall speed is given by BADA [46] for landing configuration:

$$(5) \quad v_{\text{stall,ref}} = \text{from BADA OPF file} \quad (\text{OPF} = \text{Operations Performance File})$$

The reference stall speed can be corrected for the aircraft's actual landing weight. For reasons of simplicity, the aircraft's maximum landing weight (MLW) or the BADA reference weight (whichever is smaller) is assumed:

$$(6) \quad v_{\text{stall,MLW}} = v_{\text{stall,ref}} \cdot \sqrt{\frac{m_{\text{MLW}}}{m_{\text{ref}}}}$$

The landing speed  $v_{\text{landing}}$  is calculated as incremented stall speed following BADA [46]:

$$(7) \quad v_{\text{landing}} = C_{V_{\text{min,LD}}} \cdot v_{\text{stall,MLW}} + V_{d,LD} \quad \text{with } C_{V_{\text{min,LD}}} = 1.3 \quad \text{and } V_{d,LD} = 5 \text{ kt}$$

## Appendix B ENGINE THRUST LEVELS

The BADA approach to estimate maximum engine thrust [46] and a generic thrust model from [129] are implemented in VarMission and will be described in the following paragraphs.

BADA provides engine thrust coefficients  $C_{Tc, x}$  for each aircraft model that can be used in order to estimate maximum climb thrust as function of altitude and flight speed. In the BADA methodology the maximum climb thrust of an aircraft is approximated as follows:

$$(1a) \quad T_{\max \text{ climb, ISA}} = C_{Tc,1} \cdot \left( 1 - \frac{h}{C_{Tc,2}} + C_{Tc,3} \cdot h^2 \right) \quad \text{for aircraft with jet engines}$$

$$(1b) \quad T_{\max \text{ climb, ISA}} = C_{Tc,1} \cdot \frac{1 - \frac{h}{C_{Tc,2}}}{v_{TAS}} + C_{Tc,3} \quad \text{for aircraft with turboprop engines}$$

$$(1c) \quad T_{\max \text{ climb, ISA}} = C_{Tc,1} \cdot \left( 1 - \frac{h}{C_{Tc,2}} + \frac{C_{Tc,3}}{v_{TAS}} \right) \quad \text{for aircraft with piston engines}$$

As can be seen from the formulae above, BADA estimates the maximum climb thrust as function of altitude  $h$  for jet aircraft and as function of altitude and true airspeed  $v_{TAS}$  for turboprops and aircraft with piston engines. The thrust calculated by formula (1a-c) assumes International Standard Atmospheric Conditions (ISA). Formula (2) corrects  $T_{\max \text{ climb, ISA}}$  for a temperature deviation from ISA conditions  $\Delta T_{ISA}$ :

$$(2) \quad T_{\max \text{ climb}} = T_{\max \text{ climb, ISA}} \cdot \left( 1 - C_{Tc,5} \cdot \Delta T_{ISA,eff} \right)$$

with  $\Delta T_{ISA,eff} = \Delta T_{ISA} - C_{Tc,4}$  and  $C_{Tc,5} \cdot \Delta T_{ISA,eff}$  limited to values between 0 and 0.4.

BADA thrust levels other than maximum climb thrust are obtained by multiplying maximum climb thrust with a coefficient:

- Maximum cruise thrust is calculated as follows:

$$(3) \quad T_{\max \text{ cruise}} = C_{Tcr} \cdot T_{\max \text{ climb}}$$

- A reduced climb thrust level can be calculated as function of aircraft mass  $m$  and is suggested to be used in the climb phase for a realistic climb profile:

$$(4) \quad T_{\text{red climb}} = C_{\text{pow,red}} \cdot (T_{\max \text{ climb}} - D) + D \quad \text{with} \quad C_{\text{pow,red}} = 1 - C_{\text{red}} \cdot \frac{m_{\max} - m}{m_{\max} - m_{\min}}$$

- During descent, BADA assumes a descent thrust level calculated by formula (5):

$$(5) \quad T_{des} = C_{Tdes} \cdot T_{\max \text{ climb}} \quad \text{with } C_{Tdes} \text{ given as function of aircraft type and altitude.}$$

As BADA climb thrust for jet aircraft does not depend on airspeed or flight Mach number, the formulae are not suitable for low speed segments that are typically flown at low altitudes. Furthermore, maximum take-off thrust cannot be calculated by the BADA model. In order to provide low-altitude climb thrust and take-off thrust data, a generic engine thrust model from [129] is implemented in VarMission and typically used for climb phases below flight level 100. This model will be described in the following paragraphs.

Given the maximum rated thrust of an engine type (e.g. from the ICAO engine exhaust emissions databank [78]), the maximum thrust for flight conditions is estimated as follows:

$$(6) \quad T_{\max \text{ take-off}} = T_{\max \text{ rating}} \cdot \left( \frac{T}{T_{\max \text{ rating}}} \right)_{M+h} \cdot \left( \frac{T}{T_{\max \text{ rating}}} \right)_{pl}$$

Formula (6) calculates the maximum take-off thrust of an engine using correction factors for Mach number and altitude effects and for the pressure loss in the air intake. The correction factors are calculated by formulae (7) and (8):

$$(7) \quad \left( \frac{T}{T_{\max \text{ rating}}} \right)_{M+h} = \frac{\rho}{\rho_0} \cdot \exp\left(-0.35 \cdot M \cdot \frac{p}{p_0} \cdot \sqrt{\mu}\right)$$

$$(8) \quad \left( \frac{T}{T_{\max \text{ rating}}} \right)_{pl} = 1 - (1.3 + 0.25 \cdot \mu) \cdot \frac{\Delta P}{P} \quad \text{assuming } \frac{\Delta P}{P} = 0.02$$

In the above formulae,  $\rho$  and  $\rho_0$  are the air density at flight altitude and sea level respectively,  $p$  and  $p_0$  are the static pressure at flight altitude and at sea level while  $\mu$  is the engine bypass ratio (at sea level static and maximum rated thrust). VarMission assumes ISA standard atmospheric conditions for  $p_0$  and  $\rho_0$  calculation. Maximum climb thrust is estimated based on maximum take-off thrust using a climb thrust rating factor D:

$$(9) \quad T_{\max \text{ climb}} = D \cdot T_{\max \text{ take-off}} \quad \text{with D typically equal to 0.80}$$

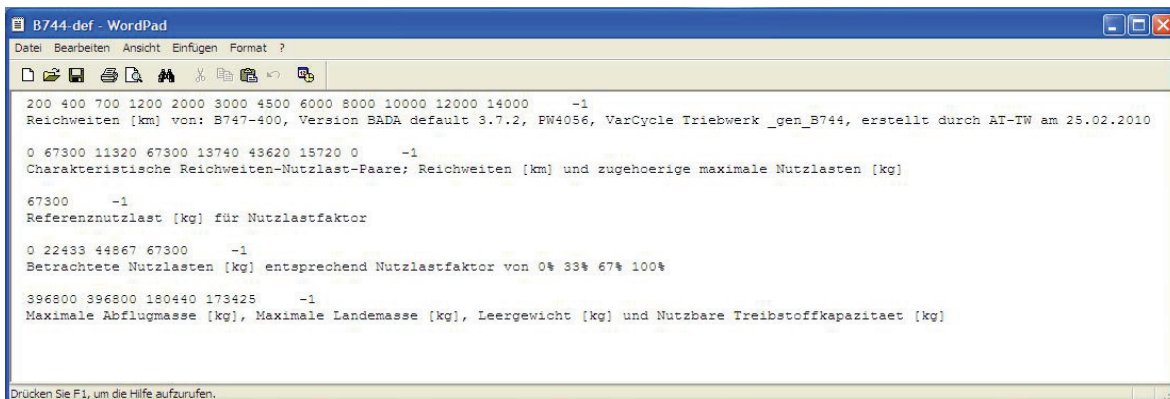
In VarMission's default flight missions, the thrust model from [129] is used for BADA aircraft with jet engines during climb phases below flight level 100 while BADA maximum or reduced climb thrust levels are applied for the climb phases above flight level 100. For non-BADA aircraft only the formulae from [129] are applied while for BADA aircraft with turboprop or piston engines only the BADA thrust model is used.

## Appendix C FORMAT OF VARMISSION AND FATE EMISSION PROFILES

This appendix contains information on the file format of emission profiles produced by VarMission. The emission profiles are intended for the FATE global inventory tool and have, in principle, the original FATE data format with some modifications.

### Information file:

The information file is a text file containing aircraft and engine information, the aircraft's payload-range-capabilities and its characteristic masses. It also lists distances and load factors for which emission profile files are available. An example is shown in Figure 98.



```

B744-def - WordPad
Datei Bearbeiten Ansicht Einfügen Format ?
200 400 700 1200 2000 3000 4500 6000 8000 10000 12000 14000 -1
Reichweiten [km] von: B747-400, Version BADA default 3.7.2, PW4056, VarCycle Triebwerk _gen_B744, erstellt durch AT-TW am 25.02.2010

0 67300 11320 67300 13740 43620 15720 0 -1
Charakteristische Reichweiten-Nutzlast-Paare; Reichweiten [km] und zugehoerige maximale Nutzlasten [kg]

67300 -1
Referenznutzlast [kg] für Nutzlastfaktor

0 22433 44867 67300 -1
Betrachtete Nutzlasten [kg] entsprechend Nutzlastfaktor von 0% 33% 67% 100%

396800 396800 180440 173425 -1
Maximale Abflugmasse [kg], Maximale Landemassee [kg], Leergewicht [kg] und Nutzbare Treibstoffkapazitaet [kg]

Drücken Sie F1, um die Hilfe aufzurufen.

```

Figure 98: Example of an information file (Boeing 747-400, default engine)

The information file is named by the aircraft code followed by the engine code. These codes are separated by a dash. The file contains data lines and comment lines that describe the data in the previous data line. All data is separated by spaces and each data line is ended by "-1". The lines contain the following information:

- Line 1: Data line with ranges in km for which emission profiles were calculated.
- Line 2: Comment line with additional information on aircraft name, aircraft model version, engine name, VarCycle engine model and date of simulation.
- Line 3: Empty line
- Line 4: Data line containing ranges in km and corresponding maximum payloads in kg. Usually four data pairs are given and sufficient to plot the payload-range diagram.
- Line 5-6: Comment line + empty line
- Line 7: Data line with the aircraft's reference payload (usually the maximum payload).
- Line 8-9: Comment line + empty line
- Line 10: Data line with payloads in kg for which emission profiles were calculated.
- Line 11-12: Comment line + empty line
- Line 13: Data line containing characteristic aircraft masses in kg, i.e. maximum take-off mass, maximum landing mass, operational empty mass, usable fuel capacity.
- Line 14-15: Comment line + empty line



## Profile files:

The profile files contain tabulated flight mission protocols including emissions data. There is one profile file per simulated flight, i.e. for a given mission distance and load factor. An example is shown in the following figure.

H[m]	dS[m]	dT[sec]	dF[kg]	dCO2[kg]	dH2O[kg]	dSOx[kg]	dNOx[kg]	dCO[kg]	dHC[kg]	dSOOT[kg]	dFART[-]	Phase[-]
10972.93	5576333.02	5999995.85	22493.65	25974.02	44866.67	73913.30						
11277.74	221623.18	1770.68	298723.65	236210.78								
0.00	0.00	660.00	496.32	1565.89	613.95	0.3971	28377	57573	0.3276	0.0000	0.00E+00	1
0.00	268.16	12206	60.50	190.88	74.84	0.0484	18799	0.0064	0.0083	0.0000	0.00E+00	2
0.00	655.36	10.00	94.98	299.66	117.49	0.0760	29384	0.0101	0.0130	0.0000	0.00E+00	2
0.00	859.59	10.00	94.38	297.60	116.68	0.0755	29045	0.0100	0.0129	0.0000	0.00E+00	2
0.00	1036.90	10.00	93.65	295.47	115.85	0.0749	28706	0.0099	0.0128	0.0000	0.00E+00	2
72.40	460.69	17624	41.76	131.74	51.65	0.0394	12796	0.0044	0.0057	0.0000	0.00E+00	3
224.80	883.83	20668	78.84	248.75	97.53	0.0631	24138	0.0084	0.0109	0.0000	0.00E+00	3
529.60	1772.27	16.98	153.80	485.25	190.26	0.1230	46967	0.0166	0.0215	0.0000	0.00E+00	3
594.37	1513.60	26634	97.42	307.35	120.51	0.0779	25543	0.0106	0.0137	0.0000	0.00E+00	4
670.57	1770.79	13.36	104.19	328.72	128.88	0.0834	27999	0.0114	0.0147	0.0000	0.00E+00	4
914.41	1860.58	40223	108.32	341.75	133.99	0.0867	28116	0.0119	0.0154	0.0000	0.00E+00	5
1219.21	2391.85	17.78	135.34	427.00	167.42	0.1083	36352	0.0151	0.0195	0.0000	0.00E+00	5
1524.02	2466.26	40347	135.34	426.98	167.41	0.1083	36268	0.0153	0.0198	0.0000	0.00E+00	5
3048.04	13614.16	95.26	679.00	2142.26	839.93	0.3432	179211	0.0805	0.1040	0.0000	0.00E+00	5
3048.04	14176.63	79.81	392.11	1237.12	485.04	0.1317	75596	0.0731	0.0623	0.0000	0.00E+00	6
4572.06	19800.54	97.81	692.04	2183.37	856.05	0.3536	192417	0.0885	0.1144	0.0000	0.00E+00	7
6096.07	25237.68	115.82	745.20	2351.10	921.81	0.3962	196355	0.1032	0.1334	0.0000	0.00E+00	7
7620.09	34038.18	144.98	837.56	2642.52	1036.07	0.4701	206096	0.1260	0.1629	0.0000	0.00E+00	7
9144.11	46362.31	183.83	940.69	2967.88	1163.64	0.5226	213018	0.1539	0.1989	0.0000	0.00E+00	7
10668.13	47179.02	185.54	809.65	2554.46	1001.54	0.4477	162393	0.1457	0.1877	0.0000	0.00E+00	7
10972.93	12696.79	50.56	195.48	616.75	241.81	0.1564	35312	0.0400	0.0478	0.0000	0.00E+00	7
10972.93	3659.76	14.76	26.60	83.93	32.91	0.0213	0.2306	0.0294	0.0103	0.0000	0.00E+00	8
10972.93	576328.87	2324.29	6073.42	19161.64	7512.82	48887	739030	29569	17295	0.0000	0.00E+00	8
10972.93	1000000.00	4032.92	10317.09	32550.43	12762.24	82537	1230201	52633	29905	0.0000	0.00E+00	9
10972.93	1000000.00	4032.92	10051.99	31714.02	12454.31	80416	1169225	54307	29778	0.0000	0.00E+00	9
10972.93	1000000.00	403.29	991.25	3127.39	1226.17	0.7930	113777	0.5522	0.2971	0.0000	0.00E+00	9
11277.74	1000000.00	403.46	1065.75	3362.43	1318.33	0.8526	134422	0.4806	0.3034	0.0000	0.00E+00	9
11277.74	8000000.00	3227.65	7702.66	24301.90	9528.19	61621	880988	43444	23870	0.0000	0.00E+00	9
11277.74	1000000.00	4034.56	9411.70	29693.92	11642.28	75294	1053512	55813	29727	0.0000	0.00E+00	9
11277.74	1000000.00	4034.56	9184.59	28977.39	11361.34	73477	1004713	57477	29609	0.0000	0.00E+00	9
11277.74	7449.65	29.51	88.01	277.69	108.87	0.0704	12548	0.0300	0.0227	0.0000	0.00E+00	10
10665.61	8659.35	34.14	30987	87.36	0.00	0.0095	0.0370	0.2466	0.0140	0.0000	0.00E+00	11

Figure 99: Example of a profile file (B744, default engine, 67% load factor, 6000km mission)

The profile file name is composed of aircraft code, engine code, load factor in percent and mission distance in 100 km; these elements are separated by dashes. The profile file consists of tabulated data separated by tabs. It contains the following data:

- Line 1: Column descriptions for lines 4 to end-of-file
- Line 2: Special data line containing the following mission-specific results: initial cruise altitude [m], cruise distance [m], mission distance [m], cruise time [s], mission time [s], payload [kg] and block fuel [kg]<sup>46</sup>.
- Line 3: Special data line containing the following mission-specific data: final cruise altitude [m], climb distance [m], climb time [s], take-off weight [kg], landing weight [mg].
- Line 4-x: The following lines contain the flight mission data. Each line can be regarded as one point along the flight profile. The column H specifies the instantaneous altitude in m while columns dF, dNO<sub>x</sub>, ... specify the delta in fuel burn and NO<sub>x</sub> emissions compared to the previous line.

<sup>46</sup> Block fuel includes trip fuel, taxi fuel and reserve fuel quantities.

## Appendix D TYPICAL CRUISE FLIGHT LEVELS

VarMission suggests typical cruise altitudes for a given flight mission in case the user of the software does not specify details of the cruise phase trajectory. Typical cruise flight levels are estimated as function of aircraft type and mission distance and are based on average cruise flight levels observed in the air traffic system. The underlying data are taken from a statistical evaluation of cruise flight levels in the Aero2k inventory of global aviation [90], [58]. The Aero2k inventory covers flight movements of the year 2002 and is based on European and US radar trajectories provided by EUROCONTROL and the FAA [53].

Figure 100 presents an example of the data examined in the statistical evaluation from [90]. The diagram shows the maximum flight levels of all flights performed by Airbus A321 aircraft in December 2002. Given such information, the average maximum flight level of the aircraft type can be determined for different distance categories. These analyses have been performed at the DLR Institute of Atmospheric Physics for 49 different aircraft types using range steps of 500 nautical miles [58]. Regional differences in the Air Traffic Management and a dependency of the maximum flight level on the load factor are neglected. If such statistical data are available for a given aircraft type and distance, the corresponding average flight level is assumed by VarMission as the flight level at top-of-descent.

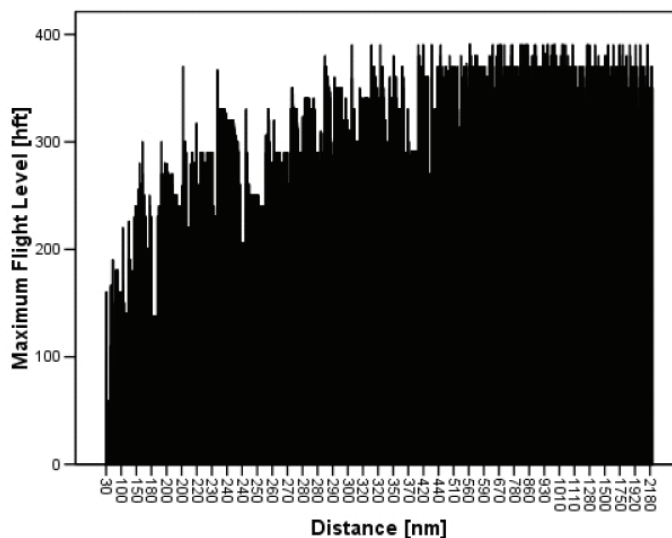


*Figure 100: Maximum flight level of Airbus A321 by mission distance in flight movements of the Aero2k inventory for December 2002 [90]*

The flight level at top-of-descent may not correspond to the flight level at the top-of-climb, as one or more step climbs may have been performed during cruise flight. Unfortunately, only the maximum flight levels of each flight were analysed in the statistical evaluation described above. As a consequence, VarMission estimates the initial cruise altitude as function of aircraft type, mission distance and load factor.

Given the “typical” final cruise flight level from the aforementioned statistics, the initial cruise flight level (which equals the flight level at top-of-climb) is determined as follows:

- VarMission estimates both the initial cruise weight and the final cruise weight of the aircraft on the given flight mission. The maximum flight levels that can be reached at these two gross weights and at the aircraft’s typical cruise Mach number are determined by the aircraft performance model.
- Given the typical flight level at top-of-descent from the statistical evaluation, the delta between the maximum flight level and the typical flight level at top-of-descent conditions can be calculated.
- The same delta is assumed for top-of-climb conditions. This way, the initial cruise flight level can be calculated.

A mid-cruise step climb is performed between the initial and final cruise flight levels. No step climb is assumed if the initial cruise altitude estimated by VarMission equals the final cruise altitude and for short distance flights of less than 270 nautical miles<sup>47</sup>. While the aforementioned approach is a rough simplification, it leads to plausible flight profiles: Initial cruise flight levels depend on aircraft type, mission distance and payload while final cruise flight levels correspond to the average maximum flight levels described above.

For aircraft types with no available reference data, average flight levels for an aircraft category derived from the data in [90] and [58] are used by VarMission. Given such average values for top-of-descent conditions, the initial cruise flight level is calculated as described above. Average top-of-descent flight levels have been derived for 12 aircraft categories including widebody and narrowbody aircraft, regional jets and business jets, turboprops and piston aircraft. Each of these categories is split further into “old” and “modern” aircraft types. This simplified approach regarding cruise flight levels is also followed for simulated flight missions performed by the newly created aircraft models of the future, which were described in chapter 3.4.5.

---

<sup>47</sup> Short distance flights of less than 270 nautical miles are assumed to fly at a constant cruise flight level which equals the initial cruise flight level as calculated by VarMission.

## Appendix E SPECIFIC SOOT PARTICLE NUMBER VS. ALTITUDE

The curve describing the average specific soot particle number  $N_{soot}$  [ $10^{15}/g$ ] vs. altitude  $H$  [km] from [33] can be approximated by the following function:

For  $H$  [km]  $\leq 11.3$ :

$$N_{soot} = a \cdot H^6 + b \cdot H^5 + c \cdot H^4 + d \cdot H^3 + e \cdot H^2 + f \cdot H + g$$

with  $a = -0.0000728$        $e = -0.1970238$

$b = 0.0020713$        $f = 0.6372580$

$c = -0.0217709$        $g = 4.8185084$

$d = 0.1071162$

For  $H$  [km]  $> 11.3$ :

$$N_{soot} = m \cdot H + t$$

with  $m = 0.0100312$        $t = 16.3945469$

The original diagram from [33] shows decreasing values of  $N_{soot}$  at very high altitudes ( $> 14$  km), but based on measurements for one single engine (from Concorde) only. As Concorde aircraft have been retired, high-altitude data was omitted in both the above formulae and the diagram below.

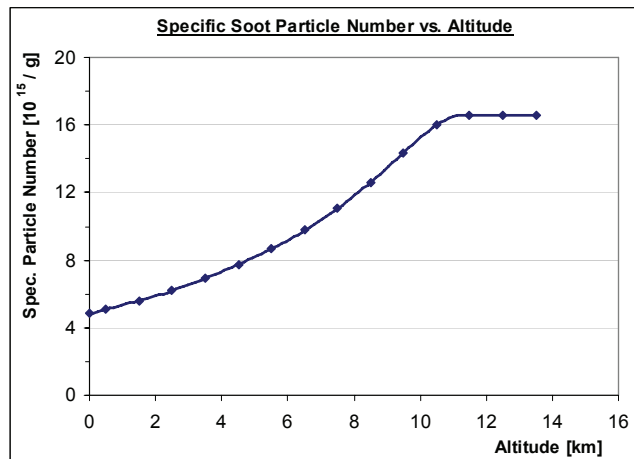


Figure 101: Average soot particle number per gram of soot vs. flight altitude

## Appendix F OAG AIRCRAFT AND VARMISSION MODELS

Specific or General Aircraft ID (OAG)	OAG Aircraft Name	Equivalent OAG IDs for Forecast	VarMission Aircraft ID	VarMission Aircraft Variant	User-defined model	Represent. Aircraft
ND2	Aerospatiale (Nord) 262		SH36	BADA v3.9		x
AB3	Airbus A300 Passenger	AB4,AB6	A306	BADA v3.9		
AB6	Airbus A300-600 Passenger		A306	BADA v3.9		
AB4	Airbus A300B2 /B4 Passenger		A30B	BADA v3.9		
ABX	Airbus A300B4 /A300C4 /A300F4		A30B	BADA v3.9		x
310	Airbus A310 Passenger	312,313	A310	BADA v3.9		
312	Airbus A310-200 Passenger		A310	BADA v3.9		
313	Airbus A310-300 Passenger		A310	BADA v3.9		x
318	Airbus A318		A318	BADA v3.9		
32S	Airbus A318 /319 /320 /321	318,319,320,321	A320	BADA v3.8*		
319	Airbus A319		A319	BADA v3.9		
320	Airbus A320		A320	BADA v3.8*		
321	Airbus A321		A321	BADA v3.9		
330	Airbus A330	332,333	A332	BADA v3.9		
332	Airbus A330-200		A332	BADA v3.9		
333	Airbus A330-300		A333	BADA v3.9		
340	Airbus A340	342,343,345,346	A343	BADA v3.9		
342	Airbus A340-200		A343	BADA v3.9		x
343	Airbus A340-300		A343	BADA v3.9		
345	Airbus A340-500		A345	BADA v3.9		
346	Airbus A340-600		A346	BADA v3.9		
380	Airbus A380	388,389	A388	BADA v3.9		
388	Airbus A380-800 Passenger		A388	BADA v3.9		
389	Airbus A380-900 Passenger		A388	BADA v3.9		x
ANF	Antonov AN-12		C130	BADA v3.9		x
A4F	Antonov AN-124		B742	BADA v3.9		x
A40	Antonov AN-140		AT45	BADA v3.9		x
A81	Antonov An148-100		B462	BADA v3.9		x
AN4	Antonov AN-24		F27	BADA v3.9		x
AN6	Antonov AN-26 /30 /32		F27	BADA v3.9		x
A28	Antonov An28 /Pzl Mielec M-28 Skytruck		E120	BADA v3.9		x
AN7	Antonov AN-72 /74		F28	BADA v3.9		x
AT3	ATR 42 300 /400		AT43	BADA v3.9		
AT5	ATR 42 500		AT45	BADA v3.9		
AT4	ATR 42-300 /320	AT3	AT43	BADA v3.9		
AT7	ATR 72		AT73	BADA v3.9		
ATR	ATR42 /ATR72	AT3,AT5,AT7	AT73	BADA v3.9		
AR1	Avro RJ100		RJ85	BADA v3.9		x
AR7	Avro RJ70		RJ85	BADA v3.9		x
ARJ	Avro RJ70 /RJ85 /RJ100	AR1,AR7,AR8	RJ85	BADA v3.9		
AR8	Avro RJ85		RJ85	BADA v3.9		
B15	BAe (BAC /ROMBAC) 1-11 500	B11	BA11	BADA v3.9		x
B11	BAe (BAC) 1-11		BA11	BADA v3.9		
B12	BAe (BAC) 1-11 200	B11	BA11	BADA v3.9		x
B13	BAe (BAC) 1-11 300	B11	BA11	BADA v3.9		x
HS7	BAe (HS) 748		F27	BADA v3.9		x
14F	BAe 146 (Freighter)		B462	BADA v3.9		x
146	BAe 146 Passenger	141,142,143	B462	BADA v3.9		
141	BAe 146-100 Passenger		B462	BADA v3.9		x
142	BAe 146-200 Passenger		B462	BADA v3.9		
143	BAe 146-300 Passenger		B462	BADA v3.9		x
ATP	BAe ATP		ATP	BADA v3.9		
JST	BAe Jetstream	J31,J32,J41	JS32	BADA v3.9		
J31	BAe Jetstream 31		JS32	BADA v3.9		x
J32	BAe Jetstream 32		JS32	BADA v3.9		
J41	BAe Jetstream 41		JS41	BADA v3.9		
BET	Beechcraft (Lght Acft - Twin Turboprop)	BEC	JS32	BADA v3.9		x
BEC	Beechcraft (Light Aircraft)		BE9L	BADA v3.9		
BE1	Beechcraft 1900 Airliner	BEH,BES	JS32	BADA v3.9		x
BES	Beechcraft 1900C Airliner		JS32	BADA v3.9		x
BEH	Beechcraft 1900D Airliner		JS32	BADA v3.9		x
BE9	Beechcraft C99 Airliner		BE99	BADA v3.9		
BE2	Beechcraft-Lght Acft-Twin Piston Engine	BEC	BE58	BADA v3.9		x

Table 29: Assignment of VarMission / BADA models to OAG aircraft types, part 1

Specific or General Aircraft ID (OAG)	OAG Aircraft Name	Equivalent OAG IDs for Forecast	VarMission Aircraft ID	VarMission Aircraft Variant	User-defined model	Represent. Aircraft
BN1	BN BN-2A /BN-2B Islander		PA31	BADA v3.9		x
BNT	BN BN-2A MkIII Trislander		PA31	BADA v3.9		x
D10	Boeing (Douglas) DC10 Passenger	D1C,D11	DC10	BADA v3.9		
D11	Boeing (Douglas) DC10-10 /15 Passenger		DC10	BADA v3.9		x
D1C	Boeing (Douglas) DC10-30 /40 Passenger		DC10	BADA v3.9		
D3F	Boeing (Douglas) DC3 Freighter	DC3	F27	BADA v3.9		x
DC3	Boeing (Douglas) DC-3 Passenger		F27	BADA v3.9		x
D6F	Boeing (Douglas) DC6A /B /C Freighter		C130	BADA v3.9		x
DC6	Boeing (Douglas) DC-6b Passenger		C130	BADA v3.9		x
DC8	Boeing (Douglas) DC-8 Passenger		DC87	BADA v3.9		x
D9F	Boeing (Douglas) DC9 Freighter		DC94	BADA v3.9		x
DC9	Boeing (Douglas) DC-9 Passenger	D92,D93,D95	DC94	BADA v3.9		x
D92	Boeing (Douglas) DC-9-20		DC94	BADA v3.9		x
D93	Boeing (Douglas) DC9-30 Passenger		DC94	BADA v3.9		x
D95	Boeing (Douglas) DC9-50 Passenger		DC94	BADA v3.9		x
M1M	Boeing (Douglas) MD-11 Mixed Config		MD11	BADA v3.9		x
M11	Boeing (Douglas) MD-11 Passenger		MD11	BADA v3.9		
M80	Boeing (Douglas) MD-80	M81,M82,M83,M87,M88	MD82	BADA v3.9		
M81	Boeing (Douglas) MD-81		MD82	BADA v3.9		x
M82	Boeing (Douglas) MD-82		MD82	BADA v3.9		
M83	Boeing (Douglas) MD-83		MD83	BADA v3.9		
M87	Boeing (Douglas) MD-87		MD82	BADA v3.9		x
M88	Boeing (Douglas) MD-88		MD83	BADA v3.9		x
M90	Boeing (Douglas) MD-90		MD83	BADA v3.9		x
707	Boeing 707 /720 Passenger		B703	BADA v3.9		
70F	Boeing 707-320B /320C (Freighter)		B703	BADA v3.9		
717	Boeing 717-200		B712	BADA v3.9		
72M	Boeing 727 (Mixed Configuration)		B722	BADA v3.9		x
727	Boeing 727 (Passenger)	721,722	B722	BADA v3.9		
721	Boeing 727-100 Passenger		B722	BADA v3.9		x
72S	Boeing 727-200 Passenger	722	B722	BADA v3.9		
72A	Boeing 727-200 Advanced	722	B722	BADA v3.9		
722	Boeing 727-200 Passenger		B722	BADA v3.9		
73M	Boeing 737 (Mixed Configuration)	73L,73Q	B732	BADA v3.9		x
73S	Boeing 737 Advanced all Series	732	B732	BADA v3.9		
737	Boeing 737 Passenger	731,732,733,734,735,736,73G,738,739	B738	BADA v3.9		
731	Boeing 737-100 Passenger		B732	BADA v3.9		x
73L	Boeing 737-200 (Mixed Configuration)		B732	BADA v3.9		x
73A	Boeing 737-200 /200C Advanced (Pax)	732	B732	BADA v3.9		
732	Boeing 737-200 Passenger		B732	BADA v3.9		
73C	Boeing 737-300 (Winglets) Passenger	733	B733	BADA v3.9		
733	Boeing 737-300 Passenger		B733	BADA v3.9		
73Q	Boeing 737-400 (Mixed Configuration)		B734	BADA v3.9		x
734	Boeing 737-400 Passenger		B734	BADA v3.9		
735	Boeing 737-500 Passenger		B735	BADA v3.9		
73E	Boeing 737-500 (Winglets) Passenger	735	B735	BADA v3.9		
736	Boeing 737-600 Passenger		B736	BADA v3.9		
73W	Boeing 737-700 (Winglets) Passenger	73G	B737	BADA v3.9		
73G	Boeing 737-700 Passenger		B737	BADA v3.9		
73H	Boeing 737-800 (Winglets) Passenger	738	B738	BADA v3.9		
738	Boeing 737-800 Passenger		B738	BADA v3.9		
73J	Boeing 737-900 (Winglets) Passenger	739	B739	BADA v3.9		
739	Boeing 737-900 Passenger		B739	BADA v3.9		
74M	Boeing 747 (Mixed Configuration)	74C,74D,74E	B744	BADA v3.9		x
747	Boeing 747 (Passenger)	741,742,743,744,748	B744	BADA v3.9		
741	Boeing 747-100 (Passenger)		B742	BADA v3.9		x
74C	Boeing 747-200 (Mixed Configuration)		B742	BADA v3.9		x
742	Boeing 747-200 (Passenger)		B742	BADA v3.9		
743	Boeing 747-300 /747-100 /200 SUD (Pax)		B743	BADA v3.9		
74D	Boeing 747-300 /747-200 SUD (Mxd Config)		B743	BADA v3.9		x
74E	Boeing 747-400 (Mixed Configuration)		B744	BADA v3.9		x
744	Boeing 747-400 (Passenger)		B744	BADA v3.9		
74L	Boeing 747SP Passenger		B742	BADA v3.9		x
74R	Boeing 747SR Passenger		B742	BADA v3.9		x
757	Boeing 757 (Passenger)	752,753	B752	BADA v3.9		
75W	Boeing 757-200 (Winglets) Passenger		B752	BADA v3.9		
75M	Boeing 757-200 (Mixed Configuration)	752	B752	BADA v3.9		x
752	Boeing 757-200 Passenger		B752	BADA v3.9		

Table 30: Assignment of VarMission / BADA models to OAG aircraft types, part 2

Specific or General Aircraft ID (OAG)	OAG Aircraft Name	Equivalent OAG IDs for Forecast	VarMission Aircraft ID	VarMission Aircraft Variant	User-defined model	Represent. Aircraft
753	Boeing 757-300 Passenger		B753	BADA v3.9		
75T	Boeing 757-300 (Winglets) Passenger	753	B753	BADA v3.9		
767	Boeing 767 Passenger	762,763,764	B763	BADA v3.9		
762	Boeing 767-200 Passenger		B762	BADA v3.9		
763	Boeing 767-300 Passenger		B763	BADA v3.9		
76W	Boeing 767-300 (Winglets) Passenger	763	B763	BADA v3.9		
764	Boeing 767-400 Passenger		B764	BADA v3.9		
777	Boeing 777 Passenger	772,773,77L,77W	B772	BADA v3.9		
772	Boeing 777-200 Passenger		B772	BADA v3.9		
77L	Boeing 777-200LR		B77L	BADA v3.9		
773	Boeing 777-300 Passenger		B773	BADA v3.9		
77W	Boeing 777-300ER Passenger		B77W	BADA v3.9		
CL4	Canadair CL-44		C130	BADA v3.9		
CRA	Canadair Crj Series 705		CRJ9	BADA v3.9		x
CRJ	Canadair Regional Jet	CR1,CR2,CR7,CR9,CRX,CRA	CRJ2	BADA v3.9		
CR1	Canadair Regional Jet 100		CRJ1	BADA v3.9		
CRX	Canadair Regional Jet 1000		CRJ9	BADA v3.9		x
CRK	Canadair Regional Jet 1000	CRX	E170	BADA v3.9		x
CR2	Canadair Regional Jet 200		CRJ2	BADA v3.9		
CR7	Canadair Regional Jet 700		CRJ9	BADA v3.9		x
CR9	Canadair Regional Jet 900		CRJ9	BADA v3.9		
CS5	Casa /Nusantara CN-235		DH8A	BADA v3.9		x
CS2	Casa C212 /Nusantara NC-212 Aviocar		D228	BADA v3.9		x
CNA	Cessna (Light Aircraft)		C421	BADA v3.9		x
CN1	Cessna Light Aircraft (Single Piston Engine)	CNA	P28A	BADA v3.9		x
CNF	Cessna 208b Freighter	CNA	C421	BADA v3.9		x
CNJ	Cessna Citation		C550	BADA v3.9		x
CNC	Cessna Light Aircraft (Single Turboprop)	CNA	P28A	BADA v3.9		x
CNT	Cessna Light Aircraft (Twin Turboprop)	CNA	MU2	BADA v3.9		x
CVR	Convair 240 /440 /580 (Passenger)		F27	BADA v3.9		x
CVF	Convair 440 /580 /600 /640 (Freighter)		F27	BADA v3.9		x
CV5	Convair 580 Passenger	CVR	F27	BADA v3.9		x
CWC	Curtiss C-46 Commando		F27	BADA v3.9		x
DFL	Dassault Falcon	DF2	F2TH	BADA v3.9		
DF2	Dassault Falcon 10 /20 /100 /200 /2000		F2TH	BADA v3.9		
DHS	De Havilland DHC 3 Otter	DHO	C421	BADA v3.9		x
DHP	De Havilland DHC-2 Beaver	DHB	BE58	BADA v3.9		x
DHB	De Havilland DHC2 Beaver /Turbo Beaver		BE58	BADA v3.9		x
DHO	De Havilland DHC-3 Otter /Turbo Otter		C421	BADA v3.9		x
DHL	De Havilland DHC-3 Turbo Otter	DHO	C421	BADA v3.9		x
DHC	De Havilland DHC-4 Caribou		F27	BADA v3.9		x
DHT	De Havilland DHC-6 Twin Otter		BE20	BADA v3.9		x
DH7	De Havilland DHC-7 Dash 7		F27	BADA v3.9		x
DH8	De Havilland DHC-8 Dash 8	DH1,DH2,DH3,DH4	DH8A	BADA v3.9		
DH1	De Havilland DHC-8-100 Dash 8 /8Q		DH8A	BADA v3.9		
DH2	De Havilland DHC-8-200 Dash 8 /8Q		DH8A	BADA v3.9		x
DH3	De Havilland DHC-8-300 Dash 8 /8Q		DH8C	BADA v3.9		
DH4	De Havilland DHC-8-400 Dash 8Q		DH8D	BADA v3.9		
EMB	Embraer 110 Bandeirante		D228	BADA v3.9		x
EM2	Embraer 120 Brasilia		E120	BADA v3.9		
E70	Embraer 170		E170	BADA v3.9		
EMJ	Embraer 170 /195	E70,E75,E90,E95	E170	BADA v3.9		
E75	Embraer 175		E170	BADA v3.9		x
E90	Embraer 190		E190	BADA v3.9		
E95	Embraer 195		E190	BADA v3.9		x
ERJ	Embraer RJ 135 /140 /145	ER3,ER4,ERD	E145	BADA v3.9		
ER3	Embraer RJ135		E135	BADA v3.8**		
ERD	Embraer RJ140		E145	BADA v3.9		x
EM4	Embraer RJ145	ER4	E145	BADA v3.9		
ER4	Embraer RJ145		E145	BADA v3.9		
D28	Fairchild Dornier 228		D228	BADA v3.9		
D38	Fairchild Dornier 328-100		D328	BADA v3.9		
FRJ	Fairchild Dornier 328JET		C750	BADA v3.9		x
FK7	Fairchild Industries FH227		F27	BADA v3.9		
SWM	Fairchild SA26 /SA226 /SA277 Merlin /Me		SW4	BADA v3.9		x
100	Fokker 100		F100	BADA v3.9		
F50	Fokker 50		F50	BADA v3.9		
F70	Fokker 70		F70	BADA v3.9		

Table 31: Assignment of VarMission / BADA models to OAG aircraft types, part 3



Specific or General Aircraft ID (OAG)	OAG Aircraft Name	Equivalent OAG IDs for Forecast	VarMission Aircraft ID	VarMission Aircraft Variant	User-defined model	Represent. Aircraft
F27	Fokker F27 Friendship /Fairchild F27		F27	BADA v3.9		
F28	Fokker F28 Fellowship	F21,F22,F23,F24	F28	BADA v3.9		
F21	Fokker F28-1000 Fellowship		F28	BADA v3.9		x
F22	Fokker F28-2000 Fellowship		F28	BADA v3.9		x
F23	Fokker F28-3000 Fellowship		F28	BADA v3.9		x
F24	Fokker F28-4000 Fellowship		F28	BADA v3.9		
CD2	GAF N22B /N24A Nomad		E120	BADA v3.9		x
GRG	Grumman G-21 Goose (Amphibian)		F27	BADA v3.9		x
GRM	Grumman G-73 Mallard (Amphibian)		E120	BADA v3.9		x
GRS	Gulfstream Aerospace G159 G 1		F27	BADA v3.9		x
YN2	Harbin Yunshuji Y12		E120	BADA v3.9		x
I14	Ilyushin IL114		SB20	BADA v3.9		x
IL8	Ilyushin IL-18		C130	BADA v3.9		x
IL6	Ilyushin IL-62		B703	BADA v3.9		x
IL7	Ilyushin IL-76		B703	BADA v3.9		x
ILW	Ilyushin IL-86		B703	BADA v3.9		x
IL9	Ilyushin IL-96 Passenger		A343	BADA v3.9		x
WWP	Israel Aircraft Ind.1124 Westwind		H25A	BADA v3.9		x
LRJ	Learjet		LJ35	BADA v3.9		
L4T	Let 410		D228	BADA v3.9		x
L11	Lockheed L1011 TriStar 1 /50 /100 /150		L101	BADA v3.9		
L15	Lockheed L1011 TriStar 500 Passenger		L101	BADA v3.9		x
L1F	Lockheed L1011 TriStar Freighter		L101	BADA v3.9		x
L10	Lockheed L1011 TriStar Passenger	L11,L15	L101	BADA v3.9		
LOH	Lockheed L182 /L282 /L382 (L100) Hercul		C130	BADA v3.9		
LOF	Lockheed L188 Electra (Freighter)		C130	BADA v3.9		x
LOM	Lockheed L188 Electra (Mixed Config.)	LOF	C130	BADA v3.9		x
D9S	McD-Douglas DC9 30 /40 /50	D93,D94,D95	DC94	BADA v3.9		x
D94	McD-Douglas DC9-40		DC94	BADA v3.9		
MU2	Mitsubishi MU-2		MU2	BADA v3.9		
YS1	NAMC YS-11		F27	BADA v3.9		x
PN6	Partenavia P68		DA42	BADA v3.9		x
PL2	Pilatus PC-12		BE9L	BADA v3.9		x
PA1	Piper (Light Aircraft - Single Piston)	PAG	P28A	BADA v3.9		x
PA2	Piper (Light Aircraft - Twin Piston)	PAG	PA31	BADA v3.9		
PAT	Piper (Light Aircraft - Twin Turboprop)	PAG	PAY3	BADA v3.9		
PAG	Piper (Light Aircraft)		P28A	BADA v3.9		
S20	Saab 2000		SB20	BADA v3.9		
SFB	Saab 340	SF3	SF34	BADA v3.9		
SF3	Saab 340		SF34	BADA v3.9		
SH3	Shorts 330 (SD3-30)		SH36	BADA v3.9		x
SH6	Shorts 360 (SD3-60)		SH36	BADA v3.9		
SHB	Shorts SC.5 Belfast		C130	BADA v3.9		
SHS	Shorts Skyvan (SC-7)		E120	BADA v3.9		x
TU3	Tupolev TU134		T134	BADA v3.9		
TU5	Tupolev TU154		T154	BADA v3.9		
T20	Tupolev TU-204 /TU-214		B752	BADA v3.9		x
T2F	Tupolev TU-204 Freighter		B752	BADA v3.9		x
ACD	Twin (aero) Commander /turbo /jetprop		MU2	BADA v3.9		x
YN7	Xian Yunshuji Y7 /MA60		F27	BADA v3.9		x
YK4	Yakovlev Yak-40		FA50	BADA v3.9		x
YK2	Yakovlev Yak-42 /142		B722	BADA v3.9		x

\* The Airbus A320 model from BADA v3.8 was used as reference aircraft for the development of future narrowbody and A320 NEO aircraft models. The BADA v3.9 model of the A320 refers to another engine version. For reasons of consistency, the BADA v3.8 version of the A320 is used in this study.

\*\* The Embraer E135 model from BADA v3.8 refers to the "LR" version of this aircraft and is used in this study. The BADA v3.9 model of the E135 refers to a business jet version and may be less representative for the aircraft in airline service.

Table 32: Assignment of VarMission / BADA models to OAG aircraft types, part 4

Specific or General Aircraft ID	User-defined Aircraft Name	Equivalent OAG IDs for Forecast	VarMission Aircraft ID	VarMission Aircraft Variant	User-defined model	Represent. Aircraft
ABF	Airbus A300 Freighter	ABX,ABY	A306	A300-600F	x	
ABY	Airbus A300-600 Freighter		A306	A300-600F	x	
31F	Airbus A310 Freighter		A310	A310-200F	x	
31Y	Airbus A310-300 Freighter	31F	A310	A310-300F	x	
33F	Airbus A330 Freighter		A332	A330-200F	x	
33X	Airbus A330-200 Freighter	33F	A332	A330-200F	x	
35F	Airbus A350-900 Freighter		B772	777F	x	x
38F	Airbus A380-800 Freighter		A388	A380F	x	
D1Y	Boeing (Douglas) DC10 - 30 /40 Freighter	D1F	DC10	DC10-30AF	x	
D1F	Boeing (Douglas) DC10 Freighter		DC10	DC10-30AF	x	
D8F	Boeing (Douglas) DC8 Freighter		DC87	DC-8-72F	x	
D8Y	Boeing (Douglas) DC-8-71 /72 /73 Freighter	D8F	DC87	DC-8-72F	x	
M1F	Boeing (Douglas) MD-11 Freighter		MD11	MD-11F	x	
72F	Boeing 727 Freighter		B722	727-200F	x	
73F	Boeing 737 Freighter	73P,73X,73Y	B733	737-300SF	x	
73X	Boeing 737-200 Freighter		B732	737-200F	x	
73Y	Boeing 737-300 Freighter		B733	737-300SF	x	
73P	Boeing 737-400 Freighter		B734	737-400SF	x	
73R	Boeing 737-700 Freighter		B737	737-700C	x	
74F	Boeing 747 Freighter	74T,74X,74Y,74Z	B744	747-400F	x	
74T	Boeing 747-100 Freighter		B742	747-200F	x	x
74X	Boeing 747-200 Freighter		B742	747-200F	x	
74Y	Boeing 747-400F Freighter		B744	747-400F	x	
74Z	Boeing 747-8F Freighter		B748	747-8F	x	
75F	Boeing 757-200F Freighter		B752	757-200PF	x	
76F	Boeing 767 Freighter		B763	767-300F	x	
76X	Boeing 767-200 Freighter	76F	B762	767-200F	x	
76Y	Boeing 767-300 Freighter	76F	B763	767-300F	x	
77F	Boeing 777 Freighter		B772	777F	x	
77X	Boeing 777-200F Freighter	77F	B772	777F	x	
78F	Boeing 787-800 Freighter		A332	A330-200F	x	x
D8X	McD-Douglas DC-8-50 /61 /62 /63 Freighter	D8F	DC87	DC-8-72F	x	x

Table 33: Assignment of VarMission cargo aircraft models to OAG aircraft types

Specific or General Aircraft ID	User-defined Aircraft Name	Equivalent OAG IDs for Forecast	VarMission Aircraft ID	VarMission Aircraft Variant	User-defined model	Represent. Aircraft
19N	Airbus A319 NEO		A319N	user defined	x	
20N	Airbus A320 NEO		A320N	user defined	x	
21N	Airbus A321 NEO		A321N	user defined	x	
35X	Airbus A350-1000 XWB Passenger		A359	user defined	x	x
358	Airbus A350-800 XWB Passenger		A359	user defined	x	x
359	Airbus A350-900 XWB Passenger		A359	user defined	x	
37N	Boeing 737 MAX 7		A319N	user defined	x	x
38N	Boeing 737 MAX 8		A320N	user defined	x	x
39N	Boeing 737 MAX 9		A321N	user defined	x	x
748	Boeing 747-8I		B748	user defined	x	
788	Boeing 787-8		B788	user defined	x	
789	Boeing 787-9		B788	user defined	x	x
CS1	Bombardier CSeries 100		FURJ	user defined	x	x
CS3	Bombardier CSeries 300		A319N	user defined	x	x
F7B	Bombardier Future 70 Seat Regional Jet		E170	BADA v3.9	x	x
F9B	Bombardier Future 90 Seat Regional Jet		FURJ	user defined	x	x
C91	Comac 919-100		A319N	user defined	x	x
C92	Comac 919-200		A320N	user defined	x	x
C93	Comac 919-300		A321N	user defined	x	x
217	Comac ARJ21-700		E190	BADA v3.9	x	x
219	Comac ARJ21-900		E190	BADA v3.9	x	x
FE	Embraer Future 100 Seat Regional Jet		FURJ	user defined	x	x
F5E	Embraer Future 50 Seat Regional Jet		E145	BADA v3.9	x	x
F7E	Embraer Future 70 Seat Regional Jet		E170	BADA v3.9	x	x
FU1	Future Narrowbody (134 seats)		FUN1	user defined	x	
FU2	Future Narrowbody (164 seats)		FUN2	user defined	x	
FU3	Future Narrowbody (199 seats)		FUN3	user defined	x	
FP9	Future Turboprop (90 seats)		AT73	BADA v3.9	x	x
FUQ	Future Turboprop ATR (50 seats)		AT45	BADA v3.9	x	x
FUP	Future Turboprop ATR (70 seats)		AT73	BADA v3.9	x	x
FQQ	Future Turboprop Bombardier (70 seats)		AT73	BADA v3.9	x	x
72N	Future Widebody / 777-200 Successor		A359	user defined	x	x
73N	Future Widebody / 777-300 Successor		A359	user defined	x	x
MJ7	Mitsubishi MRJ70		FURJ	user defined	x	x
MJ9	Mitsubishi MRJ90		FURJ	user defined	x	
S75	Suchoi SSJ 100-75		FURJ	user defined	x	x
S95	Suchoi SSJ 100-95		FURJ	user defined	x	x

Table 34: Assignment of VarMission passenger aircraft models to future aircraft types

## Appendix G EN-ROUTE EXTENSION

Inefficiencies in the Air Traffic Management (ATM) lead to flight distances that are larger than the great-circle distances between departure and arrival airports. This appendix explains the approximation of the flight distances in the Air Traffic Emissions Module based on reference data from the EUROCONTROL Performance Review Commission (PRC) [47], [48], [49].

The flight distance extension (or en-route extension) compared to the great-circle distance consists of the direct route extension and the TMA interface. Figure 102 explains the interrelations between these elements. In the terminology used by EUROCONTROL PRC, the direct route extension is given by A-D while the TMA interface is described by D-G.

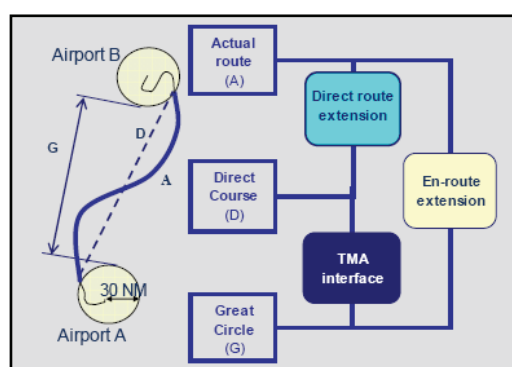


Figure 102: Contributions to route extension [49]

Table 35 shows average values for the elements that contribute to en-route extension. As can be seen from the table, the TMA interface distance in Europe is approximately constant in recent years (~15.3 km). The same is true for the direct route extension. It should be noted, however, that the direct route extension of a flight is dependent on the flight's great-circle distance. In Europe, the average distance per flight is increasing. Consequently, the relative en-route extension in percent of the great-circle distance has decreased in the same timeframe (see Table 35).

In this study, the en-route extension is modelled as function of time and great-circle distance. In this appendix, the distance-dependency is derived for the reference year 2008. The resulting en-route extension is corrected as function of time, as described in chapter 3.3.5.

	2005	2006	2007	2008	2009
En-route extension [% of great-circle]	5.9	5.8	5.8	5.6	5.4
En-route extension [km]	48.7	48.2	48.9	48.8	47.6
Average great-circle distance per flight [km]	822	830	842	868	874
Direct route extension [km]	33.45	32.95	33.4	33.6	32.2
TMA interface [km]	15.25	15.25	15.5	15.2	15.3

Table 35: Development of en-route extension in Europe [47], [48], [49]

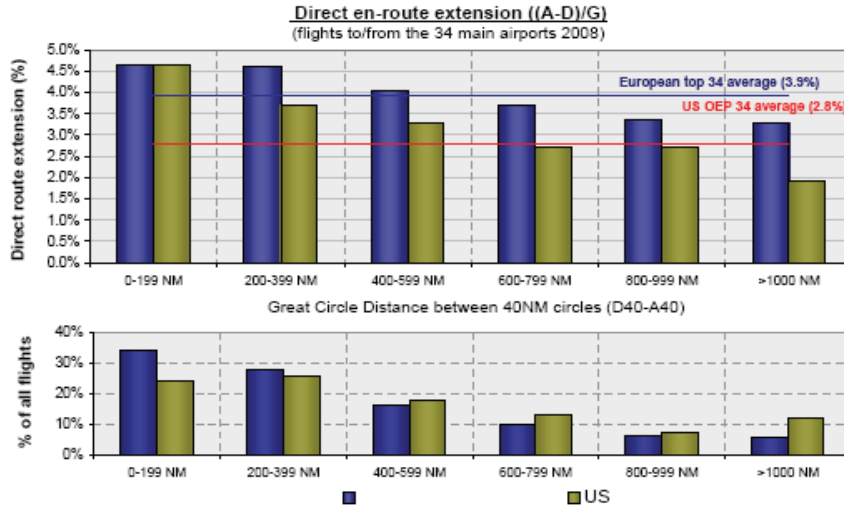


Figure 103: Direct route extension in Europe and the US per distance category [48]

Figure 103 shows distance-dependent reference data for the direct route extension in the US and Europe. Unfortunately, such information is not available for the global air traffic system. Assuming that the average distance per distance category in Figure 103 is the mean of a given interval<sup>48</sup> and using the mean percentages from the US and European columns for a further analysis, the direct en-route extension in kilometres can be plotted versus the great-circle distance (see Figure 104).

The graph shown in Figure 104 is a parabolic trend function through the reference points supplemented by a linear relationship assumed for distances above 8500 km. As no reference data for route extensions of long-haul flights is available, the graph must be regarded as a rough estimate only.

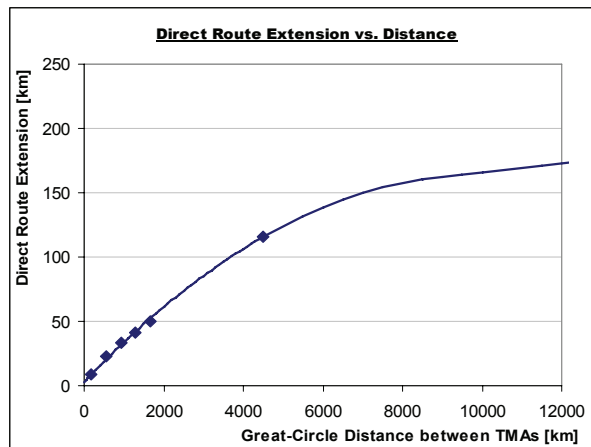


Figure 104: Direct route extension as function of great-circle distance (approximation)

<sup>48</sup> The average great-circle distance of the interval labelled „>1000 NM“ was determined such that the average great-circle distance per flight in Europe equals the value for the year 2008 shown in Table 10.

---

The function of the curve shown in Figure 104 is described by formulae (1a)-(1b):

$$(1a) \quad \textit{DirectRouteExtension} = -1.6273 \cdot 10^{-6} \cdot G^2 + 0.03236 \cdot G + 2.9926 \quad \textit{for } G < 8500 \textit{ km}$$

$$(1b) \quad \textit{DirectRouteExtension} = 0.003435 \cdot G + 131.3043 \quad \textit{for } G \geq 8500 \textit{ km}$$

In the above formulae, G refers to the great-circle distance between the airports' terminal areas. The terminal areas can be assumed as circles around the airports with a radius of 40 nautical miles [48]. When using formulae (1a)-(1b), 2·40 nautical miles (i.e. 148 kilometre) need to be subtracted from a flight's great-circle distance between departure and arrival airports.

While the direct route extension is modelled as function of distance, the TMA interface extension is assumed as a constant. Formulae (2)-(3) consider both elements when calculating the total en-route extension:

$$(2) \quad \textit{TMAInterface} = \textit{const.} = 15.3 \textit{ km}$$

$$(3) \quad \textit{EnRouteExtension} = \textit{DirectRouteExtension} + \textit{TMAInterface}$$

Formula (1)-(3) can be used to calculate the en-route extension for every flight in the movements database of the Air Traffic Emissions Module. It should be noted, however, that the above formulae are based on statistics from the European and US airspace and the distance-dependency is a rough estimate only.

## Appendix H ATM EFFICIENCY IN AIR TRAFFIC EMISSIONS MODULE

When calculating fuel burn and emissions in the Air Traffic Emissions Module, inefficiencies due to Air Traffic Management (ATM) are initially neglected. Given aircraft and engine identifiers as well as great-circle distance and payload information, fuel burn and emissions of NO<sub>x</sub>, CO, HC and soot can be calculated for each flight. Emission profiles, i.e. interpolation tables produced by the VarMission module are applied for this purpose (see chapter 3.2.6).

In a second step, inefficiencies in the ATM system are accounted for. The following contributions to ATM inefficiency are modelled explicitly:

- A ground-based inefficiency component.
- A terminal manoeuvring area (TMA) flight inefficiency.
- A horizontal flight inefficiency component (en-route).

Furthermore, a vertical flight inefficiency component of small magnitude is assumed to be implicitly included in the emission profiles. As was described in chapter 3.3.4, all inefficiency components in the model are given as fraction of aviation's total fuel consumption in an ideal air traffic system. The total fuel consumption for ideal conditions (i.e. without inefficiencies) can be approximated as follows:

$$(1) \quad TotalFuel_{ideal} = \frac{1}{1 + Inefficiency_{ATM,air,vertical}} \cdot \sum_{Flights} (FuelConsumption_{profiles} \cdot Frequency)$$

FuelConsumption<sub>profiles</sub> represents a flight schedule entry's fuel consumption as calculated by use of the emission profiles. The flight mission represented by the emission profiles includes 16 minutes of ground operations with engines in idle. This time is assumed as typical for engine start, taxi-out and taxi-in in a system without inefficiencies. The corresponding fuel consumption can be determined for each flight by use of the emission profiles:

$$(2) \quad TotalIdleFuel_{ideal} = \sum_{Flights} (IdleFuel_{profiles} \cdot Frequency)$$

In order to account for the **ground-based ATM inefficiency**, taxi times of all flights are increased equally such that the additional fuel consumption reflects the given inefficiency level. The additional fuel consumption of all flights amounts to:

$$(3) \quad AdditionalTaxiFuel_{ATM} = Inefficiency_{ATM,Ground} \cdot TotalFuel_{ideal}$$

This increase in fuel corresponds to an increase in taxi time, which is estimated as follows:

$$(4) \quad AdditionalTaxiTime_{ATM} = AdditionalTaxiFuel_{ATM} \cdot \frac{IdleTime_{ideal}}{TotalIdleFuel_{ideal}}$$



The additional taxi time is applied to each flight from the movements database. Hence, both fuel consumption and emission during the idle phases can be corrected to account for ground-based ATM inefficiencies:

$$(5a) \quad IdleFuel_{corrected} = IdleFuel_{profiles} \cdot \left( 1 + \frac{AdditionalTaxiTime_{ATM}}{IdleTime_{ideal}} \right)$$

$$(5b) \quad IdleEmissions_{corrected} = IdleEmissions_{profiles} \cdot \left( 1 + \frac{AdditionalTaxiTime_{ATM}}{IdleTime_{ideal}} \right)$$

A similar approach is followed when modelling ATM inefficiency in the terminal area (TMA). **TMA inefficiency** is simulated by holding segments at the destination airports of all flights from the movements database. No holding phase is included in the fuel burn and emission results for ideal conditions. However, the holding fuel and emissions tables described in chapter 3.2.6 can be used to estimate holding fuel and emissions. The additional fuel consumption of all flights due to TMA inefficiency is given as:

$$(6) \quad HoldingFuel_{ATM} = Inefficiency_{ATM,air,TMA} \cdot TotalFuel_{ideal}$$

In order to estimate the average holding time that corresponds to the fuel consumption from formula (6), a holding phase of 1 minute is added temporarily to each flight in the movements database. For simplicity, a holding altitude of 6000 feet and an initial aircraft gross weight equal to the landing weight obtained from the mission analysis is assumed. The holding time corresponding to the TMA inefficiency amounts to:

$$(7) \quad HoldingTime_{ATM} = HoldingFuel_{ATM} \cdot \frac{HoldingTime_{temp}}{HoldingFuel_{temp}}$$

On this basis, fuel consumption and emissions for individual flights are calculated as follows:

$$(8a) \quad HoldingFuel_{corrected} = HoldingTime_{ATM} \cdot \frac{HoldingFuel_{temp}}{HoldingTime_{temp}}$$

$$(8b) \quad HoldingEmissions_{corrected} = HoldingTime_{ATM} \cdot \frac{HoldingEmissions_{temp}}{HoldingTime_{temp}}$$

When considering the **horizontal flight inefficiency**, a flight distance extension compared to the great-circle is estimated such that the additional fuel in the cruise phase corresponds to the given inefficiency level:

$$(9) \quad AdditionalCruiseFuel_{ATM} = Inefficiency_{ATM,Air,horizontal} \cdot TotalFuel_{ideal}$$

Unlike in the approach for taxi times and holding segments – where all flights are treated equally – the en-route flight distance extension depends on the flights’ great-circle distances. In an interim step, the emission profiles are used to re-calculate fuel burn and emissions for each flight, this time including a “default” distance extension. Figure 105 shows the relationship used to calculate this extension as function of great-circle distance. The data in Figure 105 is derived from EUROCONTROL statistics, more details are found in Appendix G.

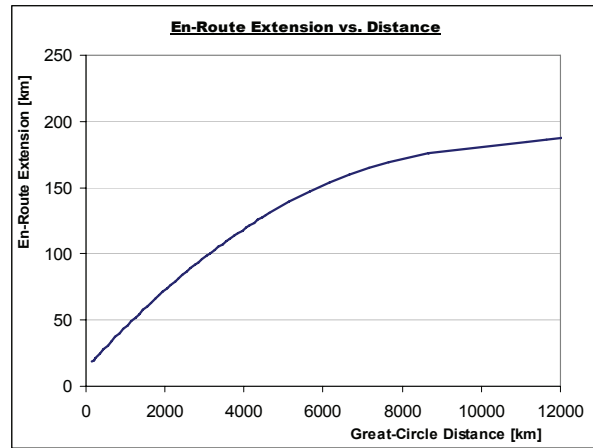


Figure 105: En-route extension vs. great-circle distance [48]

The additional fuel resulting from the interim calculation can be estimated as follows:

$$(10) \text{ AdditionalCruiseFuel}_{temp} = \sum_{Flights} (FuelConsumption_{profile,temp} \cdot Frequency) - \sum_{Flights} (FuelConsumption_{profiles} \cdot Frequency)$$

On this basis, a correction factor for the en-route extension can be determined. Applying this factor to the default distance extension described above, the target fuel consumption from formula (9) will be reached. The correction factor is calculated as follows:

$$(11) \text{ Correction}_{RouteExtension} = \frac{\text{AdditionalCruiseFuel}_{ATM}}{\text{AdditionalCruiseFuel}_{temp}}$$

In a final step, the emission profiles are used again for fuel-burn and emission calculation of all flights, this time assuming the corrected flight distance extensions. Nominating a flight’s fuel consumption from this calculation step as  $FuelConsumption_{profiles, corrected}$ , the fuel consumption and emissions including taxi and holding inefficiencies can be estimated as:

$$(12a) \text{ FuelConsumption}_{corrected} = \text{FuelConsumption}_{profiles,corrected} + (\text{IdleFuel}_{corrected} - \text{IdleFuel}_{profiles}) + \text{HoldingFuel}_{corrected}$$

$$(12b) \text{ Emissions}_{corrected} = \text{Emissions}_{profiles,corrected} + (\text{IdleEmissions}_{corrected} - \text{IdleEmissions}_{profiles}) + \text{HoldingEmissions}_{corrected}$$

The corrected results are written to the Flight Movements and Emissions Database.

## Appendix I DATABASE STRUCTURE OF AIR TRAFFIC EMISSIONS MODULE

The following figures give an insight into the main database tables and their relations in Microsoft Access. Figure 106 shows the database structure used by the Air Traffic Emissions Module, which is equally applied by the Emissions Forecast Module. Figure 107 to Figure 109 refer to load factor information from ICAO [77] and other data sources while Figure 110 and Figure 111 focus on fleet information from ASCEND [11], which is required by the Air Traffic Emissions Module for the assignment of aircraft and engine models to each flight.

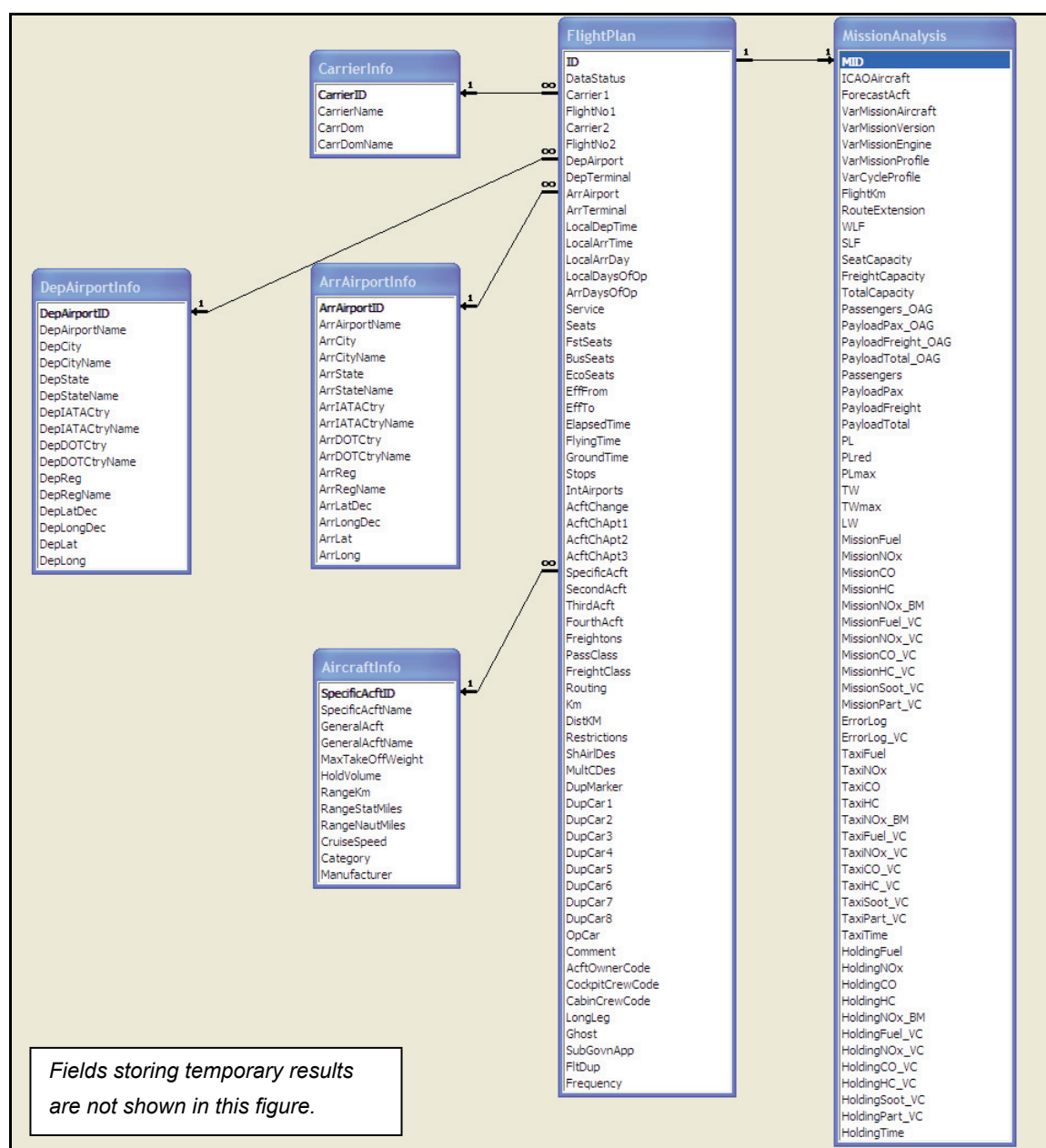


Figure 106: Movements and Emissions Database based on OAG flight schedules [100]

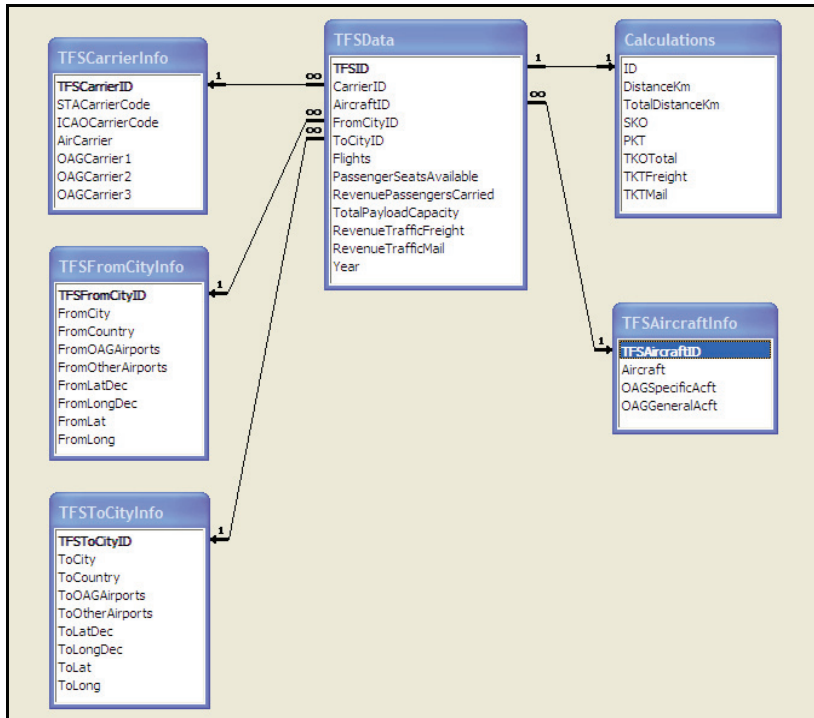


Figure 107: ICAO TFS data [77] as used by the Air Traffic Emissions Module

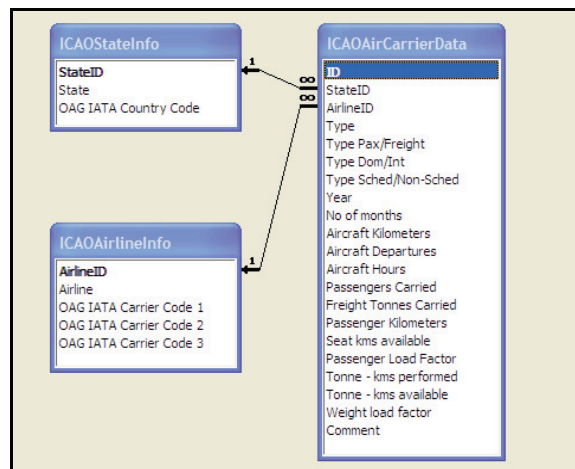


Figure 108: ICAO Air Carrier data [77] as used by the Air Traffic Emissions Module

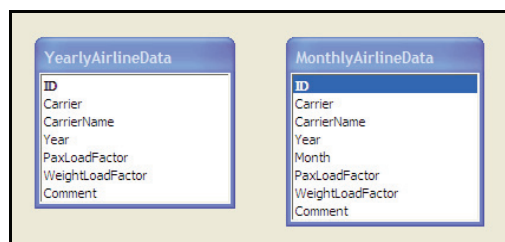


Figure 109: Data from airline publications as used by the Air Traffic Emissions Module

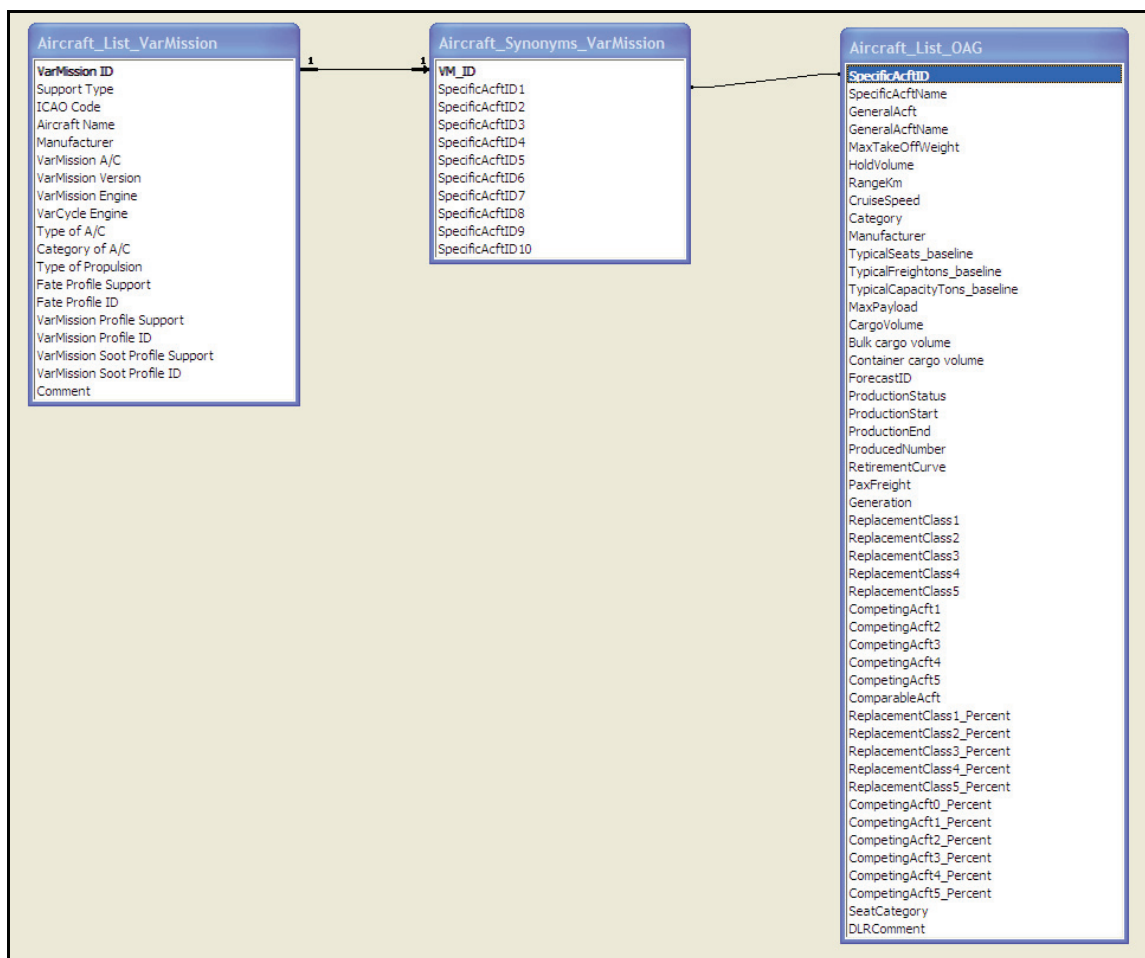


Figure 110: Excerpt of the VarMission database as used by the Air Traffic Emissions Module for the assignment of aircraft models to flight movements

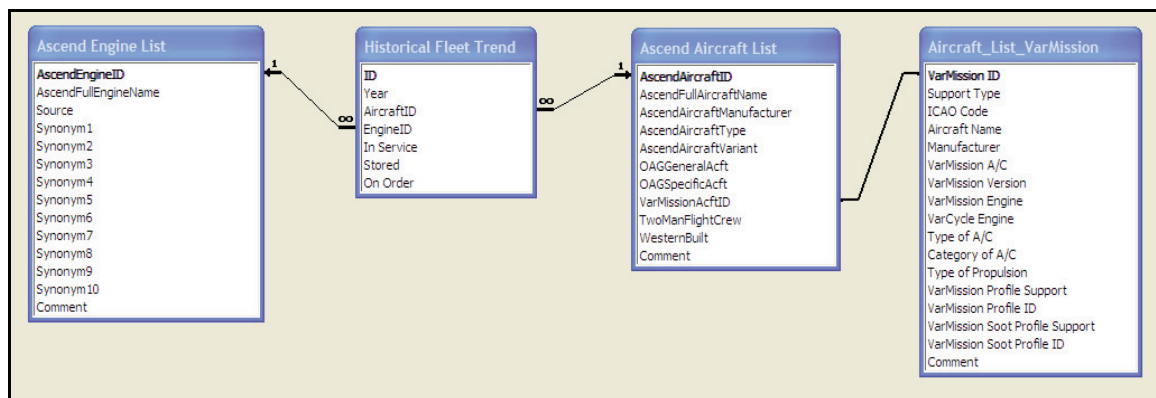


Figure 111: Excerpt of ASCEND fleets data [11] as used by the Air Traffic Emissions Module for the assignment of engine types to flight movements

## Appendix J GROWTH RATES FOR PASSENGER AND CARGO AIR TRAFFIC

From Region	Region Codes	Country Codes	To Region	Region Codes	Country Codes	Dom / Int	Average Annual Growth Rate		
							2011-2015	2016-2020	2021-2030
Africa Sub Sahara	AF2,AF3,AF4		Asia	AS2,AS3,AS4			6.6%	5.4%	4.4%
Africa Sub Sahara	AF2,AF3,AF4		Australia/NZ		AU,NZ		5.3%	4.6%	4.0%
Africa Sub Sahara	AF2,AF3,AF4		Caribbean	LA1			13.0%	8.8%	6.4%
Africa Sub Sahara	AF2,AF3,AF4		Indian Sub	AS1			7.9%	8.1%	6.3%
Africa Sub Sahara	AF2,AF3,AF4		Middle East	ME1			10.7%	7.5%	5.6%
Africa Sub Sahara	AF2,AF3,AF4		North Africa	AF1			11.9%	8.0%	5.8%
Africa Sub Sahara	AF2,AF3,AF4		Pacific	SW1			5.3%	4.6%	4.0%
Africa Sub Sahara	AF2,AF3,AF4		PRC		CN		12.2%	8.9%	6.5%
Africa Sub Sahara	AF2,AF3,AF4		Russia		RU		4.9%	4.1%	3.6%
Africa Sub Sahara	AF2,AF3,AF4		South Africa		ZA		7.2%	6.6%	5.9%
Africa Sub Sahara	AF2,AF3,AF4		South America	LA3,LA4			13.0%	8.8%	6.4%
Africa Sub Sahara	AF2,AF3,AF4		United States		US		9.2%	6.8%	5.3%
Africa Sub Sahara	AF2,AF3,AF4		Western Europe	EU1			5.3%	4.5%	3.9%
Asia	AS2,AS3,AS4		Australia/NZ		AU,NZ		6.1%	5.3%	4.8%
Asia	AS2,AS3,AS4		Canada		CA		5.7%	4.7%	3.9%
Asia	AS2,AS3,AS4		Central Europe	EU2			8.0%	6.7%	4.6%
Asia	AS2,AS3,AS4		CIS		AM,AZ,BY,KZ,GE,KG,MD,TJ,TM,UA,UZ		9.1%	6.7%	5.0%
Asia	AS2,AS3,AS4		Indian Sub	AS1			9.1%	7.9%	6.9%
Asia	AS2,AS3,AS4		Japan		JP		1.9%	3.2%	2.4%
Asia	AS2,AS3,AS4		Middle East	ME1			7.5%	5.3%	4.6%
Asia	AS2,AS3,AS4		North Africa	AF1			7.3%	5.8%	4.5%
Asia	AS2,AS3,AS4		Pacific	SW1			6.6%	5.4%	4.3%
Asia	AS2,AS3,AS4		PRC		CN		9.4%	6.7%	5.6%
Asia	AS2,AS3,AS4		Russia		RU		8.6%	6.3%	4.8%
Asia	AS2,AS3,AS4		South Africa		ZA		9.1%	7.2%	5.5%
Asia	AS2,AS3,AS4		South America	LA3,LA4			8.3%	6.7%	5.6%
Asia	AS2,AS3,AS4		United States		US		6.1%	4.6%	4.3%
Asia	AS2,AS3,AS4		Western Europe	EU1			5.3%	4.5%	3.8%
Australia/NZ		AU,NZ	Canada		CA		5.6%	4.9%	4.4%
Australia/NZ		AU,NZ	Caribbean	LA1			5.6%	4.9%	4.4%
Australia/NZ		AU,NZ	Indian Sub	AS1			6.1%	5.2%	4.3%
Australia/NZ		AU,NZ	Japan		JP		3.6%	3.6%	2.9%
Australia/NZ		AU,NZ	Middle East	ME1			10.1%	6.6%	5.5%
Australia/NZ		AU,NZ	Pacific	SW1			9.1%	6.1%	4.5%
Australia/NZ		AU,NZ	PRC		CN		6.3%	6.0%	5.9%
Australia/NZ		AU,NZ	South Africa		ZA		6.3%	6.0%	5.5%
Australia/NZ		AU,NZ	South America	LA3,LA4			9.9%	7.2%	5.7%
Australia/NZ		AU,NZ	United States		US		5.6%	4.9%	4.4%
Australia/NZ		AU,NZ	Western Europe	EU1			3.0%	3.4%	3.1%
Canada		CA	Caribbean	LA1			7.6%	5.6%	4.1%
Canada		CA	Central America	LA2			12.9%	8.7%	6.2%
Canada		CA	Central Europe	EU2			6.8%	6.1%	4.5%
Canada		CA	CIS		AM,AZ,BY,KZ,GE,KG,MD,TJ,TM,UA,UZ		9.0%	6.0%	4.4%
Canada		CA	Indian Sub	AS1			13.7%	9.9%	6.3%
Canada		CA	Japan		JP		1.8%	5.4%	4.0%
Canada		CA	Middle East	ME1			11.5%	7.3%	5.2%
Canada		CA	North Africa	AF1			7.2%	5.3%	4.1%
Canada		CA	PRC		CN		8.3%	7.2%	6.5%
Canada		CA	Russia		RU		5.5%	4.4%	3.7%
Canada		CA	South America	LA3,LA4			13.7%	7.0%	4.3%
Canada		CA	United States		US		3.0%	3.6%	3.2%
Canada		CA	Western Europe	EU1			3.6%	4.6%	4.4%
Caribbean	LA1		Central America	LA2			6.5%	6.4%	5.5%
Caribbean	LA1		Russia		RU		6.9%	5.2%	4.3%
Caribbean	LA1		South America	LA3,LA4			2.9%	3.2%	3.2%
Caribbean	LA1		United States		US		3.1%	2.3%	2.3%
Caribbean	LA1		Western Europe	EU1			3.8%	3.4%	2.8%
Central America	LA2		Japan		JP		8.2%	4.4%	3.3%
Central America	LA2		PRC		CN		7.3%	7.1%	7.0%
Central America	LA2		Russia		RU		8.2%	6.2%	5.7%
Central America	LA2		South America	LA3,LA4			9.5%	7.4%	6.0%
Central America	LA2		United States		US		5.1%	4.9%	4.2%
Central America	LA2		Western Europe	EU1			4.5%	4.3%	3.3%
Central Europe	EU2		CIS		AM,AZ,BY,KZ,GE,KG,MD,TJ,TM,UA,UZ		10.9%	7.4%	4.9%
Central Europe	EU2		Middle East	ME1			6.5%	5.1%	4.3%
Central Europe	EU2		North Africa	AF1			7.6%	5.6%	4.0%
Central Europe	EU2		PRC		CN		5.4%	5.1%	4.0%
Central Europe	EU2		Russia		RU		9.1%	6.9%	5.0%
Central Europe	EU2		United States		US		4.5%	3.9%	3.6%
Central Europe	EU2		Western Europe	EU1			7.3%	6.2%	4.7%

Table 36: Average annual growth rates for passenger air traffic from [24], part 1

From Region	Region Codes	Country Codes	To Region	Region Codes	Country Codes	Dom / Int	Average Annual Growth Rate		
							2011-2015	2016-2020	2021-2030
CIS		AM,AZ,BY,KZ,GE,KG,MD,TJ,TM,UA,UZ	Indian Sub	AS1			4.7%	4.7%	4.0%
CIS		AM,AZ,BY,KZ,GE,KG,MD,TJ,TM,UA,UZ	Japan		JP		7.1%	5.4%	4.0%
CIS		AM,AZ,BY,KZ,GE,KG,MD,TJ,TM,UA,UZ	Middle East	ME1			8.8%	6.1%	4.5%
CIS		AM,AZ,BY,KZ,GE,KG,MD,TJ,TM,UA,UZ	North Africa	AF1			8.7%	5.7%	4.0%
CIS		AM,AZ,BY,KZ,GE,KG,MD,TJ,TM,UA,UZ	PRC		CN		11.1%	8.9%	6.8%
CIS		AM,AZ,BY,KZ,GE,KG,MD,TJ,TM,UA,UZ	Russia		RU		8.9%	6.5%	5.8%
CIS		AM,AZ,BY,KZ,GE,KG,MD,TJ,TM,UA,UZ	United States		US		8.7%	5.8%	4.4%
CIS		AM,AZ,BY,KZ,GE,KG,MD,TJ,TM,UA,UZ	Western Europe	EU1			5.6%	5.3%	4.5%
Africa Sub Sahara	AF2,AF3,AF4		Africa Sub Sahara	AF2,AF3,AF4		D	9.1%	6.9%	5.3%
Asia	AS2,AS3,AS4		Asia	AS2,AS3,AS4		D	7.6%	5.5%	4.7%
Australia/NZ		AU,NZ	Australia/NZ		AU,NZ	D	5.7%	4.1%	3.7%
Brazil		BR	Brazil		BR	D	8.1%	6.8%	5.8%
Canada		CA	Canada		CA	D	2.8%	2.7%	2.4%
Caribbean	LA1		Caribbean	LA1		D	1.6%	1.8%	1.9%
Central America	LA2		Central America	LA2		D	8.1%	7.5%	6.2%
Central Europe	EU2		Central Europe	EU2		D	4.6%	4.5%	3.7%
CIS		AM,AZ,BY,KZ,GE,KG,MD,TJ,TM,UA,UZ	CIS		AM,AZ,BY,KZ,GE,KG,MD,TJ,TM,UA,UZ	D	8.7%	5.6%	3.9%
India		IN	India		IN	D	13.9%	10.4%	7.5%
Indian Sub	AS1		Indian Sub	AS1		D	4.5%	4.5%	4.3%
Japan		JP	Japan		JP	D	2.5%	1.7%	1.1%
Mexico		MX	Mexico		MX	D	6.0%	5.7%	5.0%
Middle East	ME1		Middle East	ME1		D	4.4%	3.6%	3.5%
North Africa	AF1		North Africa	AF1		D	7.8%	5.7%	4.5%
Pacific	SW1		Pacific	SW1		D	7.6%	5.4%	3.9%
PRC		CN	PRC		CN	D	11.0%	7.5%	5.1%
Russia		RU	Russia		RU	D	5.1%	4.9%	4.6%
South Africa		ZA	South Africa		ZA	D	5.5%	5.9%	5.9%
South America	LA3,LA4		South America	LA3,LA4		D	3.8%	3.8%	3.7%
Turkey		TR	Turkey		TR	D	6.7%	6.1%	4.6%
United States		US	United States		US	D	3.0%	2.3%	2.2%
Western Europe	EU1		Western Europe	EU1		D	2.7%	2.9%	2.7%
Indian Sub	AS1		Japan		JP		7.4%	6.0%	4.8%
Indian Sub	AS1		Middle East	ME1			7.4%	5.9%	5.8%
Indian Sub	AS1		North Africa	AF1			7.9%	8.1%	6.3%
Indian Sub	AS1		PRC		CN		13.8%	10.0%	6.6%
Indian Sub	AS1		Russia		RU		4.9%	4.8%	4.1%
Indian Sub	AS1		South Africa		ZA		7.7%	7.9%	6.5%
Indian Sub	AS1		United States		US		10.5%	9.4%	6.4%
Indian Sub	AS1		Western Europe	EU1			7.9%	5.8%	5.7%
Africa Sub Sahara	AF2,AF3,AF4		Africa Sub Sahara	AF2,AF3,AF4		I	8.0%	6.3%	5.1%
Asia	AS2,AS3,AS4		Asia	AS2,AS3,AS4		I	9.7%	5.9%	5.1%
Australia/NZ		AU,NZ	Australia/NZ		AU,NZ	I	4.1%	3.4%	3.1%
Caribbean	LA1		Caribbean	LA1		I	2.3%	2.4%	2.5%
Central America	LA2		Central America	LA2		I	8.3%	7.0%	5.7%
Central Europe	EU2		Central Europe	EU2		I	8.5%	7.1%	4.8%
CIS		AM,AZ,BY,KZ,GE,KG,MD,TJ,TM,UA,UZ	CIS		AM,AZ,BY,KZ,GE,KG,MD,TJ,TM,UA,UZ	I	9.0%	5.9%	4.1%
Indian Sub	AS1		Indian Sub	AS1		I	7.5%	7.5%	5.6%
Middle East	ME1		Middle East	ME1		I	8.2%	6.3%	4.9%
North Africa	AF1		North Africa	AF1		I	7.6%	5.1%	4.1%
Pacific	SW1		Pacific	SW1		I	7.5%	5.1%	3.7%
South America	LA3,LA4		South America	LA3,LA4		I	7.9%	6.5%	5.5%
Western Europe	EU1		Western Europe	EU1		I	3.8%	3.4%	2.8%
Japan		JP	Middle East	ME1			12.8%	6.4%	4.4%
Japan		JP	North Africa	AF1			9.3%	5.3%	3.7%
Japan		JP	Pacific	SW1			5.8%	3.5%	2.4%
Japan		JP	PRC		CN		6.0%	5.9%	6.1%
Japan		JP	Russia		RU		5.5%	4.4%	3.4%
Japan		JP	South America	LA3,LA4			5.9%	4.3%	3.2%
Japan		JP	United States		US		1.8%	5.4%	4.0%
Japan		JP	Western Europe	EU1			2.0%	3.5%	2.8%
Mexico		MX	United States		US		5.5%	4.6%	4.2%
Middle East	ME1		North Africa	AF1			9.7%	6.6%	5.0%
Middle East	ME1		PRC		CN		9.9%	8.2%	6.4%
Middle East	ME1		Russia		RU		8.3%	6.0%	4.2%
Middle East	ME1		South Africa		ZA		11.7%	9.0%	7.1%
Middle East	ME1		South America	LA3,LA4			26.5%	12.7%	8.2%
Middle East	ME1		United States		US		10.3%	6.7%	5.8%
Middle East	ME1		Western Europe	EU1			7.9%	5.8%	4.6%

Table 37: Average annual growth rates for passenger air traffic from [24], part 2



From Region	Region Codes	Country Codes	To Region	Region Codes	Country Codes	Dom / Int	Average Annual Growth Rate		
							2011-2015	2016-2020	2021-2030
North Africa	AF1		PRC		CN		12.8%	9.7%	7.1%
North Africa	AF1		Russia		RU		9.3%	6.5%	5.0%
North Africa	AF1		South Africa		ZA		8.6%	7.4%	6.2%
North Africa	AF1		United States		US		8.7%	6.0%	4.6%
North Africa	AF1		Western Europe	EU1			6.1%	4.7%	3.9%
Pacific	SW1		PRC		CN		6.8%	6.3%	5.5%
Pacific	SW1		South America	LA3,LA4			5.9%	4.3%	3.2%
Pacific	SW1		United States		US		4.2%	3.3%	2.8%
Pacific	SW1		Western Europe	EU1			5.1%	4.0%	3.2%
PRC		CN	Russia		RU		10.4%	8.6%	6.7%
PRC		CN	South Africa		ZA		8.9%	8.3%	7.8%
PRC		CN	South America	LA3,LA4			7.3%	7.1%	7.0%
PRC		CN	United States		US		8.1%	6.9%	5.8%
PRC		CN	Western Europe	EU1			7.4%	6.5%	5.4%
Russia		RU	South America	LA3,LA4			8.2%	6.2%	5.7%
Russia		RU	United States		US		8.2%	6.2%	5.7%
Russia		RU	Western Europe	EU1			5.8%	5.0%	4.4%
South Africa		ZA	South America	LA3,LA4			6.9%	6.6%	6.1%
South Africa		ZA	United States		US		5.2%	4.1%	3.2%
South Africa		ZA	Western Europe	EU1			3.5%	4.6%	4.9%
South America	LA3,LA4		United States		US		5.9%	5.4%	4.9%
South America	LA3,LA4		Western Europe	EU1			5.8%	5.3%	4.6%
United States		US	Western Europe	EU1			4.5%	3.9%	3.6%
World	World		World	World			5.8%	5.0%	4.3%

Table 38: Average annual growth rates for passenger air traffic from [24], part 3

From Region	Region Codes	Country Codes	To Region	Region Codes	Country Codes	Dom / Int	AAGR
							2009-2029*
Africa	AF1,AF2,AF3,AF4		Africa	AF1,AF2,AF3,AF4			4.7%
Africa	AF1,AF2,AF3,AF4		Asia	AS2,AS3,AS4			4.7%
Africa	AF1,AF2,AF3,AF4		Central America	LA1,LA2			7.7%
Africa	AF1,AF2,AF3,AF4		CIS		AM,AZ,BY,KZ,GE,KG,MD,TJ,TM,UA,UZ,RU		4.5%
Africa	AF1,AF2,AF3,AF4		Europe	EU1,EU2			5.1%
Africa	AF1,AF2,AF3,AF4		Indian Subcontinent	AS1			5.1%
Africa	AF1,AF2,AF3,AF4		Japan		JP		1.9%
Africa	AF1,AF2,AF3,AF4		Middle East	ME1			5.4%
Africa	AF1,AF2,AF3,AF4		North America	NA1			4.9%
Africa	AF1,AF2,AF3,AF4		Pacific	SW1			3.8%
Africa	AF1,AF2,AF3,AF4		PRC		CN		6.3%
Africa	AF1,AF2,AF3,AF4		South America	LA3,LA4			5.3%
Asia	AS2,AS3,AS4		Africa	AF1,AF2,AF3,AF4			5.3%
Asia	AS2,AS3,AS4		Asia	AS2,AS3,AS4			5.7%
Asia	AS2,AS3,AS4		Central America	LA1,LA2			7.8%
Asia	AS2,AS3,AS4		CIS		AM,AZ,BY,KZ,GE,KG,MD,TJ,TM,UA,UZ,RU		6.3%
Asia	AS2,AS3,AS4		Europe	EU1,EU2			4.7%
Asia	AS2,AS3,AS4		Indian Subcontinent	AS1			6.8%
Asia	AS2,AS3,AS4		Japan		JP		4.8%
Asia	AS2,AS3,AS4		Middle East	ME1			4.6%
Asia	AS2,AS3,AS4		North America	NA1			5.4%
Asia	AS2,AS3,AS4		Pacific	SW1			5.4%
Asia	AS2,AS3,AS4		PRC		CN		8.6%
Asia	AS2,AS3,AS4		South America	LA3,LA4			6.1%
Central America	LA1,LA2		Africa	AF1,AF2,AF3,AF4			8.3%
Central America	LA1,LA2		Asia	AS2,AS3,AS4			4.1%
Central America	LA1,LA2		Central America	LA1,LA2			8.4%
Central America	LA1,LA2		CIS		AM,AZ,BY,KZ,GE,KG,MD,TJ,TM,UA,UZ,RU		7.8%
Central America	LA1,LA2		Europe	EU1,EU2			4.9%
Central America	LA1,LA2		Indian Subcontinent	AS1			8.5%
Central America	LA1,LA2		Japan		JP		6.3%
Central America	LA1,LA2		Middle East	ME1			7.1%
Central America	LA1,LA2		North America	NA1			4.7%
Central America	LA1,LA2		Pacific	SW1			8.1%
Central America	LA1,LA2		PRC		CN		6.0%
Central America	LA1,LA2		South America	LA3,LA4			7.6%

Table 39: Average annual growth rates for cargo air traffic from [3], part 1

From Region	Region Codes	Country Codes	To Region	Region Codes	Country Codes	Dom / Int	AAGR 2009-2029*
CIS		AM,AZ,BY,KZ,GE,KG, MD,TJ,TM,UA,UZ,RU	Africa	AF1,AF2,AF3,AF4			3.3%
CIS		AM,AZ,BY,KZ,GE,KG, MD,TJ,TM,UA,UZ,RU	Asia	AS2,AS3,AS4			4.7%
CIS		AM,AZ,BY,KZ,GE,KG, MD,TJ,TM,UA,UZ,RU	Central America	LA1,LA2			7.1%
CIS		AM,AZ,BY,KZ,GE,KG, MD,TJ,TM,UA,UZ,RU	Europe	EU1,EU2			3.6%
CIS		AM,AZ,BY,KZ,GE,KG, MD,TJ,TM,UA,UZ,RU	Indian Subcontinent	AS1			4.6%
CIS		AM,AZ,BY,KZ,GE,KG, MD,TJ,TM,UA,UZ,RU	Japan		JP		4.0%
CIS		AM,AZ,BY,KZ,GE,KG, MD,TJ,TM,UA,UZ,RU	Middle East	ME1			4.4%
CIS		AM,AZ,BY,KZ,GE,KG, MD,TJ,TM,UA,UZ,RU	North America	NA1			3.8%
CIS		AM,AZ,BY,KZ,GE,KG, MD,TJ,TM,UA,UZ,RU	Pacific	SW1			4.2%
CIS		AM,AZ,BY,KZ,GE,KG, MD,TJ,TM,UA,UZ,RU	PRC		CN		5.4%
CIS		AM,AZ,BY,KZ,GE,KG, MD,TJ,TM,UA,UZ,RU	South America	LA3,LA4			4.2%
India		IN	India		IN	D	11.3%
PRC		CN	PRC		CN	D	9.4%
US		US	US		US	D	2.9%
Europe	EU1,EU2		Africa	AF1,AF2,AF3,AF4			4.6%
Europe	EU1,EU2		Asia	AS2,AS3,AS4			5.1%
Europe	EU1,EU2		Central America	LA1,LA2			6.2%
Europe	EU1,EU2		CIS		AM,AZ,BY,KZ,GE,KG, MD,TJ,TM,UA,UZ,RU		5.3%
Europe	EU1,EU2		Europe	EU1,EU2			4.5%
Europe	EU1,EU2		Indian Subcontinent	AS1			8.2%
Europe	EU1,EU2		Japan		JP		3.0%
Europe	EU1,EU2		Middle East	ME1			4.7%
Europe	EU1,EU2		North America	NA1			4.2%
Europe	EU1,EU2		Pacific	SW1			4.3%
Europe	EU1,EU2		PRC		CN		7.7%
Europe	EU1,EU2		South America	LA3,LA4			4.2%
Indian Subcontinent	AS1		Africa	AF1,AF2,AF3,AF4			6.7%
Indian Subcontinent	AS1		Asia	AS2,AS3,AS4			5.8%
Indian Subcontinent	AS1		Central America	LA1,LA2			9.6%
Indian Subcontinent	AS1		CIS		AM,AZ,BY,KZ,GE,KG, MD,TJ,TM,UA,UZ,RU		4.5%
Indian Subcontinent	AS1		Europe	EU1,EU2			6.3%
Indian Subcontinent	AS1		Indian Subcontinent	AS1			6.2%
Indian Subcontinent	AS1		Japan		JP		5.4%
Indian Subcontinent	AS1		Middle East	ME1			6.3%
Indian Subcontinent	AS1		North America	NA1			5.2%
Indian Subcontinent	AS1		Pacific	SW1			4.9%
Indian Subcontinent	AS1		PRC		CN		6.6%
Indian Subcontinent	AS1		South America	LA3,LA4			7.1%
Japan		JP	Africa	AF1,AF2,AF3,AF4			5.3%
Japan		JP	Asia	AS2,AS3,AS4			5.1%
Japan		JP	Central America	LA1,LA2			6.5%
Japan		JP	CIS		AM,AZ,BY,KZ,GE,KG, MD,TJ,TM,UA,UZ,RU		5.7%
Japan		JP	Europe	EU1,EU2			4.8%
Japan		JP	Indian Subcontinent	AS1			5.5%
Japan		JP	Middle East	ME1			5.2%
Japan		JP	North America	NA1			4.2%
Japan		JP	Pacific	SW1			5.2%
Japan		JP	PRC		CN		8.1%
Japan		JP	South America	LA3,LA4			3.4%
Middle East	ME1		Africa	AF1,AF2,AF3,AF4			5.1%
Middle East	ME1		Asia	AS2,AS3,AS4			4.7%
Middle East	ME1		Central America	LA1,LA2			9.4%
Middle East	ME1		CIS		AM,AZ,BY,KZ,GE,KG, MD,TJ,TM,UA,UZ,RU		4.9%
Middle East	ME1		Europe	EU1,EU2			3.6%
Middle East	ME1		Indian Subcontinent	AS1			6.1%
Middle East	ME1		Japan		JP		3.1%
Middle East	ME1		Middle East	ME1			4.4%
Middle East	ME1		North America	NA1			4.3%
Middle East	ME1		Pacific	SW1			4.1%
Middle East	ME1		PRC		CN		6.4%
Middle East	ME1		South America	LA3,LA4			4.2%
North America	NA1		Africa	AF1,AF2,AF3,AF4			6.0%
North America	NA1		Asia	AS2,AS3,AS4			5.1%

Table 40: Average annual growth rates for cargo air traffic from [3], part 2

From Region	Region Codes	Country Codes	To Region	Region Codes	Country Codes	Dom / Int	AAGR 2009-2029*
North America	NA1		Central America	LA1,LA2			4.8%
North America	NA1		CIS		AM,AZ,BY,KZ,GE,KG, MD,TJ,TM,UA,UZ,RU		6.0%
North America	NA1		Europe	EU1,EU2			4.7%
North America	NA1		Indian Subcontinent	AS1			8.9%
North America	NA1		Japan		JP		4.1%
North America	NA1		Middle East	ME1			5.0%
North America	NA1		North America	NA1			3.2%
North America	NA1		Pacific	SW1			3.8%
North America	NA1		PRC		CN		8.0%
North America	NA1		South America	LA3,LA4			5.6%
Pacific	SW1		Africa	AF1,AF2,AF3,AF4			4.2%
Pacific	SW1		Asia	AS2,AS3,AS4			4.2%
Pacific	SW1		Central America	LA1,LA2			8.4%
Pacific	SW1		CIS		AM,AZ,BY,KZ,GE,KG, MD,TJ,TM,UA,UZ,RU		5.2%
Pacific	SW1		Europe	EU1,EU2			4.0%
Pacific	SW1		Indian Subcontinent	AS1			4.8%
Pacific	SW1		Japan		JP		4.3%
Pacific	SW1		Middle East	ME1			5.3%
Pacific	SW1		North America	NA1			2.5%
Pacific	SW1		Pacific	SW1			2.3%
Pacific	SW1		PRC		CN		3.4%
Pacific	SW1		South America	LA3,LA4			7.4%
PRC		CN	Africa	AF1,AF2,AF3,AF4			7.0%
PRC		CN	Asia	AS2,AS3,AS4			8.2%
PRC		CN	Central America	LA1,LA2			7.4%
PRC		CN	CIS		AM,AZ,BY,KZ,GE,KG, MD,TJ,TM,UA,UZ,RU		6.6%
PRC		CN	Europe	EU1,EU2			8.4%
PRC		CN	Indian Subcontinent	AS1			7.3%
PRC		CN	Japan		JP		2.8%
PRC		CN	Middle East	ME1			7.0%
PRC		CN	North America	NA1			8.7%
PRC		CN	Pacific	SW1			6.8%
PRC		CN	South America	LA3,LA4			7.5%
South America	LA3,LA4		Africa	AF1,AF2,AF3,AF4			5.8%
South America	LA3,LA4		Asia	AS2,AS3,AS4			5.8%
South America	LA3,LA4		Central America	LA1,LA2			8.6%
South America	LA3,LA4		CIS		AM,AZ,BY,KZ,GE,KG, MD,TJ,TM,UA,UZ,RU		5.8%
South America	LA3,LA4		Europe	EU1,EU2			6.0%
South America	LA3,LA4		Indian Subcontinent	AS1			7.6%
South America	LA3,LA4		Japan		JP		5.1%
South America	LA3,LA4		Middle East	ME1			3.5%
South America	LA3,LA4		North America	NA1			3.8%
South America	LA3,LA4		Pacific	SW1			4.9%
South America	LA3,LA4		PRC		CN		7.4%
South America	LA3,LA4		South America	LA3,LA4			6.0%
World	World		World	World			5.9%

\* Average annual growth rates (AAGR) for 2009-2029 are equally assumed until 2030.

Table 41: Average annual growth rates for cargo air traffic from [3], part 3

---

## Appendix K STANDARDIZATION OF AIRCRAFT CAPACITIES

In the original flight schedules compiled by OAG, each flight has given seat- and freight capacities. Depending on airline policy, these capacities may vary considerably even for a single aircraft type. Comfortable seating configurations are often used on longer flights while higher seat densities are typically found on short-haul flights. Furthermore, the most modern aircraft types are often used in more comfortable seating configurations than older aircraft of the same size and range category.

In order to reduce the complexity of the model, a simplified approach was chosen for modelling seat and freight capacities in the Air Traffic Forecast module: in this module, seat capacities depend on the aircraft type and the great-circle distance between origin and destination airports only. Baseline seat capacities have been obtained for each passenger aircraft type based on standardized seating configurations. The baseline seat capacities are corrected as function of aircraft category and great-circle distance using results from an evaluation of actual seat capacities from the OAG flight schedules. Given the seat capacity of a flight, the corresponding freight capacity can be calculated considering aircraft-specific limits with respect to cargo volume and maximum structural payload. For all-cargo aircraft, baseline freight capacities per aircraft type have been calculated that are applied to all flights of such aircraft (i.e. independently from the flight distance). To determine the baseline seat capacities and to calculate freight capacities, the following approach is used:

- Three-class seating configurations described as “typical” by aircraft manufacturers are assumed as baseline configurations for widebody aircraft types, whereas all-economy configurations are assumed for most narrowbody aircraft. Exceptions are older long-range aircraft like the Boeing 707 and Douglas DC-8 and the medium-range Boeing 757 and TU-204. For these aircraft types, two-class configurations are assumed as a baseline. Typical seat capacities for such configurations have been obtained from websites of the aircraft manufacturers, from aircraft airport planning manuals [2], [17], [37] or reference look-up sources like Jane’s All The World Aircraft [85].
- Limits for each aircraft type’s cargo volume and payload capacity were obtained from manufacturers’ documents [2], [17], [37] and sources like OAG [100] or BADA [46]. As cargo volumes quoted in literature vary considerably for some aircraft types, both type and number of loadable unit load devices (ULD) have been determined for large commercial aircraft types in order to calculate the aircrafts’ cargo volumes in a standardized way. Table 42 shows the data assumed for different types of ULDs.
- As will be described later, freight capacities can be calculated based on seat capacities, cargo volumes and structural payload limits. A passenger mass of 90 kg (including 14kg of checked-in baggage), an average cargo density of 161 kg/m<sup>3</sup> and a loadability of

baggage and cargo of 85% are assumed for this purpose. The average passenger mass and the cargo density values are suggested by ICAO and IATA documents [77], [80].

ULD Type	Assumed cargo volume	Suitable for aircraft types
LD1 container	4.9 m <sup>3</sup>	Boeing 747
LD2 container	3.4 m <sup>3</sup>	Boeing 767
LD3 container	4.3 m <sup>3</sup>	Most widebody aircraft
LD7 pallet, 96x125in	11.8 m <sup>3</sup>	
LD7 pallet, 88x125in	10.8 m <sup>3</sup>	

Table 42: Cargo volumes of different unit load devices

A full list of the baseline capacities determined for this study is found in Appendix N. While the baseline capacities reflect the aircrafts' capabilities and should be comparable between aircraft types of the same category, the actual number of seats used by different airlines and on different routes may vary. In a comparison of actual seat capacities from the OAG flight schedules of September 2009 with the baseline seat capacities described above, the flight distance was identified as one of the most influential factors. Figure 112 shows the average deviation of OAG seat capacities from the baseline capacities as function of flight distance.

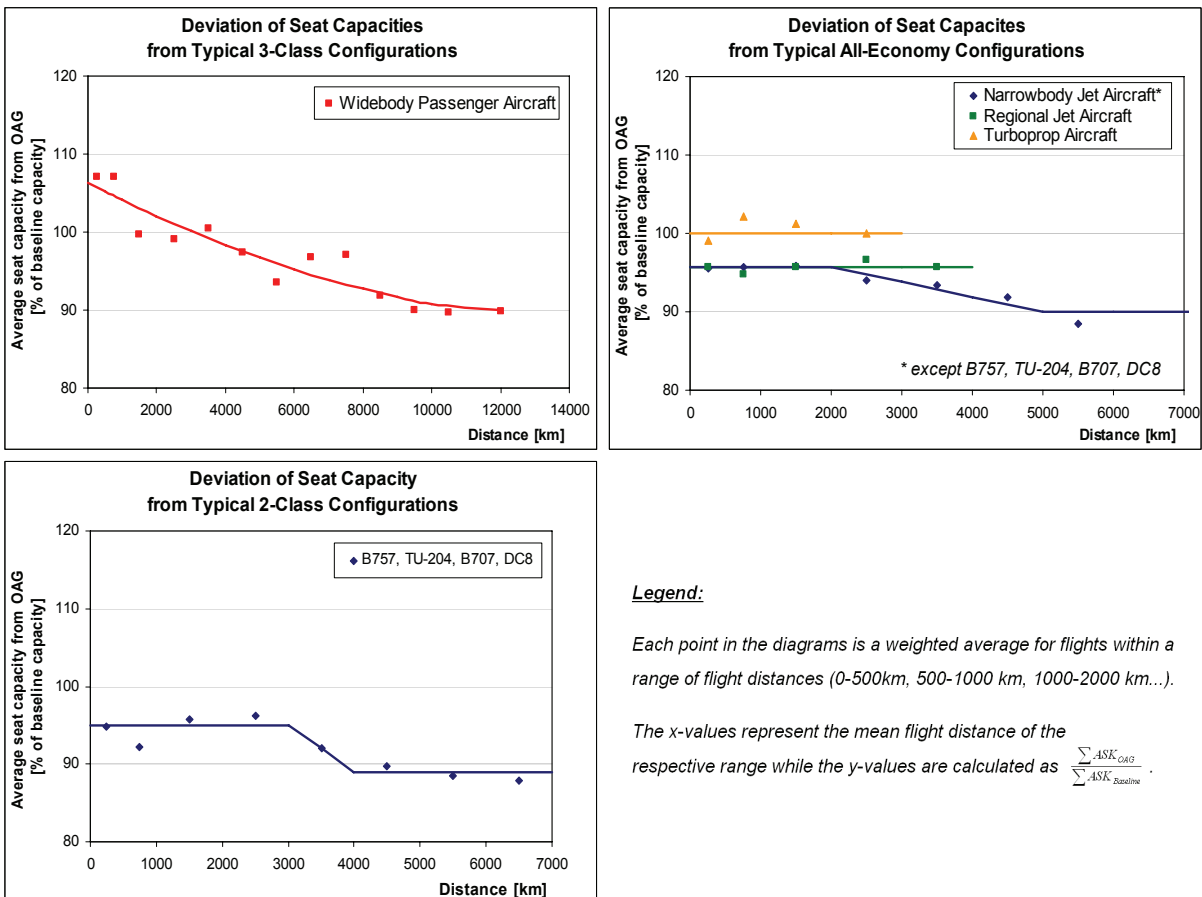


Figure 112: Deviation of OAG seat capacities from baseline seating configurations

In order to consider the influence of flight distance on seat capacity in the forecast model and in order to keep transport performance values on regional or global levels (measured e.g. in available seat kilometres, ASK) comparable between the forecast model and historical OAG data, the following correction is applied to the baseline seat capacities:

$$(1) \quad n_{\text{Seats}} = k_{\text{correction}} \cdot n_{\text{seats, baseline}}$$

$$\text{with } k_{\text{correction}} = f(\text{aircraft category, flight distance})$$

$k_{\text{correction}}$  corresponds to the functions shown in Figure 112 for five different aircraft categories. The formulae which deliver the correction factor as function of the great-circle distance GCD (in km) between origin and destination airports are approximated as follows:

(2a) *For widebody aircraft:*

$$k_{\text{correction}} = \frac{7.44 \cdot 10^{-8} \cdot \text{GCD}^2 - 0.0023 \cdot \text{GCD} + 106.37}{100} \quad \text{for } \text{GCD} < 11,000 \text{ (km)}$$

$$k_{\text{correction}} = 0.9 \quad \text{for } \text{GCD} \geq 11,000 \text{ (km)}$$

(2b) *For narrowbody jet aircraft (except B757, TU204, B707, DC8 and regional jets):*

$$k_{\text{correction}} = 0.957 \quad \text{for } \text{GCD} < 2000 \text{ (km)}$$

$$k_{\text{correction}} = \frac{-0.0019 \cdot \text{GCD} + 99.5}{100} \quad \text{for } 2000 \leq \text{GCD} < 5000$$

$$k_{\text{correction}} = 0.9 \quad \text{for } \text{GCD} \geq 5000 \text{ (km)}$$

(2c) *For aircraft with two-class configurations as baseline configurations (i.e. B757, TU204 and old long-range aircraft B707 and DC8):*

$$k_{\text{correction}} = 0.95 \quad \text{for } \text{GCD} < 3000 \text{ (km)}$$

$$k_{\text{correction}} = \frac{-0.006 \cdot \text{GCD} + 113}{100} \quad \text{for } 3000 \leq \text{GCD} < 4000$$

$$k_{\text{correction}} = 0.89 \quad \text{for } \text{GCD} \geq 4000 \text{ (km)}$$

(2d) *For regional jet aircraft with less than 110 seats:*  $k_{\text{correction}} = 0.957 = \text{const.}$

(2e) *For turboprop and piston-powered aircraft:*  $k_{\text{correction}} = 1 = \text{const.}$

By using the above correction, the total transport performance in ASK covered by each of the five aircraft categories deviates by less than 0.4% from OAG reference values in a flight schedule sample for September 2009. The total ASKs for all flights in this sample are underestimated by just 0.04%. These figures confirm that the corrected seat capacities used by the model reflect average seat capacities from the OAG schedules at sufficient accuracy.

Given an aircraft type with a number of seat  $n_{Seats}$ , a total cargo volume  $V_{Cargo}$  and the maximum structural payload  $PL_{max}$ , the freight that can be transported additionally to passenger baggage is calculated as follows:

$$(3) \quad m_{Freight,VolumeLimited} = V_{Cargo} \cdot CargoDensity \cdot Loadability - n_{Seats} \cdot m_{Baggage}$$

$$(4) \quad m_{Freight,MassLimited} = PL_{max} - n_{Seats} \cdot m_{Passenger+Baggage}$$

$$(5) \quad FreightCapacity = Minimum(m_{Freight,VolumeLimited}, m_{Freight,MassLimited})$$

While for passenger aircraft,  $n_{Seats}$  varies with flight distance,  $n_{Seats}$  equals to zero for all-cargo aircraft. Given the freight capacity from formula (5), the aircraft's typical payload capacity is calculated by the following formula:

$$(6) \quad PayloadCapacity = n_{Seats} \cdot m_{Passenger+Baggage} + FreightCapacity$$

As mentioned before, a passenger mass of 90 kg (including 14kg of checked-in baggage), an average cargo density of 161 kg/m<sup>3</sup> and a loadability of baggage and cargo of 85% are assumed in this study (see [77] and [80]).

Freight capacities are also given in the OAG flight schedules, although the quality and calculation methodology of this data are unknown. Freight capacities in OAG may vary with airline, aircraft type and city pair. In the September 2009 flight schedule, the total transport performance with respect to freight (measured in tonne-kilometres offered, TKO) that is calculated by the above model is 3.6% lower than the respective OAG figure. The transport performance on all-cargo flights is underestimated by 4.3% while on passenger flights the transport performance with respect to freight transport is underestimated by 2.8%. For reasons of simplicity, a calibration of aircraft freight capacities is omitted in this study. When considering the total transport performance for both passenger and freight transport, the Air Traffic Forecast Model underestimates the TKOs from OAG by 1.35%. This deviation of the total transport performance seems acceptable considering the focus of this study on aircraft emissions.



## Appendix L DEVELOPMENT OF RETIREMENT CURVES

Aircraft lifetimes assumed by the Air Traffic Emissions Forecast Module have been derived from an analysis of fleet statistics for jet and turboprop aircraft. These analyses have been performed as part of this study based on the ASCEND Fleets Database [11]. Using the online version of the database, which is limited to pre-defined queries via an online interface, the required data was gained from a number of different queries. These queries include:

- Aircraft deliveries by individual aircraft for 1950-2010.
- Aircraft retirements by individual aircraft for 1950-2010.
- Freighter conversions by individual aircraft for 1950-2010.
- Storage events by individual aircraft for 1950-2010.
- Historical fleets by individual aircraft for 1950-2010.

All data from the aforementioned queries were imported into a Microsoft Access database. In the data tables, each individual aircraft can be identified by a combination of information from the “aircraft type”, “aircraft series” and “serial number” data fields. The data required for retirement analyses were transferred into a unified data table using database scripts written in Visual Basic for Applications (VBA). The unified table contains – amongst other information – an aircraft’s unique ID as well as its order date, build year, delivery date, conversion date to freighter (if applicable), retirement date (if applicable) and storage dates (begin and end of each storage period, as far as available). From this information, the age at retirement, conversion or storage can be calculated for each aircraft. For this purpose, an aircraft’s delivery date is used as the reference for all age calculations<sup>49</sup>.

Given this information, a VBA script was used to calculate the fraction of all aircraft that were retained in the fleet (“survival percentage”) as function of aircraft age. This function is often referred to as “retirement curve” and was evaluated in age steps of 1 year for three groups of aircraft, namely widebody aircraft, narrowbody aircraft and turboprop aircraft. In principle, the survival percentage is calculated as follows:

$$(4) \quad \text{SurvivalPercentage}(\text{age}) = \frac{\text{NumberSurvived}(\text{age})}{\text{TotalNumber}(\text{age})}$$

with:  $\text{NumberSurvived}(\text{age}) = \text{aircraft retained in fleet at a given age (or older)}$

$\text{TotalNumber}(\text{age}) = \text{all aircraft in database at a given age (or older)}$

---

<sup>49</sup> The build year is used for a small number of aircraft without available delivery date.

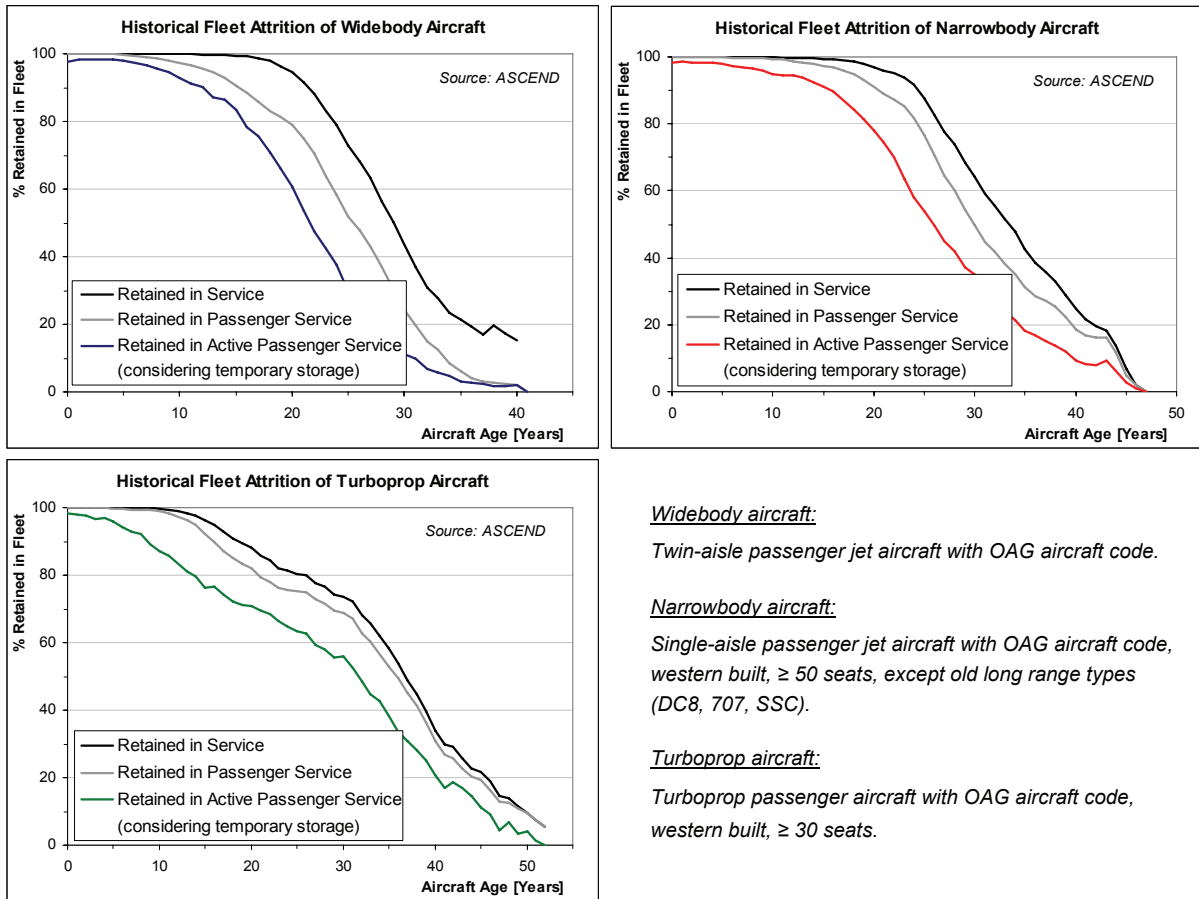


Figure 113: Analysis of typical aircraft lifetimes by aircraft category

Figure 113 shows the resulting graphs that were obtained for widebody aircraft, narrowbody aircraft and turboprops. These curves depend largely on:

- a) The exact definition of the group of aircraft examined;
- b) The meaning of “retained in fleet” (i.e. the definition of aircraft “survival”).

The groups of aircraft used for this evaluation are described on the right hand side of the figure. Passenger aircraft that can be attributed to an aircraft code from the OAG flight schedules [100] were considered for this evaluation (i.e. ignoring military, research, VIP and other “exotic” aircraft types that are not primarily used by commercial airlines). Besides, only western built aircraft have been considered in the narrowbody and turboprop segments<sup>50</sup>.

Each diagram in Figure 113 contains three graphs which differ by the definition of aircraft “survival”. The retirement curves required by the Air Traffic Emissions Forecast Module are those which consider both conversions to freighters and storage events. These curves can

<sup>50</sup> Due to better data availability and -quality for western built aircraft plus the dominance of western aircraft manufacturers in the near future.

be approximated by polynomial functions as shown in Figure 114. The retirement curves are used by the fleet rollover model to predict the number of aircraft of an existing fleet that will be kept in active passenger service in the future. More details regarding the fleet rollover model and the way the retirement curves are applied are found in chapter 3.4.4.2.

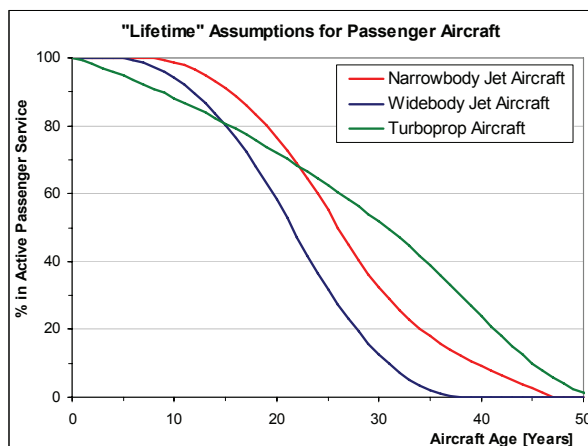


Figure 114: Reference retirement curves for different groups of aircraft

Similar analyses as described above for passenger aircraft were performed for all-cargo aircraft. Reliable trends, however, are much more difficult to identify in this segment given the small number of aircraft, the high share of converted passenger aircraft and rather heterogeneous lifetimes in general. As a consequence, retirement curves for cargo aircraft were not implemented into the fleet rollover model. Instead, an average lifetime of 30 years is assumed for widebody cargo aircraft types while 25 years are assumed for narrowbody freighters<sup>51</sup>.

<sup>51</sup> A small number of (comparably old) cargo aircraft were assigned to retirement curves for passenger aircraft, if in-service numbers and recent retirements seemed to indicate respective trends (see Appendix N).

## Appendix M FLEET FORECAST DETAILS

This appendix provides additional information on specific aspects of the fleet rollover model described in chapter 3.4.4.

### Estimating transport performance per aircraft for newly introduced aircraft types

In order to provide a link between aircraft in-service numbers and transport performance in terms of available tonne-kilometres (TKO), fleet statistics from the ASCEND Online Fleets Database [11] have been combined with TKO obtained from OAG flight schedules [100]. This way, the average transport performance per individual aircraft is estimated for each aircraft type that is listed in the base year flight schedules. For newly introduced aircraft types, however, this value needs to be estimated (see chapter 3.4.4.1). Reference data for older aircraft types with similar size, range and operating patterns are used for this purpose. The following paragraphs describe the procedure for estimating the average tonne-kilometres per individual aircraft for newly introduced aircraft types.

Each new aircraft type is assigned to one or more comparable reference aircraft types of the previous generation. Formula (1) sums up the TKO of these reference aircraft in the baseyear flight movements from OAG:

$$(1) \quad TKO_{Sum,ref} = \sum_i (TKO_{ref,i} \cdot k_{Frequency,i})$$

$$\text{with} \quad k_{Frequency,i} = \frac{PayloadCapacity_{ref,i}}{PayloadCapacity_{new\ aircraft}}$$

The correction factor  $k_{Frequency,i}$  accounts for different payload capacities of the new aircraft type and the comparable aircraft types assigned to it. Similarly, the total number of reference aircraft that are in-service in the base year of the forecast are determined as follows:

$$(2) \quad n_{Sum,ref} = \sum_i n_{ref,i}$$

Combining equations (1) and (2) leads to:

$$(3) \quad TKOperAircraft_{new} = \frac{TKO_{Sum,ref}}{n_{Sum,ref}} \cdot (1 + k_{Efficiency})$$

$k_{Efficiency}$  is an optional parameter which provides the possibility to specify an improvement of the  $TKOperAircraft$  from one aircraft generation to another (e.g. by improved utilization). In this study,  $k_{Efficiency}$  is not used and set to zero. This way,  $TKOperAircraft_{new}$  assumed for the new aircraft type corresponds to the average of this value for the reference aircraft.

### Retirement modelling when fleet statistics are missing

The retirement model described in chapter 3.4.4.2 is based on aircraft lifetime assumptions (retirement curves) in combination with historical fleet statistics. Delivery numbers per aircraft type and year are required as input data. For some aircraft types, statistics on delivery numbers and/or in-service numbers are not available from the ASCEND Fleets Database [11]. This applies mostly to small turboprop-powered aircraft with less than 30 seats and some old aircraft types with piston engines.

If in-service numbers are available for an aircraft type while delivery numbers are missing, delivery numbers have to be estimated from in-service numbers. An automated function performing this task has been developed and is part of the fleet rollover model. Potential retirements during the production period of the aircraft type need to be considered, as many aircraft types are produced for several decades. As a consequence, a retirement curve needs to be assumed for the aircraft type in order to perform this task.

Another approach is followed for aircraft with no historical in-service numbers available from the fleets database. For these aircraft types, the production periods as well as the total number of produced aircraft were obtained from Jane's All The World's Aircraft [85]. Based on this information, a generic distribution of delivery numbers per year is assumed and modelled by linear and parabolic functions as shown on the left hand side of Figure 115. Given the assumed delivery numbers per year and a retirement curve, in-service numbers can be calculated. Although the uncertainty of this approach must be regarded as high, the method should be sufficient for the purpose of this study considering that the aircraft types affected by the simplification account for less than 1% of the base year transport performance. In-production aircraft types and new types not yet in production in the base year of the forecast are not affected, as their delivery numbers will be calculated on a yearly basis depending on the forecasted traffic demand.

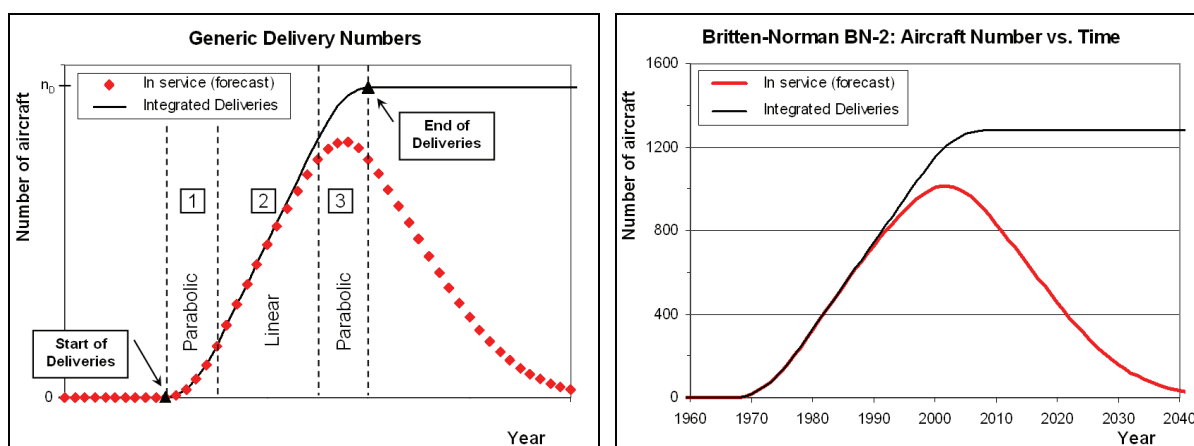


Figure 115: Estimated aircraft numbers vs. time (without detailed fleet statistics)

## Appendix N AIRCRAFT DELIVERY PERIODS, CAPACITIES AND LIFETIME ASSUMPTIONS

Table 44 to Table 52 list the aircraft types used in this study and present the assumptions about:

- a) the delivery periods for each aircraft type in the baseline scenario of the forecast,
- b) the standardized (baseline) capacities for each aircraft type and underlying assumptions,
- c) the identifier of the assumed retirement curves as explained in Table 43<sup>52</sup>.

Retirement curve ID	Description of retirement curve / retirement assumptions
103	Average retirement curve derived from ASCEND fleet statistics [1] for widebody aircraft types
113 / 114 / 115 / 116 / 117 / 118	Variations of baseline curve for widebody aircraft types with much lower / lower / slightly lower / slightly higher / higher / much higher aircraft lifetime
203	Average retirement curve derived from ASCEND fleet statistics [1] for narrowbody aircraft types
213 / 214 / 215 / 216 / 217 / 218	Variations of baseline curve for narrowbody aircraft types with much lower / lower / slightly lower / slightly higher / higher / much higher aircraft lifetime
303	Average retirement curve derived from ASCEND fleet statistics [1] for turboprop aircraft types
313 / 314 / 315 / 316 / 317 / 318	Variations of baseline curve for turboprop aircraft types with much lower / lower / slightly lower / slightly higher / higher / much higher aircraft lifetime
Other number x < 100	Constant aircraft lifetime of x years until retirement (assumed for freight aircraft)
OS = "Out of Service" / PO = "Phase Out" / PO2 = "Phase Out 2"	The number of active aircraft is assumed to decrease linearly until all aircraft are retired in the years 2015 / 2018 / 2021 (assumed for some old aircraft types near the end of their operational lifes)

Table 43: Description of identifier for aircraft retirement curves

<sup>52</sup> The maximum payload shown in Table 44 to Table 52 is valid for a specific (exemplary) aircraft configuration. For aircraft types with an entry into service before 2010, the year of first deliveries shown in the tables was estimated as the year after the aircraft type's first appearance according to ASCEND fleet statistics [11].

Specific Aircraft	Specific Aircraft Name	First Deliveries	Last Deliveries	Retirement Curve	Baseline		Cargo Volume [m <sup>3</sup> ]	Maximum Payload [t]	Assumptions for Passenger and Freight Capacities
					Seats	Baseline Freight Cap. [t]			
389	Airbus A380-900	2019	2050	103	650	18,0	198	100,0	three-class seating, 42 LD3 container + bulk, maximum payload estimated
388	Airbus A380-800	2005	2050	103	525	17,4	181	90,6	three-class seating, 38 LD3 container + bulk, max. payload from Airbus Airport Planning Manual
748	Boeing 747-8I	2012	2030	103	467	18,0	179	76,7	three-class seating, 16 LD1 container + 7 pallets + bulk, maximum payload estimated
744	Boeing 747-400	1989	2005	103	416	18,8	180	67,3	three-class seating, 32 LD1 container + bulk, max. payload from Boeing Airport Planning Manual
743	Boeing 747-300	1983	1990	117	412	18,2	175	67,8	three-class seating, 30 LD1 container + bulk, max. payload from Boeing Airport Planning Manual
346	Airbus A340-600	2001	2010	103	380	22,1	200	65,6	three-class seating, 42 LD3 container + bulk, max. payload from Airbus Airport Planning Manual
73N	Boeing 777-300/-300ER Successor	2020	2050	103	368	23,1	206	69,9	three-class seating, capacity equal to 777-300ER
77W	Boeing 777-300ER	2003	2021	103	368	23,1	206	69,9	three-class seating, 44 LD3 container + bulk, max. payload from Boeing Airport Planning Manual
773	Boeing 777-300	1998	2006	118	368	23,1	206	65,0	three-class seating, 44 LD3 container + bulk, max. payload from Boeing Airport Planning Manual
742	Boeing 747-200	1971	1988	PO	366	18,8	175	68,2	three-class seating, 30 LD1 container + bulk, max. payload from Boeing Airport Planning Manual
741	Boeing 747-100	1969	1973	OS	366	18,8	175	76,3	three-class seating, 30 LD1 container + bulk, max. payload from Boeing Airport Planning Manual
35X	Airbus A350-1000 XWB	2018	2050	103	350	22,5	201	70,0	three-class seating, 44 LD3 container + bulk, maximum payload estimated

Table 44: Aircraft production periods and capacities, seat categories 6-7



Specific Aircraft	Specific Aircraft Name	First Deliveries	Last Deliveries	Retirement Curve	Baseline Seats	Baseline Freight Cap. [t]	Baseline Capacity [t]	Cargo Volume [m <sup>3</sup> ]	Maximum Payload [t]	Assumptions for Passenger and Freight Capacities
74L	Boeing 747SP	1976	1989	117	316	9.8	36.3	109	38.3	three-class seating, 20 LD1 container + bulk, max. payload from Boeing Airport Planning Manual
359	Airbus A350-900 XWB	2014	2050	103	314	18.3	46.6	166	60.0	three-class seating, 36 LD3 container + bulk, maximum payload estimated
345	Airbus A340-500	2002	2011	103	313	16.0	44.1	149	59.6	three-class seating, 30 LD3 container + bulk, max. payload from Airbus Airport Planning Manual
72N	Boeing 777-200/200LR Successor	2019	2050	103	305	16.9	44.3	155	56.9	three-class seating, capacity equal to 777-200
772	Boeing 777-200	1994	2016	103	305	16.9	44.3	155	56.9	three-class seating, 32 LD3 container + bulk, max. payload from Boeing Airport Planning Manual
77L	Boeing 777-200LR	2005	2016	103	305	16.9	44.3	155	64.0	three-class seating, 32 LD3 container + bulk, max. payload from Boeing Airport Planning Manual
333	Airbus A330-300	1992	2016	103	295	17.4	43.9	157	49.1	three-class seating, 32 LD3 container + bulk, max. payload from Airbus Airport Planning Manual
343	Airbus A340-300	1991	2009	116	295	17.4	43.9	157	52.8	three-class seating, 32 LD3 container + bulk, max. payload from Airbus Airport Planning Manual
M11	Boeing (Douglas) MD-11	1990	1997	PO	293	16.7	43.1	152	49.4	three-class seating, 32 LD3 container + bulk, max. payload from MDD Airport Planning Manual
789	Boeing 787-9	2014	2050	103	280	18.8	44.0	166	50.0	three-class seating, 36 LD3 container + bulk, maximum payload estimated
358	Airbus A350-800 XWB	2017	2050	103	270	14.2	36.5	132	50.0	three-class seating, 28 LD3 container + bulk, maximum payload estimated
D11	Boeing (Douglas) DC10-10/15	1971	1983	OS	255	13.7	36.7	126	43.0	three-class seating, 24 LD3 container + bulk, max. payload from MDD Airport Planning Manual
D1C	Boeing (Douglas) DC10-30/40	1972	1984	OS	255	13.7	36.7	126	46.2	three-class seating, 24 LD3 container + bulk, max. payload from MDD Airport Planning Manual
AB6	Airbus A300-600	1983	2000	115	255	10.9	33.9	106	43.8	three-class seating, 22 LD3 container + bulk, max. payload from Airbus Airport Planning Manual
332	Airbus A330-200	1997	2019	103	253	14.5	37.2	132	51.2	three-class seating, 26 LD3 container + bulk, max. payload from Airbus Airport Planning Manual
AB4	Airbus A300B2/B4	1972	1987	OS	250	10.5	33.0	102	35.5	three-class seating, 20 LD3 container + bulk, max. payload from Airbus Airport Planning Manual
L11	Lockheed L1011 TriStar	1970	1983	OS	248	8.4	30.8	87	n/a	three-class seating, 16 LD3 container + bulk, data estimated
764	Boeing 767-400	2000	2008	102	243	15.6	37.5	139	46.5	three-class seating, 38 LD2 container + bulk, max. payload from Boeing Airport Planning Manual
753	Boeing 757-300	1999	2004	203	243	5.8	27.7	68	30.7	two-class seating, max. payload and cargo volume from Boeing Airport Planning Manual
342	Airbus A340-200	1992	1998	117	239	14.6	36.2	132	43.8	three-class seating, 26 LD3 container + bulk, max. payload from Airbus Airport Planning Manual
788	Boeing 787-8	2012	2050	103	237	14.7	36.0	132	45.4	three-class seating, 28 LD3 container + bulk, maximum payload estimated
IL9	Ilyushin Il-96	1988	2011	103	237	10.4	31.7	100	40.0	three-class seating, 16 LD3 container + bulk, data estimated
ILW	Ilyushin Il-86	1976	1994	OS	234	10.4	31.5	100	42.0	three-class seating, 16 LD3 container + bulk, data estimated
L15	Lockheed L1011 TriStar 500	1979	1984	PO	234	10.4	31.5	100	n/a	three-class seating, 19 LD3 container + bulk, data estimated
763	Boeing 767-300	1986	2014	103	218	12.6	32.2	114	42.2	three-class seating, 30 LD2 container + bulk, max. payload from Boeing Airport Planning Manual
312	Airbus A310-200	1982	1989	OS	212	7.6	26.7	78	31.9	three-class seating, 14 LD3 container + bulk, max. payload from Airbus Airport Planning Manual
313	Airbus A310-300	1985	1997	103	212	7.6	26.7	78	31.9	three-class seating, data for A310-200
752	Boeing 757-200	1982	2001	215	200	3.3	21.3	51	21.3	two-class seating, maximum payload and cargo volume from Boeing Airport Planning Manual
762	Boeing 767-200	1981	1984	103	181	9.4	25.7	87	35.6	three-class seating, 22 LD2 container + bulk, max. payload from Boeing Airport Planning Manual

Table 45. Aircraft production periods and capacities, seat category 5

Specific Aircraft	Specific Aircraft Name	First Deliveries	Last Deliveries	Retirement Curve	Baseline Seats	Baseline Freight Cap. [t]	Baseline Capacity [t]	Cargo Volume [m <sup>3</sup> ]	Maximum Payload [t]	Assumptions for Passenger and Freight Capacities
321	Airbus A321	1993	2020	203	199	4.3	22.2	52	26.9	all economy seating, maximum payload and cargo volume from Airbus Airport Planning Manual
21N	Airbus A321 NEO	2018	2040	203	199	4.3	22.2	52	26.9	all economy seating, capacity equal to A321
C93	Comac 919-300	2020	2050	203	199	4.3	22.2	52	26.9	all economy seating, capacity assumed equal to A321
739	Boeing 737-900	2001	2021	203	187	3.9	20.7	52	20.7	all economy seating, maximum payload and cargo volume from Boeing Airport Planning Manual
39N	Boeing 737 MAX 9	2019	2050	203	187	3.9	20.7	52	20.7	all economy seating, capacity equal to 737-900
T20	Tupolev TU-204 / TU-214	1989	2012	203	184	3.0	19.6	n/a	21.0	two-class seating, data estimated
738	Boeing 737-800	1989	2019	203	175	3.7	19.5	45	21.3	all economy seating, maximum payload and cargo volume from Boeing Airport Planning Manual
38N	Boeing 737 MAX 8	2017	2050	203	175	3.7	19.5	45	21.3	all economy seating, capacity equal to 737-800
320	Airbus A320	1987	2018	203	164	2.8	17.6	37	21.3	all economy seating, maximum payload and cargo volume from Airbus Airport Planning Manual
20N	Airbus A320 NEO	2016	2037	203	164	2.8	17.6	37	21.3	all economy seating, capacity equal to A320
C92	Comac 919-200	2017	2050	203	164	2.8	17.6	37	21.3	all economy seating, capacity assumed equal to A320
M90	Boeing (Douglas) MD-90	1993	2000	213	160	2.8	17.2	37	19.0	all economy seating, maximum payload and cargo volume from MDD Airport Planning Manual
M81	Boeing (Douglas) MD-81	1979	1994	OS	160	2.6	17.0	36	18.2	all economy seating, maximum payload and cargo volume from MDD Airport Planning Manual
M88	Boeing (Douglas) MD-88	1987	1997	216	160	2.6	17.0	36	20.0	all economy seating, maximum payload and cargo volume from MDD Airport Planning Manual
M82	Boeing (Douglas) MD-82	1981	1998	215	160	2.6	17.0	36	20.0	all economy seating, maximum payload and cargo volume from MDD Airport Planning Manual
M83	Boeing (Douglas) MD-83	1985	2004	216	160	1.7	16.1	29	19.2	all economy seating, maximum payload and cargo volume from MDD Airport Planning Manual
TU5	Tupolev TU154	1968	1993	214	160	1.6	16.0	n/a	18.0	all economy seating, data estimated
734	Boeing 737-400	1988	2000	203	159	2.0	16.3	31	19.4	all economy seating, maximum payload and cargo volume from Boeing Airport Planning Manual
IL6	Ilyushin IL-62	1963	1985	PO	158	3.8	18.0	n/a	21.0	two-class seating, data estimated
722	Boeing 727-200	1967	1983	OS	155	3.7	17.7	43	19.2	all economy seating, maximum payload and cargo volume from Boeing Airport Planning Manual
DC8	Boeing (Douglas) DC-8	1958	1971	OS	147	4.2	17.4	46	19.0	two-class seating, maximum payload and cargo volume from MDD Airport Planning Manual
707	Boeing 707 / 720	1958	1974	OS	147	4.8	18.0	50	21.4	two-class seating, maximum payload and cargo volume from Boeing Airport Planning Manual
73G	Boeing 737-700	1997	2020	203	140	1.9	14.5	28	17.6	all economy seating, maximum payload and cargo volume from Boeing Airport Planning Manual
37N	Boeing 737 MAX 7	2018	2050	203	140	1.9	14.5	28	17.6	all economy seating, capacity equal to 737-700
733	Boeing 737-300	1984	1999	215	137	1.6	14.0	26	15.4	all economy seating, maximum payload and cargo volume from Boeing Airport Planning Manual
D95	Boeing (Douglas) DC9-50	1975	1981	217	135	2.7	14.8	33	15.3	all economy seating, maximum payload and cargo volume from Boeing Airport Planning Manual
M87	Boeing (Douglas) MD-87	1986	1992	214	135	1.8	13.9	27	17.6	all economy seating, maximum payload and cargo volume from MDD Airport Planning Manual
319	Airbus A319	1995	2019	203	134	1.9	14.0	28	18.8	all economy seating, maximum payload and cargo volume from MDD Airport Planning Manual
19N	Airbus A319 NEO	2017	2038	203	134	1.9	14.0	28	18.8	all economy seating, maximum payload and cargo volume from MDD Airport Planning Manual
C91	Comac 919-100	2019	2050	203	134	1.9	14.0	28	18.8	all economy seating, capacity assumed equal to A319
CS3	CSeries 300	2014	2050	203	130	2.3	14.0	30	n/a	all economy seating, cargo volume from wikipedia

Table 46: Aircraft production periods and capacities, seat category 4

Specific Aircraft	Specific Aircraft Name	First Deliveries	Last Deliveries	Retirement Curve	Baseline Seats	Baseline Freight Cap. [t]	Baseline Capacity [t]	Cargo Volume [m <sup>3</sup> ]	Maximum Payload [t]	Assumptions for Passenger and Freight Capacities
D94	Boeing (Douglas) DC9-40	1968	1979	PO	125	2.2	13.5	29	14.4	all economy seating, maximum payload and cargo volume from MDD Airport Planning Manual
721	Boeing 727-100	1963	1972	PO	125	1.7	12.9	25	13.8	all economy seating, maximum payload and cargo volume from Boeing Airport Planning Manual
732	Boeing 737-200	1967	1987	PO	124	1.7	12.8	25	16.0	all economy seating, maximum payload and cargo volume from Boeing Airport Planning Manual
736	Boeing 737-600	1998	2015	203	123	1.2	12.3	21	15.6	all economy seating, maximum payload and cargo volume from Boeing Airport Planning Manual
735	Boeing 737-500	1990	1999	215	123	0.9	11.9	19	15.2	all economy seating, maximum payload and cargo volume from Boeing Airport Planning Manual
717	Boeing 717-200	1998	2006	213	117	2.0	12.5	27	12.9	all economy seating, maximum payload and cargo volume from Boeing Airport Planning Manual
318	Airbus A318	2002	2015	203	117	1.3	11.8	21	14.2	all economy seating, maximum payload and cargo volume from Airbus Airport Planning Manual
D93	Boeing (Douglas) DC9-30	1967	1982	OS	115	1.9	12.2	25	13.7	all economy seating, maximum payload and cargo volume from MDD Airport Planning Manual
CS1	C-Series 100	2013	2050	203	110	1.6	11.5	23	n/a	all economy seating, cargo volume from wikipedia
731	Boeing 737-100	1967	1969	OS	110	1.0	10.9	18	12.7	all economy seating, maximum payload and cargo volume from Boeing Airport Planning Manual
E95	Embraer 195	2006	2021	203	108	2.0	11.7	26	13.8	all economy seating, maximum payload and cargo volume from Embraer Airport Planning Manual
100	Fokker 100	1986	1996	214	107	0.8	10.5	17	11.1	all economy seating, maximum payload from BADA, cargo volume from OAG
219	Comac ARJ21-900	2015	2035	203	105	2.0	11.5	n/a	n/a	all economy seating, data estimated
YK2	Yakovlev Yak-42/142	1975	1986	215	104	2.5	11.9	29	n/a	all economy seating, cargo volume from OAG
CRX	Canadair Regional Jet 1000	2011	2020	203	100	2.0	11.0	25	12.1	all economy seating, maximum payload from Bombardier website, cargo volume from OAG
143	BAe 146-300	1987	1994	213	100	1.7	10.7	23	11.7	all economy seating, maximum payload and cargo volume from BAE documents
AR1	Avro RJ100	1992	2001	213	100	1.7	10.7	23	12.3	all economy seating, maximum payload and cargo volume from BAE documents
E90	Embraer 190	2005	2020	203	98	1.7	10.5	23	12.9	all economy seating, maximum payload and cargo volume from Embraer Airport Planning Manual
FXE	Embraer 190 Successor	2019	2060	203	98	1.7	10.5	23	12.9	all economy seating, capacity equal to E190
S95	Superjet 100-95	2012	2050	203	98	1.6	10.5	22	12.2	all economy seating, maximum payload and cargo volume from wikipedia

Table 47: Aircraft production periods and capacities, seat category 3

Specific Aircraft	Specific Aircraft Name	First Deliveries	Last Deliveries	Retirement Curve	Baseline Seats	Baseline Freight Cap. [t]	Baseline Capacity [t]	Cargo Volume [m <sup>3</sup> ]	Maximum Payload [t]	Assumptions for Passenger and Freight Capacities
CR9	Canadair Regional Jet 900	2001	2024	203	90	1.3	9.4	19	10.3	all economy seating, maximum payload from Bombardier website, cargo volume estimated
F9B	CRJ 900 Successor	2022	2050	203	90	1.3	9.4	19	10.3	all economy seating, capacity equal to CRJ-900
217	Comac ARJ21-700	2012	2035	203	90	1.3	9.4	n/a	n/a	all economy seating, data estimated
FP9	Future Turboprop (90 seats)	2019	2050	303	90	0.9	9.0	n/a	n/a	all economy seating, data estimated
D92	Boeing (Douglas) DC-9-20	1968	1969	OS	90	1.1	9.2	17	11.5	all economy seating, maximum payload and cargo volume from MDD Airport Planning Manual
IL8	Ilyushin IL-18	1957	1969	PO	90	0.9	9.0	n/a	n/a	all economy seating, data estimated
B11	BAe (BAC) 1-11	1965	1986	OS	90	0.7	8.8	14	9.6	all economy seating, maximum payload from BADA, cargo volume from OAG
MJ9	MRJ90	2014	2050	203	88	1.5	9.4	n/a	n/a	all economy seating, data estimated
142	BAe 146-200	1982	1984	214	85	1.3	9.0	18	11.2	all economy seating, maximum payload and cargo volume from BAE documents
AR8	Avro RJ85	1992	2001	213	85	1.3	9.0	18	11.2	all economy seating, maximum payload and cargo volume from BAE documents
F24	Fokker F28-4000 Fellowship	1976	1987	214	79	1.1	8.2	16	10.5	all economy seating, maximum payload from BADA, cargo volume from OAG
F22	Fokker F28-2000 Fellowship	1971	1976	OS	79	1.1	8.2	16	n/a	all economy seating, data for F28-4000
F70	Fokker 70	1993	1997	203	79	0.7	7.8	13	10.8	all economy seating, maximum payload from BADA, cargo volume from OAG
E75	Embraer 175	2005	2020	203	78	1.3	8.3	17	10.2	all economy seating, maximum payload and cargo volume from Embraer Airport Planning Manual
S75	Superjet 100-75	2015	2050	203	78	1.0	8.0	15	9.1	all economy seating, maximum payload and cargo volume from Embraer Airport Planning Manual
CRA	Canadair Regional Jet 705	2005	2022	203	75	1.6	8.3	19	9.9	all economy seating, maximum payload and cargo volume from wikipedia
A81	Antonov An148-100	2009	2010	203	75	1.0	7.8	15	9.0	two-class seating, maximum payload from Bombardier website, cargo volume estimated
MJ7	MRJ70	2017	2050	203	72	1.2	7.7	n/a	n/a	all economy seating, maximum payload and cargo volume from wikipedia
TU3	Tupolev TU134	1964	1984	203	72	1.0	7.5	15	8.0	all economy seating, maximum payload from BADA, cargo volume from OAG
CR7	Canadair Regional Jet 700	1999	2021	203	70	0.9	7.2	14	8.5	all economy seating, maximum payload from Bombardier website, cargo volume estimated
F7B	CRJ 700 Successor	2020	2050	203	70	1.0	7.3	14	9.1	all economy seating, capacity equal to E170
E70	Embraer 170	2004	2019	203	70	1.0	7.3	14	9.1	all economy seating, maximum payload and cargo volume from Embraer Airport Planning Manual
F7E	Embraer 170 Successor	2018	2050	203	70	1.0	7.3	14	9.1	all economy seating, capacity equal to E170
DH4	De Havilland DHC-8-400 Dash 8Q	1998	2020	303	70	0.9	7.2	14	8.7	all economy seating, maximum payload from BADA, cargo volume from OAG
FQQ	Bombardier DHC-8 Successor	2018	2050	303	70	0.7	7.0	n/a	n/a	all economy seating, data estimated
141	BAe 146-100	1981	1992	215	70	0.9	7.2	14	7.8	all economy seating, maximum payload and cargo volume from BAE documents
AR7	Avro RJ70	1992	1996	213	70	0.9	7.2	14	9.4	all economy seating, maximum payload and cargo volume from BAE documents
AT7	ATR 72	1988	2019	303	70	0.3	6.6	9	7.4	all economy seating, maximum payload from BADA, cargo volume from OAG
FUP	ATR 72 Successor	2017	2050	303	70	0.7	7.0	n/a	n/a	all economy seating, data estimated
DC6	Boeing (Douglas) DC-6b	1952	1959	318	66	0.7	6.6	n/a	n/a	all economy seating, data estimated
F21	Fokker F28-1000 Fellowship	1967	1977	PO	65	0.9	6.7	13	n/a	all economy seating, cargo volume from OAG
F23	Fokker F28-3000 Fellowship	1977	1984	216	65	0.9	6.7	13	n/a	all economy seating, cargo volume from OAG
ATP	BAe ATP	1986	1985	313	64	0.7	6.5	12	7.2	all economy seating, maximum payload from BADA, cargo volume from OAG
YS1	NAMC YS-11	1965	1973	PO	60	1.1	6.5	14	n/a	all economy seating, cargo volume from OAG
IL4	Ilyushin IL114	1990	2015	303	60	0.5	5.9	10	n/a	all economy seating, cargo volume from OAG

Table 48: Aircraft production periods and capacities, seat category 2

Specific Aircraft	Specific Aircraft Name	First Deliveries	Last Deliveries	Retirement Curve	Baseline Seats	Baseline Freight Cap. [t]	Baseline Capacity [t]	Cargo Volume [m <sup>3</sup> ]	Maximum Payload [t]	Assumptions for Passenger and Freight Capacities
AN7	Antonov AN-72/74	1978	1988	203	52	0.5	5.2	n/a	n/a	all economy seating, data estimated
CR1	Canadair Regional Jet 100	1991	2000	213	50	0.5	5.0	9	5.9	all economy seating, maximum payload from Bombardier website, cargo volume estimated
CR2	Canadair Regional Jet 200	1996	2012	203	50	0.5	5.0	9	5.9	all economy seating, maximum payload from Bombardier website, cargo volume estimated
S20	Saab 2000	1992	1999	303	50	0.7	5.2	10	5.9	all economy seating, maximum payload from BADA, cargo volume from OAG
ER4	Embraer RJ145	1995	2026	203	50	0.6	5.1	9	5.8	all economy seating, maximum payload from wikipedia, cargo volume from OAG
F8E	Embraer RJ145 Successor	2025	2050	203	50	0.6	5.1	9	5.8	all economy seating, capacity equal to E145
DH3	De Havilland DHC-8-300	1987	2008	317	50	0.5	5.0	9	6.1	all economy seating, maximum payload from BADA, cargo volume from OAG
CVR	Convair 240 /440 /580	1960	1969	PO2	50	0.5	5.0	n/a	n/a	all economy seating, data estimated
F50	Fokker 50	1987	1997	215	50	0.4	4.9	8	6.1	all economy seating, maximum payload from BADA, cargo volume from OAG
DH7	De Havilland DHC-7 Dash 7	1975	1988	315	50	0.3	4.8	7	n/a	all economy seating, cargo volume from OAG
FUQ	ATR 42 Successor	2023	2050	303	50	0.5	5.0	n/a	n/a	all economy seating, data estimated
HS7	BAe (HS) 748	1960	1985	303	48	0.7	5.0	10	n/a	all economy seating, cargo volume from OAG
A40	Antonov AN-140	1998	2015	303	48	0.6	4.9	9	n/a	all economy seating, cargo volume from OAG
FK7	Fairchild Industries FH27	1966	1971	OS	48	0.4	4.7	8	6.1	all economy seating, maximum payload from BADA, cargo volume from OAG
AN4	Antonov AN-24	1959	1977	216	46	1.0	5.1	12	n/a	all economy seating, cargo volume from OAG
YN7	Xian Yunshuji Y7 /MA60	1976	1995	313	46	0.9	5.0	11	n/a	all economy seating, cargo volume from OAG
AN6	Antonov AN-26 /30 /32	1969	1994	217	46	0.5	4.6	n/a	n/a	all economy seating, data estimated
CS5	Casa /Nusantara CN-235	1983	2009	318	45	0.2	4.2	6	n/a	all economy seating, cargo volume from OAG
ERD	Embraer RJ140	2000	2003	203	44	0.6	4.6	9	5.3	all economy seating, maximum payload from wikipedia, cargo volume from OAG
F27	Fokker F27 Friendship	1955	1986	PO2	44	0.5	4.4	8	6.1	all economy seating, maximum payload from BADA, cargo volume from OAG
AT3	ATR 42 300 /400	1985	1997	303	42	0.5	4.3	8	4.9	all economy seating, maximum payload from BADA, cargo volume from OAG
AT5	ATR 42 500	1994	2027	303	42	0.5	4.3	8	5.5	all economy seating, maximum payload from BADA, cargo volume from OAG
ER3	Embraer RJ135	1998	2027	203	37	0.7	4.1	9	4.5	all economy seating, maximum payload from wikipedia, cargo volume from OAG
DH2	De Havilland DHC-6-200	1992	2008	303	37	0.7	4.0	9	n/a	all economy seating, cargo volume from OAG
DH1	De Havilland DHC-6-100	1983	2000	316	37	0.7	4.0	9	4.0	all economy seating, maximum payload from BADA, cargo volume from OAG
GRS	Gulfstream Aerospace G159	1960	1969	318	36	0.0	3.2	3	n/a	all economy seating, cargo volume from OAG
SH6	Shorts 360 (SD3-60)	1981	1991	315	36	0.0	3.2	6	3.2	all economy seating, maximum payload from BADA, cargo volume from OAG
SF3	Saab 340	1983	1999	315	33	0.5	3.5	7	3.8	all economy seating, maximum payload from BADA, cargo volume from OAG
FRJ	Fairchild Dornier 328JET	1998	2008	213	32	0.4	3.3	6	n/a	all economy seats, cargo volume from OAG
D38	Fairchild Dornier 328-100	1991	2001	314	32	0.4	3.3	6	3.5	all economy seating, maximum payload from BADA, cargo volume from OAG
DHC	De Havilland DHC-4 Caribou	1994	1994	303	30	0.3	3.0	n/a	n/a	all economy seating, data estimated
YK4	Yakovlev Yak-40	1966	1981	216	30	0.3	3.0	n/a	n/a	all economy seating, data estimated
EM2	Embraer 120 Brasilia	1983	1999	313	30	0.3	3.0	6	3.0	all economy seating, maximum payload from BADA, cargo volume from OAG
SH3	Shorts 330 (SD3-30)	1974	1986	313	30	0.1	2.8	4	n/a	all economy seating, cargo volume from OAG

Table 49: Aircraft production periods and capacities, seat category 1

Specific Aircraft	Specific Aircraft Name	First Deliveries	Last Deliveries	Retirement Curve	Baseline Seats	Baseline Cap. [t]	Baseline Freight Capacity [t]	Cargo Volume [m <sup>3</sup> ]	Maximum Payload [t]	Assumptions for Passenger and Freight Capacities
J41	BAe Jetstream 41	1991	1998	313	29	0.4	3.0	7	3.0	maximum payload from BADA, cargo volume from OAG
DC3	Boeing (Douglas) DC-3	1949	2007	303	28	0.2	2.7	4	n/a	cargo volume from OAG
ND2	Aerospatiale (Nord) 262	1962	1977	OS	26	0.3	2.7	5	n/a	cargo volume from OAG
CS2	Casa C212 Aviocar	1971	1989	315	22	0.2	2.2	4	n/a	cargo volume from OAG
BEH	Beechcraft 1900D Airliner	1990	2002	303	19	0.4	2.1	5	n/a	cargo volume from OAG
BES	Beechcraft 1900C Airliner	1984	1992	317	19	0.4	2.1	5	n/a	cargo volume from OAG
SWM	Fairchild SA26 Merlin	1969	1997	303	19	0.3	2.0	4	n/a	data estimated
SHS	Shorts Skyvan (SC-7)	1984	1984	303	19	0.2	1.9	n/a	n/a	data estimated
J31	BAe Jetstream 31	1982	1989	313	19	0.1	1.9	3	n/a	cargo volume from OAG
J32	BAe Jetstream 32	1988	1993	314	19	0.1	1.8	3	1.8	maximum payload from BADA, cargo volume from OAG
DHT	De Havilland DHC-6 Twin Otter	1965	2050	303	18	0.3	1.9	4	n/a	cargo volume from OAG
D28	Fairchild Dornier 228	1981	2050	303	18	0.2	1.8	3	2.2	maximum payload from BADA, cargo volume from OAG
E1MB	Embraer 110 Bandeirante	1968	1990	315	18	0.2	1.8	3	n/a	cargo volume from OAG
YN2	Harbin Yunshuji Y12	1985	2050	303	17	0.2	1.7	3	n/a	cargo volume from OAG
A28	Antonov An28	1969	1992	313	17	0.0	1.5	1	n/a	cargo volume from OAG
L4T	Let 410	1969	2050	303	17	0.0	1.5	1	n/a	cargo volume from OAG
BNT	BN BN-2A Mikilil Trislander	1972	1982	303	16	0.0	1.4	1	n/a	cargo volume from OAG
BE9	Beechcraft C99 Airliner	1966	1986	318	15	0.1	1.4	2	1.5	maximum payload from BADA, cargo volume from OAG
DF2	Dassault Falcon	1963	2050	203	15	0.0	1.4	1	n/a	cargo volume from OAG
CD2	GAF NZ2B /NZ4A Nomad	1971	1988	314	12	0.1	1.2	2	n/a	cargo volume from OAG
GRM	Grumman G-73 Mallard	1969	1985	314	10	0.1	1.0	2	n/a	cargo volume from OAG
DHO	De Havilland DHC-3	1956	1967	318	9	0.1	1.0	2	n/a	cargo volume from OAG
PL2	Pilatus PC-12	1995	2050	303	9	0.0	0.8	1	n/a	cargo volume from OAG
ACD	Twin (Aero) Commander	1963	1969	318	9	0.0	0.8	1	n/a	cargo volume from OAG
BEC	Beechcraft (Light Aircraft)	1951	2050	303	9	0.0	0.8	1	n/a	cargo volume from OAG
BNI	BN BN-2A /BN-2B Islander	1968	2008	303	9	0.0	0.8	1	n/a	cargo volume from OAG
CNA	Cessna (Light Aircraft)	1971	2050	303	9	0.0	0.8	1	n/a	cargo volume from OAG
MU2	Mitsubishi MU-2	1965	1986	303	9	0.0	0.8	1	1.9	maximum payload from BADA, cargo volume from OAG
WWP	Israel Aircraft Ind.1124	1970	1987	203	8	0.2	0.9	2	n/a	cargo volume from OAG
CNU	Cessna Citation	1969	2050	203	8	0.2	0.9	2	n/a	cargo volume from OAG
LRJ	Learjet	1963	2050	203	8	0.0	0.7	1	1.5	maximum payload from BADA, cargo volume from OAG
GRG	Grumman G-21 Goose	1938	1946	318	8	0.0	0.7	1	n/a	cargo volume from OAG
PAG	Piper (Light Aircraft)	1951	2050	303	7	0.0	0.7	1	n/a	cargo volume from OAG
DHB	De Havilland DHC2	1949	1968	318	7	0.0	0.7	1	n/a	cargo volume from OAG
PN6	Pariseravia P68	1975	1994	303	5	0.1	0.5	1	n/a	cargo volume from OAG

Table 50: Aircraft production periods and capacities, seat category 0 (very small passenger aircraft)

Specific Aircraft	Specific Aircraft Name	First Deliveries	Last Deliveries	Retirement Curve	Baseline Seats	Baseline Freight Cap. [t]	Baseline Capacity [t]	Cargo Volume [m <sup>3</sup> ]	Maximum Payload [t]	Assumptions for Passenger and Freight Capacities
										maximum payload and cargo volume from Airbus Airport Planning Manual
38F	Airbus A380-800 (Freighter)	2020	2050	30	0	128.4	128.4	938	151.4	maximum payload and cargo volume from Airbus Airport Planning Manual
A4F	Antonov AN-124	1982	1996	103	0	120.0	120.0	1000	120.0	maximum payload from wikipedia, cargo volume from OAG
74Z	Boeing 747-8F (Freighter)	2012	2050	30	0	117.5	117.5	868	133.9	maximum payload from Boeing Airport Planning Manual, cargo volume from Boeing website
74Y	Boeing 747-400F (Freighter)	1993	2018	30	0	106.6	106.6	779	122.9	maximum payload from Boeing Airport Planning Manual, cargo volume from Boeing website
74X	Boeing 747-200 (Freighter)	1972	2003	113	0	95.1	95.1	695	111.0	maximum payload and cargo volume from Boeing Airport Planning Manual
74T	Boeing 747-100 (Freighter)	1974	1995	PO	0	94.6	94.6	694	94.6	maximum payload from Ascend Online Fleets, cargo volume from Boeing Airport Planning Manual data estimated
35F	Airbus A350-900 (Freighter)	2018	2050	30	0	90.0	90.0	n/a	n/a	
77F	Boeing 777 (Freighter)	2010	2050	30	0	89.4	89.4	653	103.7	maximum payload from Boeing Airport Planning Manual, cargo volume from OAG
M1F	Boeing MD-11 (Freighter)	1991	2012	30	0	81.8	81.8	588	90.7	maximum payload from MDD Airport Planning Manual, cargo volume from Boeing website
D1F	Boeing (Douglas) DC10 (Freighter)	1984	2002	103	0	65.4	65.4	478	69.4	maximum payload and cargo volume from MDD Airport Planning Manual
33F	Airbus A330-200F (Freighter)	2011	2050	30	0	63.9	63.9	475	63.9	maximum payload from Airbus Airport Planning Manual, cargo volume from Airbus website data estimated
78F	Boeing 787-8 (Freighter)	2024	2050	30	0	59.0	59.0	n/a	n/a	
ABY	Airbus A300-600F (Freighter)	1994	2017	30	0	54.1	54.1	416	54.1	max. payload from Airbus Airport Planning Manual, cargo volume from Airbus Product Presentation
76F	Boeing 767 (Freighter)	1995	2020	30	0	50.0	50.0	400	50.0	data estimated (averaged for 767-200F and 767-300F)
L1F	Lockheed L1011 (Freighter)	1991	1996	OS	0	50.0	50.0	n/a	n/a	data estimated
IL7	Ilyushin IL-76	1971	1994	215	0	45.0	45.0	n/a	n/a	data estimated
ABX	Airbus A300B4 / C4 / F4	1980	2002	113	0	40.0	40.0	412	40.0	maximum payload from Airbus Airport Planning Manual, cargo volume estimated
31F	Airbus A310 (Freighter)	1995	2016	30	0	34.5	34.5	300	34.5	maximum payload from Airbus Airport Planning Manual, cargo volume from OAG
75F	Boeing 757-200F (Freighter)	1987	2014	25	0	39.0	39.0	239	39.0	maximum payload from Boeing Airport Planning Manual, cargo volume from OAG
70F	Boeing 707 (Freighter)	1963	1978	OS	0	37.9	37.9	277	42.9	maximum payload and cargo volume from Boeing Airport Planning Manual
D8F	Douglas DC8 (Freighter)	1963	1995	PO	0	37.7	37.7	276	40.7	maximum payload and cargo volume from MDD Airport Planning Manual
SHB	Shorts SC.5 Belfast	1966	1971	OS	0	30.0	30.0	n/a	36.2	data estimated
72F	Boeing 727 (Freighter)	1978	2000	213	0	26.4	26.4	193	29.5	maximum payload and cargo volume from Boeing Airline Startup data
T2F	Tupolev TU-204 (Freighter)	1998	2015	25	0	25.0	25.0	n/a	n/a	data estimated
CL4	Canadair CL-44	1960	1965	OS	0	20.5	20.5	150	30.0	data estimated, cargo volume from OAG
73P	Boeing 737-400 (Freighter)	2006	2017	25	0	19.7	19.7	150	19.7	maximum payload estimated from Ascend Online Fleets data, cargo volume estimated
LOH	Lockheed Hercules	1966	1992	303	0	19.4	19.4	n/a	19.4	data estimated, maximum payload from BADA
ANF	Antonov AN-12	1957	1972	317	0	19.0	19.0	n/a	n/a	data estimated
73R	Boeing 737-700 (Freighter)	2010	2050	25	0	17.4	17.4	127	18.8	maximum payload and cargo volume from Boeing Airline Startup data
73Y	Boeing 737-300 (Freighter)	1992	2015	25	0	16.6	16.6	130	16.6	max. payload estimated from Ascend Online Fleets, cargo volume from Boeing Airline Startup data
D9F	Douglas DC9 (Freighter)	1967	1999	PO2	0	15.7	15.7	114	16.3	maximum payload and cargo volume from Boeing Airline Startup data
73X	Boeing 737-200 (Freighter)	1985	2007	213	0	15.1	15.1	112	15.1	max. payload from Boeing Airport Planning Manual, cargo volume from Boeing Airline Startup data
LOF	Lockheed L188 (Freighter)	1968	1978	PO	0	15.0	15.0	n/a	n/a	data estimated
D6F	Douglas DC6 (Freighter)	1947	1959	318	0	15.0	15.0	n/a	n/a	data estimated
14F	BAe 146 (Freighter)	1986	2008	25	0	12.0	12.0	n/a	n/a	data estimated
CVF	Convair 440 /580 /600 /640	1966	1992	314	0	7.0	7.0	n/a	n/a	data estimated
CWC	Curtiss C-46 Commando	1946	1947	318	0	4.0	4.0	n/a	n/a	data estimated

Table 51: Aircraft production periods and capacities, seat category 101-103 (freighter)



Specific Aircraft	Specific Aircraft Name	First Deliveries	Last Deliveries	Retirement Curve	Baseline Seats	Baseline Cap. [t]	Baseline Freight Capacity [t]	Cargo Volume [m <sup>3</sup> ]	Maximum Payload [t]	Assumptions for Passenger and Freight Capacities
74E	Boeing 747-400	1989	2002	103	345	35,5	66,6	295	73,5	three-class seating + 7 pallets, maximum payload from Boeing Airport Planning Manual
74D	Boeing 747-300 / 747-200 SUD	1983	1990	115	360	34,4	66,8	288	78,1	three-class seating + 6 pallets, maximum payload from Boeing Airport Planning Manual
74C	Boeing 747-200	1973	1988	PO	316	36,4	64,8	298	69,6	three-class seating + 7 pallets, maximum payload from Boeing Airport Planning Manual
M1M	Boeing (Douglas) MD-11	1991	1992	OS	181	32,9	49,2	259	66,5	three-class seating + 6 pallets, maximum payload from MDD Airport Planning Manual
73Q	Boeing 737-400	2007	2008	203	72	9,9	16,4	80	19,4	maximum payload estimated from Ascend Online Fleets data, cargo volume estimated
72M	Boeing 727	1965	1971	OS	70	11,5	17,8	n/a	19,2	data estimated from 737-400 (mixed configuration)
73L	Boeing 737-200	1968	1984	216	56	7,8	12,8	n/a	12,8	data estimated from 737-400 (mixed configuration)

Table 52: Aircraft production periods and capacities, seat category 200 (aircraft in mixed configuration)

## Appendix O VISUALIZATION OF AIRCRAFT DELIVERY PERIODS

This appendix provides an overview on the assumed delivery periods of aircraft types in the fleet scenarios covered in this study. Details regarding assumptions about delivery periods are found in chapter 3.4.4.4. The following figures are presented in this appendix:

- Figure 116 visualises the aircraft delivery periods in the baseline scenario of this study.
- Figure 117 shows the aircraft delivery periods in an alternative fleet scenario assuming development and delivery delays for future aircraft types.
- Figure 118 shows the aircraft delivery periods in an alternative fleet scenario assuming new single-aisle aircraft instead of re-engined A320 and 737 families.
- Figure 119 shows the aircraft delivery periods in a hypothetical fleet scenario assuming no new aircraft types after the year 2010.

Details about the alternative fleet scenarios and resulting effects on fuel burn and emissions of air traffic are found in chapter 4.4.

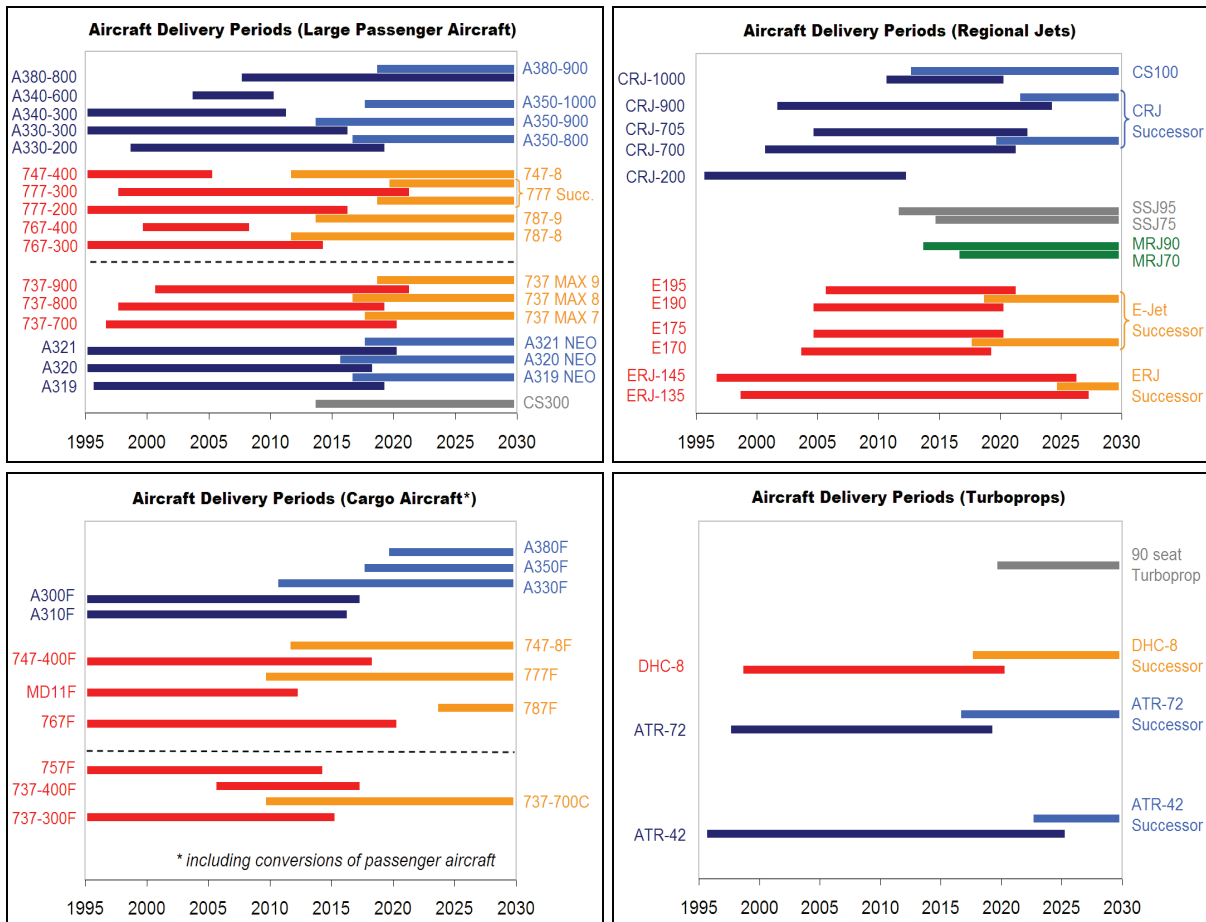


Figure 116: Aircraft delivery periods in the baseline scenario of the forecast



Figure 117: Aircraft delivery periods in an alternative fleet scenario assuming development and delivery delays of future aircraft types

More information regarding the alternative fleet scenario with assumed delivery delays of future aircraft types is found in chapter 4.4.3.

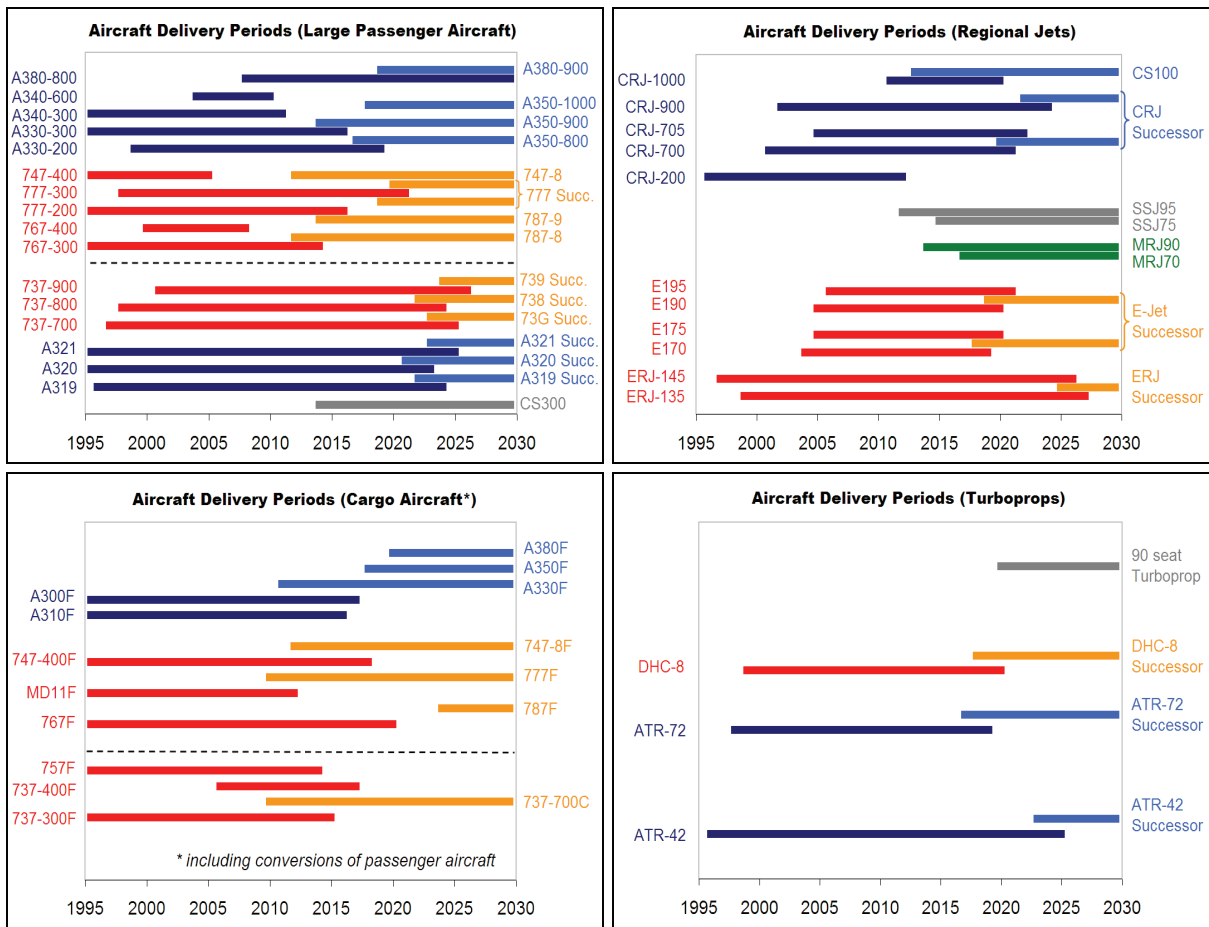


Figure 118: Aircraft delivery periods in an alternative fleet scenario assuming all-new single-aisle aircraft instead of re-engined A320 and 737 families

More information regarding the alternative fleet scenario with new single-aisle aircraft types is found in chapter 4.4.4.



Figure 119: Aircraft delivery periods in a hypothetical fleet scenario assuming no new aircraft types after the year 2010

More information regarding the hypothetical fleet scenario without new aircraft types is found in chapter 4.4.3

## Appendix P AIRCRAFT REPLACEMENT SCHEMES

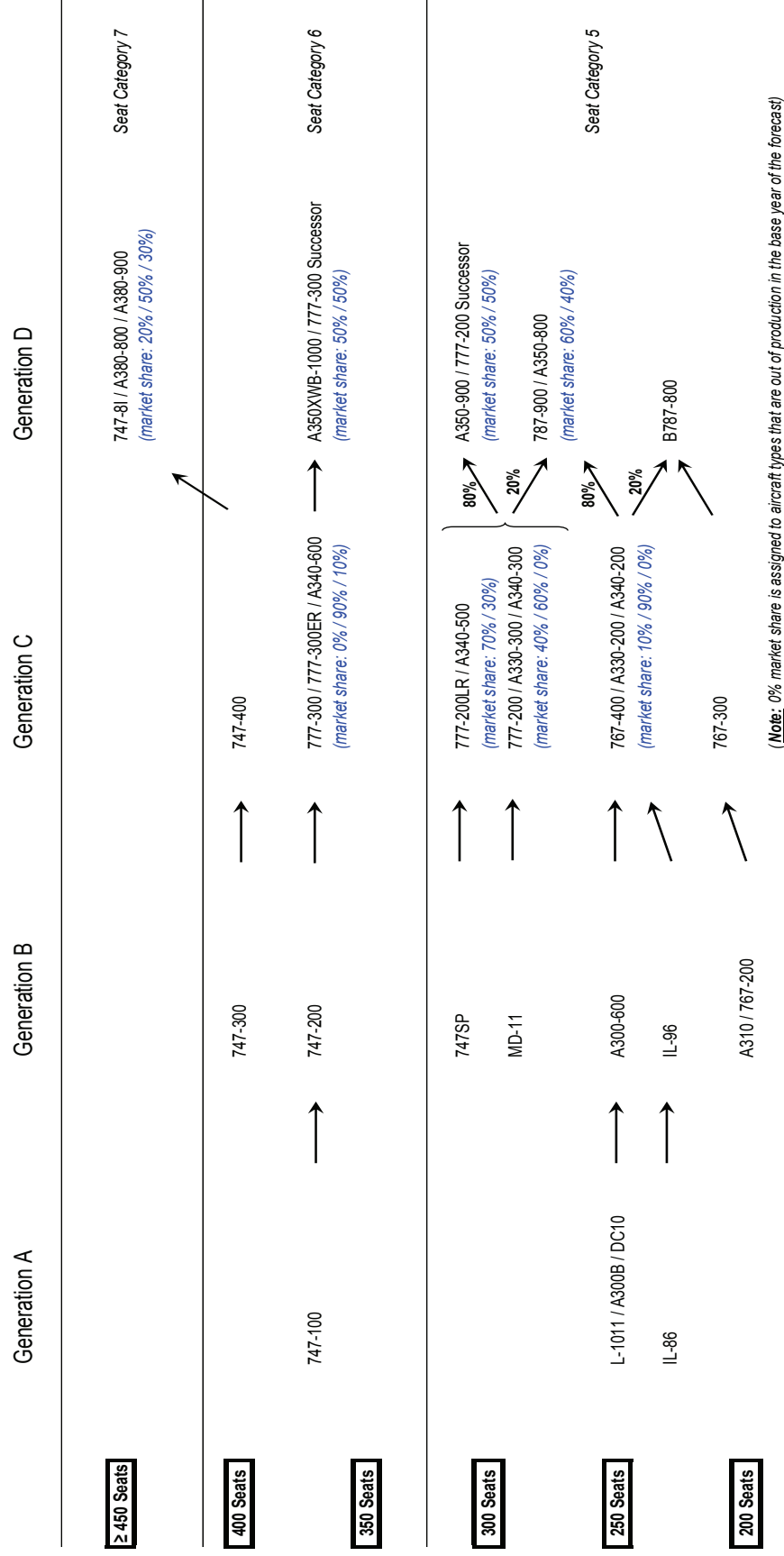


Figure 120: Replacement scheme for widebody jet aircraft in baseline forecast

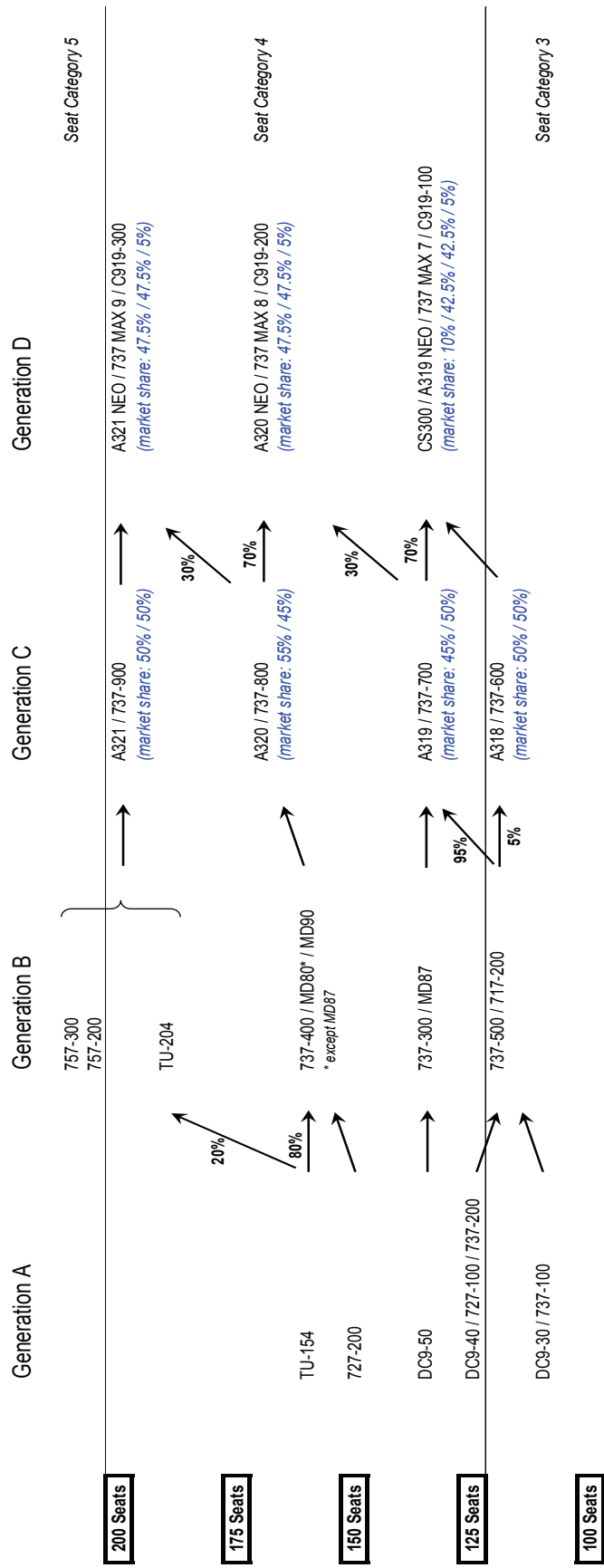


Figure 121: Replacement scheme for narrowbody jet aircraft in baseline forecast



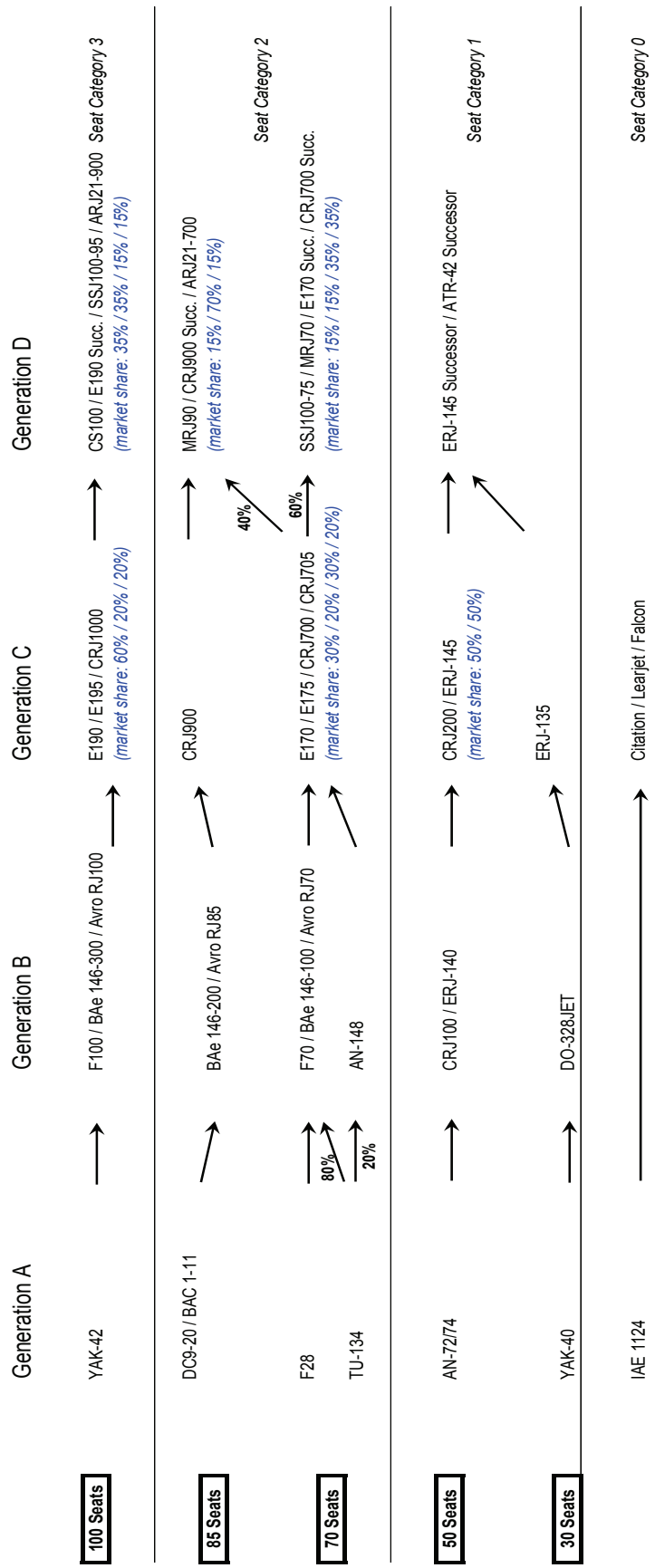


Figure 122: Replacement scheme for regional jet aircraft in baseline forecast

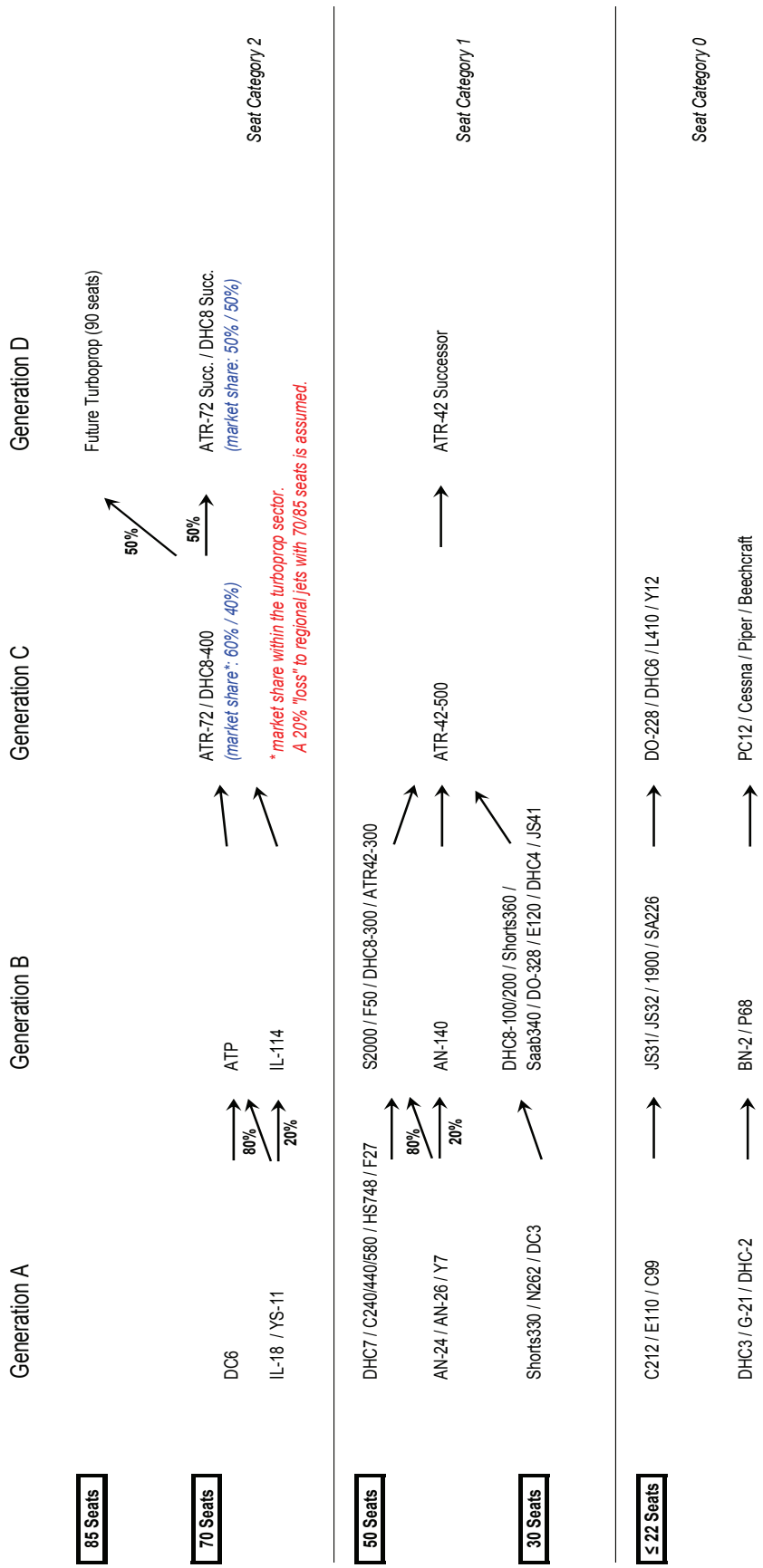


Figure 123: Replacement scheme for aircraft with turboprop and piston engines in baseline forecast

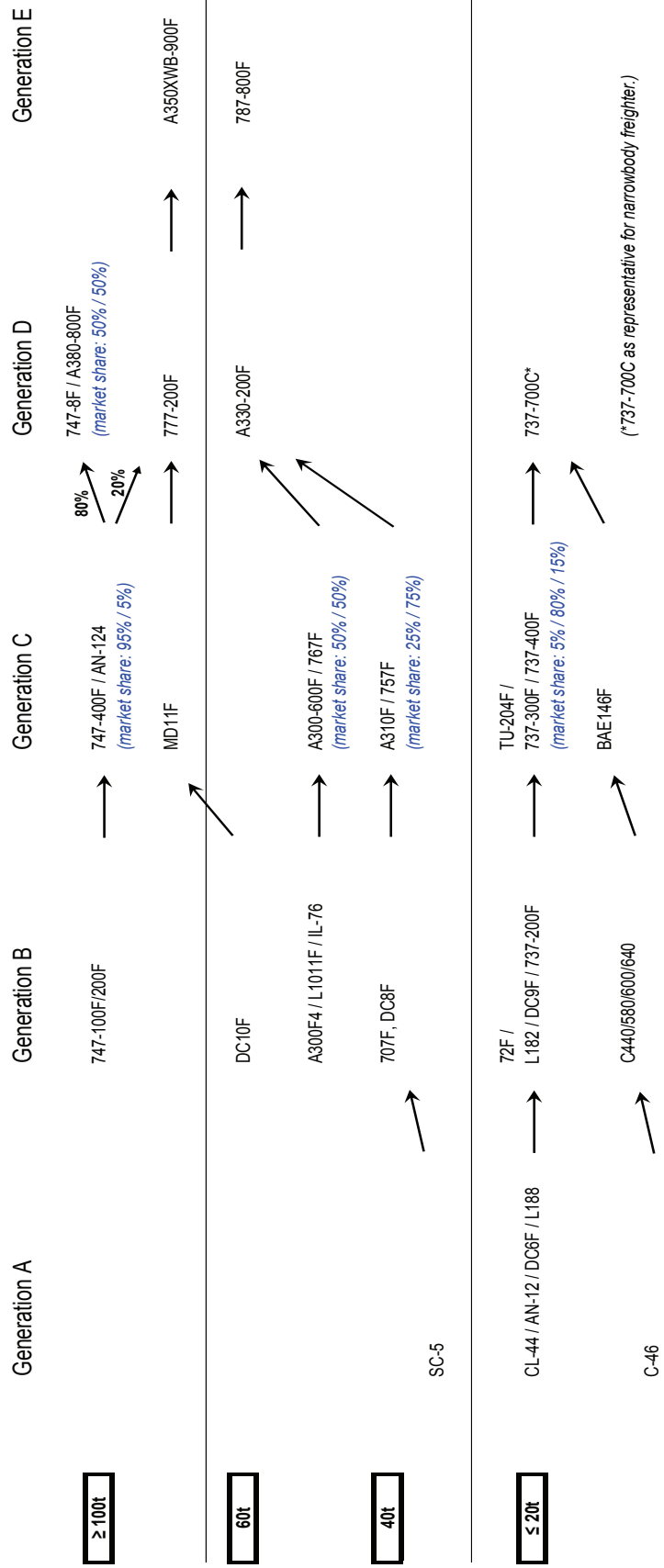


Figure 124: Replacement scheme for all-cargo aircraft / freighter in baseline forecast

## Appendix Q AIRCRAFT AND ENGINE MODELS OF THE NEAR FUTURE

Simulation models for aircraft and engine types of the near future have been created for this study in order to estimate fuel consumption and NO<sub>x</sub> emissions on flight mission level. Major characteristics of these models including weight, lift-to-drag ratios, fuel efficiency and specific NO<sub>x</sub> emissions were described in chapter 3.4.5. This appendix provides additional information on engine models and aircraft aerodynamics.

Table 53 present aerodynamic characteristics assumed for the newly created aircraft models. The data shown in the table refer to cruise conditions at the aircrafts' typical cruise speed. Mach-number dependent drag polars for the Boeing 787-8 have been derived from a freely available model of this aircraft developed by Lissys Ltd [93]. As an approximation, the polars for the 787-8 are equally assumed for the Airbus A350 XWB-900. Drag polars for an Airbus A320 were obtained from [92] and are assumed for the A320 NEO. This assumption implies that aerodynamic improvements on the NEO compared to the baseline A320 (e.g. by sharklets) compensate for a drag penalty from larger engine dimensions. The aerodynamic characteristics of the A319 NEO and A321 NEO models differ from the A320 NEO by a delta C<sub>D0</sub> which was estimated by handbook methods for aircraft design. These methods were described by Roskam [111] and Thorenbeek [130] and have also been applied here to derive polars for the 747-8 and a generic regional jet.

	747-8	787-8*	A350-900*	Generic RJ	A319 NEO	A320 NEO**	A321 NEO
Wing area [m <sup>2</sup> ]	525	360	443	77	123	123	123
C <sub>D0</sub>	0.0147	0.0122	0.0122	0.0204	0.0193	0.0200	0.0210
C <sub>D</sub> at (L/D) <sub>max</sub>	0.0294	0.0238	0.0238	0.0397	0.0337	0.0343	0.0354
C <sub>L</sub> at (L/D) <sub>max</sub>	0.56	0.50	0.50	0.66	0.60	0.60	0.60
(L/D) <sub>max</sub>	18.9	21.0	21.0	16.7	17.8	17.4	17.0
Cruise Mach number [-]	0.85	0.85	0.85	0.77	0.78	0.78	0.78
* Lift-to-drag ratios assumed for 787-8 and A350-900 correspond to the PIANO model of the Boeing 787-8 [93].							
** Lift-to-drag ratios assumed for the A320 NEO correspond to the PIANO model of the Airbus A320 [92].							

Table 53: Aerodynamic assumptions for aircraft models in cruise flight

Engine performance models simulated by the VarCycle software were provided by DLR [106]. Models of the GENx-1B for the Boeing 787-8 and the Trent XWB for the A350 XWB-900 are used in this study. No detailed models are currently available for the GENx-2B engines on the 747-8 and the Trent 1000 option for the 787. An updated version of the GENx-1B model is assumed for the 747-8<sup>53</sup>. Similarly, the Trent 1000 engine is assumed to have the same fuel specific consumption as the GENx-1B. Differences in the NO<sub>x</sub> emissions

<sup>53</sup> A 2% increase of engine SFC is assumed for to account for the smaller fan diameter of the GENx-2B.

between Trent 1000 and GENx-1B are accounted for, as will be described below. For use with the narrowbody aircraft, an engine similar to the PW1217G is simulated. This engine powers the generic regional jet, which resembles the Mitsubishi MRJ-90ER. An upscaled version of this engine with slightly improved specific fuel consumption is assumed as representative engine for the A320 NEO family.

All engine models were developed before the respective engine types were certified. Only limited and preliminary specifications from [29] and [110] were available as input data. Emission indices of  $\text{NO}_x$  have been estimated for sea-level conditions based on the characteristic  $\text{NO}_x$  levels per kN take-off thrust that are currently predicted by engine manufacturers [110]<sup>54</sup>. A diagram showing the characteristic  $\text{NO}_x$  levels is found in Figure 48 on page 85. The fuel flow from the engine models and the assumed emission indices of  $\text{NO}_x$ , which depend on engine thrust, are shown in Figure 125 to Figure 129. Correlation methods can be used to calculate in-flight emissions of  $\text{NO}_x$  based on reference emissions for sea-level static conditions. In this study, the  $p_3T_3$  approach [119] is applied when simulating the TAPS combustor of the GENx whereas the DLR fuel flow correlation [31] is applied as the standard method for engines with RQL combustors. Given the lack of reliable data, it is difficult to estimate emissions of  $\text{NO}_x$  for future engine types. It is particularly difficult to estimate the potential of the TAPS combustor to reduce emissions during cruise flight. A significant potential is predicted in [97], but depends on the transition point between pilot mode and combined pilot/main mode. The emission characteristics shown in Figure 125 reflect such claims, as the transition point was chosen such that cruise flight operating points are predominantly in the pilot/main zone. However, the uncertainty of the modelled  $\text{NO}_x$  characteristics for TAPS combustors must be regarded as high.

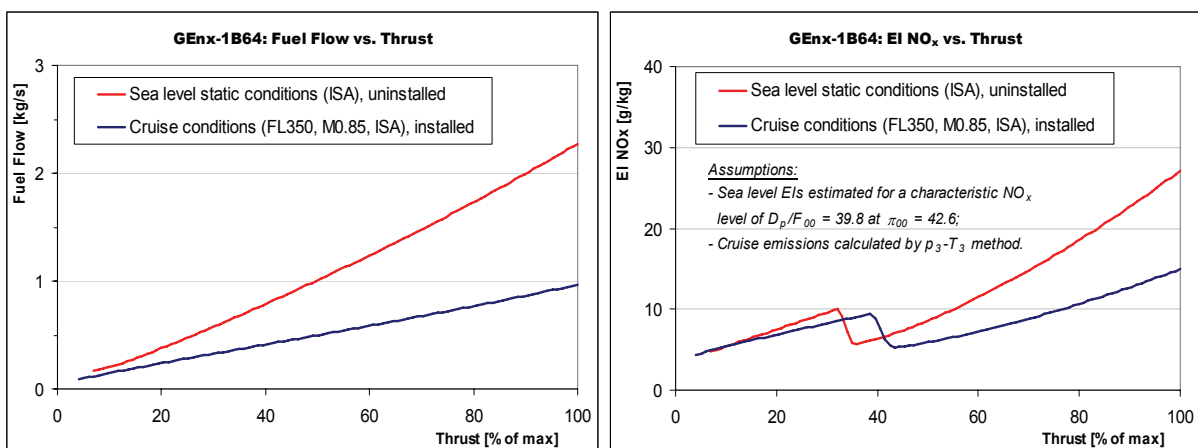


Figure 125: Fuel flow and  $\text{NO}_x$  emission index vs. thrust for GENx-1B engine (simulation)

<sup>54</sup> Assumptions about the number of engines tested for certification are required when estimating emission indices from a given characteristic  $\text{NO}_x$  level. One test engine is assumed for large turbofans above 200kN take-off thrust while two such engines are assumed for smaller turbofans.

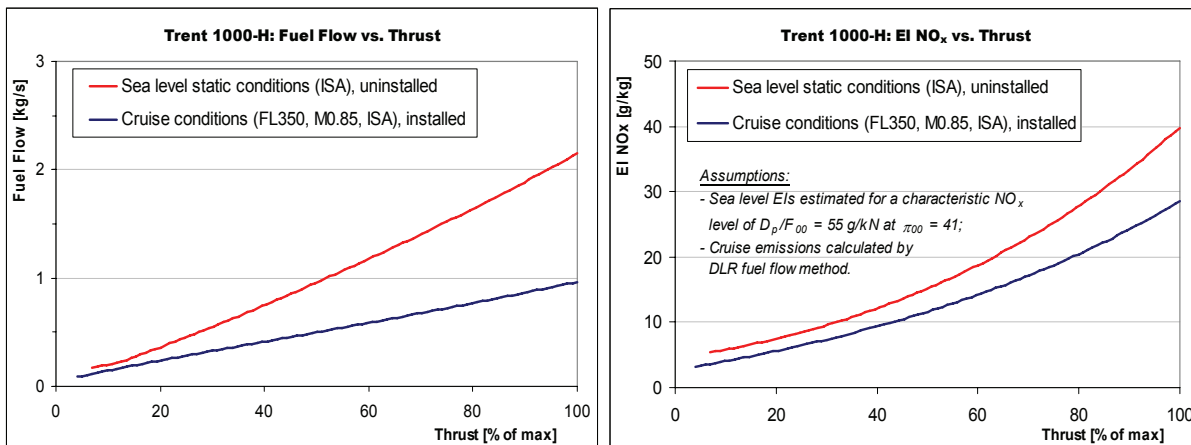


Figure 126: Fuel flow and NO<sub>x</sub> emission index vs. thrust for Trent 1000 engine (simulation)<sup>55</sup>

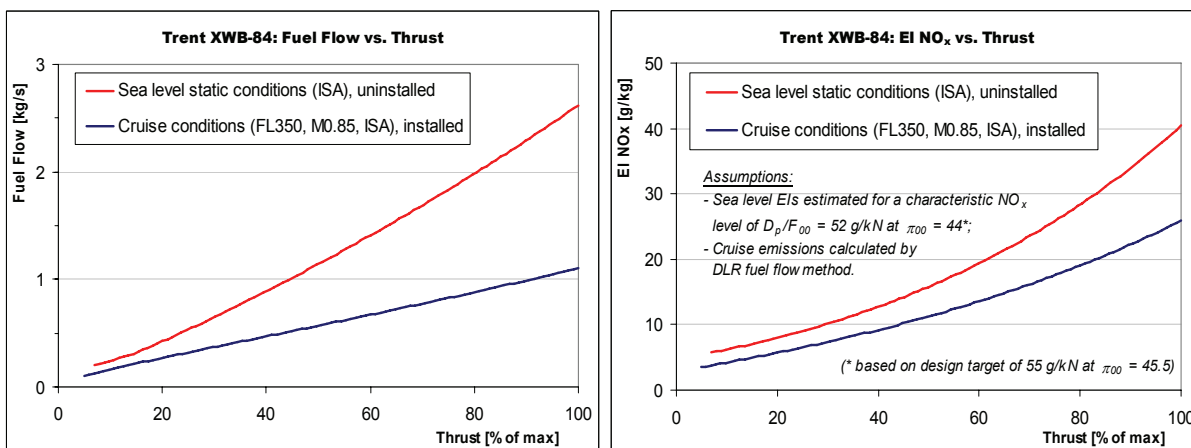


Figure 127: Fuel flow and NO<sub>x</sub> emission index vs. thrust for Trent XWB engine (simulation)

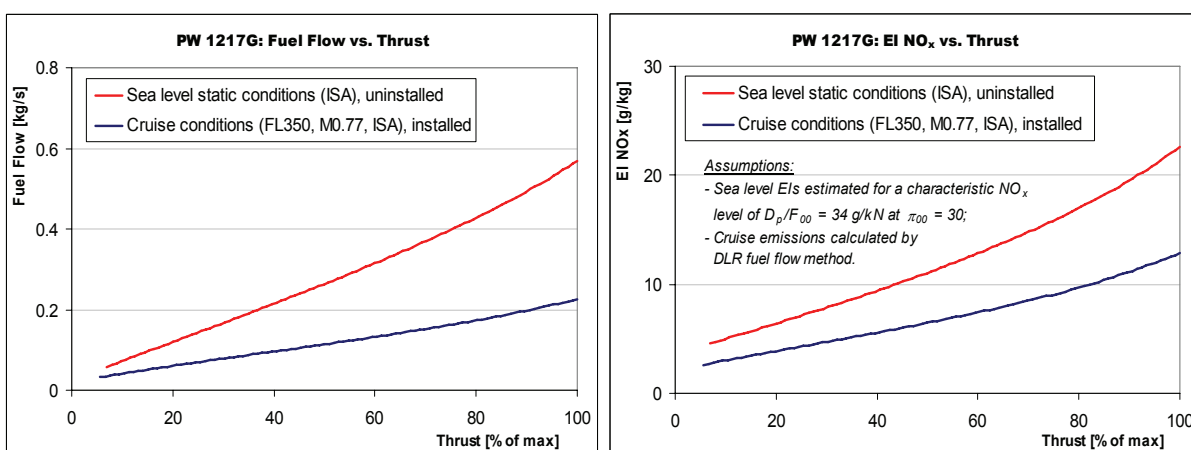


Figure 128: Fuel flow and NO<sub>x</sub> emission index vs. thrust for PW 1217G engine (simulation)

<sup>55</sup> The diagrams for the Trent 1000 refer to the version with 285kN maximum thrust at sea level.

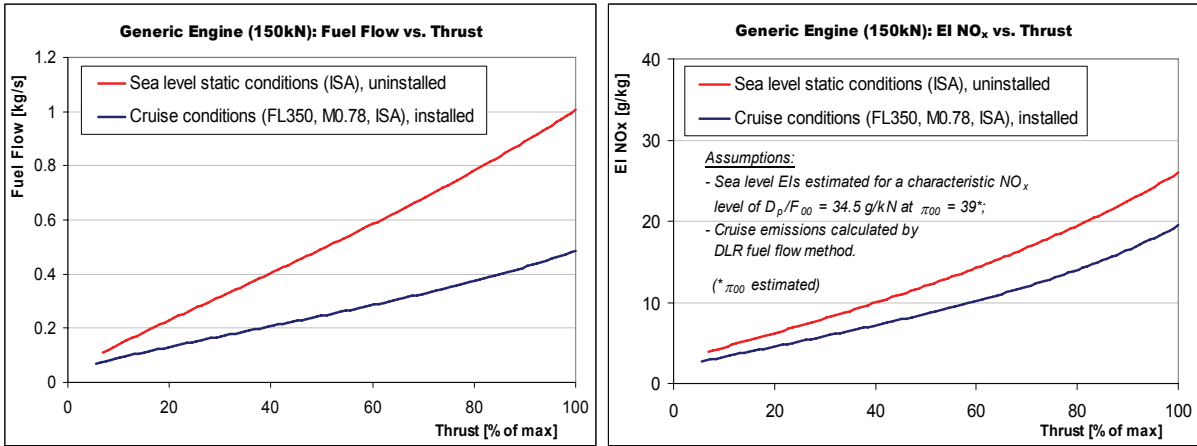


Figure 129: Fuel flow and NO<sub>x</sub> emission index vs. thrust for A321 NEO engine (simulation)<sup>56</sup>

Given the aircraft and engine models, the VarMission software can be used for flight mission simulation. For each aircraft-engine combination, a full set of emission profiles was created, i.e. standardized flight mission protocols for different load factors and ranges. The resulting fuel efficiencies measured in fuel burn per passenger-kilometre or per tonne-kilometre are in line with expectations by aircraft manufacturers (see chapter 3.4.5).

In addition to analyses on mission level, payload-range diagrams can be calculated for the aircraft models (see Figure 130). The payload-range chart for the Boeing 747-8I shown in the left hand diagram compares well to published reference data in Boeing’s airport planning manual [17]. The difference in terms of maximum range at maximum payload is less than 1% while the model delivers a maximum range at maximum fuel load that is 2.6% higher than in the manual. No reference data is currently available for the remaining aircraft types.

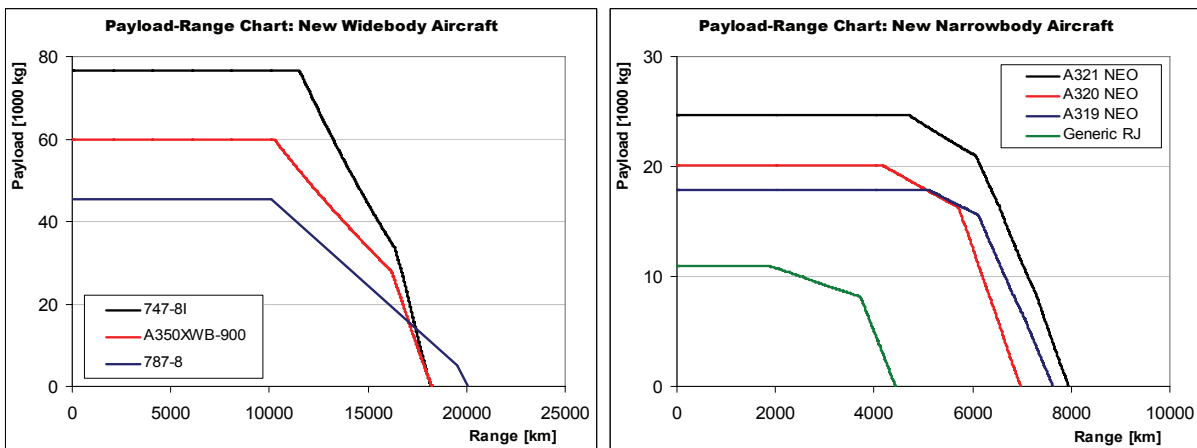


Figure 130: Payload-range performance of new aircraft types (simulation)

<sup>56</sup> Data refers to a RQL combustor. 20% lower NO<sub>x</sub> emissions on flight mission level are assumed for a similar engine with TAPS combustor (see chapter 3.4.5.3).



## Appendix R DESIGN APPROACH FOR A FUTURE NARROWBODY AIRCRAFT FAMILY

Performance models have been created for a generic family of narrowbody aircraft expected to enter service during the early 2020s. These aircraft are intended to replace the Boeing 737 and Airbus A320 families in a hypothetical fleet scenario. While aircraft design specifications and most aircraft characteristics are described in chapter 3.4.5.4, this appendix provides additional information on the engine model and presents an overview on the design process.

An ultra-high bypass ratio (UHBR) engine originating from the CLAIRE 2 project by DLR and MTU [35] is assumed to power the aircraft family. The engine model from CLAIRE 2 has been scaled to meet the thrust requirements of the aircraft. Engine emission characteristics of  $\text{NO}_x$  have been estimated assuming a TAPS combustor with a characteristic  $\text{NO}_x$  level  $D_p/F_{00}$  of about 29 g/kN at an overall pressure ratio  $\pi_{00}$  of 42.8 (and assuming two engines are tested for certification). This corresponds to a technology level that can be expected for the year 2020. Figure 131 shows fuel burn and  $\text{NO}_x$  emissions of the UHBR engine.

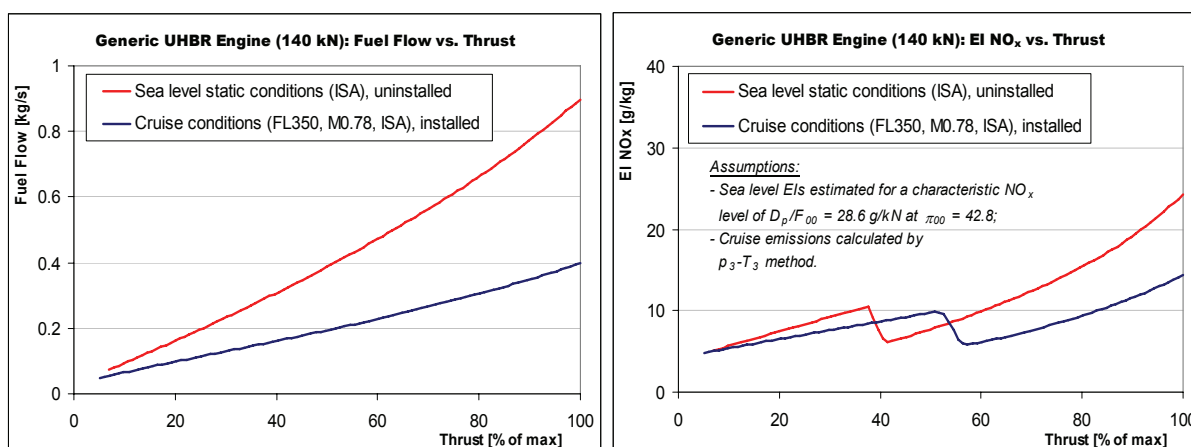


Figure 131: Fuel flow and  $\text{NO}_x$  emission index vs. thrust for UHBR engine (simulation)

The following steps were performed iteratively during the design process:

- Operational empty weight and maximum take-off weight are calculated following Roskam [111]. Engine weight is estimated separately and structural modifications on the aircraft required for engine installation are accounted for. Correction factors are applied in order to consider improvements in the fields of lightweight construction and materials: A 7.5% reduction<sup>57</sup> of the maximum zero fuel weight (MZFW) compared to state-of-the-art materials used for the A320 generation is assumed in this study [132].

<sup>57</sup> Compared to aircraft of the A320 generation including “snow-ball” effects, but not considering the extra weight from the new engine systems. 7.5% of the MZFW correspond to roughly 11.1% of the OEW.

- Aircraft aerodynamics are evaluated using methods from Roskam [111] and Torenbeek [130]. A 4% improvement of the lift-to-drag ratio during cruise compared to the previous generation of narrowbody aircraft is assumed [65]. This value is based on the assumption that revolutionary concepts in aircraft aerodynamics e.g. laminar flow control are not yet introduced on this aircraft.
- Engine thrust requirements are calculated for take-off and top-of-climb conditions according to certification requirements. The engine model has been scaled in order to deliver the required thrust.

The iterative design process is repeated until aircraft weights, aerodynamics and engine characteristics are matched. Assuming a family concept, both a stretch and a shrink version have been derived from the baseline aircraft. Figure 132 compares the payload-range performance of the future narrowbody aircraft compared to the Airbus A320 family. The design mission of the baseline aircraft is also shown in the figure. More details regarding preliminary design methods and more information on the assumptions for the future narrowbody family can be found in a separate report [131].

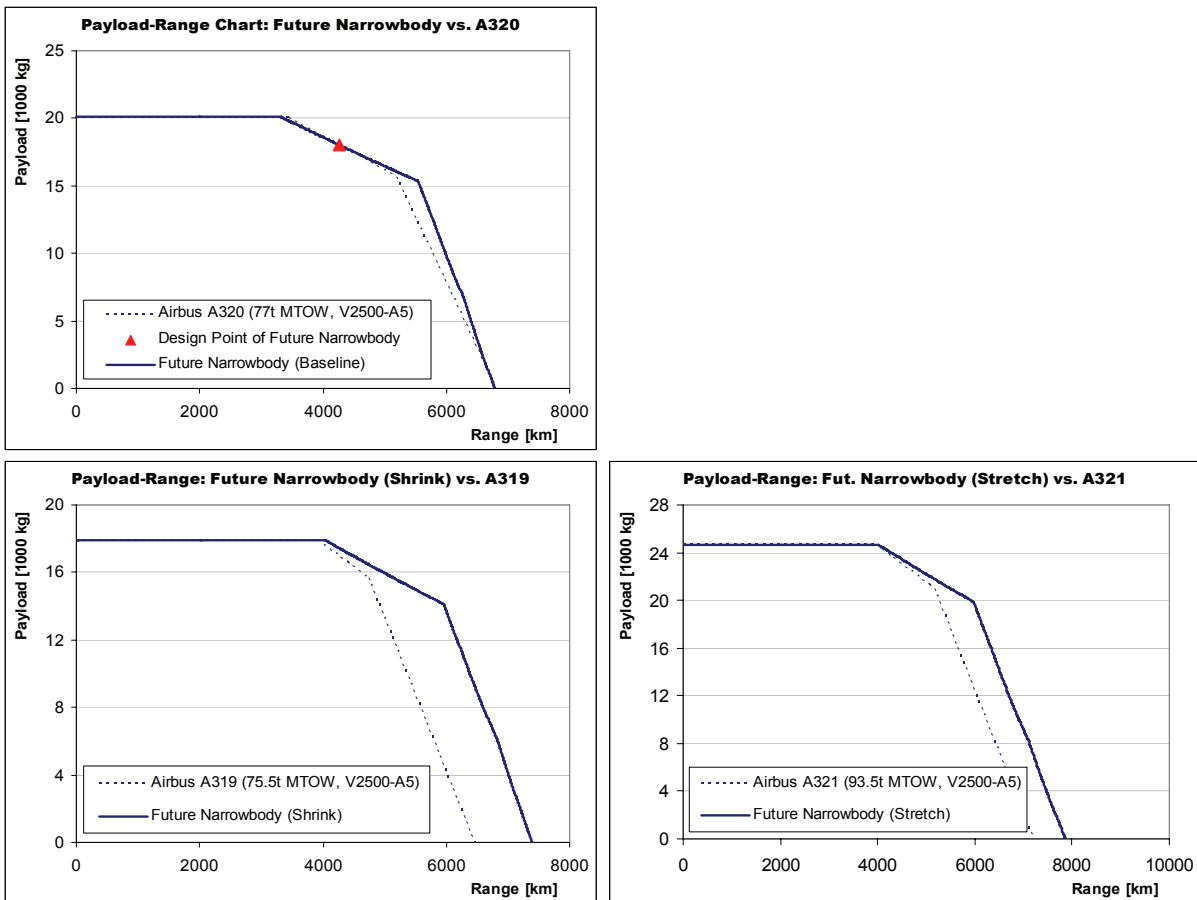


Figure 132: Payload-range performance of a future narrowbody aircraft family compared to the Airbus A320 family (simulation) [2]

## Appendix S ASSUMPTIONS FOR CARGO AIRCRAFT

Performance models for cargo aircraft are currently not available from the BADA database. Cargo aircraft are often variants of passenger aircraft types with similar characteristics in terms of aerodynamics and engine performance. Their characteristic weights, however, usually differ from the passenger version. Particularly the empty weight of cargo aircraft (which is typically lower than for the corresponding passenger versions) and the maximum structural payload (which is typically higher) will influence fuel consumption and emissions on flight mission level.

When simulating flights of cargo aircraft, VarMission uses existing models of passenger aircraft in combination with characteristic weights of the corresponding cargo version. This way, the differences between passenger and cargo variants are accounted for. As a first order approximation, aircraft aerodynamics and engine parameters are assumed to remain unchanged. Table 54 to Table 57 show the characteristic weights assumed for the most important cargo aircraft. A full list of all simulated aircraft types is found in Appendix F.

	Boeing 747-8F*	Boeing 747-400F	Boeing 777-200F
Maximum take-off weight (MTOW) [kg]	442 253	396 894	347 815
Operating empty weight (OEW) [kg]	191 053	165 087	144 379
Maximum payload (MPL) [kg]	133 901	122 945	103 736
Maximum fuel capacity (MFC) [kg]	182 981	173 425	145 379
Source of data	Preliminary airplane characteristics [17]	Boeing airplane characteristics [17]	Boeing airplane characteristics [17]
<i>* Used in combination with the newly developed aircraft model described in chapter 3.4.5.2.</i>			

Table 54: Characteristic weights of major cargo aircraft types

	Boeing MD-11F	Boeing 767-300F	Boeing 757-200PF
Maximum take-off weight (MTOW) [kg]	273 294	186 880	116 650
Operating empty weight (OEW) [kg]	112 748	85 275	51 700
Maximum payload (MPL) [kg]	90 719	54 885	39 000
Maximum fuel capacity (MFC) [kg]	115 000	73 364	34 260
Source of data	Boeing airplane characteristics [17]	Boeing airplane characteristics [17]	Boeing airplane characteristics [17]

Table 55: Characteristic weights of major cargo aircraft types (continued)

	Airbus A380-800F	Airbus A330-200F	Airbus A300-600F
Maximum take-off weight (MTOW) [kg]	590 000	233 000	170 500
Operating empty weight (OEW) [kg]	250 560	109 100	81 900
Maximum payload (MPL) [kg]	151 440	63 900	50 340
Maximum fuel capacity (MFC) [kg]	243 350	109 185	48 980
Source of data	Preliminary airplane characteristics [2]	Airbus airplane characteristics [2]	Airbus airplane characteristics [2]

Table 56: Characteristic weights of major cargo aircraft types (continued)

	Boeing 737-700C	Boeing 737-400SF	Boeing 737-300SF
Maximum take-off weight (MTOW) [kg]	77 560	65 921	63 049
Operating empty weight (OEW) [kg]	38 360	32 458	31 910
Maximum payload (MPL) [kg]	18 780	19 705	16 639
Maximum fuel capacity (MFC) [kg]	20 816	19 131	19 131
Source of data	Boeing website / information for airline startups	ASCEND online fleets, average [11]	ASCEND online fleets, average [11]

Table 57: Characteristic weights of major cargo aircraft types (continued)

While the aforementioned aircraft are modelled by VarMission, fuel burn and NO<sub>x</sub> emissions of aircraft types with no available performance model can be estimated by using a “representative” aircraft model with similar characteristics. As was described for passenger aircraft in chapter 3.4.5.5, deltas of specific fuel burn and emissions can be specified between the actual aircraft type and its representative model. Table 58 presents the assumptions made for future cargo aircraft types with no available performance model. The improvements in terms of specific fuel consumption and NO<sub>x</sub> emissions compared to the representative aircraft model correspond roughly to the deltas that were observed for the respective passenger versions.

Aircraft type	Representative model	Assumption for aircraft representation
Boeing 787 Freighter	Airbus A330-200F	15% reduction of fuel burn and 15% reduction of NO <sub>x</sub> emissions per kg payload*
Airbus A350 XWB Freighter	Boeing 777-200F	25% reduction of fuel burn and 40% reduction of NO <sub>x</sub> emissions per kg payload
* assuming an “average” engine between the GENx with TAPS combustor and the Trent-1000 with RQL combustor.		

Table 58: Simplified assumptions for future cargo aircraft without available performance models

## Appendix T ASSUMED STRINGENCY OF NO<sub>x</sub> EMISSION STANDARDS

This appendix summarizes the assumed stringency scenarios for engine NO<sub>x</sub> emission standards:

- Table 59 shows the assumptions used in the baseline scenario of the forecast.
- Table 60 refers to an alternative scenario assuming a delayed introduction of low-NO<sub>x</sub> technology.

Detailed information regarding the baseline assumptions are found in chapter 3.4.6.2.

The alternative stringency scenario for NO<sub>x</sub> emission standards is discussed in chapter 4.4.3.

Year	NO <sub>x</sub> regulatory limit for newly certified engines	NO <sub>x</sub> regulatory limit for in-production engines
2004	CAEP/4	CAEP/2
2008	CAEP/6	CAEP/2
2014	CAEP/8	CAEP/6 (from 2013)
2017	CAEP/8 – 17%	CAEP/6
2020	CAEP/8 – 35% (~Mid-term goal from [109] for low $\pi_{00}$ *)	CAEP/8
2025	CAEP/8 – 50%	CAEP/8
2030	Long-term goal from [109]	CAEP/8 – 35% (~ Mid-term goal from [109] for low $\pi_{00}$ *)
* higher slope compared to mid-term technology goal for $\pi_{00} > 30$ , see Figure 55.		

Table 59: Stringency of NO<sub>x</sub> emission standards in baseline scenario

Year	NO <sub>x</sub> regulatory limit for newly certified engines	NO <sub>x</sub> regulatory limit for in-production engines
2004	CAEP/4	CAEP/2
2008	CAEP/6	CAEP/2
2014	CAEP/8	CAEP/6 (from 2013)
2018	CAEP/8 – 17%	CAEP/6
2023	CAEP/8 – 35% (~Mid-term goal from [109] for low $\pi_{00}$ *)	CAEP/8
2030	CAEP/8 – 50%	CAEP/8
2035	Long-term goal from [109]	CAEP/8 – 35% (~ Mid-term goal from [109] for low $\pi_{00}$ *)
* higher slope compared to mid-term technology goal for $\pi_{00} > 30$ , see Figure 55.		

Table 60: Stringency of NO<sub>x</sub> emission standards in scenario with development delays

## Appendix U TABULATED RESULTS FOR BASELINE SCENARIO

Year* [ ]	Flights [10 <sup>5</sup> ]	Distance** [10 <sup>9</sup> km]	ASK [10 <sup>5</sup> ]	RPK [10 <sup>5</sup> ]	TKO [10 <sup>9</sup> ]	TKT [10 <sup>5</sup> ]	Fuel [10 <sup>9</sup> kg]	NO <sub>x</sub> (DLR FF) [10 <sup>9</sup> kg]	NO <sub>x</sub> (BM2) [10 <sup>9</sup> kg]	CO [10 <sup>9</sup> kg]	HC [10 <sup>9</sup> kg]	Soot [10 <sup>9</sup> kg]	Soot PM [10 <sup>25</sup> ]
2000	27.62	27.64	4518	3245	671.2	412.1	155.1	1.953	2.064	0.631	0.107	6.779	6.672
2003	26.24	27.47	4455	3195	661.2	399.0	145.0	1.829	1.956	0.554	0.081	5.617	5.721
2004	27.18	29.99	4868	3604	727.2	451.2	156.5	1.989	2.131	0.582	0.080	5.828	6.013
2005	28.36	32.25	5211	3918	791.1	495.4	167.5	2.138	2.298	0.600	0.081	6.012	6.246
2006	28.82	33.41	5445	4150	811.2	518.6	171.8	2.211	2.378	0.603	0.077	6.024	6.251
2007	30.06	35.43	5795	4478	862.2	556.7	180.7	2.340	2.521	0.615	0.074	6.084	6.335
2008	30.17	36.36	6014	4684	895.0	567.4	184.9	2.398	2.589	0.621	0.071	6.170	6.457
2009	29.13	35.27	5918	4530	874.1	548.6	178.3	2.326	2.516	0.583	0.062	5.755	6.020
2010	30.51	37.48	6327	4949	924.6	602.6	188.4	2.466	2.670	0.604	0.062	6.089	6.404

\*Only September schedules available for 2000; only January and July schedules available for 2003-2005. Results are upscaled to estimate yearly values.

\*\*Great-circle distance between departure and destination airports.

Table 61: Transport performance and emissions for historical scheduled air traffic (based on OAG flight schedules)

Year* [ ]	Flights [10 <sup>5</sup> ]	Distance** [10 <sup>9</sup> km]	ASK [10 <sup>5</sup> ]	RPK [10 <sup>5</sup> ]	TKO [10 <sup>9</sup> ]	TKT [10 <sup>5</sup> ]	Fuel [10 <sup>9</sup> kg]	NO <sub>x</sub> (DLR FF) [10 <sup>9</sup> kg]	NO <sub>x</sub> (BM2) [10 <sup>9</sup> kg]	CO [10 <sup>9</sup> kg]	HC [10 <sup>9</sup> kg]	Soot [10 <sup>9</sup> kg]	Soot PM [10 <sup>25</sup> ]
2011	31.89	39.33	6689	5247	976.7	637.9	198.3	2.606	2.824	-	-	-	-
2012	33.33	41.24	7066	5554	1029.1	675.3	208.4	2.745	2.976	-	-	-	-
2013	34.86	43.28	7464	5879	1086.2	714.9	219.0	2.891	3.136	-	-	-	-
2014	36.45	45.44	7885	6222	1146.9	756.8	230.0	3.043	3.300	-	-	-	-
2015	38.13	47.69	8330	6586	1211.2	801.1	241.4	3.201	3.471	-	-	-	-
2016	39.63	49.76	8724	6912	1273.4	842.8	251.7	3.344	3.623	-	-	-	-
2017	41.19	51.88	9137	7254	1335.9	886.6	261.9	3.489	3.778	-	-	-	-
2018	42.82	54.11	9570	7613	1402.0	932.7	272.2	3.629	3.927	-	-	-	-
2019	44.49	56.41	10023	7989	1472.4	981.3	282.6	3.768	4.073	-	-	-	-
2020	46.23	58.79	10497	8385	1545.1	1032.3	293.2	3.890	4.200	-	-	-	-
2021	47.72	60.88	10924	8743	1614.8	1081.0	302.9	4.007	4.318	-	-	-	-
2022	49.26	63.04	11367	9117	1688.3	1132.1	312.7	4.113	4.426	-	-	-	-
2023	50.86	65.29	11829	9507	1764.0	1185.6	322.7	4.222	4.535	-	-	-	-
2024	52.51	67.62	12309	9913	1844.1	1241.7	333.1	4.323	4.637	-	-	-	-
2025	54.23	70.05	12809	10337	1927.4	1300.5	343.8	4.428	4.743	-	-	-	-
2026	56.03	72.59	13330	10779	2015.1	1362.2	355.1	4.530	4.845	-	-	-	-
2027	57.92	75.27	13871	11240	2106.7	1426.9	366.6	4.638	4.952	-	-	-	-
2028	59.88	78.03	14435	11721	2202.8	1494.7	378.7	4.744	5.059	-	-	-	-
2029	61.96	80.96	15021	12222	2304.2	1565.8	391.3	4.863	5.177	-	-	-	-
2030	64.11	84.00	15632	12744	2410.3	1640.4	404.5	4.958	5.271	-	-	-	-

\*Only September traffic is currently forecasted. Results are upscaled to yearly values in accordance with the monthly traffic shares in the base year 2010.

\*\*Great-circle distance between departure and destination airports.

Table 62: Transport performance and emissions for forecasted scheduled air traffic

Specific Aircraft	Specific Aircraft Name	2010	2012	2014	2016	2018	2020	2022	2024	2026	2028	2030
389	Airbus A380-900	0	0	0	0	0	25	60	96	148	194	243
388	Airbus A380-800	41	107	169	233	304	354	419	480	551	615	688
748	Boeing 747-8I	0	12	39	66	90	114	144	183	204	244	280
744	Boeing 747-400	353	314	272	228	186	145	108	77	51	32	19
743	Boeing 747-300	37	32	27	22	17	13	10	7	4	3	1
742	Boeing 747-200	18	13	9	4	0	0	0	0	0	0	0
741	Boeing 747-100	4	0	0	0	0	0	0	0	0	0	0
73N	Boeing 777-300/-300ER Successor	0	0	0	0	0	0	0	0	0	0	0
77W	Boeing 777-300ER	261	382	515	654	760	826	853	818	772	715	647
773	Boeing 777-300	59	59	57	56	54	51	48	45	41	37	32
346	Airbus A340-600	96	95	93	89	84	78	71	62	52	42	33
35X	Airbus A350-1000 XWB	0	0	0	0	32	87	165	271	380	500	628

Table 63: Number of active aircraft by aircraft type in baseline forecast, seat categories 6-7



Specific Aircraft	Specific Aircraft Name	2010	2012	2014	2016	2018	2020	2022	2024	2026	2028	2030
74L	Boeing 747SP	16	12	9	7	5	3	2	1	0	0	0
359	Airbus A350-900 XWB	0	0	22	77	207	295	364	442	518	603	710
358	Airbus A350-800 XWB	0	0	0	0	44	96	139	189	250	311	385
345	Airbus A340-500	31	34	33	32	31	28	26	23	19	16	13
343	Airbus A340-300	202	193	182	169	153	135	116	97	78	61	46
342	Airbus A340-200	25	24	22	20	18	16	14	11	9	7	5
M11	Boeing (Douglas) MD-11	17	13	9	4	0	0	0	0	0	0	0
72N	Boeing 777-200/-200LR Successor	0	0	0	0	0	0	0	0	0	0	0
772	Boeing 777-200	469	516	559	576	535	486	432	377	322	269	220
77L	Boeing 777-200LR	48	56	67	75	73	71	68	63	58	52	45
333	Airbus A330-300	323	400	468	521	500	474	443	407	366	322	276
332	Airbus A330-200	387	453	507	537	560	553	517	475	427	376	322
AB6	Airbus A300-600	97	76	56	39	26	15	8	4	2	1	0
AB4	Airbus A300B2/B4	17	10	3	0	0	0	0	0	0	0	0
789	Boeing 787-9	0	0	22	84	166	234	299	381	462	548	628
788	Boeing 787-8	0	33	103	237	375	519	632	730	831	938	1038
D11	Boeing (Douglas) DC10-10 /15	0	0	0	0	0	0	0	0	0	0	0
D1C	Boeing (Douglas) DC10-30 /40	13	8	3	0	0	0	0	0	0	0	0
764	Boeing 767-400	38	37	36	34	32	30	27	24	20	16	12
763	Boeing 767-300	494	533	542	486	430	374	321	270	225	185	150
762	Boeing 767-200	92	72	54	39	27	18	11	7	5	3	2
753	Boeing 757-300	55	54	53	51	48	45	41	37	32	26	21
752	Boeing 757-200	676	606	530	452	377	308	244	189	142	104	73
L11	Lockheed L1011 TriStar	1	0	0	0	0	0	0	0	0	0	0
L15	Lockheed L1011 TriStar 500	7	5	4	2	0	0	0	0	0	0	0
IL9	Ilyushin Il-96	16	17	16	14	13	12	10	9	7	6	4
ILW	Ilyushin Il-86	6	0	0	0	0	0	0	0	0	0	0
312	Airbus A310-200	3	0	0	0	0	0	0	0	0	0	0
313	Airbus A310-300	98	81	64	48	35	23	14	8	4	1	0

Table 64: Number of active aircraft by aircraft type in baseline forecast, seat category 5

Specific Aircraft	Specific Aircraft Name	2010	2012	2014	2016	2018	2020	2022	2024	2026	2028	2030
319	Airbus A319	1262	1459	1667	1866	1966	1975	1899	1804	1690	1559	1417
320	Airbus A320	2444	2792	3178	3496	3667	3540	3390	3215	3013	2785	2536
321	Airbus A321	617	727	850	970	1056	1100	1063	1017	962	898	827
19N	Airbus A319 NEO	0	0	0	0	81	172	301	456	615	798	995
20N	Airbus A320 NEO	0	0	0	126	328	664	1029	1445	1870	2349	2839
21N	Airbus A321 NEO	0	0	0	0	80	255	459	703	951	1240	1555
707	Boeing 707 / 720	0	0	0	0	0	0	0	0	0	0	0
722	Boeing 727-200	58	35	12	0	0	0	0	0	0	0	0
733	Boeing 737-300	726	625	527	434	349	274	210	156	112	75	48
734	Boeing 737-400	407	376	340	299	255	213	174	140	111	87	67
73G	Boeing 737-700	1043	1193	1348	1480	1548	1619	1555	1475	1380	1272	1154
738	Boeing 737-800	2101	2368	2669	2934	3090	3137	3030	2891	2719	2519	2299
739	Boeing 737-900	134	242	358	479	587	649	678	666	648	624	593
37N	Boeing 737 MAX 7	0	0	0	0	35	131	265	412	574	734	926
38N	Boeing 737 MAX 8	0	0	0	0	181	470	825	1188	1612	2061	2570
39N	Boeing 737 MAX 9	0	0	0	0	0	167	380	632	915	1224	1531
C91	Comac 919-100	0	0	0	0	0	13	37	56	75	98	114
C92	Comac 919-200	0	0	0	0	23	57	97	135	188	237	298
C93	Comac 919-300	0	0	0	0	0	8	35	58	86	110	143
CS3	CSeries 300	0	0	15	50	66	87	122	160	197	239	287
D95	Boeing (Douglas) DC9-50	45	38	31	26	22	18	15	12	9	7	5
DC8	Boeing (Douglas) DC-8	10	0	0	0	0	0	0	0	0	0	0
M81	Boeing (Douglas) MD-81	5	0	0	0	0	0	0	0	0	0	0
M82	Boeing (Douglas) MD-82	300	246	197	154	118	89	65	45	29	17	9
M83	Boeing (Douglas) MD-83	220	207	191	173	153	133	114	96	80	65	53
M87	Boeing (Douglas) MD-87	36	27	20	15	11	7	5	3	1	0	0
M88	Boeing (Douglas) MD-88	127	119	109	98	85	72	60	49	40	33	26
M90	Boeing (Douglas) MD-90	89	75	60	44	32	22	15	9	5	2	0
IL6	Ilyushin IL-62	30	22	15	7	0	0	0	0	0	0	0
T20	Tupolev TU-204 / TU-214	52	66	65	64	62	59	56	52	48	44	39
TU5	Tupolev TU154	214	163	121	87	62	44	30	20	12	7	3

Table 65: Number of active aircraft by aircraft type in baseline forecast, seat category 4

Specific Aircraft	Specific Aircraft Name	2010	2012	2014	2016	2018	2020	2022	2024	2026	2028	2030
100	Fokker 100	170	138	107	80	59	42	30	20	11	5	1
143	BAe 146-300	21	15	11	7	4	2	1	0	0	0	0
219	Comac ARJ21-900	0	0	0	36	80	120	178	241	307	382	443
318	Airbus A318	74	117	162	178	177	174	170	164	156	147	135
717	Boeing 717-200	145	135	121	104	84	64	47	33	22	14	9
721	Boeing 727-100	26	19	13	6	0	0	0	0	0	0	0
731	Boeing 737-100	0	0	0	0	0	0	0	0	0	0	0
732	Boeing 737-200	288	229	178	136	104	78	56	38	23	11	4
735	Boeing 737-500	305	273	236	197	160	126	98	75	56	41	28
736	Boeing 737-600	68	87	110	122	119	115	110	103	95	87	78
AR1	Avro RJ100	53	45	36	28	20	14	10	6	3	2	1
CRX	Canadair Regional Jet 1000	1	44	81	122	157	186	185	184	180	175	168
CS1	C-Series 100	0	0	60	130	219	298	402	534	686	841	1004
D93	Boeing (Douglas) DC9-30	48	0	0	0	0	0	0	0	0	0	0
D94	Boeing (Douglas) DC9-40	6	4	3	1	0	0	0	0	0	0	0
E90	Embraer 190	333	461	558	648	755	817	804	784	757	722	677
E95	Embraer 195	64	105	137	175	207	231	250	245	239	231	219
FXE	Embraer 190 Successor	0	0	0	0	0	96	240	399	565	755	973
S95	Superjet 100-95	0	14	41	73	115	152	212	278	346	418	506
YK2	Yakovlev Yak-42/142	100	85	70	56	44	34	25	18	13	9	5

Table 66: Number of active aircraft by aircraft type in baseline forecast, seat category 3

Specific Aircraft	Specific Aircraft Name	2010	2012	2014	2016	2018	2020	2022	2024	2026	2028	2030
141	BAe 146-100	16	13	10	8	6	4	3	2	1	1	0
142	BAe 146-200	37	28	21	15	10	7	4	2	1	0	0
217	Comac ARJ21-700	0	7	19	30	44	61	75	94	112	133	165
A81	Antonov An148-100	6	6	6	6	6	6	6	6	5	5	5
AR7	Avro RJ70	7	6	4	3	2	1	1	0	0	0	0
AR8	Avro RJ85	66	56	45	34	25	17	12	8	4	2	1
AT7	ATR 72	441	520	605	693	754	757	728	698	665	630	594
ATP	BAe ATP	37	33	28	23	18	13	9	5	3	1	1
B11	BAe (BAC) 1-11	0	0	0	0	0	0	0	0	0	0	0
CR7	Canadair Regional Jet 700	302	336	373	403	423	443	441	420	394	364	329
CR9	Canadair Regional Jet 900	240	286	332	375	416	455	480	492	473	450	422
CRA	Canadair Regional Jet 705	16	34	50	65	80	93	110	109	106	103	98
D92	Boeing (Douglas) DC-9-20	1	0	0	0	0	0	0	0	0	0	0
DC6	Boeing (Douglas) DC-6b	0	0	0	0	0	0	0	0	0	0	0
DH4	De Havilland DHC-8-400 Dash 8Q	318	365	417	478	516	554	536	517	497	476	454
E70	Embraer 170	184	236	296	344	380	394	385	373	356	336	310
E75	Embraer 175	134	162	193	223	250	279	274	266	256	243	227
F21	Fokker F28-1000 Fellowship	9	7	5	2	0	0	0	0	0	0	0
F22	Fokker F28-2000 Fellowship	1	1	0	0	0	0	0	0	0	0	0
F23	Fokker F28-3000 Fellowship	8	7	5	4	4	3	2	2	1	1	0
F24	Fokker F28-4000 Fellowship	18	13	8	5	3	1	0	0	0	0	0
F70	Fokker 70	43	41	38	35	31	27	22	18	14	12	9
F7B	CRJ 700 Successor	0	0	0	0	0	11	44	87	140	199	250
F7E	Embraer 170 Successor	0	0	0	0	11	34	71	113	159	210	263
F9B	CRJ 900 Successor	0	0	0	0	0	0	27	95	199	305	426
FP9	Future Turboprop (90 seats)	0	0	0	0	0	28	125	226	322	449	566
FQQ	Bombardier DHC-8 Successor	0	0	0	0	19	62	113	162	205	265	327
FUP	ATR 72 Successor	0	0	0	0	43	92	148	203	271	314	393
I14	Ilyushin IL114	6	7	8	11	11	10	10	9	9	9	8
IL8	Ilyushin IL-18	69	56	44	31	19	6	0	0	0	0	0
MJ7	MRJ70	0	0	0	0	7	21	36	53	75	94	116
MJ9	MRJ90	0	0	7	20	33	47	61	73	94	120	141
S75	Superjet 100-75	0	0	0	9	19	29	41	65	85	106	123
TU3	Tupolev TU134	181	142	109	82	59	41	26	15	7	3	1
YS1	NAMC YS-11	0	0	0	0	0	0	0	0	0	0	0

Table 67: Number of active aircraft by aircraft type in baseline forecast, seat category 2

Specific Aircraft	Specific Aircraft Name	2010	2012	2014	2016	2018	2020	2022	2024	2026	2028	2030
A40	Antonov AN-140	17	20	20	21	20	20	19	18	17	16	15
AN4	Antonov AN-24	203	161	123	90	60	36	19	8	2	0	0
AN6	Antonov AN-26 /30 /32	939	831	726	628	537	456	383	318	261	211	165
AN7	Antonov AN-72 /74	0	0	0	0	0	0	0	0	0	0	0
AT3	ATR 42 300 /400	202	191	180	168	156	143	129	114	98	81	64
AT5	ATR 42 500	103	115	128	145	163	179	232	252	257	246	235
CR1	Canadair Regional Jet 100	166	137	108	80	57	39	26	16	9	4	1
CR2	Canadair Regional Jet 200	781	775	756	728	691	646	592	529	459	386	315
CS5	Casa /Nusantara CN-235	0	0	0	0	0	0	0	0	0	0	0
CVR	Convair 240 /440 /580	43	35	27	20	12	4	0	0	0	0	0
D38	Fairchild Dornier 328-100	85	80	75	69	63	57	50	43	35	27	20
DH1	De Havilland DHC-8-100	221	211	201	190	179	168	156	143	129	114	99
DH2	De Havilland DHC-8-200	85	82	79	76	72	68	65	61	56	52	47
DH3	De Havilland DHC-8-300	221	215	208	201	194	186	178	170	162	153	144
DH7	De Havilland DHC-7 Dash 7	53	47	40	33	26	19	13	8	4	2	1
DHC	De Havilland DHC-4 Caribou	1	1	1	1	1	1	1	1	0	0	0
EM2	Embraer 120 Brasilia	206	181	155	127	100	74	51	32	19	11	6
ER3	Embraer RJ135	302	301	300	296	289	280	274	266	250	230	203
ER4	Embraer RJ145	714	708	703	687	664	636	630	625	582	516	452
ERD	Embraer RJ140	74	73	71	69	65	61	56	51	44	37	30
F27	Fokker F27 Friendship	88	72	56	40	24	8	0	0	0	0	0
F50	Fokker 50	145	125	104	84	66	51	39	29	21	15	9
F5E	Embraer 145 Successor	0	0	0	0	0	0	0	0	47	134	230
FK7	Fairchild Industries FH227	0	0	0	0	0	0	0	0	0	0	0
FRJ	Fairchild Dornier 328JET	98	91	81	68	54	40	29	20	14	9	5
FUQ	ATR 42 Successor	0	0	0	0	0	0	0	33	78	134	198
GRS	Gulfstream Aerospace G159	0	0	0	0	0	0	0	0	0	0	0
HS7	BAe (HS) 748	108	89	71	54	41	30	21	14	9	5	3
S20	Saab 2000	49	48	46	43	41	39	36	34	31	28	25
SF3	Saab 340	313	293	272	250	227	202	175	148	121	94	70
SH3	Shorts 330 (SD3-30)	35	26	18	11	7	4	2	1	1	0	0
SH6	Shorts 360 (SD3-60)	96	88	79	69	59	49	38	28	19	12	6
YK4	Yakovlev Yak-40	261	212	170	135	105	77	53	31	15	5	1
YN7	Xian Yunshuji Y7 /MA60	53	46	38	31	23	17	11	7	4	2	1

Table 68: Number of active aircraft by aircraft type in baseline forecast, seat category 1

Specific Aircraft	Specific Aircraft Name	2010	2012	2014	2016	2018	2020	2022	2024	2026	2028	2030
14F	BaE 146 (Freighter)	23	20	9	2	0	0	0	0	0	0	0
31F	Airbus A310 (Freighter)	84	84	83	83	83	83	83	83	81	75	66
33F	Airbus A330-200F (Freighter)	0	31	58	86	136	218	356	468	539	619	737
35F	Airbus A350-900 (Freighter)	0	0	0	0	5	31	62	100	149	209	274
38F	Airbus A380-800 (Freighter)	0	0	0	0	0	5	19	37	57	83	124
70F	Boeing 707 (Freighter)	0	0	0	0	0	0	0	0	0	0	0
72F	Boeing 727 (Freighter)	244	192	144	103	71	47	30	18	9	4	1
73P	Boeing 737-400 (Freighter)	10	12	11	12	13	13	13	13	13	13	13
73R	Boeing 737-700 (Freighter)	0	9	44	80	126	179	246	329	430	551	690
73X	Boeing 737-200 (Freighter)	20	18	16	15	13	11	9	7	5	4	2
73Y	Boeing 737-300 (Freighter)	71	99	104	121	118	112	101	87	74	60	47
74T	Boeing 747-100 (Freighter)	9	7	5	2	0	0	0	0	0	0	0
74X	Boeing 747-200 (Freighter)	71	52	35	21	11	5	2	0	0	0	0
74Y	Boeing 747-400F (Freighter)	220	236	253	275	296	296	296	291	277	254	224
74Z	Boeing 747-8F (Freighter)	0	2	8	18	28	43	61	80	107	135	167
75F	Boeing 757-200F (Freighter)	162	145	130	123	112	100	88	75	63	50	38
76F	Boeing 767 (Freighter)	113	141	147	163	176	203	203	203	200	190	174
77F	Boeing 777 (Freighter)	20	33	53	74	97	120	146	172	211	253	301
78F	Boeing 787-8 (Freighter)	0	0	0	0	0	0	0	50	187	349	517
A4F	Antonov AN-124	28	24	20	16	12	9	6	4	3	2	1
ABX	Airbus A300B4 / C4 / F4	44	33	22	13	6	2	0	0	0	0	0
ABY	Airbus A300-600F (Freighter)	156	181	236	288	324	324	324	323	311	287	252
ANF	Antonov AN-12	355	303	251	201	154	112	76	47	25	12	4
CL4	Canadair CL-44	0	0	0	0	0	0	0	0	0	0	0
CVF	Convair 440 /580 /600 /640	0	0	0	0	0	0	0	0	0	0	0
CWC	Curtiss C-46 Commando	14	5	0	0	0	0	0	0	0	0	0
D1F	Boeing DC-10 (Freighter)	105	97	89	79	69	58	47	37	28	20	13
D6F	Douglas DC6 (Freighter)	89	65	44	27	15	7	2	0	0	0	0
D8F	Douglas DC8 (Freighter)	34	25	17	8	0	0	0	0	0	0	0
D9F	Douglas DC9 (Freighter)	22	18	14	10	6	2	0	0	0	0	0
IL7	Ilyushin IL-76	408	336	270	212	164	124	91	66	45	30	18
L1F	Lockheed L1011 (Freighter)	0	0	0	0	0	0	0	0	0	0	0
LOF	Lockheed L188 (Freighter)	0	0	0	0	0	0	0	0	0	0	0
LOH	Lockheed Hercules	54	49	43	37	31	25	20	16	11	8	5
M1F	Boeing MD-11 (Freighter)	168	174	174	174	174	174	171	159	140	119	98
SHB	Shorts SC.5 Belfast	0	0	0	0	0	0	0	0	0	0	0
T2F	Tupolev TU-204 (Freighter)	0	0	0	0	0	0	0	0	0	0	0

Table 69: Number of active aircraft by aircraft type in baseline forecast, seat categories 101-103 (freighter)

Specific Aircraft	Specific Aircraft Name	2010	2012	2014	2016	2018	2020	2022	2024	2026	2028	2030
72M	Boeing 727	0	0	0	0	0	0	0	0	0	0	0
73L	Boeing 737-200	34	28	23	18	14	11	8	6	4	3	1
73Q	Boeing 737-400	44	42	40	38	34	31	28	25	22	19	16
74C	Boeing 747-200	9	7	5	2	0	0	0	0	0	0	0
74D	Boeing 747-300 / 747-200 SUD	5	3	2	1	0	0	0	0	0	0	0
74E	Boeing 747-400	43	37	31	26	20	15	11	7	4	2	1
M1M	Boeing (Douglas) MD-11	0	0	0	0	0	0	0	0	0	0	0

**Table 70: Number of active aircraft by aircraft type in baseline forecast, seat category 200 (aircraft in mixed configuration)<sup>58</sup>**

<sup>58</sup> As a simplification, no new aircraft in mixed configuration are considered in the forecast. Existing aircraft from the base year fleet are gradually phased out.

## Appendix V VISUALIZATION OF AIR TRAFFIC EMISSIONS

This appendix presents figures that visualize the regional distribution of air traffic emissions. The diagrams have been produced by the FATE software based on results from this study.



Figure 133: Visualization of global scheduled aviation's fuel consumption in September 2000 and September 2010 (Source: DLR-FW)



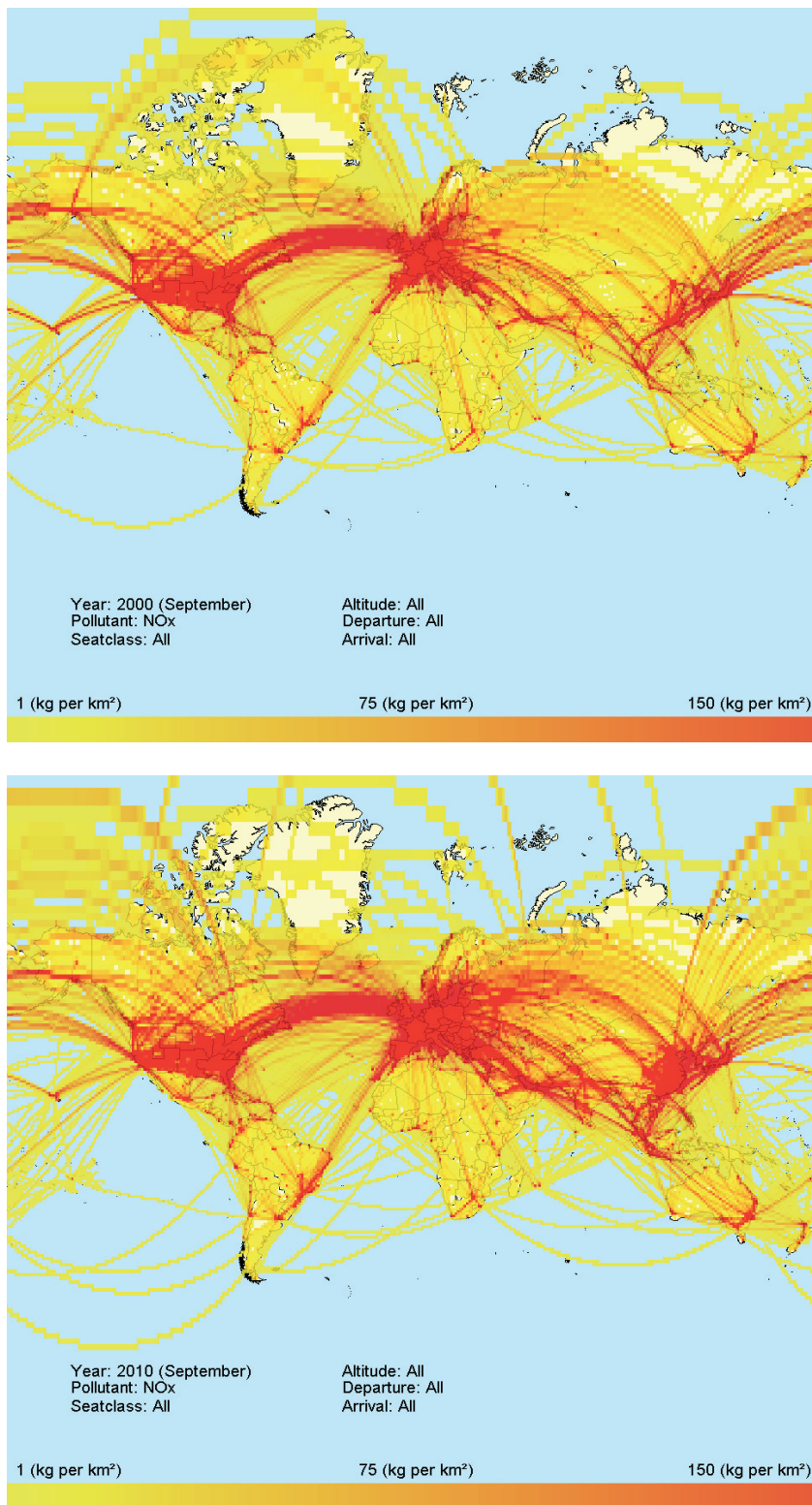
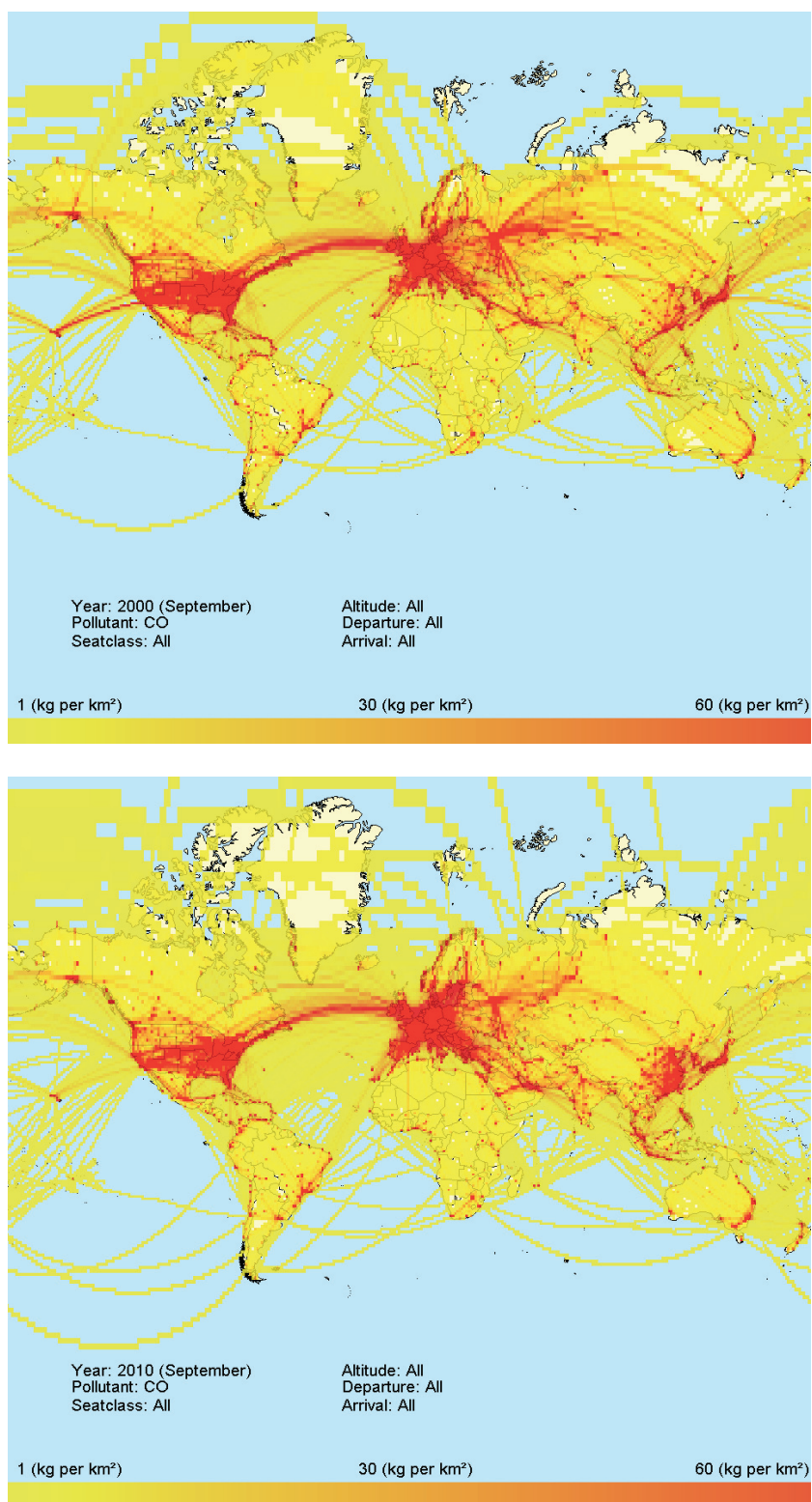


Figure 134: Visualization of global scheduled aviation's NO<sub>x</sub> emissions in September 2000 and September 2010 (Source: DLR-FW)



*Figure 135: Visualization of global scheduled aviation's CO emissions in September 2000 and September 2010 (Source: DLR-FW)*

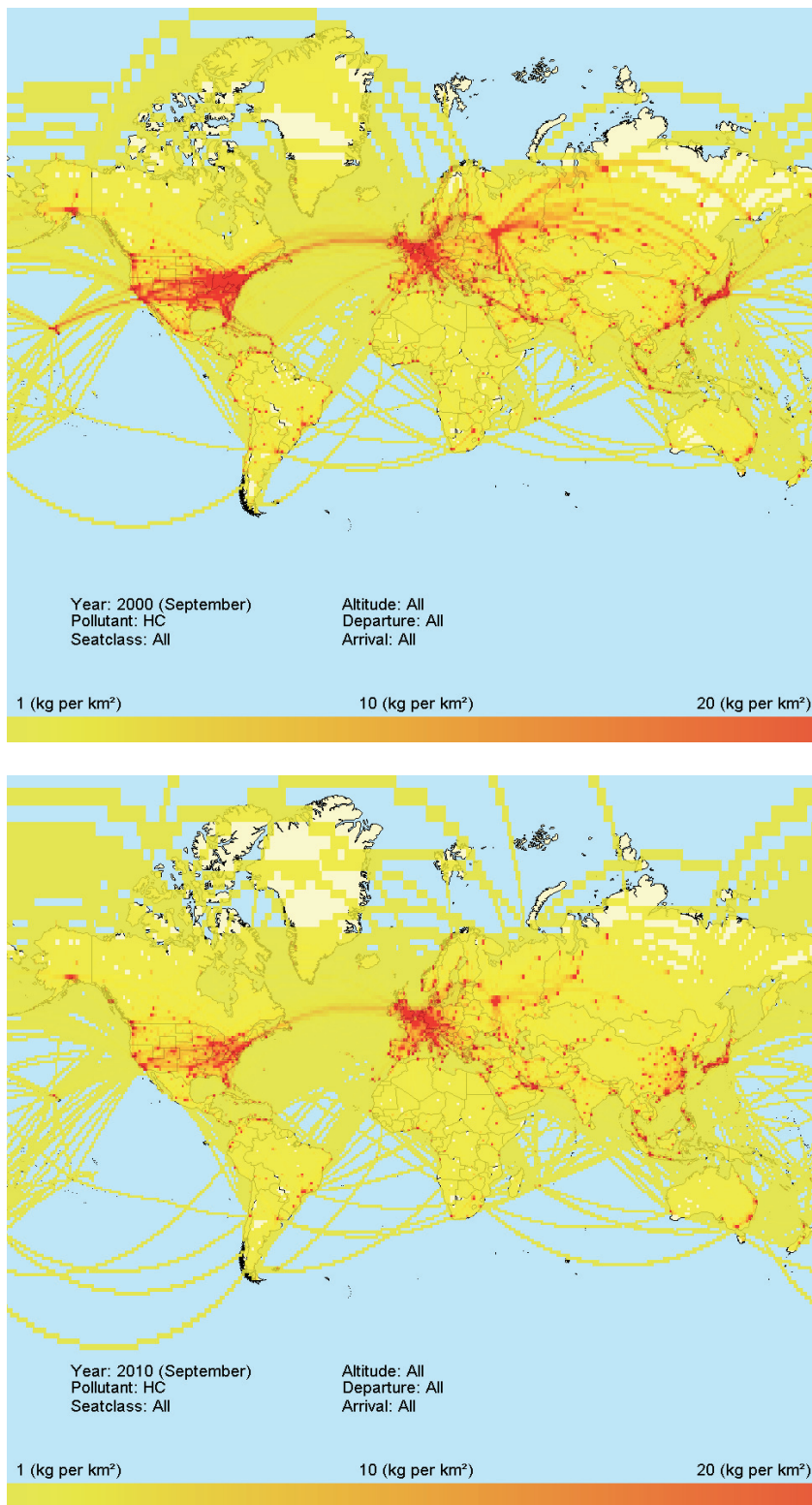
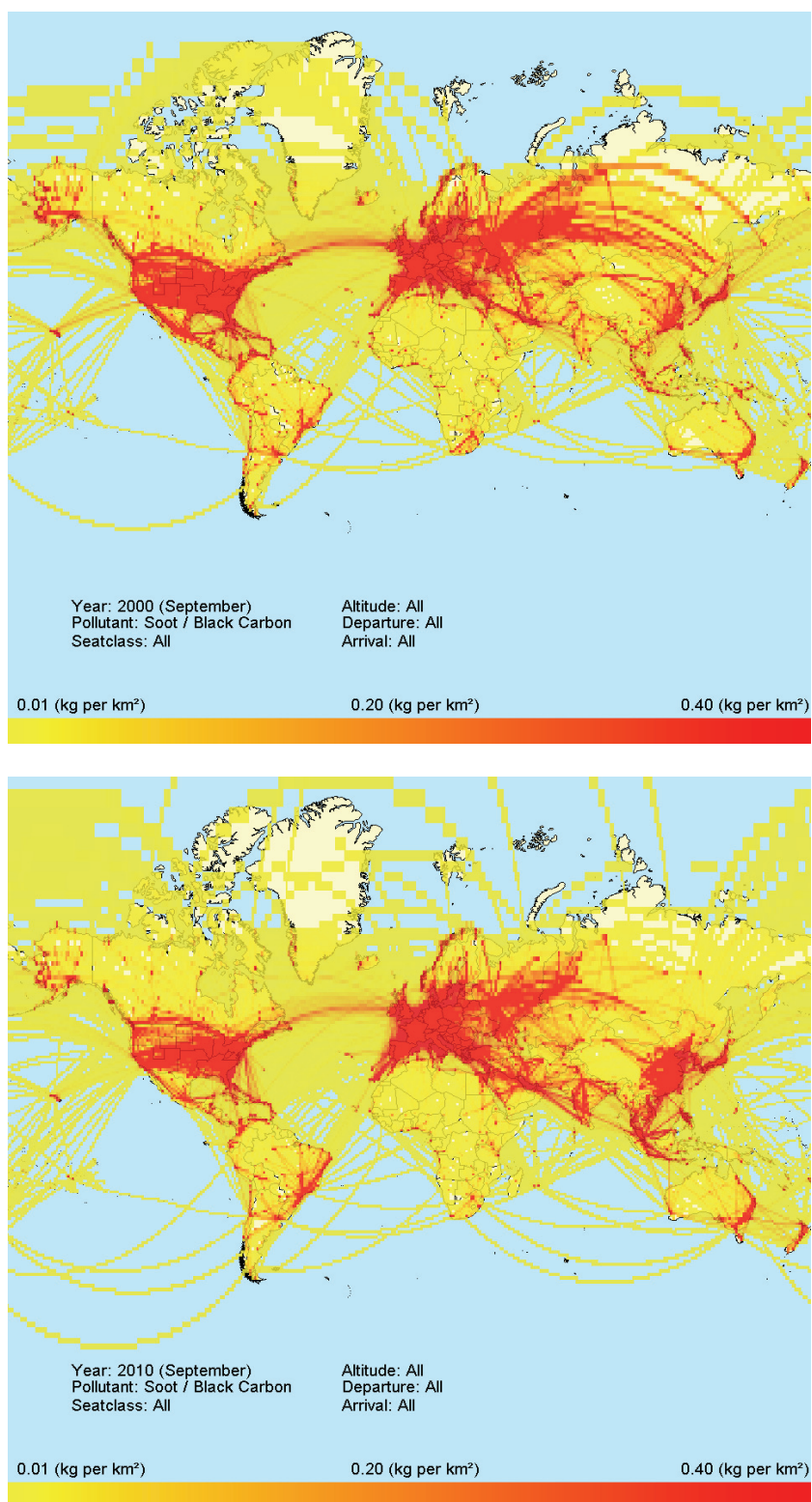


Figure 136: Visualization of global scheduled aviation's HC emissions in September 2000 and September 2010 (Source: DLR-FW)





*Figure 137: Visualization of global scheduled aviation's soot emissions in September 2000 and September 2010 (Source: DLR-FW)*